Beyond LC3-associated phagocytosis: cross-talk between autophagy and efferocytosis during microglial corpse clearance

Sanjna Singh, B. Hlth. Sc. (Hons)

THE UNIVERSITY of ADELAIDE

A thesis submitted for the degree of Doctor of Philosophy in

Adelaide Medical School

Faculty of Health and Medical Sciences

University of Adelaide

August 2023

Nothing in life is to be feared, it is only to be understood. Now is the time to understand more, so that we may fear less.

– Marie Curie

DECLARATION

I certify that this work contains no material which has been accepted for the award of any other degree or diploma in my name, in any university or other tertiary institution and, to the best of my knowledge and belief, contains no material previously published or written by another person, except where due reference has been made in the text. In addition, I certify that no part of this work will, in the future, be used in a submission in my name, for any other degree or diploma in any university or other tertiary institution without the prior approval of the University of Adelaide and where applicable, any partner institution responsible for the joint award of this degree.

I give permission for the digital version of my thesis to be made available on the web, via the University's digital research repository, the Library Search and also through web search engines, unless permission has been granted by the University to restrict access for a period of time.

I acknowledge the support I have received for my research through the provision of an Australian Government Research Training Program Scholarship.

Sanjna Singh

August 2023

ACKNOWLEDGEMENT

The work in this thesis would not have been possible without the support of the people around me. Firstly, I would like to extend immense gratitude towards my primary supervisor Dr. Timothy Sargeant. Tim – when I first joined your lab during honours, I barely knew how to hold a pipette. You have been an amazing mentor; your guidance has turned me into the scientist I am today, and I will always be thankful that you gave me the opportunity to work in your group. To my co-supervisors Dr. Ville-Petteri Mäkinen and Emeritus Professor John Hopwood – I greatly value our discussions, and the constructive feedback you gave me helped improve this project. I would especially like to thank my lab manager Sophie Lazenkas, who, in addition to keeping our lab running smoothly, very kindly volunteered her time and laser sharp cross-checking skills to ensure that everything in this thesis was in order. And lastly, I would like to thank every member of the Lysosomal Health in Ageing and EMBL Mäkinen research groups. Julien, Julian, Aaron, Leanne, Kat, Linh, Sofia, Célia and Lexi – thank you for your advice, training, lively discussions and technical expertise. Most of all, thank you for making the lab fun. Scientific research can, at times, be draining: for every successful experiment, there are several failures and inconclusive results. It helps to have someone to share these highs and lows with, and I could not have asked for a more supportive team.

To my husband, Louis – I do not have the words to adequately convey how much your love means to me. From your endless patience to your daily morning coffees: I will never forget the sheer magnitude of support I received from you. And lastly, to my parents – you have always believed in me. I could not imagine doing this without your love and guidance.

This research was supported by an Australian Research Training Program Scholarship.

ABSTRACT

Every day, billions of cells die in the human body, both as part of programmed cellular turnover and during injury or disease. These cells are engulfed and removed by specialised subsets of phagocytic immune cells, via a process termed efferocytosis. The efficient removal of apoptotic cells prevents necrosis and subsequent inflammatory damage to surrounding healthy tissue. Microglia are phagocytes that reside in the brain, where they serve as the primary executors of efferocytosis. However, corpse clearance in microglia is relatively under-studied, with most research performed in macrophages. Proper clearance of waste material and preventing inflammation is particularly crucial in the brain, where a tightly controlled environment must be maintained to ensure optimal function. Autophagy is another important waste disposal process in the brain; it involves the packaging and breakdown of intracellular cargo such as protein aggregates and organelles via double-membraned vesicles termed autophagosomes. Some the autophagy-related (ATG) machinery also facilitates the efficient clearance of apoptotic cells during efferocytosis in an autophagy-independent manner, via the conjugation of ATG8/LC3 to endolysosomal single membranes (CASM), also referred to as non-canonical autophagy. Importantly, both autophagy and efferocytosis shuttle their respective cargoes towards lysosomes for degradation and recycling of components. Defects in autophagy, efferocytosis, and CASM have been linked to pathological conditions such as stroke and neurodegeneration in the brain. However, beyond CASM, it is not known whether autophagy and efferocytosis interact with each other. Recent work connecting corpse clearance to amino acid metabolism and mammalian target of rapamycin complex 1 (mTORC1) signalling – two potent regulators of autophagy – hints at potential cross-talk between these pathways.

Given the strong links between autophagy and nutrition, I hypothesised that microglial efferocytosis interacts with autophagy to co-ordinate cargo clearance in a nutrient-sensitive manner. During efferocytosis, apoptotic material is engulfed within phagosomes: these eventually mature, become acidic, and fuse with lysosomes for cargo breakdown. At present, fluorescent dye-based techniques to measure efferocytosis cannot adequately discriminate between changes to the engulfment and acidification of material. In this thesis, I generated the novel tool 'epHero', harnessing variations in the pH-sensitivity of red and green fluorescent proteins to simultaneously track the uptake and acidification of apoptotic cells. The epHero probe could be used to measure efferocytosis via flow cytometry and imaging in both microglia- and macrophage-like cells. Further, epHero was able to detect changes to phagolysosomal acidification in a mouse model of efferocytosis. Thus, epHero is a specific, pH-responsive reporter of corpse clearance and offers significant improvements over conventional techniques.

Amino acid starvation is a well-established inducer of autophagy. Although metabolism of some apoptotic cell-derived amino acids has been implicated in corpse clearance, it is not known whether extracellular nutrient availability can modify efferocytosis. Here, the epHero reporter revealed that amino acid starvation increased acidification, but not uptake, of apoptotic material during microglial efferocytosis. Proteomic profiling of this phenomenon implicated proteins involved in arginine and fatty acid regulation, which have previously been linked to efferocytosis, as well as novel pathways such as branched chain amino acid metabolism, which will be explored in future work.

Next, CASM was pharmacologically inhibited during microglial efferocytosis to determine whether autophagic and corpse clearance pathways interacted with each other beyond CASM. Efferocytosis reduced the lysosomal delivery of autophagic cargo. This defect could be partly rescued by stimulating autophagy via amino acid starvation or mTORC1 inhibition. Pro-autophagy stimuli exerted different effects on microglial corpse clearance: amino acid starvation boosted apoptotic cargo acidification whereas pharmacological mTORC1 inhibition reduced it. This occurred even though mTORC1 inhibition elevated lysosomal activity to a higher degree compared to starvation. These results indicate a role for mTORC1 in the efficient acidification of apoptotic material during efferocytosis. Residual levels of mTORC1 activity were observed in microglia during starvation, a stimulus that normally suppresses mTORC1. Efferocytosis further increased mTORC1 function in amino acid-starved microglia. In contrast, pharmacological inhibition completely blocked mTORC1 activity. Increasing the intracellular pool of amino acids via cycloheximide treatment reverted mTORC1 function to basal levels in starved microglia, consequently abolishing the increased corpse acidification response. Taken together, these data suggest that low levels of mTORC1 activity are, counter-intuitively, required for the efficient clearance of apoptotic cargo. When mTORC1 is either fully functional or completely suppressed microglial efferocytosis is compromised.

Collectively, findings from this thesis demonstrate cross-talk between corpse clearance and autophagic pathways in microglia, whereby efferocytosis reduces autophagy. Limiting amino acid availability promotes catabolism of both autophagic and efferocytic cargo via an mTORC1-dependent mechanism. Differences between corpse clearance in mTORC1-inhibited and amino acid-starved cells were detected using the newly generated epHero reporter, highlighting the importance of accurate measurement of efferocytosis dynamics.

TABLE OF CONTENTS

LIST OF FIGURES

Chapter 1: Introduction

Chapter 4: epHero – a tandem-fluorescent probe to track the fate of apoptotic cells during efferocytosis

Chapter 5: Amino acid starvation promotes the acidification of phagosomes during apoptotic corpse clearance

LIST OF ABBREVIATIONS

AMPK	Adenosine monophosphate-activated protein kinase
ANOVA	Analysis of variance
ATG	Autophagy related
BCAA	Branched chain amino acids
BSA	Bovine serum albumin
CASM	Conjugation of ATG8 to endolysosomal single membranes
CHX	Cycloheximide
CNS	Central nervous system
DMEM	Dulbecco's minimum essential medium
DNA	Deoxyribonucleic acid
EBSS	Earle's buffered salt solution
ECL	Enhanced chemiluminescence
ECM	Extracellular matrix
EMEM	Eagle's minimum essential medium
FACS	Fluorescence activated cell sorting
FCS	Foetal calf serum
FDR	False discovery rate
GCN2	General control nonderepressible 2
HBSS	Hank's buffered salt solution
HEK293T	Human embryonic kidney 293T
HMC3	Human microglial clone 3
hr	Hour/s
HRP	Horseradish peroxidase
LAMP1	Lysosomal-associated membrane protein 1
LC3	Microtubule-associated protein 1 light chain 3

LRRK2	Leucine-rich repeat serine/threonine protein kinase 2
MFI	Median fluorescence intensity
min	Minutes
mTORC1	Mammalian target of rapamycin complex 1
NOX2	Nicotinamide adenine dinucleotide phosphate hydrogen oxidase
PBS	Phosphate buffered saline
PCA	Principal component analysis
PMA	Phorbol 12-myristate 13-acetate
PS	Phosphatidylserine
PVDF	Polyvinylidene fluoride
RLE	Relative log expression
RNA	Ribonucleic acid
RPMI	Roswell Park Memorial Institute
SAM	S-Adenosyl methionine
SDS-PAGE	Sodium dodecyl-sulphate polyacrylamide gel electrophoresis
SILAC	Stable isotope labelling with amino acids in cell culture
SNX17	Sorting nexin 17
SQSTM1	Sequestosome 1
STAT3	Signal transducer and activator of transcription 3
TFEB	Transcription factor EB
THP1	Tohoku Hospital Paediatrics 1
TUNEL	Terminal deoxynucleotidyl transferase dUTP nick end labelling
ULK1/2	Unc-51-like autophagy-activating kinases 1/2
v-ATPase	Vacuolar-type adenosine 5'-triphosphatase

CHAPTER 1

Introduction

1.1 A PRIMER ON EFFEROCYTOSIS

Cell death is an intrinsic part of life. Every day, nearly 330 billion cells become apoptotic and die in the human body (Sender and Milo, 2021). This number becomes even higher during development, injury, and disease. While a portion of these cells are turned over via simple shedding in the skin and digestive tract, the remainder must be removed via phagocytosis by specialised professional and non-professional phagocytes via a process termed efferocytosis. Failure to dispose of apoptotic cells in a timely manner results in secondary necrosis and the leakage of intracellular contents, resulting in inflammation and damage to surrounding healthy tissue (Cai *et al.*, 2016, Fadok *et al.*, 1998, Kumaran Satyanarayanan *et al.*, 2019). Defects in efferocytosis have been linked to atherosclerosis (Yurdagul *et al.*, 2017), autoimmune conditions (Geng *et al.*, 2022, Jorge *et al.*, 2022), and neurodegeneration (Berglund *et al.*, 2020, Heckmann *et al.*, 2019).

Efferocytosis shares several features with phagocytosis, which involves the engulfment and clearance of pathogens and other foreign cargo. Both processes are performed by the same subset of specialised cells – professional phagocytes like microglia and macrophages, as well as non-professional phagocytes such as fibroblasts, dendritic, and epithelial cells (Boada-Romero *et al.*, 2020). Further, much of the machinery involving cytoskeletal rearrangements and formation of the phagocytic cup, ingestion of extracellular material, and lysosomal turnover of cargo are similar between the two processes. However, efferocytosis utilises a distinct group

of receptors and bridging molecules to bind to and internalise apoptotic corpses (Doran, Yurdagul and Tabas, 2020). Importantly, whereas phagocytosis of pathogens triggers an inflammatory response, efferocytosis is largely considered immunologically silent and dampens the production of pro-inflammatory cytokines, while stimulating the production of pro-resolution mediators such as transforming growth factor β (Lin *et al.*, 2020). However, in certain scenarios, such as during the clearance of pathogen-infected cells (Salina *et al.*, 2022), efferocytosis can also elicit a pro-inflammatory response.

1.2 MOLECULAR MECHANISMS OF CORPSE CLEARANCE

The process of corpse clearance begins with the dead cells themselves – apoptotic cells release 'find-me' signals, including chemokines (Truman *et al.*, 2008), nucleotides such as ATP and UDP (Elliott *et al.*, 2009), and lipids (Mueller *et al.*, 2007). This creates a chemotactic gradient, triggering the movement of phagocytes towards the site of injury. The plasma membrane of apoptotic cells serves as a signalling platform that determines whether phagocytosis will take place. Apoptotic cells contain several 'eat-me' signals on their membranes. Further, expression of 'don't-eat-me' cues such as CD47 is reduced in cells undergoing apoptosis. Phagocytes engage with apoptotic cells – either via direct receptor binding or with the help of bridging molecules – and a balance between 'eat-me' and 'don't-eat-me' cues governs whether efferocytosis will proceed (Boada-Romero *et al.*, 2020). Exposure of the lipid phosphatidylserine on the outer plasma membrane of apoptotic cells is a key feature of cell death, with several phagocytic receptors able to recognise it (Mueller *et al.*, 2007). Recognition of an apoptotic cell activates the Rac1 GTPase in phagocytes

(Figure 1.1), triggering actin polymerisation and the remodelling of the cytoskeleton to engulf apoptotic cargo (Miki, Suetsugu and Takenawa, 1998, Erwig *et al.*, 2006).

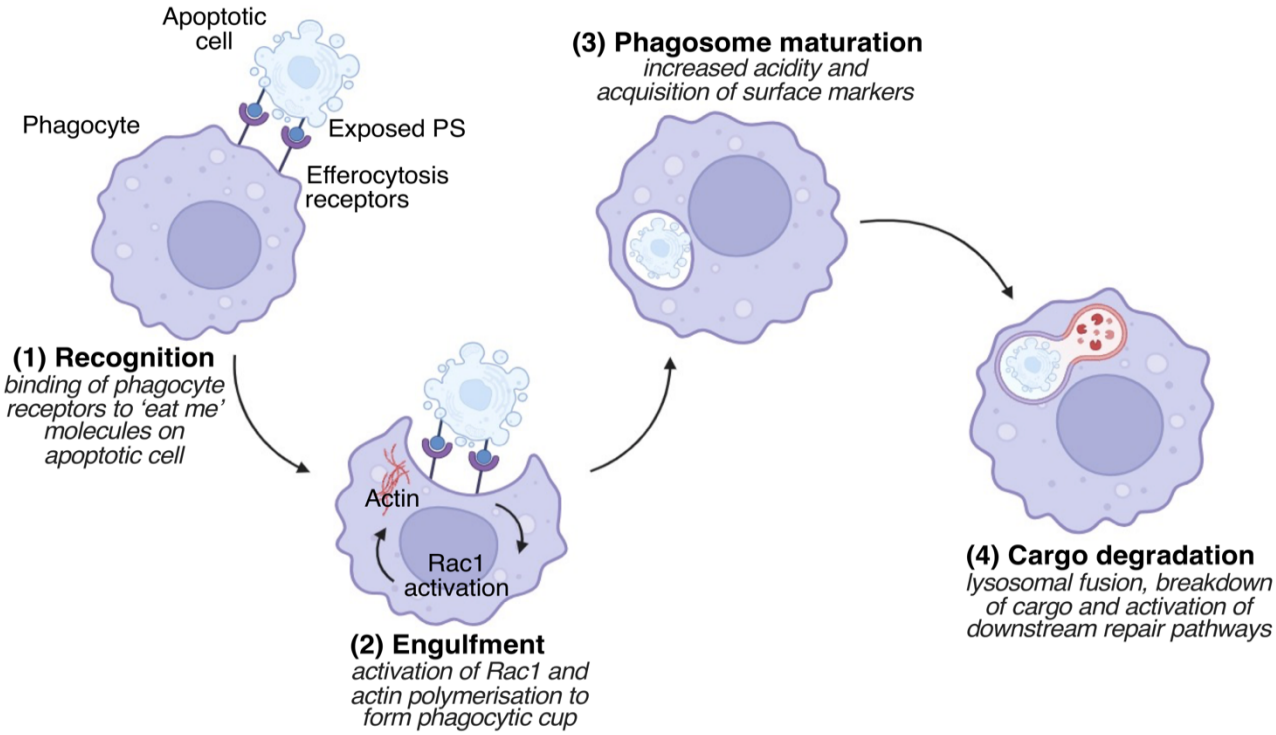

Figure 1.1 An overview of apoptotic corpse clearance.

Schematic depicting the **(1)** binding of phagocyte efferocytosis receptors to 'eat me' signals on the apoptotic cell such as exposed phosphatidylserine (PS), which **(2)** triggers Rac1 activation and actin mobilisation to form the phagocytic cup and engulf the apoptotic cell within a **(3)** phagosome. Phagosomes eventually mature, acidify and **(4)** fuse with lysosomes, resulting in the degradation of their apoptotic cargo. Figure created in BioRender.

Once an apoptotic cell is internalised into a phagosome, the phagosome undergoes a series of maturation steps facilitated by GTPases Rab5 and Rab7 (Kinchen *et al.*, 2008), enabling it to fuse with a lysosome for degradation of its contents. Apoptotic

cell-containing phagosomes may also be directed towards recycling endosomes for removal via exocytosis (Yin *et al.*, 2016). As they mature, phagosomes containing apoptotic material acquire a number of proteins on their surface, including the lysosomal marker LAMP1, autophagy-related protein LC3, and the vacuolar ATPase proton pump (Hooper *et al.*, 2022, Martinez *et al.*, 2011). These facilitate the production of reactive oxygen species to promote acidification of the phagosome lumen and subsequent breakdown of its contents (Martinez *et al.*, 2015, Hooper *et al.*, 2022). The digestion of apoptotic cells by phagocytes provides them with metabolites to sustain subsequent rounds of efferocytosis, and activates wound-healing and anti-inflammatory signalling pathways (Yurdagul *et al.*, 2020, Merlin *et al.*, 2021, Ampomah *et al.*, 2022). Conversely, incomplete digestion of apoptotic cargo can lead to pathogenic inflammation (Kawane *et al.*, 2006).

1.3 METHODS FOR MONITORING EFFEROCYTOSIS

1.3.1 *In vitro* measurement of efferocytosis

At present, techniques for measuring efferocytosis employ flow cytometry or microscopy to analyse the engulfment of labelled targets by phagocytes. These targets may be apoptotic cells (Miksa *et al.*, 2009, Aziz, Yang and Wang, 2013, Stöhr *et al.*, 2018) or synthetic cargo such as inert latex beads (Yin *et al.*, 2016, Evans *et al.*, 2017, Erwig *et al.*, 2006). While synthetic targets can be ingested by phagocytes, they cannot be degraded – thus, this technique can only be used to measure the engulfment of material or to study signalling pathways activated by ligand-receptor interactions. Recent work has shown that phagocytes derive amino and fatty acids from the breakdown of their incoming cargo, which fuels successive rounds of

efferocytosis (Zhang *et al.*, 2019, Yurdagul *et al.*, 2020, Ampomah *et al.*, 2022). As this process cannot be recapitulated in phagocytes engulfing beads, true phagocytic uptake may be underestimated using this method.

Apoptotic cells provide a more physiologically relevant target for phagocytes: they are generally labelled using fluorescent dyes and incubated with phagocytes, with fluorescent signal development within phagocytes used to quantify efferocytosis. However, this does not allow for separation between apoptotic cargo merely bound to the surface of phagocytes from that which has been engulfed. This issue can be partly mitigated by labelling apoptotic cells with pH-sensitive dyes such as pHrodo (Miksa *et al.*, 2009, Aziz, Yang and Wang, 2013, Stöhr *et al.*, 2018) and CypHer5E (Kumaran Satyanarayanan *et al.*, 2019, Schappe *et al.*, 2022). These dyes have low levels of fluorescence at neutral pH, but they fluoresce brightly upon entering an acidic environment such as within a phagosome. This difference in signal intensity ensures that only internalised targets are included in analyses. However, this presents a new problem – an increase in pHrodo signal within phagocytes could represent either greater uptake or acidification. Conversely, a reduction of the pHrodo signal may indicate complete cargo digestion or defects in acidification. These differences can only be elucidated by supplementing this technique with temporal and imaging data, which can be time-consuming and laborious.

1.3.2 Measuring efferocytosis in organisms

While *in vitro* models can be useful, it is important to study efferocytosis *in vivo*, where phagocytes in a three-dimensional network are surrounded by different cell types and

must detect, travel towards, and engulf apoptotic material. Recently, a pH-sensitive tool 'CharON' was developed, employing a system whereby apoptotic cells express engineered red and green fluorescent proteins – which vary in terms of their signal intensity under different pH environments – to simultaneously measure corpse uptake and acidification during embryogenesis in *Drosophila* (Raymond *et al.*, 2022). However, this reporter is activated in response to caspase 3-induced cell death, which, while innovative, cannot measure efferocytosis during caspase 3-independent programmed cell death (Turner *et al.*, 2003, van Delft *et al.*, 2010).

In mice, the most widely used technique to monitor corpse clearance *in vivo* involves the injection of labelled targets into the peritoneal cavity (Wang *et al.*, 2023, Schappe *et al.*, 2022). The peritoneal cavity contains a significant proportion of macrophages, and this number can be increased further under elicited conditions such as thioglycollate injection (Schneider, 2013). After a few hours, macrophages can be isolated from the peritoneal cavity and, similar to *in vitro* techniques, the target-derived signal within macrophages measured to estimate efferocytosis. This approach has also been adapted to study efferocytosis within other phagocyte populations. For instance, apoptotic targets can be inoculated into mice intranasally or intratracheally to study efferocytosis by alveolar macrophages (Subramaniam *et al.*, 2016, Hodge *et al.*, 2019). It is worth noting that these techniques measure the clearance of 'non-self' targets: how an organism phagocytoses externally sourced material may vary from how it removes its own dead cells. This limitation can be overcome by injecting mice with dexamethasone – which induces robust apoptosis in the thymus – and measuring macrophage uptake of apoptotic thymocytes (Yurdagul *et al.*, 2020, Wang *et al.*,

2023). However, unless employed in fluorescent transgenic mouse lines, this requires staining for dead cells within thymus macrophages, which does not provide a dynamic readout of uptake and degradation.

Recently, a technique termed '2Phatal', which combines the targeted induction of cell death using a two-photon laser with time-lapse imaging, has been used to study corpse clearance in the brains of live mice (Hill *et al.*, 2017, Damisah *et al.*, 2020). This is discussed further in '*1.4.3 Measuring corpse removal in the brain – the how'*.

1.4 CORPSE CLEARANCE IN THE BRAIN

1.4.1 Efferocytosis in the brain – the when?

The mammalian brain controls all functions essential for sustaining life. Consequently, the brain parenchyma has evolved to become a tightly regulated environment, as even small disruptions to homeostasis can have catastrophic implications. The efficient removal of apoptotic cells and debris in the brain is, therefore, crucial. Efferocytosis plays an important role in maintaining brain homeostasis during development – where large numbers of neurons, axons, and synapses are removed to facilitate the development of neural circuits – as well as injury, ageing, and disease (Gabandé-Rodríguez, Keane and Capasso, 2020).

Under physiological conditions, it is extremely challenging to detect efferocytosis in the brain. This is because the rate of cell death is remarkably limited in the mature central nervous system (CNS). Neurons are post-mitotic cells with limited regenerative potential, making it crucial for the neuronal pool to survive throughout an organism's

lifespan despite probable exposure to various stressors during that time (Kole, Annis and Deshmukh, 2013). The threshold for apoptosis is markedly increased in mature neurons, with these cells having several apoptotic 'brakes' conferring resistance to pro-apoptotic factors and downstream caspase effectors (Hollville, Romero and Deshmukh, 2019). Thus, unlike peripheral tissue where billions of cells undergo programmed cell death on a daily basis (Sender and Milo, 2021), cellular turnover is low in healthy brain. Further, the limited number of neurons that *do* die are rapidly cleared by microglia – within less than two days (Damisah *et al.*, 2020). The low rate of neuronal cell death coupled with a highly efficient clearance process makes detecting CNS efferocytosis a difficult proposition. While new technologies such as 2Phatal – discussed further in '*1.4.3 Measuring corpse removal in the brain: the how?*' – provide an exciting avenue for measuring basal corpse clearance in the brain (Hill *et al.*, 2017, Damisah *et al.*, 2020), they are time-, cost- and labour-intensive. Given this, the neurodevelopmental period offers the best opportunity to study efferocytosis in a brain free from pathological, genetic or pharmacological perturbations. The developing brain contains an excess of neurons, axonal projections, and synapses, which are systematically eliminated by microglia, leaving behind a refined network (Schafer and Stevens, 2013), most of which is maintained throughout the remainder of an organism's life. This results in a unique scenario whereby there is a high efferocytic burden in an otherwise healthy brain. Several groups have utilised this neurodevelopmental period to study neuronal corpse clearance in model organisms including mice (Paolicelli *et al.*, 2011), zebrafish (Möller *et al.*, 2022, Villani *et al.*, 2019), and *Drosophila* (Etchegaray *et al.*, 2016, Raymond *et al.*, 2022).

Efferocytosis is also important during pathological disturbances in the brain, particularly when there is excess cell death, where clean-up becomes crucial for preventing necrosis and subsequent inflammatory damage. During stroke, enhancing efferocytosis reduces inflammation and improves neurological outcomes (Nakahashi-Oda *et al.*, 2021, Campana *et al.*, 2018). In Alzheimer's disease, neurons containing toxic protein aggregates express the efferocytosis signal phosphatidylserine and are engulfed by phagocytes (Brelstaff *et al.*, 2018), contributing to cellular senescence and the spread of disease (Brelstaff *et al.*, 2021). Parkinson's disease-related mutations in leucine rich repeat kinase 2 (LRRK2) result in abnormally increased phagocytosis of dopaminergic neurons (Kim *et al.*, 2018), possibly contributing to excessive neuronal loss and subsequent neurodegeneration.

1.4.2 Key players mediating corpse clearance in the brain – the who?

Microglia are the professional phagocytes of the brain. While the precise origins of microglia and other tissue macrophages remains contested, the general consensus is that microglia are a unique subset of phagocytes that descend almost entirely from yolk sac progenitors, unlike other tissue-resident macrophages that are derived predominantly from haematopoietic stem cells (Alliot, Godin and Pessac, 1999, Ginhoux and Prinz, 2015). In addition to microglia, astrocytes and infiltrating monocytes also perform phagocytic functions in the brain. However, the extent of apoptotic cargo clearance by these cells is limited – either it occurs less efficiently compared to microglia (Damisah *et al.*, 2020, Morizawa *et al.*, 2017) or only under specific circumstances, for instance, during blood-brain barrier disruption in stroke (Morizawa *et al.*, 2017). For these reasons, our work will predominantly focus on

microglial efferocytosis, albeit with an important caveat: microglial markers used in several *in vivo* studies cannot distinguish between microglia and infiltrating monocytes that differentiate into 'microglia-like' cells. Therefore, when discussing previous reports on corpse clearance in the brain, what we refer to as microglial efferocytosis may well have some contribution from infiltrating phagocyte populations.

While some groups have studied efferocytosis in microglia both *in vitro* and in the brain, a majority of the research into corpse clearance has been performed in macrophages, with results extrapolated for microglia. Compared to other macrophages, microglia have different ontogeny, transcriptional profiles, and operate in the unique environment of the brain (Márquez-Ropero *et al.*, 2020). Given the importance of maintaining efficient efferocytosis in the brain and the paucity of data on microglial corpse clearance, there is an unmet need to study microglial efferocytosis under both physiological and pathological settings.

1.4.3 Measuring corpse removal in the brain – the how?

Efferocytosis in the CNS has been studied in a range of model organisms, including mice, primates, zebrafish, and *Drosophila.* One strategy used is simply counting the number of dead cells in the brain, thereby measuring efferocytosis by proxy (Etchegaray *et al.*, 2016, Beccari *et al.*, 2023), since increased levels of cell death may indicate inefficient clearance. However, this approach could yield inconclusive results, as a given stimulus may increase neuronal cell death without reducing phagocytosis. Staining for apoptotic cells within microglia – identified via abnormal nuclear morphology, TUNEL staining or the expression of cell death markers – can provide

information on the engagement of microglia with apoptotic material (Ayoub *et al.*, 2023, Kurant *et al.*, 2008), although it is difficult to determine whether a corpse is truly present inside microglia from fixed tissue imaging alone. While immunostaining-based techniques alone cannot fully capture the dynamics of phagosome maturation and degradation, they have been used in conjunction with *ex vivo* models such as primary microglia (Cai *et al.*, 2019, Beccari *et al.*, 2023) or organotypic brain slice cultures (Beccari *et al.*, 2023) to uncover novel regulators of efferocytosis.

Alternatively, live imaging can be performed to track efferocytosis. This involves measuring the disappearance of apoptotic cargo-derived signal within microglia. During development, there is a significant amount of cell death in the CNS, providing an avenue to study corpse removal in a physiological context. In zebrafish embryos, which are transparent and well-suited for imaging, transgenic approaches – where microglia and apoptotic neurons express different fluorophores – have been used to track the removal of dying neurons by microglia-like cells (Möller *et al.*, 2022, Villani *et al.*, 2019). Similarly, in the developing CNS of *Drosophila*, where there is a wave of apoptosis and subsequent removal of neurons by glia, fluorescent reporters for glia and neurons can be used to estimate corpse clearance (Shklyar, Shklover and Kurant, 2013). When using live imaging approaches, fluorophore selection should be carefully considered to ensure that signal loss results from cargo degradation and not merely the quenching of acid-sensitive fluorescent green (Morsch *et al.*, 2015) and yellow proteins (van Ham *et al.*, 2010) within phagosomes. Alternatively, the acid-sensitive nature of some fluorophores can be harnessed to provide additional information on cargo acidification. For instance, the CharON reporter employs a novel approach

whereby two fluorescent proteins with different pH properties are used to simultaneously measure engulfment and acidification of apoptotic cells during *Drosophila* development (Raymond *et al.*, 2022).

In the last few years, a powerful tool termed 2Phatal has been developed, which enables the tracking of a single apoptotic neuron as it is degraded by surrounding microglia, providing a high spatiotemporal view of efferocytosis in the mouse or zebrafish brain (Hill *et al.*, 2017). In mice, this involves creating cranial windows to provide optical access and facilitate imaging. Animals are administered with a nucleic acid binding dye, following which individual cells are targeted using a two-photon laser to induce photobleaching and cell death. When used in animals that express cell type-specific fluorescent reporters, the clearance of a single dying cell in the living brain can be tracked, providing a useful view of efferocytosis dynamics (Damisah *et al.*, 2020, Hill *et al.*, 2017). To date, this has only been used to target relatively small numbers (<100) of cells per animal and has not been used to recapitulate settings where there is a high corpse burden for phagocytes, such as during disease. This process is also expensive, time- and labour-intensive, requiring specialised skills and equipment. Consequently, in the six years since its publication, 2Phatal has only been employed by two research groups (Damisah *et al.*, 2020, Chapman *et al.*, 2023, Hill *et al.*, 2017). Future work using this technique to disseminate cell clearance under pathological settings may yield novel disease-relevant insights.

1.5 AN OVERVIEW OF AUTOPHAGY

Autophagy is an evolutionarily conserved catabolic process whereby intracellular material – including protein aggregates, organelles and pathogens – is packaged into double membraned organelles and shuttled towards lysosomes for degradation. These double membraned structures, termed autophagosomes, are thought to be initially derived from endoplasmic reticulum components, and are a defining feature of the autophagic pathway. Their formation is regulated by a key set of autophagy-related (ATG) proteins. Autophagy is a cell's fundamental response to stress, allowing it to maintain homeostasis. For instance, during nutrient deprivation, autophagy delivers dispensable intracellular cargo to the lysosome where it can be broken down and its components recycled to maintain essential cellular processes (He, 2022, Onodera and Ohsumi, 2005). The vital contribution of autophagy to an organism's well-being is highlighted by the fact that mice lacking key ATG proteins die soon after birth (Sou *et al.*, 2008, Komatsu *et al.*, 2005, Kuma *et al.*, 2004). In the brain, autophagy is highly efficient and is critical for optimal function during both development and disease, discussed further in '*1.9.3 Microglial autophagy and efferocytosis are perturbed during neurodegenerative disease'*.

1.6 THE AUTOPHAGY MACHINERY

The formation of autophagosomes is an essential step in the autophagic pathway. This involves the sequential processing of the ATG8 family of proteins, culminating in their conjugation to the lipid phosphatidylethanolamine on both the inner and outer leaflets of the autophagosomal membrane. This ATG8 lipidation on the autophagosome membrane facilitates its expansion and subsequent fusion with

lysosomes. While several ATG8 proteins have been identified, microtubule-associated protein 1 light chain 3 (LC3) is the best characterised member of this family and will be our primary focus for the remainder of this thesis.

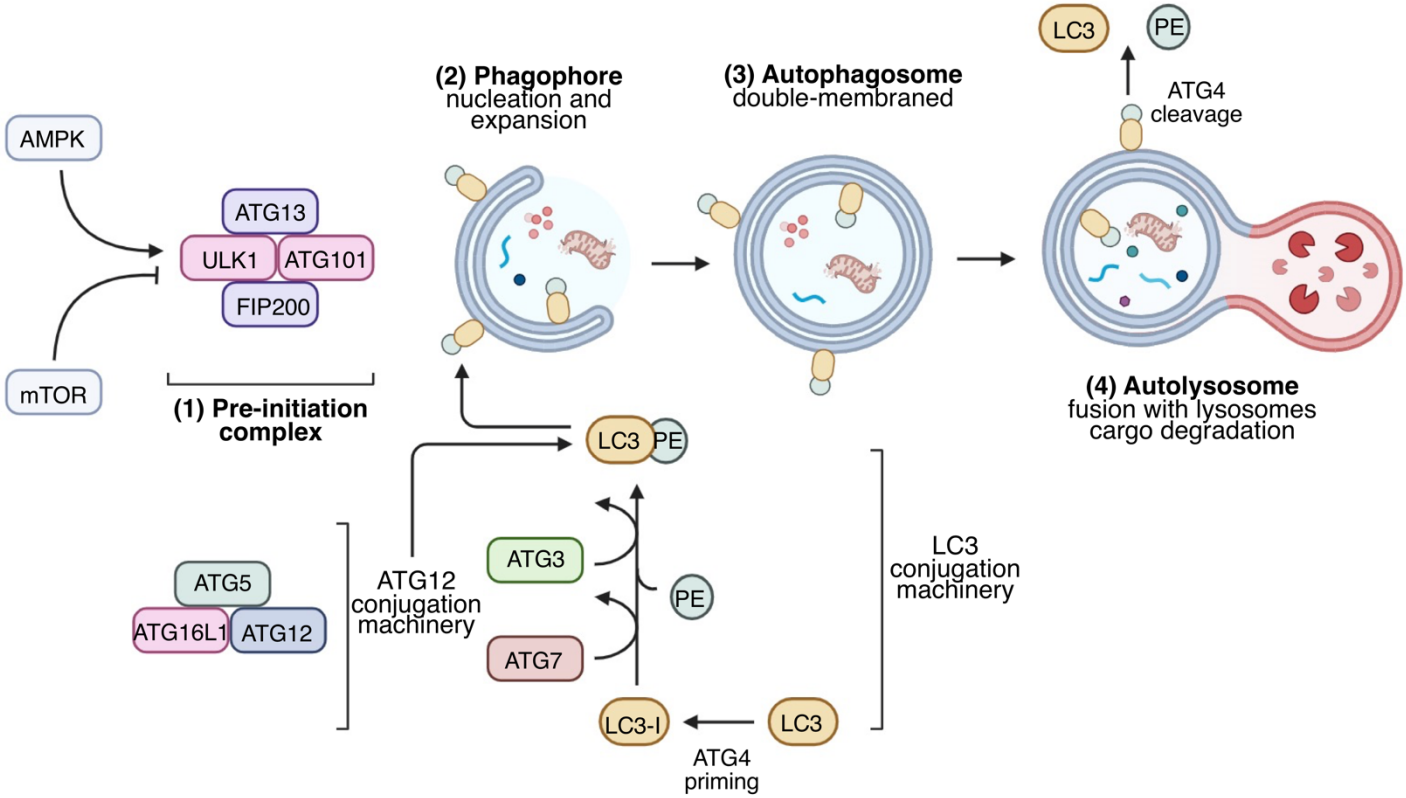

Figure 1.2 An overview of autophagy.

Schematic showing the main steps involved in autophagy including **(1)** initiation, **(2,3)** formation of double-membraned autophagosomes with LC3 lipidated to phosphatidylethanolamine (PE) on both inner and outer leaflets, and **(4)** fusion of autophagosomes with lysosomes for breakdown of autophagic cargo. Figure created using BioRender.

The initiation of autophagy involves the unc-51-like autophagy activating kinase 1/2 complex (ULK1/2) – comprising FIP200, WIPI2, ATG13 and ULK1/2 – which is recruited to the site of autophagosome assembly (Figure 1.2). Cytosolic LC3 is first

'primed' for lipidation via ATG4-mediated cleavage, exposing its C-terminus glycine residue (Tanida *et al.*, 2004). Then, in a series of sequential enzymatic reactions, ATG7 (Mizushima *et al.*, 1998) and ATG10 (Shintani *et al.*, 1999) facilitate the formation of the ligase complex ATG5–ATG12–ATG16L1, which ultimately conjugates LC3 to phosphatidylethanolamine to generate lipidated LC3 (LC3-II) on the autophagosomal membrane (Kuma *et al.*, 2002, Hanada *et al.*, 2007). Autophagy occurs in response to a wide range of stimuli, including nutrient availability, growth factor signalling, infection, and oxidative stress (Peker and Gozuacik, 2020). Notably, the induction of autophagy is largely governed by two intracellular energy sensing pathways: AMP-activated protein kinase (AMPK) and the mammalian target of rapamycin complex (mTORC1), which phosphorylate ULK1 at different sites to either promote or inhibit autophagy, respectively (Hosokawa *et al.*, 2009, Kim *et al.*, 2011).

1.7 FLUX AS A MEASUREMENT OF AUTOPHAGY

Given that autophagosome formation is a key step in the autophagic pathway, and lipidated LC3 is a core component of autophagosomes, assaying levels of LC3-II in cells or tissues can provide an estimate of autophagy. However, autophagy is a dynamic process – at any given time, material, including LC3-II, is both entering this system and being broken down in lysosomes. Therefore, simply measuring the total amount of lipidated LC3 does not provide enough information on the transit of cargo through the autophagic system: an increase in LC3 lipidation may indicate either increased induction of autophagy or compromised lysosomal degradation. For these reasons, measuring LC3-II 'flux' is, at present, the best way to study autophagy (Klionsky *et al.*, 2021). This technique involves the pharmacological inhibition of

lysosomal function, thus preventing the degradation of autophagic cargo. The resulting build-up of LC3-II (or other autophagic substrates) can be interpreted as autophagic turnover, *i.e.,* the amount of material that would have been degraded via autophagy if lysosome function had not been blocked. When used in conjunction with pro-autophagy stimuli, LC3 flux measurements can provide valuable information on the induction and degradation of autophagic cargo. This technique has been successfully used to measure flux in cultured cells, model organisms (Bensalem *et al.*, 2021a, Fourrier *et al.*, 2021), and human blood (Bensalem *et al.*, 2021b).

1.8 LC3-ASSOCIATED EFFEROCYTOSIS – WHERE AUTOPHAGY MEETS APOPTOTIC CORPSE CLEARANCE

We now know that several autophagy proteins perform functions beyond canonical autophagy. Notably, the key autophagy marker LC3-II, which usually decorates both the inner and outer leaflets of double-membraned autophagosomes, can also be recruited onto single-membraned vesicles via a process termed conjugation of LC3/ATG8 proteins to single membranes (CASM), sometimes referred to as non-canonical autophagy. This occurs in response to a wide range of stimuli, including efferocytosis (Martinez *et al.*, 2011), phagocytosis of pathogens (Sanjuan *et al.*, 2007), osmotic imbalances (Florey *et al.*, 2015), and lysosomal damage (Cross *et al.*, 2023). For the remainder of this review, we will primarily focus on CASM in the context of efferocytosis.

1.8.1 Untying the knot – separating autophagy from CASM

CASM and autophagy are two closely related, but distinct, degradative mechanisms

which share several molecular components. Complicating matters further, the primary readout for both processes is LC3 lipidation, which makes it challenging to attribute findings to one or the other. Fortunately, we now have several tools at our disposal, enabling the separation of autophagy from CASM. Given that CASM involves the tethering of lipidated LC3-II onto single-membraned vesicles, the core ubiquitin-like conjugation systems are required for both autophagy and CASM. The pre-initiation autophagy machinery – comprising FIP200, WIPI2, ATG13 and ULK1/2 – is crucial for canonical autophagy induction but dispensable during CASM (Martinez *et al.*, 2015). Disruption of ATG5 or ATG7 – involved in the lipidation of LC3, enabling its recruitment to autophagosomal or phagosomal membranes – leads to the ablation of both canonical autophagy and CASM (Martinez *et al.*, 2011, Martinez *et al.*, 2015). The autophagy protein ATG16L1, part of the ATG5-containing LC3 conjugation complex, appears to be the molecular switch co-ordinating LC3 recruitment to autophagic or phagocytic compartments. During canonical autophagy, ATG16L1 is recruited to the nascent autophagosome via its central FIP200-binding domain (Gammoh *et al.*, 2013). Conversely, this central region is dispensable for CASM. Instead, the ATG16L1 C-terminal WD40 domain is necessary for LC3-associated efferocytosis, but is not required during canonical autophagy (Fletcher *et al.*, 2018, Ulferts *et al.*, 2021). Another CASM-specific target is the protein Rubicon – a negative regulator of canonical autophagy (Matsunaga *et al.*, 2009) – which is required for CASM during phagocytosis, where it stabilises NOX2 to facilitate reactive oxygen species production and the subsequent degradation of cargo (Martinez *et al.*, 2015).

It is also possible to employ pharmacological reagents to specifically target autophagy and CASM. Since autophagy is a dynamic catabolic process, LC3-II flux is utilised as its gold-standard measure – where lysosomal turnover is pharmacologically blocked, enabling dissection of the rate of protein degradation via the autophagic pathway (Klionsky *et al.*, 2021). Chloroquine and monensin, drugs routinely used to assay autophagic flux also robustly stimulate CASM (Florey *et al.*, 2015, Hooper *et al.*, 2022). Therefore, one must employ caution when interpreting results obtained using these methods, particularly in phagocytosis-capable cells. Inhibitors of the vacuolar ATPase (v-ATPase) – a proton transport pump that enables lysosome acidification – such as bafilomycin and concanamycin, stifle both canonical and non-canonical autophagy (Florey *et al.*, 2015, Hooper *et al.*, 2022). Due to their simultaneous effects on both autophagy inhibition and CASM induction, chloroquine and monensin increase LC3 lipidation to a larger extent compared to bafilomycin. This difference between chloroquine/monensin- and bafilomycin-mediated LC3 flux can therefore be utilised to dissect the relative contribution of CASM and autophagy towards LC3 signal. Recently, the compound saliphenylhalamide, which inhibits v-ATPase activity via a different mechanism (Xie *et al.*, 2004), was shown to stimulate rather than block CASM in autophagy-deficient cells (Hooper *et al.*, 2022), although it is unclear whether it also has an impact on canonical autophagy.

Thus, despite their shared components, pharmacological inhibition or the selective targeting of proteins specific to autophagy or CASM (Figure 1.3) makes it possible to distinguish between these two related processes.

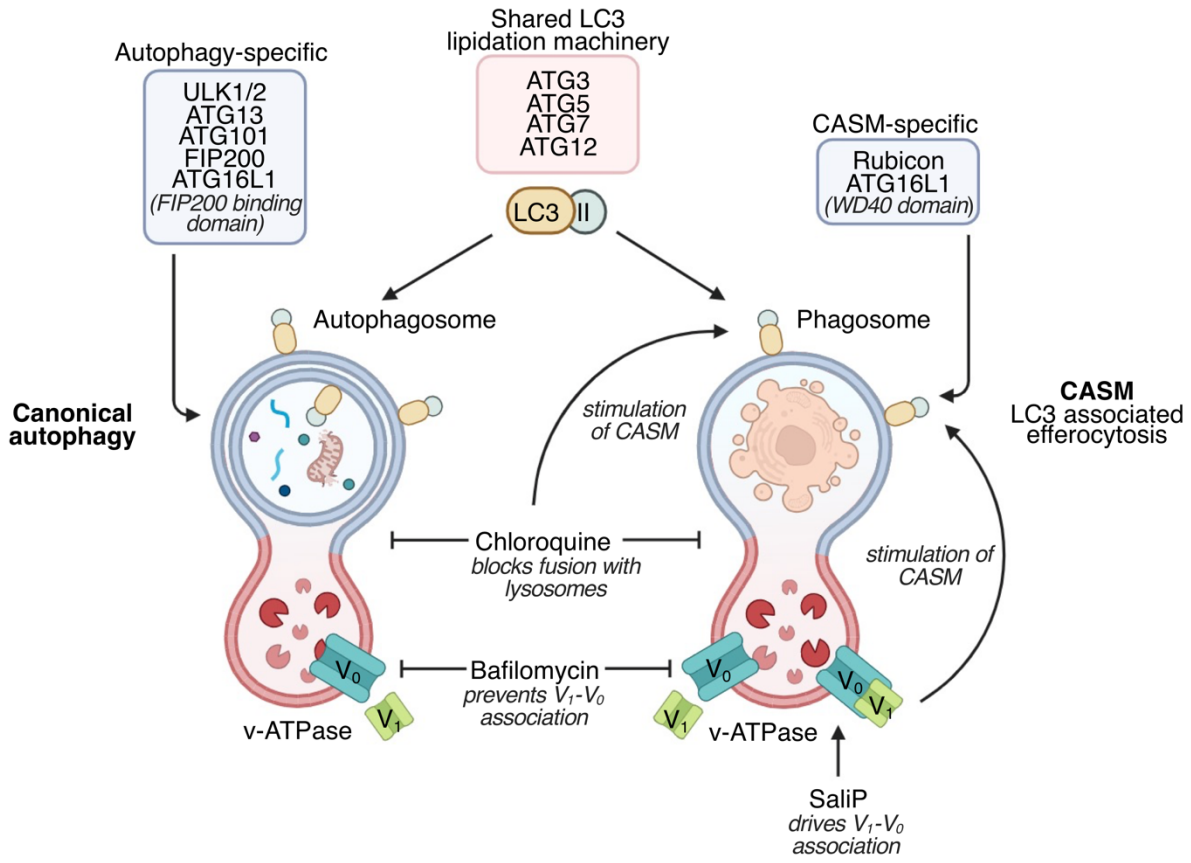

Figure 1.3 Comparison between canonical autophagy and CASM.

Schematic depicting proteins shared between canonical autophagy and CASM pathways, and those unique to either one. Also shown are targets of three commonly used pharmacological reagents: chloroquine, bafilomycin, and saliphenylhalamide (SaliP). Figure generated using Biorender.

1.9 THINKING BEYOND CASM – POTENTIAL CROSS-TALK BETWEEN AUTOPHAGIC AND CORPSE CLEARANCE PATHWAYS

Based on previous reports, CASM is thought to be regulated independently of canonical autophagy. These conclusions have been drawn primarily from experiments showing that the nutrient-sensitive autophagy pre-initiation complex, necessary for autophagy induction, is dispensable during CASM (Martinez *et al.*, 2011, Martinez *et*

al., 2015). Extracellular material can be taken up and cleared by phagocytes even in the absence of CASM and canonical autophagy proteins, albeit less efficiently (Martinez *et al.*, 2015, Heckmann *et al.*, 2019), indicating that while CASM is beneficial for efficient cargo degradation, it is not critical. Therefore, it is important to examine links between autophagy and efferocytosis beyond CASM, as canonical autophagy may modulate, or be affected by, corpse clearance in a CASM-independent manner. In line with this, recent work has demonstrated that two powerful autophagy regulators – mTORC1 activity (Krajcovic *et al.*, 2013, Fazeli *et al.*, 2023) and amino acid metabolism (Merlin *et al.*, 2021, Yurdagul *et al.*, 2020, Ampomah *et al.*, 2022) – impact corpse clearance. In this section, we will highlight potential points of interaction between canonical autophagy and efferocytosis by outlining key signalling pathways shared between the two, and pathologies where both processes are perturbed.

Cargo is delivered to the lysosome during both autophagy and efferocytosis. Consequently, proper lysosome function is required for these two processes, with lysosomal defects being detrimental for both autophagy and corpse clearance. In this thesis, we discovered key changes to the delivery and acidification of lysosome-destined cargo when both autophagy and efferocytosis were stimulated. For these reasons, although there are several pathways, such as inflammasome (Biasizzo and Kopitar-Jerala, 2020, Lang *et al.*, 2022) and toll-like receptor activation (Tricker and Cheng, 2008, Delgado *et al.*, 2008), which are known to regulate both autophagy and corpse clearance, our work will focus on lysosome-specific signalling mechanisms.

1.9.1 Lysosome signalling hubs shared by autophagy and efferocytosis

The mTORC1 complex

The mTOR machinery comprises two protein complexes – mTORC1 and mTORC2. Together, these complexes serve as master regulators of cell growth and metabolism. Autophagy and amino acid-sensing pathways are predominantly mediated by mTORC1. Further, mTORC1 can be recruited to the lysosome and directly modify cellular catabolism. Given this, our work will focus on mTORC1. Under basal conditions, mTORC1 negatively influences lysosomal activity: it localises to the lysosomal membrane, where it phosphorylates the transcription factor EB (TFEB), preventing its nuclear transport (Settembre *et al.*, 2011, Settembre *et al.*, 2012). During periods of cellular stress, such as nutrient deprivation, mTORC1 dissociates from lysosomes. This enables TFEB to enter the nucleus, where it promotes the expression of autophagy and lysosome-related genes, including cathepsins, v-ATPase components, and degradative enzymes (Settembre *et al.*, 2011, Settembre *et al.*, 2012, Sardiello *et al.*, 2009). Lysosomal acidification, which is necessary for optimal enzyme activity and breakdown of cargo, is also controlled by mTORC1. The assembly of the v-ATPase complex on lysosomal membranes is required for acidification of the lysosomal lumen. Recent work has demonstrated that the presence of mTORC1 on the lysosomal membrane reduces the association between V_1 and V_0 subunits of v-ATPase (Ratto *et al.*, 2022), although the mechanism behind this is unclear. When mTORC1 is rendered inactive via amino acid starvation or pharmacological inhibition, V_1-V_0 assemble to form the v-ATPase proton pump, thereby reducing lysosome pH and increasing proteolytic capacity. In a similar vein, a different group showed that mTORC1 phosphorylates the lysosomal substrate

STK11IP to enable its association with the V_1 domain of v-ATPase, reducing lysosome acidification (Zi *et al.*, 2022). Thus, mTORC1 regulates lysosome pH and proteolytic capacity, which are required for the efficient breakdown of cargo during both autophagy and corpse clearance.

Canonical autophagy is negatively regulated by mTORC1 activity. Under nutrient-replete conditions, mTORC1 inhibits autophagy via phosphorylation of the ULK1 complex (Hosokawa *et al.*, 2009, Kim *et al.*, 2011). When autophagy is induced – during amino acid starvation for instance – mTORC1 is rendered inactive and dissociates from this complex, permitting autophagy to occur. Unlike canonical autophagy, CASM does not appear to be modulated by mTORC1 activity because the ULK1 complex is not required for corpse uptake (Martinez *et al.*, 2011, Martinez *et al.*, 2015). However, mTORC1 may exert CASM-independent effects on efferocytosis, particularly during its later stages. mTORC1 is reactivated during the terminal stages of both autophagy (Yu *et al.*, 2010) and efferocytosis (Krajcovic *et al.*, 2013) in amino acid-starved cells, via amino acids obtained from the breakdown of autophagic or apoptotic material, respectively. During efferocytosis and entosis – a related process involving the cannibalism of living cells (Overholtzer *et al.*, 2007) – mTORC1 enables the fission of large phagosomes into smaller vesicles, facilitating faster cargo degradation (Fazeli *et al.*, 2023, Krajcovic *et al.*, 2013). Interestingly, mTORC1 is also involved in a similar process during the terminal stages of autophagy. During prolonged starvation, autophagy-mediated recycling of cellular nutrients reactivates mTORC1, allowing enlarged autolysosomes to undergo fission, thereby restoring the pool of functional lysosomes in a cell (Yu *et al.*, 2010). Thus, the resolution of

phagosomes and autolysosomes represents an mTORC1-dependent mechanism that is shared by efferocytosis and autophagy.

Together, these data indicate a dual role for mTORC1 during the lysosomal flux of both autophagic and efferocytic material. On the one hand, mTORC1 negatively regulates autophagy, lysosome proteolysis, acidification, and biogenesis. Here, inhibiting mTORC1 should improve the degradation of autophagic and apoptotic cargo. Conversely, mTORC1 activity is required for the more efficient clearance of material, as it regulates the fission and resolution of both autophagosomes and lysosomes. Thus, mTORC1 can either prevent or facilitate the clearance of lysosomal cargo delivered via autophagy or corpse clearance pathways.

The STAT3 signalling pathway

The signal transducer and activation of transcription factor-3 (STAT3) is involved in inflammation and tumorigenesis. It is present within the cytoplasm and, upon phosphorylation, translocates to the nucleus to drive target gene expression. During lysosomal stress – triggered by either protein overload or protease deficiency – phosphorylated STAT3 localises to the nucleus and promotes expression of lysosomal enzymes independently of TFEB (Martínez-Fábregas *et al.*, 2018). Further, under conditions where lysosome or cytosolic pH is disrupted, such as bafilomycin treatment, amino acid starvation or cytosol acidification, STAT3 restores homeostasis by binding to v-ATPase and facilitating the acidification of lysosomes (Liu *et al.*, 2018). This function of STAT3 appears to be independent of its transcription factor activity, as the phosphorylation status of STAT3 does not affect its ability to localise to lysosomes.

STAT3 is a negative regulator of autophagy. Upon translocation to the nucleus, phosphorylated STAT3 prevents the transcription of pro-autophagy genes (Miao *et al.*, 2014, Qin *et al.*, 2015). Depletion of STAT3 promotes autophagic flux by increasing the activity of the autophagy-regulating AMPK (Bhattacharya *et al.*, 2022). Further, pharmacological inhibition of STAT3 induces autophagy both *in vitro* and in mice (Shen *et al.*, 2012). Both wild-type and phosphorylation-deficient mutants of STAT3 impair autophagic flux (Shen *et al.*, 2012), suggesting that STAT3, at least partly, regulates autophagy in a transcription-independent manner. The STAT3 signalling pathway also plays a role in efferocytosis. Phosphorylated STAT3 is elevated in macrophages that have ingested synthetic apoptotic targets (Soki *et al.*, 2014). Pharmacologically inactivating macrophage STAT3 by inhibiting its phosphorylation and nuclear localisation reduces the uptake of apoptotic cells (Soki *et al.*, 2014, Proto *et al.*, 2018) and subsequent production of anti-inflammatory cytokines (Campana *et al.*, 2018).

Thus, STAT3 regulates lysosome homeostasis, which may have downstream effects on cargo degradation during efferocytosis and autophagy, Further, STAT3 also influences corpse uptake and autophagy. Given that STAT3 is activated during efferocytosis, the STAT3 signalling pathway may represent an important signalling node that co-ordinates cross-talk between autophagy and corpse clearance.

1.9.2 Amino acid metabolism modulates both autophagy and corpse clearance

Cell growth and metabolism are tightly governed by nutrient availability. Amino acids, in particular, co-ordinate several intracellular signalling mechanisms. There are three

major amino acid sensing pathways: (i) AMPK and (ii) general control non-derepressible 2 (GCN2), which respond to amino acid deprivation; and (iii) mTORC1, which is activated by the presence of amino acids. Autophagy is potently regulated by intracellular amino acid availability. During amino acid starvation, mTORC1 is inhibited (Hosokawa *et al.*, 2009), whereas AMPK and GCN2 are activated (Kim *et al.*, 2011, Ye *et al.*, 2015, Maurin *et al.*, 2022), resulting in the induction of autophagy to catabolise non-essential materials and restore energy balance to the cell. In addition to autophagy, corpse clearance can also be modulated by amino acid-sensing pathways. In amino acid-starved cells performing efferocytosis, mTORC1 is reactivated and contributes to the efficient degradation of apoptotic material (Krajcovic *et al.*, 2013, Fazeli *et al.*, 2023), as discussed in '*1.9.1 The mTORC1 complex*'. During corpse clearance, macrophages up-regulate AMPK, and pharmacological inhibition of AMPK reduces the uptake of apoptotic cells by macrophages both *in vitro* and in mice (Jiang *et al.*, 2013). Further, stimulating AMPK activity increases phagocytosis, likely by promoting downstream actin assembly pathways needed for the engulfment of phagocytic cargo (Bae *et al.*, 2011). Recently, GCN2 has been implicated in the phagocytic clearance of damaged red blood cells: GCN2-deficient mice are unable to properly degrade red blood cells, possibly due to impaired lysosomal maturation and acidification (Toboz *et al.*, 2022).

In addition to the general amino acid-sensing pathway, specific amino acids have also been linked to autophagic or efferocytic degradation. For instance, the presence of certain individual amino acids – including methionine, arginine and glutamine – is sufficient to activate mTORC1 even in the absence of all other amino acids (Meng *et*

al., 2020), thereby reducing autophagic flux. Notably, these amino acids have also been implicated in macrophage efferocytosis. Phagocytes derive arginine from the digestion of apoptotic cells, subsequently activating actin-mobilising pathways to facilitate the engulfment of subsequent apoptotic corpses (Yurdagul *et al.*, 2020). Similarly, intracellular levels of methionine and its metabolite S-adenosyl methionine (SAM) – an autophagy inhibitor (Sutter *et al.*, 2013) – are increased in phagocytes that have engulfed corpses, and mediate inflammation resolution following efferocytosis (Ampomah *et al.*, 2022). Phagocytes metabolise glutamine to meet the high energy demands of cytoskeletal repositioning during efferocytosis (Merlin *et al.*, 2021), although it is unclear whether they obtain glutamine from apoptotic cells or the extracellular environment. Thus, amino acid-sensing pathways and, in some cases, amino acids themselves play a role in both autophagy and efferocytosis.

1.9.3 Microglial autophagy and efferocytosis are perturbed during neurodegenerative disease

Another clue hinting at possible links between autophagy and corpse clearance pathways comes from studying pathologies where both processes are compromised. Although efferocytic and autophagic disturbances have been linked to several disease processes such as atherosclerosis and autoimmunity, here we will focus on the brain, specifically during neurodegeneration. Lysosomal dysfunction, which leads to the accumulation of material delivered via both autophagic and phagocytic mechanisms, is a key feature of several neurodegenerative pathologies, including frontotemporal dementia, Alzheimer's disease, and Parkinson's disease (Udayar *et al.*, 2022). Genetic variants associated with Alzheimer's disease strongly implicate microglial

involvement in its progression, with several risk genes influencing autophagy, phagocytosis, and immune pathways (Romero-Molina *et al.*, 2022, Huang *et al.*, 2017). Further, transcriptional analysis of neurodegenerative disease-associated microglia has revealed differential expression of genes encoding lysosomal enzymes, phagocytosis, and lipid receptors (Deczkowska *et al.*, 2018).

It is widely accepted that autophagy is compromised during neurodegeneration. Microglia-specific disruption of the key autophagy proteins ATG5 or ATG7 aggravates disease pathology in mouse models of Alzheimer's and Parkinson's diseases (Tu *et al.*, 2021, Xu *et al.*, 2021, Choi *et al.*, 2023). Given the links between autophagy and phagocytosis, particularly during CASM, there is an emerging field of work investigating how these two pathways interact with each other in neurodegeneration. ATG5 and ATG7 – involved in LC3 lipidation – are indispensable for both canonical autophagy and CASM (Martinez *et al.*, 2015, Mizushima *et al.*, 1998, Kuma *et al.*, 2002), making it unclear whether toxic protein accumulation and neurological defects in mice lacking microglial ATG5/7 are mediated by a deficiency in one pathway or whether they involve both canonical autophagy and CASM. Recent work suggests that microglial CASM, rather than autophagy, may be driving neurodegeneration, at least in certain contexts. Transgenic Alzheimer's disease mice lacking microglial ATG7 have worse cognitive and pathological outcomes compared to mice lacking FIP200 (Heckmann *et al.*, 2019), which is required for canonical autophagy but not CASM. In a similar vein, microglial depletion of ATG7 but not ULK1 results in the accumulation of myelin debris within microglia and the development of multiple sclerosis-like symptoms in mice (Berglund *et al.*, 2020). Further, aged ATG16L1 mutant mice – able

to perform autophagy but not CASM – develop Alzheimer's-like pathology with high levels of neuronal death (Heckmann *et al.*, 2020). Since CASM promotes efficient efferocytosis, this increased cell death may indicate impaired clearance of neuronal debris. In line with this, recycling of several receptors involved in phagocytosis is compromised in ATG16L1 mutant mice (Heckmann *et al.*, 2020).

Taken together, these reports highlight that pathways involved in both the autophagic and phagocytic degradation of cargo are disturbed during neurodegenerative disease; it is possible that these two processes interact with each other to modify disease progression, even beyond CASM. In Alzheimer's disease mouse models, stimulating autophagy via mTORC1 inhibition has neuroprotective effects but only when administered during early disease stages (Carosi and Sargeant, 2019). Conversely, during *Drosophila* neurodegeneration, inhibiting autophagy by activating the fly orthologue of mTORC1 improves apoptotic corpse processing and reduces histological hallmarks of brain damage (Etchegaray *et al.*, 2016). Beyond the fact that these reports did not employ the same disease models, the mixed results may be explained, at least in part, by the different roles played by mTORC1 during autophagy and corpse clearance: mTORC1 suppresses autophagy (Hosokawa *et al.*, 2009, Kim *et al.*, 2011) but is involved in the resolution of phagosomes (Krajcovic *et al.*, 2013, Fazeli *et al.*, 2023). In a healthy brain, microglia must be able to safely remove both intracellular and phagocytic cargo. Inhibiting mTORC1 could, in theory, polarise microglia towards the clearance of autophagic rather than extracellular material, which, while initially beneficial, may ultimately have limited therapeutic potential. In Alzheimer's disease mice, microglia become senescent after phagocytosing neurons

that have accumulated pathological amounts of tau protein (Brelstaff *et al.*, 2018, Brelstaff *et al.*, 2021). As cellular senescence is known to impair autophagy (Suelves *et al.*, 2023), this provides a potential mechanism by which efferocytosis communicates with autophagy. In this context, stimulating CASM to clear extracellular neuronal debris may come at a cost to microglial autophagy.

1.10 REFERENCES

Alliot, F., Godin, I. and Pessac, B. (1999) 'Microglia derive from progenitors, originating from the yolk sac, and which proliferate in the brain', *Brain Res Dev Brain Res,* 117(2), pp. 145-152.

Ampomah, P.B., Cai, B., Sukka, S.R., Gerlach, B.D., Yurdagul, A., Jr., Wang, X., Kuriakose, G., Darville, L.N.F., Sun, Y., Sidoli, S., Koomen, J.M., Tall, A.R. and Tabas, I. (2022) 'Macrophages use apoptotic cell-derived methionine and DNMT3A during efferocytosis to promote tissue resolution', *Nat Metab,* 4(4), pp. 444-457.

Ayoub, M., David, L.M., Shklyar, B., Hakim-Mishnaevski, K. and Kurant, E. (2023) 'Drosophila FGFR/Htl signaling shapes embryonic glia to phagocytose apoptotic neurons', *Cell Death Discov,* 9(1), p. 90.

Aziz, M., Yang, W.L. and Wang, P. (2013) 'Measurement of phagocytic engulfment of apoptotic cells by macrophages using pHrodo succinimidyl ester', *Curr Protoc Immunol,* Chapter 14, p. Unit 14.31.

Bae, H.B., Zmijewski, J.W., Deshane, J.S., Tadie, J.M., Chaplin, D.D., Takashima, S. and Abraham, E. (2011) 'AMP-activated protein kinase enhances the phagocytic ability of macrophages and neutrophils', *Faseb j,* 25(12), pp. 4358-4368.

Beccari, S., Sierra-Torre, V., Valero, J., Pereira-Iglesias, M., García-Zaballa, M., Soria, F.N., De Las Heras-Garcia, L., Carretero-Guillen, A., Capetillo-Zarate, E., Domercq, M., Huguet, P.R., Ramonet, D., Osman, A., Han, W., Dominguez, C., Faust, T.E., Touzani, O., Pampliega, O., Boya, P., Schafer, D., Mariño, G., Canet-Soulas, E., Blomgren, K., Plaza-Zabala, A. and Sierra, A. (2023) 'Microglial phagocytosis dysfunction in stroke is driven by energy depletion and induction of autophagy', *Autophagy,* 19(7), pp. 1952-1981.

Bensalem, J., Fourrier, C., Hein, L.K., Hassiotis, S., Proud, C.G. and Sargeant, T.J. (2021a) 'Inhibiting mTOR activity using AZD2014 increases autophagy in the mouse cerebral cortex', *Neuropharmacology,* 190, p. 108541.

Bensalem, J., Hattersley, K.J., Hein, L.K., Teong, X.T., Carosi, J.M., Hassiotis, S., Grose, R.H., Fourrier, C., Heilbronn, L.K. and Sargeant, T.J. (2021b) 'Measurement of autophagic flux in humans: an optimized method for blood samples', *Autophagy,* 17(10), pp. 3238-3255.

Berglund, R., Guerreiro-Cacais, A.O., Adzemovic, M.Z., Zeitelhofer, M., Lund, H., Ewing, E., Ruhrmann, S., Nutma, E., Parsa, R., Thessen-Hedreul, M., Amor, S., Harris, R.A., Olsson, T. and Jagodic, M. (2020) 'Microglial autophagy-associated phagocytosis is essential for recovery from neuroinflammation', *Sci Immunol,* 5(52).

Bhattacharya, S., Yin, J., Yang, C., Wang, Y., Sims, M., Pfeffer, L.M. and Chaum, E. (2022) 'STAT3 suppresses the AMPKα/ULK1-dependent induction of autophagy in glioblastoma cells', *J Cell Mol Med,* 26(14), pp. 3873-3890.

Biasizzo, M. and Kopitar-Jerala, N. (2020) 'Interplay Between NLRP3 Inflammasome and Autophagy', *Front Immunol,* 11, p. 591803.

Boada-Romero, E., Martinez, J., Heckmann, B.L. and Green, D.R. (2020) 'The clearance of dead cells by efferocytosis', *Nat Rev Mol Cell Biol,* 21(7), pp. 398-414.

Brelstaff, J., Tolkovsky, A.M., Ghetti, B., Goedert, M. and Spillantini, M.G. (2018) 'Living Neurons with Tau Filaments Aberrantly Expose Phosphatidylserine and Are Phagocytosed by Microglia', *Cell Rep,* 24(8), pp. 1939-1948.e1934.

Brelstaff, J.H., Mason, M., Katsinelos, T., McEwan, W.A., Ghetti, B., Tolkovsky, A.M. and Spillantini, M.G. (2021) 'Microglia become hypofunctional and release metalloproteases and tau seeds when phagocytosing live neurons with P301S tau aggregates', *Sci Adv,* 7(43), p. eabg4980.

Cai, B., Thorp, E.B., Doran, A.C., Subramanian, M., Sansbury, B.E., Lin, C.S., Spite, M., Fredman, G. and Tabas, I. (2016) 'MerTK cleavage limits proresolving mediator biosynthesis and exacerbates tissue inflammation', *Proc Natl Acad Sci U S A,* 113(23), pp. 6526-6531.

Cai, W., Dai, X., Chen, J., Zhao, J., Xu, M., Zhang, L., Yang, B., Zhang, W., Rocha, M., Nakao, T., Kofler, J., Shi, Y., Stetler, R.A., Hu, X. and Chen, J. (2019) 'STAT6/Arg1 promotes microglia/macrophage efferocytosis and inflammation resolution in stroke mice', *JCI Insight,* 4(20).

Campana, L., Starkey Lewis, P.J., Pellicoro, A., Aucott, R.L., Man, J., O'Duibhir, E., Mok, S.E., Ferreira-Gonzalez, S., Livingstone, E., Greenhalgh, S.N., Hull, K.L., Kendall, T.J., Vernimmen, D., Henderson, N.C., Boulter, L., Gregory, C.D., Feng, Y.,

Anderton, S.M., Forbes, S.J. and Iredale, J.P. (2018) 'The STAT3-IL-10-IL-6 Pathway Is a Novel Regulator of Macrophage Efferocytosis and Phenotypic Conversion in Sterile Liver Injury', *J Immunol,* 200(3), pp. 1169-1187.

Carosi, J.M. and Sargeant, T.J. (2019) 'Rapamycin and Alzheimer disease: a double-edged sword?', *Autophagy,* 15(8), pp. 1460-1462.

Chapman, T.W., Olveda, G.E., Bame, X., Pereira, E. and Hill, R.A. (2023) 'Oligodendrocyte death initiates synchronous remyelination to restore cortical myelin patterns in mice', *Nat Neurosci,* 26(4), pp. 555-569.

Choi, I., Wang, M., Yoo, S., Xu, P., Seegobin, S.P., Li, X., Han, X., Wang, Q., Peng, J., Zhang, B. and Yue, Z. (2023) 'Autophagy enables microglia to engage amyloid plaques and prevents microglial senescence', *Nat Cell Biol,* 25(7), pp. 963-974.

Cross, J., Durgan, J., McEwan, D.G. and Florey, O. (2023) 'Lysosome damage triggers direct ATG8 conjugation and ATG2 engagement via CASM', *bioRxiv*, p. 2023.2003.2022.533754.

Damisah, E.C., Hill, R.A., Rai, A., Chen, F., Rothlin, C.V., Ghosh, S. and Grutzendler, J. (2020) 'Astrocytes and microglia play orchestrated roles and respect phagocytic territories during neuronal corpse removal in vivo', *Sci Adv,* 6(26), p. eaba3239.

Deczkowska, A., Keren-Shaul, H., Weiner, A., Colonna, M., Schwartz, M. and Amit, I. (2018) 'Disease-Associated Microglia: A Universal Immune Sensor of Neurodegeneration', *Cell,* 173(5), pp. 1073-1081.

Delgado, M.A., Elmaoued, R.A., Davis, A.S., Kyei, G. and Deretic, V. (2008) 'Toll-like receptors control autophagy', *Embo j,* 27(7), pp. 1110-1121.

Doran, A.C., Yurdagul, A., Jr. and Tabas, I. (2020) 'Efferocytosis in health and disease', *Nat Rev Immunol,* 20(4), pp. 254-267.

Elliott, M.R., Chekeni, F.B., Trampont, P.C., Lazarowski, E.R., Kadl, A., Walk, S.F., Park, D., Woodson, R.I., Ostankovich, M., Sharma, P., Lysiak, J.J., Harden, T.K., Leitinger, N. and Ravichandran, K.S. (2009) 'Nucleotides released by apoptotic cells act as a find-me signal to promote phagocytic clearance', *Nature,* 461(7261), pp. 282-286.

Erwig, L.P., McPhilips, K.A., Wynes, M.W., Ivetic, A., Ridley, A.J. and Henson, P.M. (2006) 'Differential regulation of phagosome maturation in macrophages and dendritic cells mediated by Rho GTPases and ezrin-radixin-moesin (ERM) proteins', *Proc Natl Acad Sci U S A,* 103(34), pp. 12825-12830.

Etchegaray, J.I., Elguero, E.J., Tran, J.A., Sinatra, V., Feany, M.B. and McCall, K. (2016) 'Defective Phagocytic Corpse Processing Results in Neurodegeneration and Can Be Rescued by TORC1 Activation', *J Neurosci,* 36(11), pp. 3170-3183.

Evans, A.L., Blackburn, J.W., Yin, C. and Heit, B. (2017) 'Quantitative Efferocytosis Assays', *Methods Mol Biol,* 1519, pp. 25-41.

Fadok, V.A., Bratton, D.L., Konowal, A., Freed, P.W., Westcott, J.Y. and Henson, P.M. (1998) 'Macrophages that have ingested apoptotic cells in vitro inhibit proinflammatory cytokine production through autocrine/paracrine mechanisms involving TGF-beta, PGE2, and PAF', *J Clin Invest,* 101(4), pp. 890-898.

Fazeli, G., Levin-Konigsberg, R., Bassik, M.C., Stigloher, C. and Wehman, A.M. (2023) 'A BORC-dependent molecular pathway for vesiculation of cell corpse phagolysosomes', *Curr Biol,* 33(4), pp. 607-621.e607.

Fletcher, K., Ulferts, R., Jacquin, E., Veith, T., Gammoh, N., Arasteh, J.M., Mayer, U., Carding, S.R., Wileman, T., Beale, R. and Florey, O. (2018) 'The WD40 domain of ATG16L1 is required for its non-canonical role in lipidation of LC3 at single membranes', *Embo j,* 37(4).

Florey, O., Gammoh, N., Kim, S.E., Jiang, X. and Overholtzer, M. (2015) 'V-ATPase and osmotic imbalances activate endolysosomal LC3 lipidation', *Autophagy,* 11(1), pp. 88-99.

Fourrier, C., Bryksin, V., Hattersley, K., Hein, L.K., Bensalem, J. and Sargeant, T.J. (2021) 'Comparison of chloroquine-like molecules for lysosomal inhibition and measurement of autophagic flux in the brain', *Biochem Biophys Res Commun,* 534, pp. 107-113.

Gabandé-Rodríguez, E., Keane, L. and Capasso, M. (2020) 'Microglial phagocytosis in aging and Alzheimer's disease', *J Neurosci Res,* 98(2), pp. 284-298.

Gammoh, N., Florey, O., Overholtzer, M. and Jiang, X. (2013) 'Interaction between FIP200 and ATG16L1 distinguishes ULK1 complex-dependent and -independent autophagy', *Nat Struct Mol Biol,* 20(2), pp. 144-149.

Geng, L., Zhao, J., Deng, Y., Molano, I., Xu, X., Xu, L., Ruiz, P., Li, Q., Feng, X., Zhang, M., Tan, W., Kamen, D.L., Bae, S.C., Gilkeson, G.S., Sun, L. and Tsao, B.P. (2022) 'Human SLE variant NCF1-R90H promotes kidney damage and murine lupus

through enhanced Tfh2 responses induced by defective efferocytosis of macrophages', *Ann Rheum Dis,* 81(2), pp. 255-267.

Ginhoux, F. and Prinz, M. (2015) 'Origin of microglia: current concepts and past controversies', *Cold Spring Harb Perspect Biol,* 7(8), p. a020537.

Hanada, T., Noda, N.N., Satomi, Y., Ichimura, Y., Fujioka, Y., Takao, T., Inagaki, F. and Ohsumi, Y. (2007) 'The Atg12-Atg5 conjugate has a novel E3-like activity for protein lipidation in autophagy', *J Biol Chem,* 282(52), pp. 37298-37302.

He, C. (2022) 'Balancing nutrient and energy demand and supply via autophagy', *Curr Biol,* 32(12), pp. R684-r696.

Heckmann, B.L., Teubner, B.J.W., Boada-Romero, E., Tummers, B., Guy, C., Fitzgerald, P., Mayer, U., Carding, S., Zakharenko, S.S., Wileman, T. and Green, D.R. (2020) 'Noncanonical function of an autophagy protein prevents spontaneous Alzheimer's disease', *Sci Adv,* 6(33), p. eabb9036.

Heckmann, B.L., Teubner, B.J.W., Tummers, B., Boada-Romero, E., Harris, L., Yang, M., Guy, C.S., Zakharenko, S.S. and Green, D.R. (2019) 'LC3-Associated Endocytosis Facilitates beta-Amyloid Clearance and Mitigates Neurodegeneration in Murine Alzheimer's Disease', *Cell,* 178(3), pp. 536-551.e514.

Hill, R.A., Damisah, E.C., Chen, F., Kwan, A.C. and Grutzendler, J. (2017) 'Targeted two-photon chemical apoptotic ablation of defined cell types in vivo', *Nat Commun,* 8, p. 15837.

Hodge, M.X., Reece, S.W., Madenspacher, J.H. and Gowdy, K.M. (2019) 'In Vivo Assessment of Alveolar Macrophage Efferocytosis Following Ozone Exposure', *J Vis Exp,* (152).

Hollville, E., Romero, S.E. and Deshmukh, M. (2019) 'Apoptotic cell death regulation in neurons', *Febs j,* 286(17), pp. 3276-3298.

Hooper, K.M., Jacquin, E., Li, T., Goodwin, J.M., Brumell, J.H., Durgan, J. and Florey, O. (2022) 'V-ATPase is a universal regulator of LC3-associated phagocytosis and non-canonical autophagy', *J Cell Biol,* 221(6).

Hosokawa, N., Hara, T., Kaizuka, T., Kishi, C., Takamura, A., Miura, Y., Iemura, S., Natsume, T., Takehana, K., Yamada, N., Guan, J.L., Oshiro, N. and Mizushima, N. (2009) 'Nutrient-dependent mTORC1 association with the ULK1-Atg13-FIP200 complex required for autophagy', *Mol Biol Cell,* 20(7), pp. 1981-1991.

Huang, K.L., Marcora, E., Pimenova, A.A., Di Narzo, A.F., Kapoor, M., Jin, S.C., Harari, O., Bertelsen, S., Fairfax, B.P., Czajkowski, J., Chouraki, V., Grenier-Boley, B., Bellenguez, C., Deming, Y., McKenzie, A., Raj, T., Renton, A.E., Budde, J., Smith, A., Fitzpatrick, A., Bis, J.C., DeStefano, A., Adams, H.H.H., Ikram, M.A., van der Lee, S., Del-Aguila, J.L., Fernandez, M.V., Ibañez, L., Sims, R., Escott-Price, V., Mayeux, R., Haines, J.L., Farrer, L.A., Pericak-Vance, M.A., Lambert, J.C., van Duijn, C., Launer, L., Seshadri, S., Williams, J., Amouyel, P., Schellenberg, G.D., Zhang, B., Borecki, I., Kauwe, J.S.K., Cruchaga, C., Hao, K. and Goate, A.M. (2017) 'A common haplotype lowers PU.1 expression in myeloid cells and delays onset of Alzheimer's disease', *Nat Neurosci,* 20(8), pp. 1052-1061.

Jiang, S., Park, D.W., Stigler, W.S., Creighton, J., Ravi, S., Darley-Usmar, V. and Zmijewski, J.W. (2013) 'Mitochondria and AMP-activated protein kinase-dependent mechanism of efferocytosis', *J Biol Chem,* 288(36), pp. 26013-26026.

Jorge, A.M., Lao, T., Kim, R., Licciardi, S., El Khoury, J., Luster, A.D., Means, T.K. and Ramirez-Ortiz, Z.G. (2022) 'SCARF1-Induced Efferocytosis Plays an Immunomodulatory Role in Humans, and Autoantibodies Targeting SCARF1 Are Produced in Patients with Systemic Lupus Erythematosus', *J Immunol,* 208(4), pp. 955-967.

Kawane, K., Ohtani, M., Miwa, K., Kizawa, T., Kanbara, Y., Yoshioka, Y., Yoshikawa, H. and Nagata, S. (2006) 'Chronic polyarthritis caused by mammalian DNA that escapes from degradation in macrophages', *Nature,* 443(7114), pp. 998-1002.

Kim, J., Kundu, M., Viollet, B. and Guan, K.L. (2011) 'AMPK and mTOR regulate autophagy through direct phosphorylation of Ulk1', *Nat Cell Biol,* 13(2), pp. 132-141.

Kim, K.S., Marcogliese, P.C., Yang, J., Callaghan, S.M., Resende, V., Abdel-Messih, E., Marras, C., Visanji, N.P., Huang, J., Schlossmacher, M.G., Trinkle-Mulcahy, L., Slack, R.S., Lang, A.E. and Park, D.S. (2018) 'Regulation of myeloid cell phagocytosis by LRRK2 via WAVE2 complex stabilization is altered in Parkinson's disease', *Proc Natl Acad Sci U S A,* 115(22), pp. E5164-e5173.

Kinchen, J.M., Doukoumetzidis, K., Almendinger, J., Stergiou, L., Tosello-Trampont, A., Sifri, C.D., Hengartner, M.O. and Ravichandran, K.S. (2008) 'A pathway for phagosome maturation during engulfment of apoptotic cells', *Nat Cell Biol,* 10(5), pp. 556-566.

Klionsky, D.J., Abdel-Aziz, A.K., Abdelfatah, S., Abdellatif, M., Abdoli, A., Abel, S., Abeliovich, H., Abildgaard, M.H., Abudu, Y.P., Acevedo-Arozena, A., Adamopoulos, I.E., Adeli, K., Adolph, T.E., Adornetto, A., Aflaki, E., Agam, G., Agarwal, A., Aggarwal, B.B., Agnello, M., Agostinis, P., Agrewala, J.N., Agrotis, A., Aguilar, P.V., Ahmad, S.T., Ahmed, Z.M., Ahumada-Castro, U., Aits, S., Aizawa, S., Akkoc, Y., Akoumianaki, T., Akpinar, H.A., Al-Abd, A.M., Al-Akra, L., Al-Gharaibeh, A., Alaoui-Jamali, M.A., Alberti, S., Alcocer-Gómez, E., Alessandri, C., Ali, M., Alim Al-Bari, M.A., Aliwaini, S., Alizadeh, J., Almacellas, E., Almasan, A., Alonso, A., Alonso, G.D., Altan-Bonnet, N., Altieri, D.C., Álvarez É, M.C., Alves, S., Alves da Costa, C., Alzaharna, M.M., Amadio, M., Amantini, C., Amaral, C., Ambrosio, S., Amer, A.O., Ammanathan, V., An, Z., Andersen, S.U., Andrabi, S.A., Andrade-Silva, M., Andres, A.M., Angelini, S., Ann, D., Anozie, U.C., Ansari, M.Y., Antas, P., Antebi, A., Antón, Z., Anwar, T., Apetoh, L., Apostolova, N., Araki, T., Araki, Y., Arasaki, K., Araújo, W.L., Araya, J., Arden, C., Arévalo, M.A., Arguelles, S., Arias, E., Arikkath, J., Arimoto, H., Ariosa, A.R., Armstrong-James, D., Arnauné-Pelloquin, L., Aroca, A., Arroyo, D.S., Arsov, I., Artero, R., Asaro, D.M.L., Aschner, M., Ashrafizadeh, M., Ashur-Fabian, O., Atanasov, A.G., Au, A.K., Auberger, P., Auner, H.W., Aurelian, L., et al. (2021) 'Guidelines for the use and interpretation of assays for monitoring autophagy (4th edition)(1)', *Autophagy,* 17(1), pp. 1-382.

Kole, A.J., Annis, R.P. and Deshmukh, M. (2013) 'Mature neurons: equipped for survival', *Cell Death Dis,* 4(6), p. e689.

Komatsu, M., Waguri, S., Ueno, T., Iwata, J., Murata, S., Tanida, I., Ezaki, J., Mizushima, N., Ohsumi, Y., Uchiyama, Y., Kominami, E., Tanaka, K. and Chiba, T.

(2005) 'Impairment of starvation-induced and constitutive autophagy in Atg7-deficient mice', *J Cell Biol,* 169(3), pp. 425-434.

Krajcovic, M., Krishna, S., Akkari, L., Joyce, J.A. and Overholtzer, M. (2013) 'mTOR regulates phagosome and entotic vacuole fission', *Mol Biol Cell,* 24(23), pp. 3736-3745.

Kuma, A., Hatano, M., Matsui, M., Yamamoto, A., Nakaya, H., Yoshimori, T., Ohsumi, Y., Tokuhisa, T. and Mizushima, N. (2004) 'The role of autophagy during the early neonatal starvation period', *Nature,* 432(7020), pp. 1032-1036.

Kuma, A., Mizushima, N., Ishihara, N. and Ohsumi, Y. (2002) 'Formation of the approximately 350-kDa Apg12-Apg5.Apg16 multimeric complex, mediated by Apg16 oligomerization, is essential for autophagy in yeast', *J Biol Chem,* 277(21), pp. 18619-18625.

Kumaran Satyanarayanan, S., El Kebir, D., Soboh, S., Butenko, S., Sekheri, M., Saadi, J., Peled, N., Assi, S., Othman, A., Schif-Zuck, S., Feuermann, Y., Barkan, D., Sher, N., Filep, J.G. and Ariel, A. (2019) 'IFN-β is a macrophage-derived effector cytokine facilitating the resolution of bacterial inflammation', *Nat Commun,* 10(1), p. 3471.

Kurant, E., Axelrod, S., Leaman, D. and Gaul, U. (2008) 'Six-microns-under acts upstream of Draper in the glial phagocytosis of apoptotic neurons', *Cell,* 133(3), pp. 498-509.

Lang, C., Roy, S., Wang, Y., Graves, D., Xu, Y., Serezani, C.H., Korrer, M. and Kim, Y.J. (2022) 'Efferocytosis drives myeloid NLRP3 dependent inflammasome signaling secretion of IL-1β to promote tumor growth', *Front Immunol,* 13, p. 993771.

Lin, D., Kang, X., Shen, L., Tu, S., Lenahan, C., Chen, Y., Wang, X. and Shao, A. (2020) 'Efferocytosis and Its Associated Cytokines: A Light on Non-tumor and Tumor Diseases?', *Mol Ther Oncolytics,* 17, pp. 394-407.

Liu, B., Palmfeldt, J., Lin, L., Colaço, A., Clemmensen, K.K.B., Huang, J., Xu, F., Liu, X., Maeda, K., Luo, Y. and Jäättelä, M. (2018) 'STAT3 associates with vacuolar H(+)-ATPase and regulates cytosolic and lysosomal pH', *Cell Res,* 28(10), pp. 996-1012.

Márquez-Ropero, M., Benito, E., Plaza-Zabala, A. and Sierra, A. (2020) 'Microglial Corpse Clearance: Lessons From Macrophages', *Front Immunol,* 11, p. 506.

Martinez, J., Almendinger, J., Oberst, A., Ness, R., Dillon, C.P., Fitzgerald, P., Hengartner, M.O. and Green, D.R. (2011) 'Microtubule-associated protein 1 light chain 3 alpha (LC3)-associated phagocytosis is required for the efficient clearance of dead cells', *Proc Natl Acad Sci U S A,* 108(42), pp. 17396-17401.

Martinez, J., Malireddi, R.K., Lu, Q., Cunha, L.D., Pelletier, S., Gingras, S., Orchard, R., Guan, J.L., Tan, H., Peng, J., Kanneganti, T.D., Virgin, H.W. and Green, D.R. (2015) 'Molecular characterization of LC3-associated phagocytosis reveals distinct roles for Rubicon, NOX2 and autophagy proteins', *Nat Cell Biol,* 17(7), pp. 893-906.

Martínez-Fábregas, J., Prescott, A., van Kasteren, S., Pedrioli, D.L., McLean, I., Moles, A., Reinheckel, T., Poli, V. and Watts, C. (2018) 'Lysosomal protease deficiency or substrate overload induces an oxidative-stress mediated STAT3-dependent pathway of lysosomal homeostasis', *Nat Commun,* 9(1), p. 5343.

Matsunaga, K., Saitoh, T., Tabata, K., Omori, H., Satoh, T., Kurotori, N., Maejima, I., Shirahama-Noda, K., Ichimura, T., Isobe, T., Akira, S., Noda, T. and Yoshimori, T.

(2009) 'Two Beclin 1-binding proteins, Atg14L and Rubicon, reciprocally regulate autophagy at different stages', *Nat Cell Biol,* 11(4), pp. 385-396.

Maurin, A.-C., Parry, L., B'chir, W., Carraro, V., Coudy-Gandilhon, C., Chaouki, G., Chaveroux, C., Mordier, S., Martinie, B., Reinhardt, V., Jousse, C., Bruhat, A., Codogno, P., Averous, J. and Fafournoux, P. (2022) 'GCN2 upregulates autophagy in response to short-term deprivation of a single essential amino acid', *Autophagy Reports,* 1(1), pp. 119-142.

Meng, D., Yang, Q., Wang, H., Melick, C.H., Navlani, R., Frank, A.R. and Jewell, J.L. (2020) 'Glutamine and asparagine activate mTORC1 independently of Rag GTPases', *J Biol Chem,* 295(10), pp. 2890-2899.

Merlin, J., Ivanov, S., Dumont, A., Sergushichev, A., Gall, J., Stunault, M., Ayrault, M., Vaillant, N., Castiglione, A., Swain, A., Orange, F., Gallerand, A., Berton, T., Martin, J.C., Carobbio, S., Masson, J., Gaisler-Salomon, I., Maechler, P., Rayport, S., Sluimer, J.C., Biessen, E.A.L., Guinamard, R.R., Gautier, E.L., Thorp, E.B., Artyomov, M.N. and Yvan-Charvet, L. (2021) 'Non-canonical glutamine transamination sustains efferocytosis by coupling redox buffering to oxidative phosphorylation', *Nat Metab,* 3(10), pp. 1313-1326.

Miao, L.J., Huang, F.X., Sun, Z.T., Zhang, R.X., Huang, S.F. and Wang, J. (2014) 'Stat3 inhibits Beclin 1 expression through recruitment of HDAC3 in nonsmall cell lung cancer cells', *Tumour Biol,* 35(7), pp. 7097-7103.

Miki, H., Suetsugu, S. and Takenawa, T. (1998) 'WAVE, a novel WASP-family protein involved in actin reorganization induced by Rac', *Embo j,* 17(23), pp. 6932-6941.

Miksa, M., Komura, H., Wu, R., Shah, K.G. and Wang, P. (2009) 'A novel method to determine the engulfment of apoptotic cells by macrophages using pHrodo succinimidyl ester', *J Immunol Methods,* 342(1-2), pp. 71-77.

Mizushima, N., Noda, T., Yoshimori, T., Tanaka, Y., Ishii, T., George, M.D., Klionsky, D.J., Ohsumi, M. and Ohsumi, Y. (1998) 'A protein conjugation system essential for autophagy', *Nature,* 395(6700), pp. 395-398.

Möller, K., Brambach, M., Villani, A., Gallo, E., Gilmour, D. and Peri, F. (2022) 'A role for the centrosome in regulating the rate of neuronal efferocytosis by microglia in vivo', *Elife,* 11.

Morizawa, Y.M., Hirayama, Y., Ohno, N., Shibata, S., Shigetomi, E., Sui, Y., Nabekura, J., Sato, K., Okajima, F., Takebayashi, H., Okano, H. and Koizumi, S. (2017) 'Reactive astrocytes function as phagocytes after brain ischemia via ABCA1-mediated pathway', *Nat Commun,* 8(1), p. 28.

Morsch, M., Radford, R., Lee, A., Don, E.K., Badrock, A.P., Hall, T.E., Cole, N.J. and Chung, R. (2015) 'In vivo characterization of microglial engulfment of dying neurons in the zebrafish spinal cord', *Front Cell Neurosci,* 9, p. 321.

Mueller, R.B., Sheriff, A., Gaipl, U.S., Wesselborg, S. and Lauber, K. (2007) 'Attraction of phagocytes by apoptotic cells is mediated by lysophosphatidylcholine', *Autoimmunity,* 40(4), pp. 342-344.

Nakahashi-Oda, C., Fujiyama, S., Nakazawa, Y., Kanemaru, K., Wang, Y., Lyu, W., Shichita, T., Kitaura, J., Abe, F. and Shibuya, A. (2021) 'CD300a blockade enhances

efferocytosis by infiltrating myeloid cells and ameliorates neuronal deficit after ischemic stroke', *Sci Immunol,* 6(64), p. eabe7915.

Onodera, J. and Ohsumi, Y. (2005) 'Autophagy is required for maintenance of amino acid levels and protein synthesis under nitrogen starvation', *J Biol Chem,* 280(36), pp. 31582-31586.

Overholtzer, M., Mailleux, A.A., Mouneimne, G., Normand, G., Schnitt, S.J., King, R.W., Cibas, E.S. and Brugge, J.S. (2007) 'A nonapoptotic cell death process, entosis, that occurs by cell-in-cell invasion', *Cell,* 131(5), pp. 966-979.

Paolicelli, R.C., Bolasco, G., Pagani, F., Maggi, L., Scianni, M., Panzanelli, P., Giustetto, M., Ferreira, T.A., Guiducci, E., Dumas, L., Ragozzino, D. and Gross, C.T. (2011) 'Synaptic pruning by microglia is necessary for normal brain development', *Science,* 333(6048), pp. 1456-1458.

Peker, N. and Gozuacik, D. (2020) 'Autophagy as a Cellular Stress Response Mechanism in the Nervous System', *J Mol Biol,* 432(8), pp. 2560-2588.

Proto, J.D., Doran, A.C., Gusarova, G., Yurdagul, A., Jr., Sozen, E., Subramanian, M., Islam, M.N., Rymond, C.C., Du, J., Hook, J., Kuriakose, G., Bhattacharya, J. and Tabas, I. (2018) 'Regulatory T Cells Promote Macrophage Efferocytosis during Inflammation Resolution', *Immunity,* 49(4), pp. 666-677.e666.

Qin, B., Zhou, Z., He, J., Yan, C. and Ding, S. (2015) 'IL-6 Inhibits Starvation-induced Autophagy via the STAT3/Bcl-2 Signaling Pathway', *Sci Rep,* 5, p. 15701.

Ratto, E., Chowdhury, S.R., Siefert, N.S., Schneider, M., Wittmann, M., Helm, D. and Palm, W. (2022) 'Direct control of lysosomal catabolic activity by mTORC1 through regulation of V-ATPase assembly', *Nat Commun,* 13(1), p. 4848.

Raymond, M.H., Davidson, A.J., Shen, Y., Tudor, D.R., Lucas, C.D., Morioka, S., Perry, J.S.A., Krapivkina, J., Perrais, D., Schumacher, L.J., Campbell, R.E., Wood, W. and Ravichandran, K.S. (2022) 'Live cell tracking of macrophage efferocytosis during Drosophila embryo development in vivo', *Science,* 375(6585), pp. 1182-1187.

Romero-Molina, C., Garretti, F., Andrews, S.J., Marcora, E. and Goate, A.M. (2022) 'Microglial efferocytosis: Diving into the Alzheimer's disease gene pool', *Neuron,* 110(21), pp. 3513-3533.

Salina, A.C.G., Dos-Santos, D., Rodrigues, T.S., Fortes-Rocha, M., Freitas-Filho, E.G., Alzamora-Terrel, D.L., Castro, I.M.S., Fraga da Silva, T.F.C., de Lima, M.H.F., Nascimento, D.C., Silva, C.M., Toller-Kawahisa, J.E., Becerra, A., Oliveira, S., Caetité, D.B., Almeida, L., Ishimoto, A.Y., Lima, T.M., Martins, R.B., Veras, F., do Amaral, N.B., Giannini, M.C., Bonjorno, L.P., Lopes, M.I.F., Benatti, M.N., Batah, S.S., Santana, R.C., Vilar, F.C., Martins, M.A., Assad, R.L., de Almeida, S.C.L., de Oliveira, F.R., Arruda Neto, E., Cunha, T.M., Alves-Filho, J.C., Bonato, V.L.D., Cunha, F.Q., Fabro, A.T., Nakaya, H.I., Zamboni, D.S., Louzada-Junior, P., Oliveira, R.D.R. and Cunha, L.D. (2022) 'Efferocytosis of SARS-CoV-2-infected dying cells impairs macrophage anti-inflammatory functions and clearance of apoptotic cells', *Elife,* 11.

Sanjuan, M.A., Dillon, C.P., Tait, S.W., Moshiach, S., Dorsey, F., Connell, S., Komatsu, M., Tanaka, K., Cleveland, J.L., Withoff, S. and Green, D.R. (2007) 'Toll-

like receptor signalling in macrophages links the autophagy pathway to phagocytosis', *Nature,* 450(7173), pp. 1253-1257.

Sardiello, M., Palmieri, M., di Ronza, A., Medina, D.L., Valenza, M., Gennarino, V.A., Di Malta, C., Donaudy, F., Embrione, V., Polishchuk, R.S., Banfi, S., Parenti, G., Cattaneo, E. and Ballabio, A. (2009) 'A gene network regulating lysosomal biogenesis and function', *Science,* 325(5939), pp. 473-477.

Schafer, D.P. and Stevens, B. (2013) 'Phagocytic glial cells: sculpting synaptic circuits in the developing nervous system', *Curr Opin Neurobiol,* 23(6), pp. 1034-1040.

Schappe, M.S., Stremska, M.E., Busey, G.W., Downs, T.K., Seegren, P.V., Mendu, S.K., Flegal, Z., Doyle, C.A., Stipes, E.J. and Desai, B.N. (2022) 'Efferocytosis requires periphagosomal Ca(2+)-signaling and TRPM7-mediated electrical activity', *Nat Commun,* 13(1), p. 3230.

Schneider, M. (2013) 'Collecting resident or thioglycollate-elicited peritoneal macrophages', *Methods Mol Biol,* 1031, pp. 37-40.

Sender, R. and Milo, R. (2021) 'The distribution of cellular turnover in the human body', *Nat Med,* 27(1), pp. 45-48.

Settembre, C., Di Malta, C., Polito, V.A., Garcia Arencibia, M., Vetrini, F., Erdin, S., Erdin, S.U., Huynh, T., Medina, D., Colella, P., Sardiello, M., Rubinsztein, D.C. and Ballabio, A. (2011) 'TFEB links autophagy to lysosomal biogenesis', *Science,* 332(6036), pp. 1429-1433.

Settembre, C., Zoncu, R., Medina, D.L., Vetrini, F., Erdin, S., Erdin, S., Huynh, T., Ferron, M., Karsenty, G., Vellard, M.C., Facchinetti, V., Sabatini, D.M. and Ballabio, A. (2012) 'A lysosome-to-nucleus signalling mechanism senses and regulates the lysosome via mTOR and TFEB', *Embo j,* 31(5), pp. 1095-1108.

Shen, S., Niso-Santano, M., Adjemian, S., Takehara, T., Malik, S.A., Minoux, H., Souquere, S., Mariño, G., Lachkar, S., Senovilla, L., Galluzzi, L., Kepp, O., Pierron, G., Maiuri, M.C., Hikita, H., Kroemer, R. and Kroemer, G. (2012) 'Cytoplasmic STAT3 represses autophagy by inhibiting PKR activity', *Mol Cell,* 48(5), pp. 667-680.

Shintani, T., Mizushima, N., Ogawa, Y., Matsuura, A., Noda, T. and Ohsumi, Y. (1999) 'Apg10p, a novel protein-conjugating enzyme essential for autophagy in yeast', *Embo j,* 18(19), pp. 5234-5241.

Shklyar, B., Shklover, J. and Kurant, E. (2013) 'Live imaging of apoptotic cell clearance during Drosophila embryogenesis', *J Vis Exp,* (78).

Soki, F.N., Koh, A.J., Jones, J.D., Kim, Y.W., Dai, J., Keller, E.T., Pienta, K.J., Atabai, K., Roca, H. and McCauley, L.K. (2014) 'Polarization of prostate cancer-associated macrophages is induced by milk fat globule-EGF factor 8 (MFG-E8)-mediated efferocytosis', *J Biol Chem,* 289(35), pp. 24560-24572.

Sou, Y.S., Waguri, S., Iwata, J., Ueno, T., Fujimura, T., Hara, T., Sawada, N., Yamada, A., Mizushima, N., Uchiyama, Y., Kominami, E., Tanaka, K. and Komatsu, M. (2008) 'The Atg8 conjugation system is indispensable for proper development of autophagic isolation membranes in mice', *Mol Biol Cell,* 19(11), pp. 4762-4775.

Stöhr, R., Deckers, N., Schurgers, L., Marx, N. and Reutelingsperger, C.P. (2018) 'AnnexinA5-pHrodo: a new molecular probe for measuring efferocytosis', *Sci Rep,* 8(1), p. 17731.

Subramaniam, R., Mukherjee, S., Chen, H., Keshava, S., Neuenschwander, P. and Shams, H. (2016) 'Restoring cigarette smoke-induced impairment of efferocytosis in alveolar macrophages', *Mucosal Immunol,* 9(4), pp. 873-883.

Suelves, N., Saleki, S., Ibrahim, T., Palomares, D., Moonen, S., Koper, M.J., Vrancx, C., Vadukul, D.M., Papadopoulos, N., Viceconte, N., Claude, E., Vandenberghe, R., von Arnim, C.A.F., Constantinescu, S.N., Thal, D.R., Decottignies, A. and Kienlen-Campard, P. (2023) 'Senescence-related impairment of autophagy induces toxic intraneuronal amyloid-β accumulation in a mouse model of amyloid pathology', *Acta Neuropathol Commun,* 11(1), p. 82.

Sutter, B.M., Wu, X., Laxman, S. and Tu, B.P. (2013) 'Methionine inhibits autophagy and promotes growth by inducing the SAM-responsive methylation of PP2A', *Cell,* 154(2), pp. 403-415.

Tanida, I., Sou, Y.S., Ezaki, J., Minematsu-Ikeguchi, N., Ueno, T. and Kominami, E. (2004) 'HsAtg4B/HsApg4B/autophagin-1 cleaves the carboxyl termini of three human Atg8 homologues and delipidates microtubule-associated protein light chain 3- and GABAA receptor-associated protein-phospholipid conjugates', *J Biol Chem,* 279(35), pp. 36268-36276.

Toboz, P., Amiri, M., Tabatabaei, N., Dufour, C.R., Kim, S.H., Fillebeen, C., Ayemoba, C.E., Khoutorsky, A., Nairz, M., Shao, L., Pajcini, K.V., Kim, K.W., Giguère, V.,

Oliveira, R.L., Constante, M., Santos, M.M., Morales, C.R., Pantopoulos, K., Sonenberg, N., Pinho, S. and Tahmasebi, S. (2022) 'The amino acid sensor GCN2 controls red blood cell clearance and iron metabolism through regulation of liver macrophages', *Proc Natl Acad Sci U S A,* 119(35), p. e2121251119.

Tricker, E. and Cheng, G. (2008) 'With a little help from my friends: modulation of phagocytosis through TLR activation', *Cell Res,* 18(7), pp. 711-712.

Truman, L.A., Ford, C.A., Pasikowska, M., Pound, J.D., Wilkinson, S.J., Dumitriu, I.E., Melville, L., Melrose, L.A., Ogden, C.A., Nibbs, R., Graham, G., Combadiere, C. and Gregory, C.D. (2008) 'CX3CL1/fractalkine is released from apoptotic lymphocytes to stimulate macrophage chemotaxis', *Blood,* 112(13), pp. 5026-5036.

Tu, H.Y., Yuan, B.S., Hou, X.O., Zhang, X.J., Pei, C.S., Ma, Y.T., Yang, Y.P., Fan, Y., Qin, Z.H., Liu, C.F. and Hu, L.F. (2021) 'α-synuclein suppresses microglial autophagy and promotes neurodegeneration in a mouse model of Parkinson's disease', *Aging Cell,* 20(12), p. e13522.

Turner, C., Devitt, A., Parker, K., MacFarlane, M., Giuliano, M., Cohen, G.M. and Gregory, C.D. (2003) 'Macrophage-mediated clearance of cells undergoing caspase-3-independent death', *Cell Death Differ,* 10(3), pp. 302-312.

Udayar, V., Chen, Y., Sidransky, E. and Jagasia, R. (2022) 'Lysosomal dysfunction in neurodegeneration: emerging concepts and methods', *Trends Neurosci,* 45(3), pp. 184-199.

Ulferts, R., Marcassa, E., Timimi, L., Lee, L.C., Daley, A., Montaner, B., Turner, S.D., Florey, O., Baillie, J.K. and Beale, R. (2021) 'Subtractive CRISPR screen identifies

the ATG16L1/vacuolar ATPase axis as required for non-canonical LC3 lipidation', *Cell Rep,* 37(4), p. 109899.

van Delft, M.F., Smith, D.P., Lahoud, M.H., Huang, D.C. and Adams, J.M. (2010) 'Apoptosis and non-inflammatory phagocytosis can be induced by mitochondrial damage without caspases', *Cell Death Differ,* 17(5), pp. 821-832.

van Ham, T.J., Mapes, J., Kokel, D. and Peterson, R.T. (2010) 'Live imaging of apoptotic cells in zebrafish', *Faseb j,* 24(11), pp. 4336-4342.

Villani, A., Benjaminsen, J., Moritz, C., Henke, K., Hartmann, J., Norlin, N., Richter, K., Schieber, N.L., Franke, T., Schwab, Y. and Peri, F. (2019) 'Clearance by Microglia Depends on Packaging of Phagosomes into a Unique Cellular Compartment', *Dev Cell,* 49(1), pp. 77-88.e77.

Wang, Y.T., Trzeciak, A.J., Rojas, W.S., Saavedra, P., Chen, Y.T., Chirayil, R., Etchegaray, J.I., Lucas, C.D., Puleston, D.J., Keshari, K.R. and Perry, J.S.A. (2023) 'Metabolic adaptation supports enhanced macrophage efferocytosis in limited-oxygen environments', *Cell Metab,* 35(2), pp. 316-331.e316.

Xie, X.S., Padron, D., Liao, X., Wang, J., Roth, M.G. and De Brabander, J.K. (2004) 'Salicylihalamide A inhibits the V0 sector of the V-ATPase through a mechanism distinct from bafilomycin A1', *J Biol Chem,* 279(19), pp. 19755-19763.

Xu, Y., Propson, N.E., Du, S., Xiong, W. and Zheng, H. (2021) 'Autophagy deficiency modulates microglial lipid homeostasis and aggravates tau pathology and spreading', *Proc Natl Acad Sci U S A,* 118(27).

Ye, J., Palm, W., Peng, M., King, B., Lindsten, T., Li, M.O., Koumenis, C. and Thompson, C.B. (2015) 'GCN2 sustains mTORC1 suppression upon amino acid deprivation by inducing Sestrin2', *Genes Dev,* 29(22), pp. 2331-2336.

Yin, C., Kim, Y., Argintaru, D. and Heit, B. (2016) 'Rab17 mediates differential antigen sorting following efferocytosis and phagocytosis', *Cell Death Dis,* 7(12), p. e2529.

Yu, L., McPhee, C.K., Zheng, L., Mardones, G.A., Rong, Y., Peng, J., Mi, N., Zhao, Y., Liu, Z., Wan, F., Hailey, D.W., Oorschot, V., Klumperman, J., Baehrecke, E.H. and Lenardo, M.J. (2010) 'Termination of autophagy and reformation of lysosomes regulated by mTOR', *Nature,* 465(7300), pp. 942-946.

Yurdagul, A., Jr., Doran, A.C., Cai, B., Fredman, G. and Tabas, I.A. (2017) 'Mechanisms and Consequences of Defective Efferocytosis in Atherosclerosis', *Front Cardiovasc Med,* 4, p. 86.

Yurdagul, A., Jr., Subramanian, M., Wang, X., Crown, S.B., Ilkayeva, O.R., Darville, L., Kolluru, G.K., Rymond, C.C., Gerlach, B.D., Zheng, Z., Kuriakose, G., Kevil, C.G., Koomen, J.M., Cleveland, J.L., Muoio, D.M. and Tabas, I. (2020) 'Macrophage Metabolism of Apoptotic Cell-Derived Arginine Promotes Continual Efferocytosis and Resolution of Injury', *Cell Metab,* 31(3), pp. 518-533.e510.

Zhang, S., Weinberg, S., DeBerge, M., Gainullina, A., Schipma, M., Kinchen, J.M., Ben-Sahra, I., Gius, D.R., Yvan-Charvet, L., Chandel, N.S., Schumacker, P.T. and Thorp, E.B. (2019) 'Efferocytosis Fuels Requirements of Fatty Acid Oxidation and the Electron Transport Chain to Polarize Macrophages for Tissue Repair', *Cell Metab,* 29(2), pp. 443-456.e445.

Zi, Z., Zhang, Z., Feng, Q., Kim, C., Wang, X.D., Scherer, P.E., Gao, J., Levine, B. and Yu, Y. (2022) 'Quantitative phosphoproteomic analyses identify STK11IP as a lysosome-specific substrate of mTORC1 that regulates lysosomal acidification', *Nat Commun,* 13(1), p. 1760.

CHAPTER 2

Project overview

2.1 GENERAL SUMMARY AND RESEARCH RATIONALE

Efferocytosis and autophagy are two major quality control pathways implemented by phagocytes: efferocytosis involves the engulfment and breakdown of extracellular apoptotic material; autophagy is the process of degradation of intracellular waste, including protein aggregates and damaged organelles. Both processes are crucial for maintaining homeostasis in the brain. Defects in autophagy have long been implicated in age-associated neurodegeneration during Alzheimer's (Pickford *et al.*, 2008, Cho *et al.*, 2014, Cheng *et al.*, 2020) and Parkinson's diseases (Cheng *et al.*, 2020, Qin *et al.*, 2021) among others. Failure to efficiently clear apoptotic debris is associated with poorer outcomes in stroke (Cai *et al.*, 2019, Nakahashi-Oda *et al.*, 2021), multiple sclerosis (Berglund *et al.*, 2020, Lampron *et al.*, 2015), and Alzheimer's disease (Heckmann *et al.*, 2019, Jung *et al.*, 2022, Huang and Lemke, 2022). In addition to their autophagy roles, LC3 proteins can also be recruited to single membranes during efferocytosis (Martinez *et al.*, 2011) via a process termed CASM or non-canonical autophagy. CASM deficiency exacerbates pathological and behavioural phenotypes in mouse models of Alzheimer's disease (Heckmann *et al.*, 2019). Thus, autophagy and efferocytosis are critical for maintaining overall brain health, both individually and via CASM. We surveyed the literature on efferocytosis, autophagy, and CASM, and identified several key gaps in the field:

(1) Efferocytosis involves the recognition, engulfment, and degradation of apoptotic material by phagocytes. Flow cytometry assays are routinely used to measure

efferocytosis, as imaging phagosome dynamics in real time is costly and laborious. Following cargo engulfment, the phagocyte executes a series of steps whereby phagosomes mature, acidify, and fuse with lysosomes to ultimately degrade their contents. However, current techniques to study efferocytosis (Miksa *et al.*, 2009, Aziz, Yang and Wang, 2013) cannot adequately discriminate between cargo engulfment and degradation. Build-up of apoptotic cell signal within phagocytes could indicate either increased uptake, increased acidification or reduced degradation – all of which have different implications for efferocytosis efficiency.

(2) Efferocytosis of apoptotic cells presents a unique metabolic burden for the ingesting phagocyte, as it needs to catabolise a large volume of incoming, potentially toxin-laden cargo, relative to its own size. Phagocytes can recycle some components of this apoptotic cargo, such as arginine (Yurdagul *et al.*, 2020), methionine (Ampomah *et al.*, 2022) and fatty acids (Zhang *et al.*, 2019), as 'food' to utilise for subsequent rounds of efferocytosis or downstream tissue repair. The amino acid glutamine also helps sustain efferocytosis (Merlin *et al.*, 2021), although it is unclear whether phagocytes derive it from their extracellular environment or from digestion of the apoptotic cells themselves. Amino acid availability modulates a range of cellular functions, including growth (Dibble and Manning, 2013), secretion (van Leeuwen, van der Krift and Rabouille, 2018), and autophagy (Onodera and Ohsumi, 2005, Zhou *et al.*, 2013). A role for certain amino acids – obtained from apoptotic corpse breakdown – in efferocytosis has been established. However, beyond the corpse, we do not know if environmental nutrient availability plays a role in a phagocyte's efferocytosis capacity. Can modifying nutrition affect corpse clearance?

(3) Autophagy and efferocytosis converge during CASM. However, beyond the characterisation of the CASM machinery, not much is known about whether autophagy and efferocytosis interact with each other. When CASM was first described, targeting the nutrient-sensitive autophagy pre-initiation complex did not affect the short-term uptake of apoptotic material (Martinez *et al.*, 2011, Martinez *et al.*, 2015), leading to the widespread notion that efferocytosis is not modified by nutrition, canonical autophagy or mTORC1 activity. However, efferocytosis can occur even without CASM, albeit less efficiently (Martinez *et al.*, 2011, Raymond *et al.*, 2022). Therefore, the fact that CASM does not require the nutrient-sensitive autophagy machinery does not necessarily mean that efferocytosis *itself* cannot be modulated by nutrition. Indeed, the role of mTORC1 in a closely related process termed entosis, which involves the cannibalism of living cells (Krajcovic *et al.*, 2013), coupled with recent reports of amino acid metabolism governing the terminal stages of efferocytosis (Yurdagul *et al.*, 2020, Merlin *et al.*, 2021, Ampomah *et al.*, 2022) certainly hints that corpse clearance may be regulated by nutrient sensing pathways. Given that autophagy and corpse clearance are two mechanisms of delivering cargo to the same destination, the lysosome, they may well interact with one another beyond CASM. Does stimulating autophagy affect efferocytosis? Conversely, can efferocytosis impact canonical autophagy?

(4) To date, most of what we know about efferocytosis comes from studies performed in macrophages. Microglia, the resident immune cells of the brain, originate from the embryonic yolk sac and are an almost entirely self-renewing population (Alliot, Godin

and Pessac, 1999). Although macrophages and microglia share several common features, microglia have a different ontogenic, transcriptional, and immunomodulatory profile compared to other macrophage populations (Márquez-Ropero *et al.*, 2020). Findings from studies performed in macrophages cannot automatically be assumed to hold true in microglia.

2.1.1 Hypothesis

Microglial efferocytosis interacts with autophagy to co-ordinate cargo clearance in a nutrient-sensitive manner.

2.1.2 Research objectives

My overarching goal was to determine whether microglial corpse clearance could be modulated via autophagy and nutrition and, if so, whether this was mediated by changes to cargo engulfment, acidification or both. My key objectives were to:

(1) develop a probe capable of tracking both early and late stages of efferocytosis, *i.e.*, the uptake and acidification of apoptotic material, simultaneously, and employ it to:

(2) determine whether microglial corpse clearance changes in response to nutrient deprivation;

(3) investigate whether modulating efferocytosis alters canonical autophagy and vice-versa;

(4) elucidate the mechanisms driving the potential interaction between efferocytosis and autophagy in microglia.

2.2 REFERENCES

Alliot, F., Godin, I. and Pessac, B. (1999) 'Microglia derive from progenitors, originating from the yolk sac, and which proliferate in the brain', *Brain Res Dev Brain Res,* 117(2), pp. 145-152.

Ampomah, P.B., Cai, B., Sukka, S.R., Gerlach, B.D., Yurdagul, A., Jr., Wang, X., Kuriakose, G., Darville, L.N.F., Sun, Y., Sidoli, S., Koomen, J.M., Tall, A.R. and Tabas, I. (2022) 'Macrophages use apoptotic cell-derived methionine and DNMT3A during efferocytosis to promote tissue resolution', *Nat Metab,* 4(4), pp. 444-457.

Aziz, M., Yang, W.L. and Wang, P. (2013) 'Measurement of phagocytic engulfment of apoptotic cells by macrophages using pHrodo succinimidyl ester', *Curr Protoc Immunol,* Chapter 14, p. Unit 14.31.

Berglund, R., Guerreiro-Cacais, A.O., Adzemovic, M.Z., Zeitelhofer, M., Lund, H., Ewing, E., Ruhrmann, S., Nutma, E., Parsa, R., Thessen-Hedreul, M., Amor, S., Harris, R.A., Olsson, T. and Jagodic, M. (2020) 'Microglial autophagy-associated phagocytosis is essential for recovery from neuroinflammation', *Sci Immunol,* 5(52).

Cai, W., Dai, X., Chen, J., Zhao, J., Xu, M., Zhang, L., Yang, B., Zhang, W., Rocha, M., Nakao, T., Kofler, J., Shi, Y., Stetler, R.A., Hu, X. and Chen, J. (2019) 'STAT6/Arg1 promotes microglia/macrophage efferocytosis and inflammation resolution in stroke mice', *JCI Insight,* 4(20).

Cheng, J., Liao, Y., Dong, Y., Hu, H., Yang, N., Kong, X., Li, S., Li, X., Guo, J., Qin, L., Yu, J., Ma, C., Li, J., Li, M., Tang, B. and Yuan, Z. (2020) 'Microglial autophagy defect causes parkinson disease-like symptoms by accelerating inflammasome activation in mice', *Autophagy,* 16(12), pp. 2193-2205.

Cho, M.H., Cho, K., Kang, H.J., Jeon, E.Y., Kim, H.S., Kwon, H.J., Kim, H.M., Kim, D.H. and Yoon, S.Y. (2014) 'Autophagy in microglia degrades extracellular β-amyloid fibrils and regulates the NLRP3 inflammasome', *Autophagy,* 10(10), pp. 1761-1775.

Dibble, C.C. and Manning, B.D. (2013) 'Signal integration by mTORC1 coordinates nutrient input with biosynthetic output', *Nat Cell Biol,* 15(6), pp. 555-564.

Heckmann, B.L., Teubner, B.J.W., Tummers, B., Boada-Romero, E., Harris, L., Yang, M., Guy, C.S., Zakharenko, S.S. and Green, D.R. (2019) 'LC3-Associated Endocytosis Facilitates beta-Amyloid Clearance and Mitigates Neurodegeneration in Murine Alzheimer's Disease', *Cell,* 178(3), pp. 536-551.e514.

Huang, Y. and Lemke, G. (2022) 'Early death in a mouse model of Alzheimer's disease exacerbated by microglial loss of TAM receptor signaling', *Proc Natl Acad Sci U S A,* 119(41), p. e2204306119.

Jung, H., Lee, S.Y., Lim, S., Choi, H.R., Choi, Y., Kim, M., Kim, S., Lee, Y., Han, K.H., Chung, W.S. and Kim, C.H. (2022) 'Anti-inflammatory clearance of amyloid-β by a chimeric Gas6 fusion protein', *Nat Med,* 28(9), pp. 1802-1812.

Krajcovic, M., Krishna, S., Akkari, L., Joyce, J.A. and Overholtzer, M. (2013) 'mTOR regulates phagosome and entotic vacuole fission', *Mol Biol Cell,* 24(23), pp. 3736-3745.

Lampron, A., Larochelle, A., Laflamme, N., Préfontaine, P., Plante, M.M., Sánchez, M.G., Yong, V.W., Stys, P.K., Tremblay, M. and Rivest, S. (2015) 'Inefficient clearance of myelin debris by microglia impairs remyelinating processes', *J Exp Med,* 212(4), pp. 481-495.

Márquez-Ropero, M., Benito, E., Plaza-Zabala, A. and Sierra, A. (2020) 'Microglial Corpse Clearance: Lessons From Macrophages', *Front Immunol,* 11, p. 506.

Martinez, J., Almendinger, J., Oberst, A., Ness, R., Dillon, C.P., Fitzgerald, P., Hengartner, M.O. and Green, D.R. (2011) 'Microtubule-associated protein 1 light chain 3 alpha (LC3)-associated phagocytosis is required for the efficient clearance of dead cells', *Proc Natl Acad Sci U S A,* 108(42), pp. 17396-17401.

Martinez, J., Malireddi, R.K., Lu, Q., Cunha, L.D., Pelletier, S., Gingras, S., Orchard, R., Guan, J.L., Tan, H., Peng, J., Kanneganti, T.D., Virgin, H.W. and Green, D.R. (2015) 'Molecular characterization of LC3-associated phagocytosis reveals distinct roles for Rubicon, NOX2 and autophagy proteins', *Nat Cell Biol,* 17(7), pp. 893-906.

Merlin, J., Ivanov, S., Dumont, A., Sergushichev, A., Gall, J., Stunault, M., Ayrault, M., Vaillant, N., Castiglione, A., Swain, A., Orange, F., Gallerand, A., Berton, T., Martin, J.C., Carobbio, S., Masson, J., Gaisler-Salomon, I., Maechler, P., Rayport, S., Sluimer, J.C., Biessen, E.A.L., Guinamard, R.R., Gautier, E.L., Thorp, E.B., Artyomov, M.N. and Yvan-Charvet, L. (2021) 'Non-canonical glutamine

transamination sustains efferocytosis by coupling redox buffering to oxidative phosphorylation', *Nat Metab,* 3(10), pp. 1313-1326.

Miksa, M., Komura, H., Wu, R., Shah, K.G. and Wang, P. (2009) 'A novel method to determine the engulfment of apoptotic cells by macrophages using pHrodo succinimidyl ester', *J Immunol Methods,* 342(1-2), pp. 71-77.

Nakahashi-Oda, C., Fujiyama, S., Nakazawa, Y., Kanemaru, K., Wang, Y., Lyu, W., Shichita, T., Kitaura, J., Abe, F. and Shibuya, A. (2021) 'CD300a blockade enhances efferocytosis by infiltrating myeloid cells and ameliorates neuronal deficit after ischemic stroke', *Sci Immunol,* 6(64), p. eabe7915.

Onodera, J. and Ohsumi, Y. (2005) 'Autophagy is required for maintenance of amino acid levels and protein synthesis under nitrogen starvation', *J Biol Chem,* 280(36), pp. 31582-31586.

Pickford, F., Masliah, E., Britschgi, M., Lucin, K., Narasimhan, R., Jaeger, P.A., Small, S., Spencer, B., Rockenstein, E., Levine, B. and Wyss-Coray, T. (2008) 'The autophagy-related protein beclin 1 shows reduced expression in early Alzheimer disease and regulates amyloid beta accumulation in mice', *J Clin Invest,* 118(6), pp. 2190-2199.

Qin, Y., Qiu, J., Wang, P., Liu, J., Zhao, Y., Jiang, F. and Lou, H. (2021) 'Impaired autophagy in microglia aggravates dopaminergic neurodegeneration by regulating NLRP3 inflammasome activation in experimental models of Parkinson's disease', *Brain Behav Immun,* 91, pp. 324-338.

Raymond, M.H., Davidson, A.J., Shen, Y., Tudor, D.R., Lucas, C.D., Morioka, S., Perry, J.S.A., Krapivkina, J., Perrais, D., Schumacher, L.J., Campbell, R.E., Wood, W. and Ravichandran, K.S. (2022) 'Live cell tracking of macrophage efferocytosis during Drosophila embryo development in vivo', *Science,* 375(6585), pp. 1182-1187.

van Leeuwen, W., van der Krift, F. and Rabouille, C. (2018) 'Modulation of the secretory pathway by amino-acid starvation', *J Cell Biol,* 217(7), pp. 2261-2271.

Yurdagul, A., Jr., Subramanian, M., Wang, X., Crown, S.B., Ilkayeva, O.R., Darville, L., Kolluru, G.K., Rymond, C.C., Gerlach, B.D., Zheng, Z., Kuriakose, G., Kevil, C.G., Koomen, J.M., Cleveland, J.L., Muoio, D.M. and Tabas, I. (2020) 'Macrophage Metabolism of Apoptotic Cell-Derived Arginine Promotes Continual Efferocytosis and Resolution of Injury', *Cell Metab,* 31(3), pp. 518-533.e510.

Zhang, S., Weinberg, S., DeBerge, M., Gainullina, A., Schipma, M., Kinchen, J.M., Ben-Sahra, I., Gius, D.R., Yvan-Charvet, L., Chandel, N.S., Schumacker, P.T. and Thorp, E.B. (2019) 'Efferocytosis Fuels Requirements of Fatty Acid Oxidation and the Electron Transport Chain to Polarize Macrophages for Tissue Repair', *Cell Metab,* 29(2), pp. 443-456.e445.

Zhou, J., Tan, S.H., Nicolas, V., Bauvy, C., Yang, N.D., Zhang, J., Xue, Y., Codogno, P. and Shen, H.M. (2013) 'Activation of lysosomal function in the course of autophagy via mTORC1 suppression and autophagosome-lysosome fusion', *Cell Res,* 23(4), pp. 508-523.

CHAPTER 3

Materials

Resource	Source	Identifier
3.1 ANTIBODIES		
Rat anti-F4/80	Cell Signalling	40781
Rabbit anti-mCherry	Abcam	ab167453
Rabbit anti-GFP	Invitrogen	A-6455
Rabbit anti-SNX17	Cell Signalling	75885
Rabbit anti-ATG2B	Invitrogen	PA5-85718
Rabbit anti-LC3B	Novus Biologicals	NB1100-2220
Rabbit anti-SQSTM1	MBL	PM045
Rabbit anti-COL1A1	Cell Signalling	91144
Rabbit anti-S6K	Cell Signalling	2708
Rabbit anti-phospho-S6K	Cell Signalling	9234
Rabbit anti-phospho-ULK1	Cell Signalling	6888
Mouse anti-STAT3	Cell Signalling	9139
Mouse anti-phospho-STAT3	Cell Signalling	9145
Mouse anti-LC3B	Cell Signalling	83506
Mouse anti-Puromycin	Merck	MABE343
Mouse anti-ACTB-HRP	Sigma Aldrich	A3854
Goat anti-Cathepsin D	R&D Systems	AF1183
Sheep anti-Lamp1	In-house (Hassiotis *et al.*, 2018)	
Donkey anti-mouse IgG Cy3	Jackson Immuno	715-165-150
Donkey anti-sheep IgG Alexa 488	Jackson Immuno	713-545-003
Donkey anti-rabbit IgG Alexa 647	Jackson Immuno	711-605-152
Goat anti-mouse IgG HRP	Biorad	1706516
Goat anti-rabbit IgG HRP	Millipore	AP307P
Donkey anti-sheep/goat IgG HRP	Millipore	AB324P
3.2 REAGENTS AND CHEMICALS		
DAPI	Biolegend	422801

Chloroquine	Sigma Aldrich	C6628
AZD8055	Selleckchem	S1555
Cycloheximide	Sigma Aldrich	C1988
Bafilomycin	Sigma Aldrich	SML1661
Methanol	Chem Supply	MA004
Poly-L-lysine	Sigma Aldrich	P8920
Vectashield mountant with DAPI	Vector Labs	H-1200
ProLong gold mountant with DAPI	Invitrogen	P36941
Eagle's Minimum Essential Medium (EMEM)	Sigma Aldrich	M4655
Roswell Park Memorial Institute (RPMI) 1640 Media	Gibco	21870076
Dulbecco's Modified Eagle Media (DMEM)	Gibco	10565018
Earle's Buffered Salt Solution (EBSS)	Sigma Aldrich	E2888
Hank's Buffered Salt Solution (HBSS)	Sigma Aldrich	H8264
Foetal Calf Serum (FCS)	Gibco	10099141
Phosphate Buffered Saline (PBS)	Gibco	10010023
Trypsin-EDTA	Gibco	15400054
L-Glutamine	Gibco	25030081
MEM amino acids	Gibco	11130051
Non-essential MEM amino acids	Gibco	11140050
EDTA protease inhibitor cocktail	Roche	4693132001
Sodium pyrophosphate	Sigma Aldrich	P8135
Sodium orthovanadate	Sigma Aldrich	S6508
β-Glycerophosphate	Sigma Aldrich	G9422
Tris base	Millipore	648310
Tween 20	Millipore	817072
Bolt LDS sample buffer	Thermo Fisher	B0007
Bolt reducing agent	Thermo Fisher	B0009

Precision Plus protein kaleidoscope standard	Biorad	1610375
Super Signal West Femto substrate	Thermo Fisher	34095
Super Signal West Pico substrate	Thermo Fisher	34580
3.3 COMMERCIAL ASSAYS AND KITS		
pHrodo Deep Red	Invitrogen	P35358
Lysotracker Green	Invitrogen	L7526
Cathepsin L Magic Red	Biorad	ICT942
BCA protein assay kit	Thermo Fisher	23225
Intracellular pH calibration kit	Invitrogen	P35379
Lipofectamine 3000	Invitrogen	L3000001
Lipofectamine RNA iMax	Invitrogen	13778075
Annexin Alexa 647	Biolegend	640911
Annexin binding buffer	Biolegend	422201
No-stain protein reagent	Invitrogen	A44449
3.4 ANIMALS AND CELL LINES		
C57BL/6	Jackson Laboratory	JAX000664
HMC3	ATCC	CRL-3304
THP-1	ATCC	TIB-202
HEK293T	ATCC	CRL-11268
3.5 PLASMIDS AND OLIGONUCLEOTIDES		
pCMV-VSV-G	Addgene, a gift from Bob Weinberg	8454
psPAX2	Addgene, a gift from Didier Trono	12260
pUltra-hot	Addgene, a gift from Malcolm Moore	24130
Lenti-tf-APP	In-house (Hein *et al.*, 2017)	

3.6 SOFTWARE		
BioRender	BioRender	https://www.biorender.com/
ImageJ version 1.54	(Schneider, Rasband and Eliceiri, 2012)	https://imagej.net/
FlowJo version 5.0	BD Life Sciences	https://www.flowjo.com/
GraphPad version 8.0	GraphPad	https://www.graphpad.com
RStudio version 3.3	R-project	https://posit.co/
ShinyGO version 0.77	(Ge, Jung and Yao, 2020)	https://ge-lab.org/go/

3.7 REFERENCES

Ge, S.X., Jung, D. and Yao, R. (2020) 'ShinyGO: a graphical gene-set enrichment tool for animals and plants', *Bioinformatics,* 36(8), pp. 2628-2629.

Hassiotis, S., Manavis, J., Blumbergs, P.C., Hattersley, K.J., Carosi, J.M., Kamei, M. and Sargeant, T.J. (2018) 'Lysosomal LAMP1 immunoreactivity exists in both diffuse and neuritic amyloid plaques in the human hippocampus', *Eur J Neurosci,* 47(9), pp. 1043-1053.

Hein, L.K., Apaja, P.M., Hattersley, K., Grose, R.H., Xie, J., Proud, C.G. and Sargeant, T.J. (2017) 'A novel fluorescent probe reveals starvation controls the commitment of amyloid precursor protein to the lysosome', *Biochim Biophys Acta Mol Cell Res,* 1864(10), pp. 1554-1565.

Schneider, C.A., Rasband, W.S. and Eliceiri, K.W. (2012) 'NIH Image to ImageJ: 25 years of image analysis', *Nat Methods,* 9(7), pp. 671-675.

CHAPTER 4

epHero – a tandem-fluorescent probe to track the fate of apoptotic cells during efferocytosis

Rationale: The work presented in this chapter addresses research objective 1, the development of a probe capable of tracking both early and late stages of efferocytosis, i.e., the uptake and acidification of apoptotic material, simultaneously.

4.1 INTRODUCTION

The human body turns over nearly four million cells per second (Sender and Milo, 2021). These cells are recognised and cleared in a process termed efferocytosis – derived from the Latin *effere*, which means 'to carry to the grave'. Under physiological conditions, apoptotic cells are rapidly removed by phagocytes – both professional and non-professional – resulting in a largely anti-inflammatory response and the maintenance of homeostasis (Doran, Yurdagul and Tabas, 2020). When this process is hampered, apoptotic cells undergo secondary necrosis, releasing intracellular material that causes inflammation and tissue necrosis (Cai *et al.*, 2016, Fadok *et al.*, 1998, Kumaran Satyanarayanan *et al.*, 2019). Perturbations in efferocytosis have been linked to several disease processes, including autoimmunity (Geng *et al.*, 2022, Jorge *et al.*, 2022), atherosclerosis (Yurdagul *et al.*, 2017), and the tumour microenvironment (Lang *et al.*, 2022).

At present, techniques to measure efferocytosis involve the flow cytometric or microscopic analysis of phagocytes ingesting labelled targets (Aziz, Yang and Wang, 2013, Miksa *et al.*, 2009). Flow cytometry enables the analysis of hundreds of thousands of cells in a relatively

short period of time; it does not, however, permit discrimination between material that has merely bound to the surface of phagocytes from that which has been internalised. Whilst microscopic examination allows this distinction to be made, it can be challenging to perform in a high throughput manner and may be inaccessible to some laboratories due to the large cost, time and complexity involved. Several groups have attempted to circumvent this issue by labelling targets with pH-sensitive dyes such as pHrodo (Aziz, Yang and Wang, 2013, Miksa *et al.*, 2009) and CypHer5E (Kumaran Satyanarayanan *et al.*, 2019). These dyes exhibit minimal fluorescence in high pH environments. Upon encountering a low pH, such as within a phagosome, they fluoresce brightly: this ensures that surface-bound targets are excluded from all analyses. While this can be beneficial in some circumstances, the binding and recognition of apoptotic cells by phagocytes is a crucial first step in efferocytosis, and this is not measurable using pH-sensitive dyes. Further, since pHrodo has a single pKa (Riazanski, Sui and Nelson, 2020) the degradation of apoptotic material cannot be tracked using this method, as an increase in pHrodo signal could indicate either greater uptake or acidification of cargo by phagocytes.

To address these gaps, we have adapted a concept employed in the field of autophagy (Kimura, Noda and Yoshimori, 2007) – which studies the degradation of intracellular material. We have constructed a novel tandem-fluorescent probe called ‘epHero’, which comprises an mCherry-eGFP fusion protein, to discriminate between efferocytic uptake and degradation. eGFP has a pKa of 6 (Haupts *et al.*, 1998, Kneen *et al.*, 1998), causing its fluorescence to quench in mildly acidic environments such as those found within a late endosome or phagosome. In contrast, mCherry has a lower pKa of 4.5 (Campbell *et al.*, 2002) and is resistant to lysosomal proteases (Katayama *et al.*, 2008), enabling it to continue fluorescing

even within the acidic lysosome. By expressing this tandem probe in apoptotic cells, these differences between eGFP and mCherry fluorophores can be used to track the internalisation and degradation of apoptotic cargo within phagocytes. We show that epHero is a simple, cost-effective probe that can be used to monitor the dynamics of apoptotic corpse clearance both *in vitro* and in mice.

4.2 METHODS

Animals

All animal experiments were approved by the South Australian Health and Medical Research Institute (SAHMRI) Animal Ethics Committee (SAM-20-075) and conducted in accordance with the *NHMRC Australian Code for the Care and Use of Animals for Scientific Purposes 2018*. C57BL/6J mice were obtained from an established breeding colony at SAHMRI and housed under standard conditions with a 12 hr day/night cycle and *ad libitum* access to food and water.

Cell culture

HMC3 microglial cells were obtained from ATCC and cultured in EMEM containing 10% FCS. THP1 monocytes were purchased from ATCC and maintained in RPMI 1640 medium supplemented with 10% FCS and 2 mM L-glutamine. THP1 monocytes were differentiated into macrophages via the addition of 81 nM phorbol 12-myristate 13-acetate (PMA) for 48 hr. Following this, cells were allowed to recover in PMA-free medium for a further 24 hr before being used in experiments. HEK293T cells were purchased from ATCC and cultured in DMEM with 10% FCS.

All cell lines used in this study were maintained at 37°C with 5% CO_2, and routinely screened for mycoplasma infection.

Generation of mCherry-eGFP expressing bait cells

Production of mCherry-eGFP lentiviral plasmid: the mCherry-eGFP coding sequence was PCR-amplified from Lenti-tf-APP (Hein *et al.*, 2017) using the following primers: Forward 5' – taagcaaccggtatgGTGAGCAAGGGCGAGGA and reverse 3' – gtggccctgagaattcTTTACTTGTACAGCTCGTCCAT. The PCR amplicon was flanked by a 5' AgeI and 3' EcoRI site to facilitate restriction cloning into the pUltraHot vector (Addgene plasmid #24130, a gift from Malcolm Moore). Restriction digestion of the vector and PCR amplicon with AgeI and EcoRI enabled directional ligation of mCherry-eGFP into the pUltraHot backbone to create a pUltraHot-mCherry-eGFP plasmid.

Lentiviral transduction: HEK293T cells were plated at 1.5 x 10^5 cells per well in two wells of a six-well plate and grown overnight. The following morning cells were transfected with 5 μg mCherry-eGFP-expressing lentivector, 4 μg psPAX2 (Addgene plasmid #12260, a gift from Didier Trono) and 4 μg pCMV-VSV-G (Addgene plasmid #8454, a gift from Bob Weinberg) using Lipofectamine 3000, according to the manufacturer's instructions. The next day, THP1 target cells were seeded in two wells of a six-well plate at 1.5 x 10^5 cells per well and maintained overnight. Two days post-transfection of HEK293T cells, culture medium containing mCherry-eGFP-expressing lentivirus was filtered using a 0.45 μM filter and polybrene added at a final concentration of 4 μg/mL. This medium was used to infect THP1 target cells overnight. The following day, virus-containing medium was replaced with complete growth medium, and THP1 cells were maintained until flow cytometry analysis.

Generation of stable monoclonal cell lines: lentivirus transduced cells were harvested, and mCherry-eGFP double-positive cells were sorted into 96-well plates at 1 cell per well on a BDAria Fusion cell sorter. Sorted cells were maintained in RPMI containing 20% FCS for up to 14 days for expansion into single colonies. Colonies were screened using fluorescence microscopy, and those with stable, moderate- to high expression of mCherry and eGFP were allowed to amplify further by sequentially transferring them to 24-, 12- and six-well plates. Clonal cell lines were analysed using flow cytometry on a BDFortessa, and those with high, consistent fluorescence peaks for both mCherry and eGFP with minimal variation were deemed the best clones and selected for all future experiments.

Induction and verification of apoptosis in bait cells

THP1 bait cells expressing mCherry-eGFP were rendered apoptotic via UV irradiation at 316 nm for 3-4 min, following which they were incubated for 3 hr at 37°C with 5% CO_2. Apoptosis was confirmed by Annexin V-Alexa Fluor® 647 staining according to the manufacturer's instructions. Briefly, cells were pelleted and re-suspended in Annexin V binding buffer containing 0.25 μg/mL Annexin V-Alexa Fluor® 647 and 1 μg/mL DAPI and incubated in the dark for 15 min at room temperature before being washed with PBS. A live-dead cell cocktail was utilised to set the appropriate gating controls. All samples were analysed on a BDFortessa cytometer with >20,000 events recorded per condition.

***In vitro* efferocytosis assay**

HMC3 microglia or PMA-differentiated THP1 macrophages were seeded in a 12-well plate at 1 x 10^5 cells per well and maintained overnight. The following day, apoptotic bait cells were

prepared as described above and added to the phagocytes at a 5:1 bait to phagocyte ratio for the indicated times. Phagocytes underwent three PBS washes to remove any unattached bait, were dissociated from the plate using trypsin to cleave un-internalised bait, and then analysed using flow cytometry. For pHrodo-based efferocytosis experiments, apoptotic THP1 cells were labelled with pHrodo Deep Red as per manufacturer's instructions. Where indicated, phagocytes were pre-treated with 10 μM cytochalasin D, 100 nM bafilomycin A1 or 50 μM chloroquine for 10 min before the addition of bait cells.

Ex vivo efferocytosis measurements

Apoptotic epHero bait cells were prepared as described above. Mice were intraperitoneally injected with either chloroquine (50 mg/kg) or saline, as well as 4 x 10^5 apoptotic cells re-suspended in 200 μL of HBSS. Mice injected with either no cells or non-fluorescent apoptotic THP1 cells served as the control. At 1- or 4 hr post-injection, mice were humanely culled and peritoneal cavity lavage was performed. Recovered cells were pelleted, resuspended in FACS buffer and stained with F4/80 (1:40) for 30 min on ice. Cells were then washed and resuspended in FACS buffer. Flow cytometry measurements were performed on a BDFortessa with gating based on unstained cells and mice not injected with apoptotic epHero bait. Both male and female mice were used in this study. All flow cytometry data were analysed on FlowJo™ version 10.8 (BD Life Sciences).

Western blotting

THP1 or epHero THP1 cells were rendered apoptotic as described above, pelleted, and resuspended in cell lysis buffer containing protease and phosphatase inhibitors. Samples were sonicated on ice, and protein concentration determined via a BCA assay. Following this,

10 μg protein was loaded per well and electrophoresed through 4-12% SDS-PAGE gels before being transferred to a PVDF membrane as previously described (Hein *et al.*, 2017). The membranes were blocked in a solution comprising Tris-buffered saline containing 0.1% (v/v) Tween 20 and 5% (w/v) skim milk and incubated overnight at 4°C with anti-mCherry (1:2,000) and anti-eGFP (1:1,000) antibodies. Incubation with HRP-conjugated anti-mouse or anti-rabbit secondary antibodies (1:10,000) was performed at room temperature for 1 hr. To detect β-actin, membranes were incubated with an HRP-conjugated anti-β-actin antibody (1:10,000) for 1 hr at room temperature. Membranes were developed on the LAS4000 Luminescent Image Analyser (Fujifilm Life Science) using the West Pico or West Femto ECL systems.

Confocal microscopy

THP1 or epHero THP1 cells were seeded into 12-well plates containing poly-L-lysine-coated coverslips at 1 x 10^5 cells per well and grown overnight. Non-adherent cells were aspirated, and coverslips fixed with 10% formalin for 10 min. Coverslips were washed twice with PBS, mounted onto slides using Vectashield Hardset with DAPI, and sealed with nail polish.

For live imaging, HMC3 cells were seeded into two-well chambered coverslips at 1 x 10^5 cells per well. The following day, epHero THP1 cells were rendered apoptotic and added to HMC3 cells at a 5:1 bait to phagocyte ratio as described above. Live imaging was performed in a humidified chamber at 37°C and 5% CO_2, with z-stacks (4-5 optical sections, z range ~ 3 μm) taken every 10 min for 2 hr. All images were acquired using a TCS SP8× confocal microscope with LASX (Leica, Germany) and imported into ImageJ for analysis.

Data analysis

All statistical analysis was performed using GraphPad version 8. Sample size and statistical tests for each experiment are detailed in the Figure legend. In general, data were analysed via either t-test, one-way or two-way ANOVA. Gaussian distribution was verified using a Shapiro-Wilk test, and either parametric or non-parametric analyses were performed accordingly. Data are presented as either individual data points or means with standard error bars as indicated in the Figure legends. $p \leq 0.05$ was considered statistically significant.

4.3 RESULTS

4.3.1 Development of mCherry-eGFP 'epHero' to measure efferocytic flux

The lumen of an apoptotic corpse-containing phagosome becomes more acidic as it matures along the phagosome-lysosome pathway (Yu *et al.*, 2022, Westman and Grinstein, 2020). To engineer a probe capable of measuring efferocytosis flux, we stably transduced THP1 cells with a tandem fluorescent mCherry-eGFP reporter, which we termed epHero (Figure 4.1A). eGFP has a low pKa and photo-quenches in acidic environments, such as those found within a lysosome (Kneen *et al.*, 1998). mCherry, on the other hand, is not an acid-sensitive fluorophore and stably fluoresces within cellular compartments including lysosomes (Campbell *et al.*, 2002, Katayama *et al.*, 2008). When cells expressing the epHero probe are rendered apoptotic and co-cultured with phagocytes, the ratio of mCherry to eGFP fluorescence in the phagocyte should increase over time, enabling the dissemination of corpse digestion and acidification (Figure 4.1B). We verified expression of our tandem-fluorescent reporter in both live (Figure 4.1C) and apoptotic cells (Figure 4.1D).

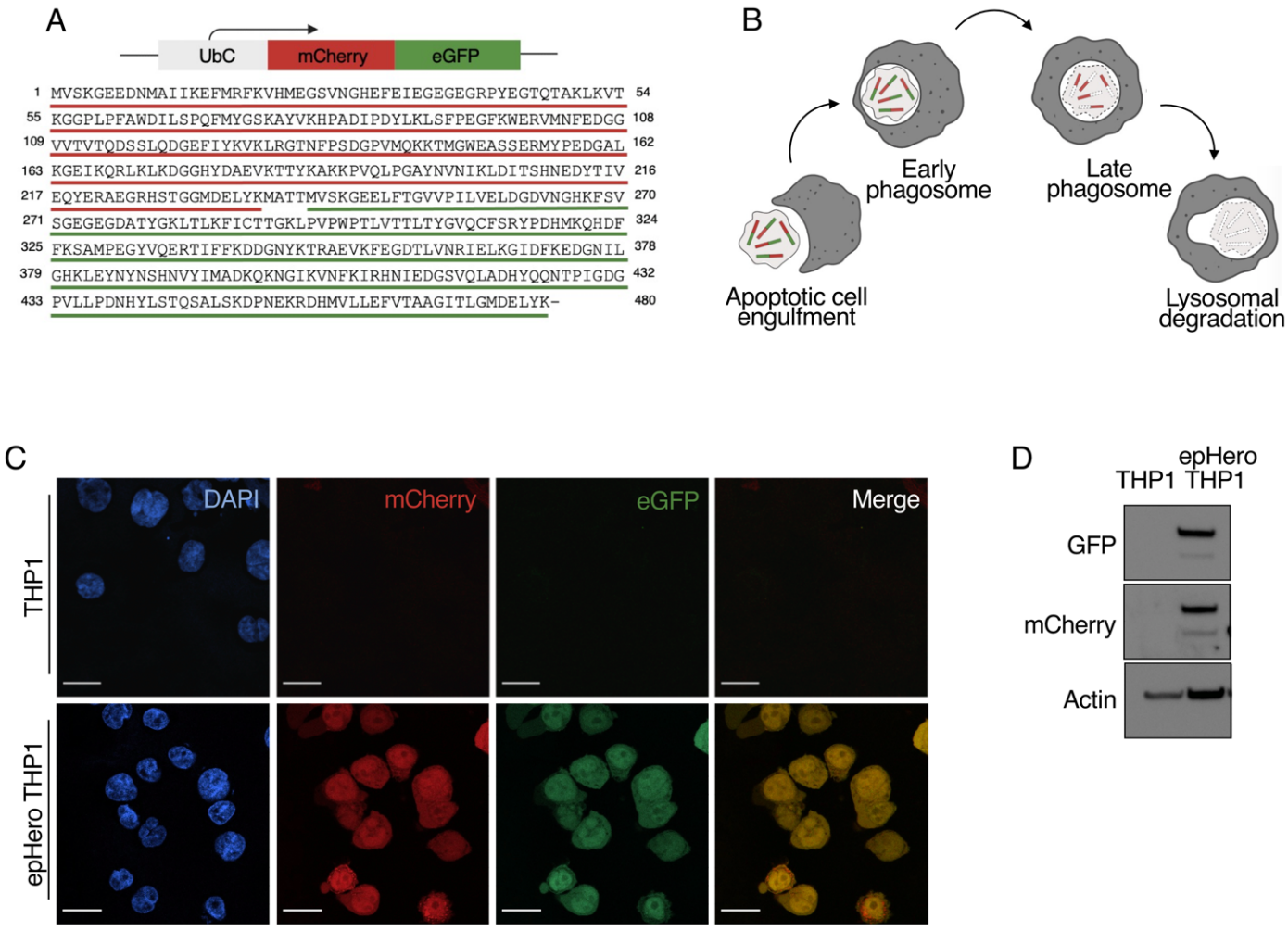

Figure 4.1 Designing a tandem-fluorescent reporter to measure efferocytosis flux.

(A) Amino acid sequence of the epHero reporter. Red, green: sequence encoding the mCherry and eGFP proteins, respectively, downstream of the ubiquitin C promoter. **(B)** Schematic of epHero probe. When expressed in apoptotic cells, changes in red and green fluorescence can be used to measure trafficking along the phagosome-lysosome pathway. **(C)** Confocal imaging of wild-type and epHero-transduced THP1 cells. Scale bar 15 μm. **(D)** Immunoblots of apoptotic wild-type and epHero-transduced THP1 cell lysates probed for mCherry and eGFP.

4.3.2 Expression of epHero in cells enables the quantification of efferocytosis following induction of apoptosis

We used UV radiation to induce apoptosis (Rehemtulla *et al.*, 1997) in THP1 cells stably transduced with the epHero reporter. This generated an Annexin V+ DAPI- early apoptotic cell population (Figure 4.2A–B). DAPI+ cells were considered late apoptotic/necrotic. The entire 'bait' cell mixture comprising viable, early apoptotic and necrotic cells was utilised in all subsequent efferocytosis experiments. In a physiological context, it is unlikely for phagocytes to be surrounded solely by apoptotic cells (Shin *et al.*, 2019). Therefore, exposing phagocytes in culture to a heterogenous mixture containing both putative efferocytosis targets and non-apoptotic cells provides a better representation of apoptotic cell clearance in an organism. To verify our probe's specificity, we pre-treated microglia with cytochalasin D, an actin polymerisation inhibitor which prevents the uptake of apoptotic cells (Casella, Flanagan and Lin, 1981), before performing the efferocytosis assay. As expected, cytochalasin D reduced the uptake of epHero bait (Figure 4.2C, F). To ensure that our assay was capturing true efferocytosis events and not the entotic cannibalism of live cells (Overholtzer *et al.*, 2007) we co-cultured both live and UV-irradiated epHero bait cells separately with microglia and measured microglial fluorescence. The uptake of epHero bait was markedly reduced in microglia co-cultured with live cells, suggesting little contribution of live cell uptake to our efferocytosis measurements (Figure 4.2 D,G). Previous work has shown that the binding and engulfment of apoptotic cells by phagocytes is dependent on the ratio of target cells to phagocytes (Wang *et al.*, 2017). We tested our probe's ability to detect these changes in apoptotic cell uptake by co-culturing microglia with varying ratios of bait: phagocyte. In line with prior studies, our results showed that the uptake of apoptotic corpses increased when the ratio of corpses to phagocytes was higher (Figure 4.2E, H). Together, these data show

that our epHero-based probe can be utilised to detect changes in the uptake of apoptotic cells.

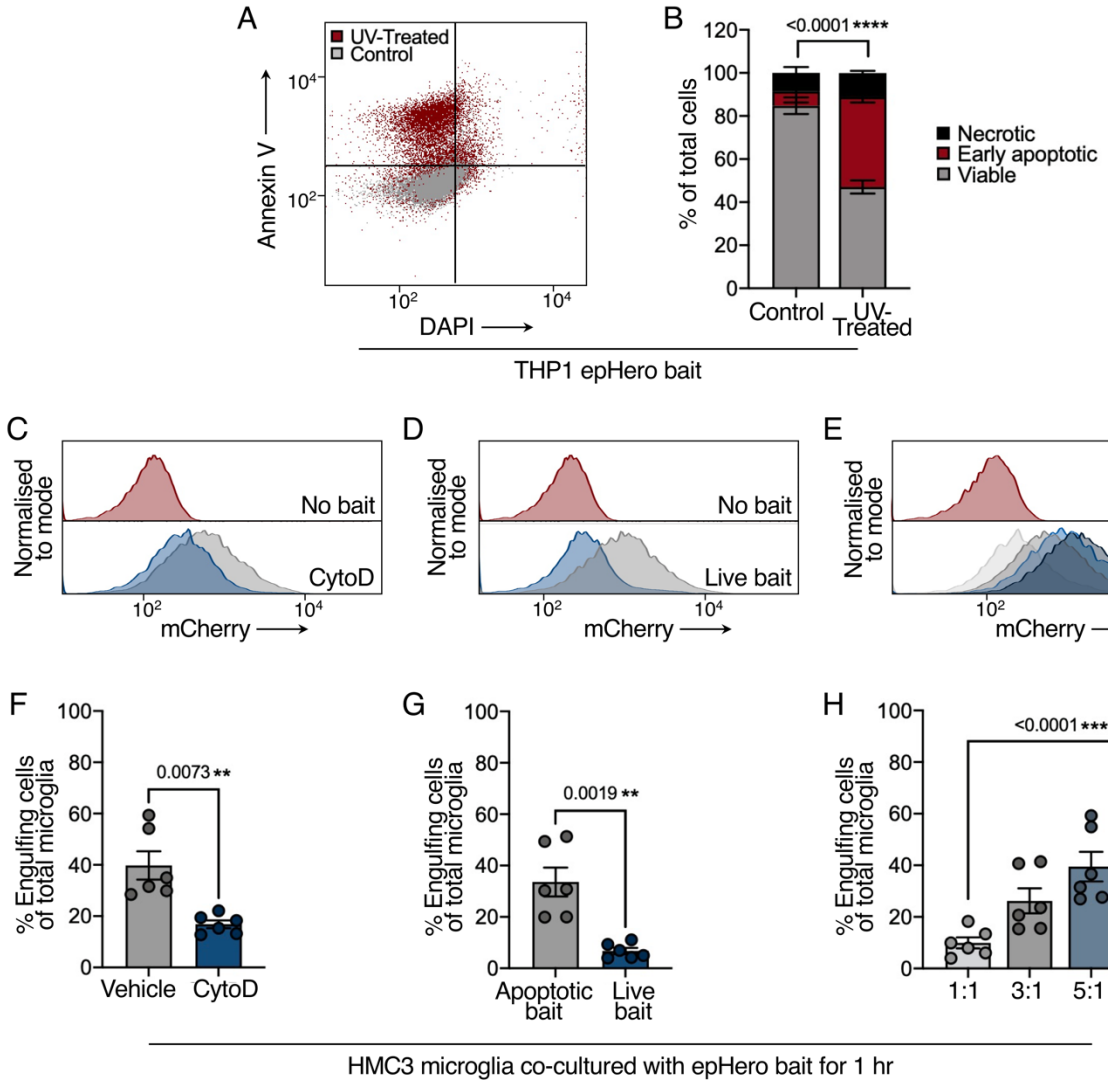

Figure 4.2 The epHero reporter can be used for the quantification of efferocytosis.

(A) Representative scatter plots from flow cytometry-based live-dead staining of epHero THP1 cells following UV-induced apoptosis. **(B)** Percentage of viable (Annexin V- DAPI-), early apoptotic (Annexin V+ DAPI-), and necrotic (Annexin V+ DAPI+ or Annexin V- DAPI+) cells from *(A).* Values represent the mean ± SEM from n = 5-6 across two independent experiments (two-way ANOVA with Šídák's multiple comparisons test; p value on graph represents the comparison of early apoptotic cells between the control and UV-treated

conditions). **(C)** Representative histograms of microglia treated with vehicle or 10 μM cytochalasin D (CytoD) for 10 min before being co-cultured with apoptotic epHero bait for 1 hr. **(D)** Histograms of microglia co-cultured with either live or UV-treated epHero bait for 1 hr before analysis via flow cytometry. **(E)** Representative histograms of microglia incubated with increasing bait:phagocyte ratios (left to right) of epHero bait for 1 hr. **(F)**,**(G)**,**(H)** Quantification of the percentage of phagocytosing cells from experiments depicted in *(C),(D)* and *(E),* respectively. Data represent mean ± SEM, with n = 6 from three independent experiments. P values are derived from either a t-test *(F,G),* or one-way ANOVA *(H)* with a test for linear left-to-right p-trend (H).

4.3.3 An epHero-based approach can be used to detect pH changes during efferocytosis

We next determined whether the epHero reporter could be employed to measure changes to the acidification and degradation of apoptotic corpses by phagocytes. First, we tested changes to the fluorescence of epHero bait cells in response to varying pH. Upon a reduction in pH, mCherry fluorescence remained stable whereas eGFP signal decreased (Figure 4.3A), highlighting the pH-responsive nature of our probe.

As phagosomes mature and fuse with lysosomes, their luminal pH decreases (Westman and Grinstein, 2020, Yu *et al.*, 2022). We modulated this process by treating phagocytes with chloroquine and bafilomycin A1, two inhibitors of phagosomal acidification that act via distinct mechanisms (Fedele and Proud, 2020, Yoshimori *et al.*, 1991). When chloroquine or bafilomycin-treated microglia were co-cultured with epHero bait, their corpse-containing phagosomes failed to acidify, as evidenced by the complete lack of mCherry/eGFP signal

development over time (Figure 4.3B–E). This occurred despite only minor changes to the uptake of apoptotic corpses by microglia (Supplementary Figure 4.2A–B). Next, we compared epHero to pHrodo, another pH-sensitive reporter that is commonly used to track efferocytosis (Miksa *et al.*, 2009). pHrodo-labelled targets exhibit weak signal in neutral environments, with their fluorescence increasing in a pH-dependent manner following cargo internalisation. We co-cultured microglia with epHero-expressing or pHrodo-labelled apoptotic bait and tracked fluorescent signal development within microglia over time. At early time-points (< 3 hr), signal development was comparable between the two probes. However, there was less uptake detected in microglia cultured with pHrodo-labelled bait at 6 hr (Figure 4.3F, $p = 0.0540$). Further, at 6 hr post-treatment there was a sizeable decrease in phagosome acidification as detected by pHrodo compared to epHero, likely due to the complete digestion of a subset of pHrodo-labelled cargo (Figure 4.3G) by phagocytes. In line with this, eGFP fluorescence was lowest 6 hr post-treatment (Supplementary Figure 4.2C), indicating that complete quenching of the pHrodo probe affects its ability to detect efferocytosis flux at its terminal stages. Thus, the epHero reporter is pH-sensitive and can detect changes to phagosomal acidification in phagocytes.

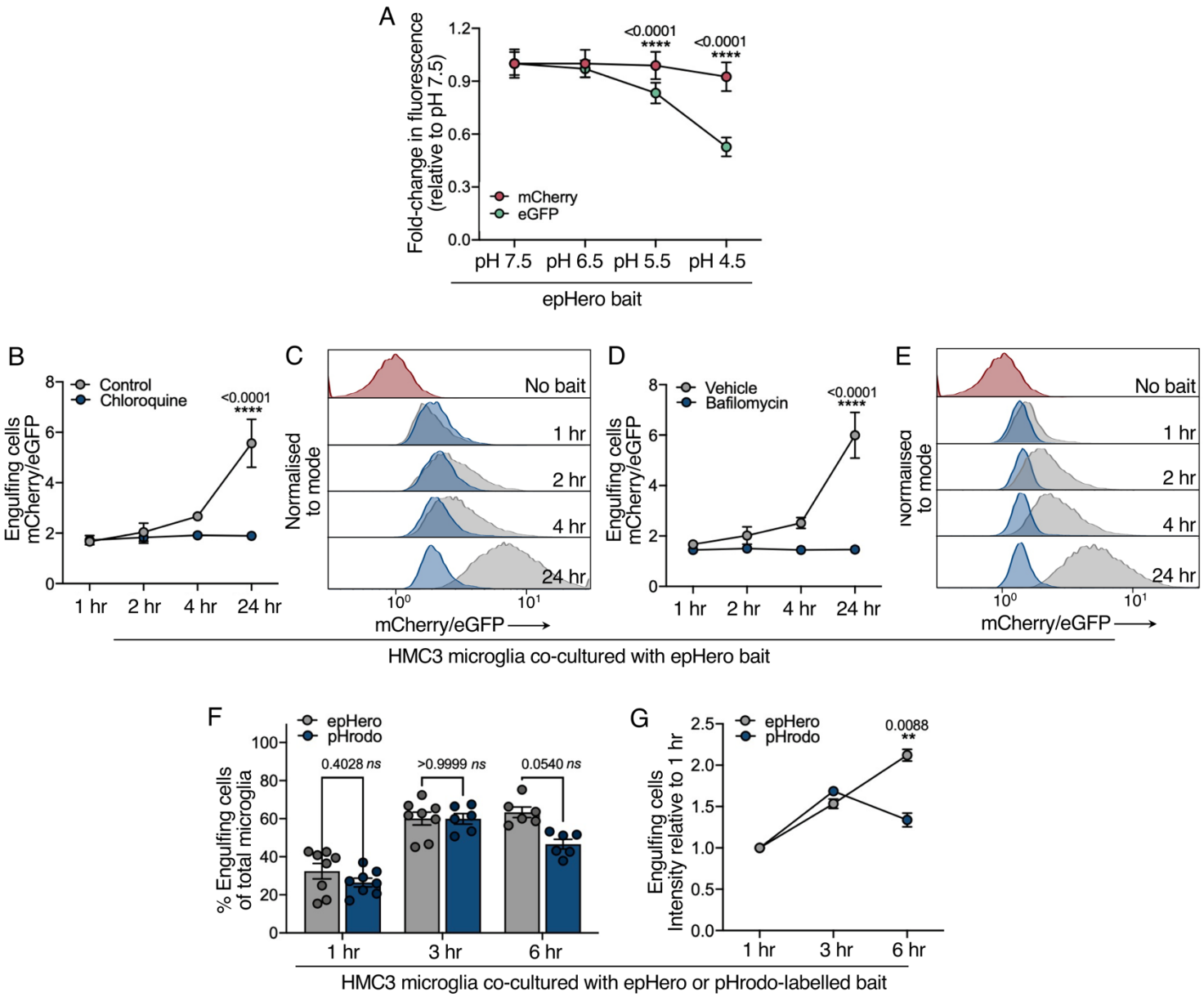

Figure 4.3 epHero is a pH-sensitive reporter of phagosomal acidification during efferocytosis. (A) Relative mCherry and eGFP signal from THP1 cells incubated in different pH buffers. Data represent mean ± SEM, n = 4 from two independent experiments (two-way ANOVA with Šídák's multiple comparisons test). **(B)** mCherry/eGFP ratio from microglia that have phagocytosed cargo after being co-cultured with apoptotic epHero bait for 1-, 2-, 4- or 24-hr, with or without 50 μM chloroquine. Data represent mean ± SEM from three independent experiments (two-way ANOVA with Šídák's multiple comparisons test). **(C)** Representative histograms from *(B).* Grey: Control; Blue: Chloroquine. **(D)** mCherry/eGFP

ratio from microglia that have phagocytosed cargo after being co-cultured with apoptotic epHero bait for 1-, 2-, 4- or 24-hr, with or without 100 nM bafilomycin. Values denote mean ± SEM from three independent experiments (two-way ANOVA with Šídák's multiple comparisons test for a difference between treatment groups at each time-point). **(E)** Representative histograms from *(D).* Grey: Vehicle; Blue: Bafilomycin. **(F)** Percentage of phagocytosing cells from microglia co-cultured with either epHero or pHrodo-labelled apoptotic THP1 bait for 1-, 3- or 6-hr. Data points centred on mean ± SEM; n = 6-8 from three- to four biologically independent experiments (two-way ANOVA with Šídák's multiple comparisons test). **(G)** epHero (mCherry/eGFP) or pHrodo signal intensity of phagocytosing microglia from *(F).* Data represent mean ± SEM from n = 6-8 across three- to four independent experiments (two-way ANOVA with Šídák's multiple comparisons test). *Abbreviations:* ns -not significant

4.3.4 The epHero reporter can track changes to efferocytosis over time

To determine whether our probe would be useful for tracking temporal changes in efferocytosis, we co-cultured microglia with apoptotic epHero bait for varying lengths of time. Live cell imaging revealed that the acidification of engulfed apoptotic cargo was detectable via microscopy (Figure 4.4A). Flow cytometry revealed that the proportion of efferocytic microglia increased over time (Figure 4.4B); examination of cell fluorescence showed an increase in the ratio of mCherry to eGFP signal – the readout of phagosomal acidification (Figure 4.4C). While mCherry fluorescence remained relatively stable, eGFP fluorescence decreased progressively as the corpse-containing phagosome matured and became more acidic over time (Figure 4.4D). Given that all our previous measurements were performed in human microglia, it was important to ensure that our probe was also capable of tracking

efferocytosis in macrophages. Consistent with our microglia data, incubating macrophages with epHero bait yielded both increased uptake and acidification of the apoptotic corpse-containing phagosome over time (Figure 4.4E–G). Taken together, these data demonstrate that epHero can be used to measure temporal changes in both cargo uptake and acidification during efferocytosis in different cell types.

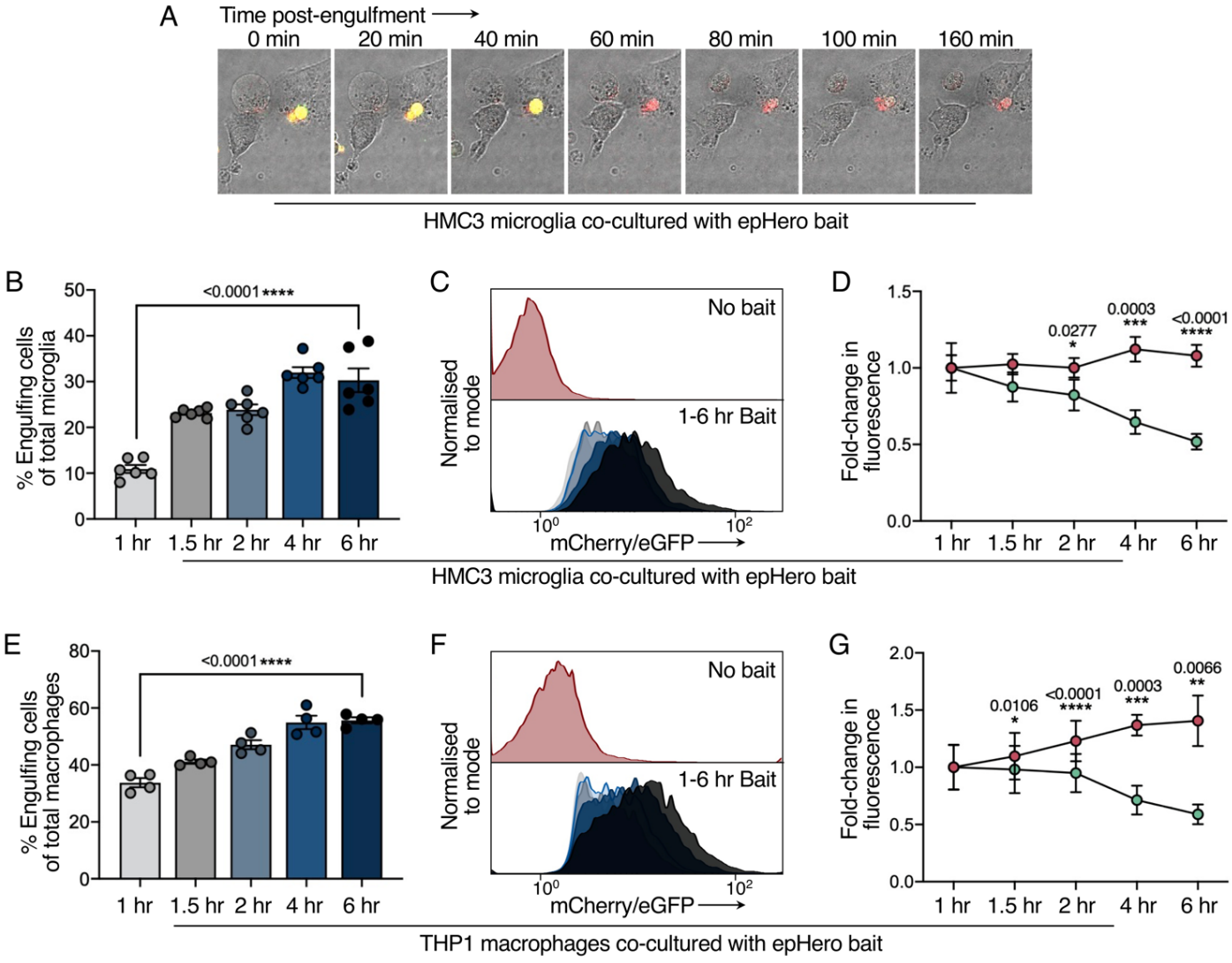

Figure 4.4 epHero can track changes in efferocytic flux over time. (A) Stills taken from confocal live imaging of microglia co-cultured with apoptotic epHero bait for 3 hr. **(B)** Percentage of phagocytosing cells from microglia co-cultured with apoptotic epHero bait for up to 6 hr. Data points centred on mean ± SEM with n = 6 from three independent

experiments (one-way ANOVA with test for linear left-to-right trend). **(C)** Representative flow cytometry histograms from *(B)*. **(D)** Fold-change in fluorescent signal (relative to 1 hr) over time in phagocytosing microglia from *(B).* Red: mCherry fluorescence; Green: eGFP fluorescence. Data points denote mean ± SD (two-way ANOVA with Šídák's multiple comparisons test). **(E)** Percentage of phagocytosing cells from THP1 macrophages co-cultured with apoptotic epHero bait for up to 6 hr. Data points centred on mean ± SEM with n = 4 from two independent experiments (one-way ANOVA with test for linear left-to-right p-trend). **(F)** Representative flow cytometry histograms from *(E)*. **(G)** Fold-change in fluorescence signal (relative to 1 hr) over time in phagocytosing THP1 macrophages from *(E).* Red: mCherry fluorescence; Green: eGFP fluorescence. Data points denote mean ± SD (two-way ANOVA with Šídák's multiple comparisons test).

4.3.5 The epHero probe can be used for the *ex vivo* measurement of efferocytic flux

Finally, we sought to ascertain whether the epHero reporter could be used to provide information on efferocytosis in organisms. The peritoneal cavity of mice contains a sizeable macrophage population, and the injection of material into the mouse peritoneal cavity is a well-established method to study *in vivo* phagocytosis by proxy (Stöhr *et al.*, 2018, Schappe *et al.*, 2022). We injected apoptotic epHero bait into the peritoneal cavity of mice and harvested the peritoneal exudate at 1- and 4 hr time-points. To further ensure that our probe provided a pH-sensitive measurement of efferocytosis, mice were also injected with either saline or the lysosomotropic agent chloroquine at the same time (Figure 4.5A). Akin to our *in vitro* measurements, the mCherry/eGFP ratio was higher at 4 hr compared to 1 hr post-injection, consistent with an increase in phagosomal acidification over time (Figure 4.5C–D). Chloroquine treatment abolished this response, with the macrophages from chloroquine-

injected mice having consistently reduced mCherry/eGFP ratios compared to their saline-injected counterparts. Further, this ratiometric response was primarily driven by changes to eGFP fluorescence, with mCherry fluorescence and cargo uptake remaining consistent between the saline and chloroquine treatment groups (Figure 4.5B). Overall, these results demonstrate that epHero can be used to simultaneously evaluate both cargo uptake and acidification during efferocytosis in mice.

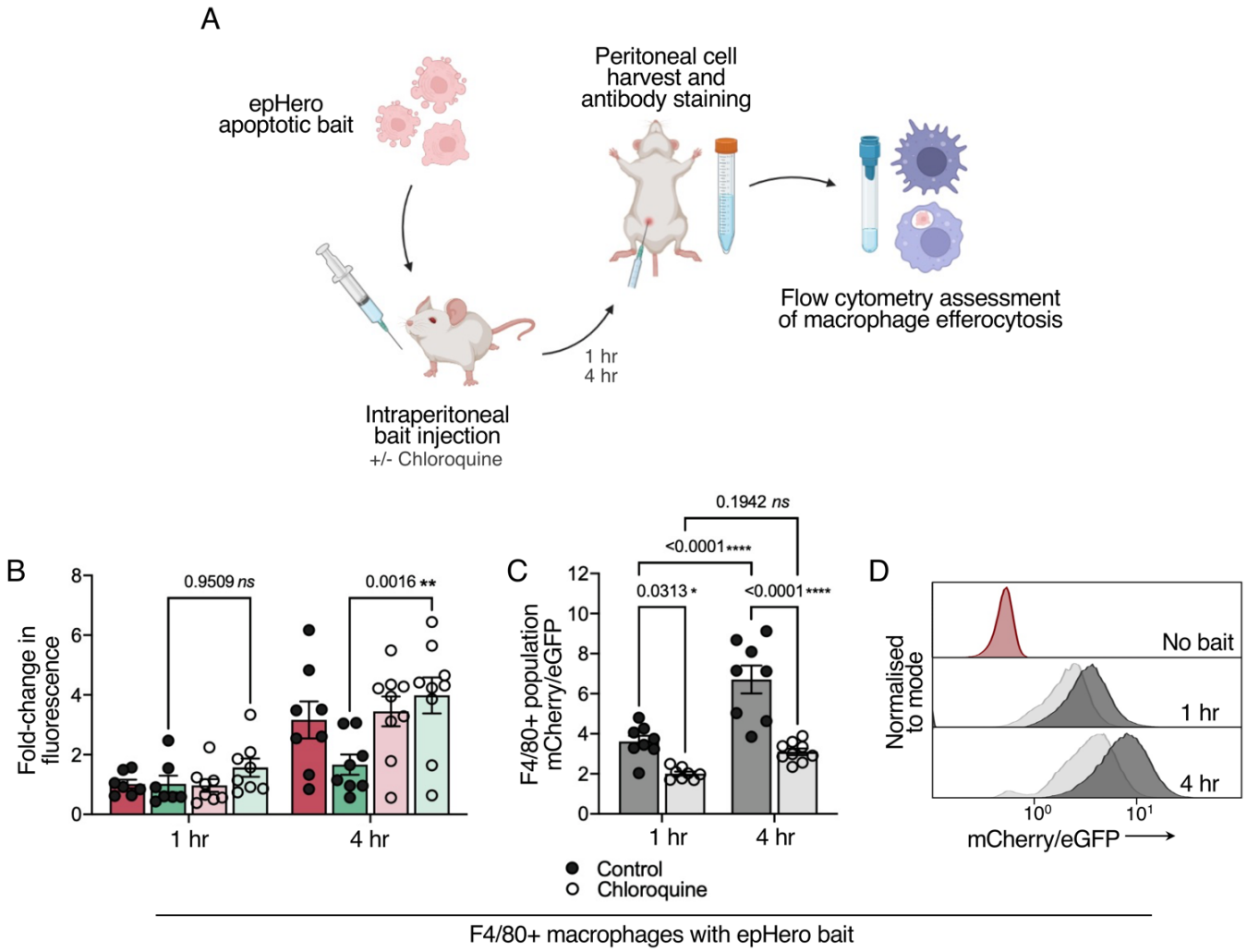

Figure 4.5. The epHero reporter is a pH-responsive measure of efferocytosis in mice.

(A) Schematic showing the experimental design to measure efferocytic flux in control or chloroquine-treated mice. **(B)** Fold-change in fluorescence (relative to 1 hr) in F4/80+

peritoneal macrophages from control (closed circles) or chloroquine-treated (open circles) mice 1- to 4 hr following injection with apoptotic epHero bait. Red: mCherry fluorescence; Green: eGFP fluorescence. Data points are centred on mean ± SEM, with 7-9 mice per condition (two-way ANOVA with Šídák's multiple comparisons test). **(C)** mCherry/eGFP ratio of F4/80+ peritoneal macrophages from *(B).* Error bars represent SEM, *n* = 7-9 mice per condition (two-way ANOVA with Šídák's multiple comparisons test). **(D).** Representative flow cytometry histograms denoting mCherry/eGFP from (*B).* Black: Control; Grey: Chloroquine. *Abbreviations:* ns - not significant.

4.4 DISCUSSION

The efficient removal of dead cells via efferocytosis is essential for maintaining homeostasis in an organism. Defects in this process have been implicated in a range of pathologies, from neurodegeneration (Etchegaray *et al.*, 2016) to cardiovascular disease (Yurdagul *et al.*, 2017) and autoimmune conditions (Geng *et al.*, 2022, Jorge *et al.*, 2022). Here, we have harnessed differences in the fluorescent properties of mCherry and eGFP to generate a tandem-fluorescent epHero probe capable of tracking the acidification of the apoptotic corpse-containing phagosome. We show that epHero is a specific pH-sensitive reporter of efferocytosis flux in both microglia- and macrophage-like cell lines and is compatible with flow cytometry and imaging modalities – two of the most widely used phagocytosis readouts in the field.

Efferocytosis is a multi-step process, comprising an initial 'find-me' stage where phagocytes respond to factors released by apoptotic cells by moving towards the site of injury, an 'eat-me' stage where phagocytic receptors make initial contact with ligands expressed by

apoptotic cells, and, finally, the internalisation and digestion of apoptotic cargo by the phagocyte (Doran, Yurdagul and Tabas, 2020). However, to date, the efferocytosis field has largely focused on the uptake and engulfment of apoptotic material, with few studies examining post-engulfment processes. This has been driven, at least in part, by the paucity of readily available techniques to track the fate of the apoptotic corpse after phagocytic engulfment. At present, the most widely used assay to measure efferocytosis involves labelling apoptotic cargo with pH-responsive dyes such as pHrodo (Aziz, Yang and Wang, 2013, Miksa *et al.*, 2009, Stöhr *et al.*, 2018) and CypHer (Kumaran Satyanarayanan *et al.*, 2019) which brightly fluoresce once the cargo has been taken up by phagocytes. This technique cannot provide a sensitive measure of cargo acidification because an increase in signal could be driven by changes in either uptake or acidification. Further, quenching of the pHrodo or CypHer signal could indicate complete cargo digestion or defects in acidification. These differences can only be elucidated by combining these techniques with temporal and imaging data, making this a time- and labour-intensive undertaking. We addressed some of these limitations with our dual fluorescent probe, which enabled simultaneous measurement of both the uptake and acidification of apoptotic cargo. We compared our epHero probe to pHrodo, the current gold-standard in the field, and demonstrated that at early time-points, epHero performs very similarly to pHrodo. However, 6 hr post-engulfment, there is a decrease in pHrodo signal compared to epHero. This is likely driven by lysosomal degradation of the pHrodo dye, whereas mCherry remains stable within lysosomes (Katayama *et al.*, 2008). If solely utilising the pHrodo probe, this decrease in both the proportion of pHrodo-containing cells and the total pHrodo signal could be misinterpreted as an overall decrease in efferocytosis rather than an increase in the acidification of phagosomal

cargo. Thus, while previous studies have attempted to address the challenges of measuring efferocytosis, our epHero reporter provides distinct advantages over existing approaches.

To date, efferocytosis has been mostly measured in macrophages, with the results extrapolated to microglia (Márquez-Ropero *et al.*, 2020). This is not ideal, as microglia have a different lineage to tissue macrophages and operate in the brain's unique environment (Alliot, Godin and Pessac, 1999). In the present study, we tested our epHero probe in both macrophage and microglial cell lines and showed that it can be used to track corpse clearance in a variety of phagocytes.

In recent years, several groups have reported the importance of phagosomal acidification and cargo degradation during efferocytosis (Yurdagul *et al.*, 2020, Schappe *et al.*, 2022), highlighting the need to successfully measure these processes. One study circumvented the limitations of conventional efferocytosis techniques by combining the pHrodo approach with GFP-expressing apoptotic cells, and employing the ratio of pHrodo to GFP fluorescence to measure acidification (Schappe *et al.*, 2022). However, the signal of a fluorescent dye and an intracellular fluorophore can vary greatly. Given that our tandem fluorescent approach bypasses the need for an extra labelling step and ensures that mCherry and eGFP are expressed in equal amounts and present within the same cellular compartments, we consider that our reporter offers several improvements over this technique. Another group has developed an efferocytosis tool based on engineered red and green fluorophores and utilised it to measure efferocytosis in *Drosophila* (Raymond et al., 2022), in an approach similar to our own. However, their probe is activated by caspase 3-induced cell death, which, while innovative, cannot be used to measure efferocytosis during caspase 3-independent

programmed cell death (Turner *et al.*, 2003, van Delft *et al.*, 2010). Additionally, our reporter relies on mCherry and eGFP fluorophores, which should be simple for most cell biology laboratories to repurpose for their own experiments. Further, we demonstrate that epHero can be used to detect changes to acidification during efferocytosis in mice.

In summary, our epHero reporter provides efferocytosis researchers with a new tool to concomitantly measure the uptake and acidification of apoptotic cargo, both *in vitro* and in *ex vivo* models of efferocytosis. By expressing this probe downstream of a cell type-specific driver, future studies could build on work reported here to provide a true *in vivo* measure of murine efferocytosis. With its ability to track efferocytosis over time, the epHero reporter can be used to dissect the molecular mechanisms underlying dead cell clearance and their role in health and disease.

4.5 SUPPLEMENTARY INFORMATION

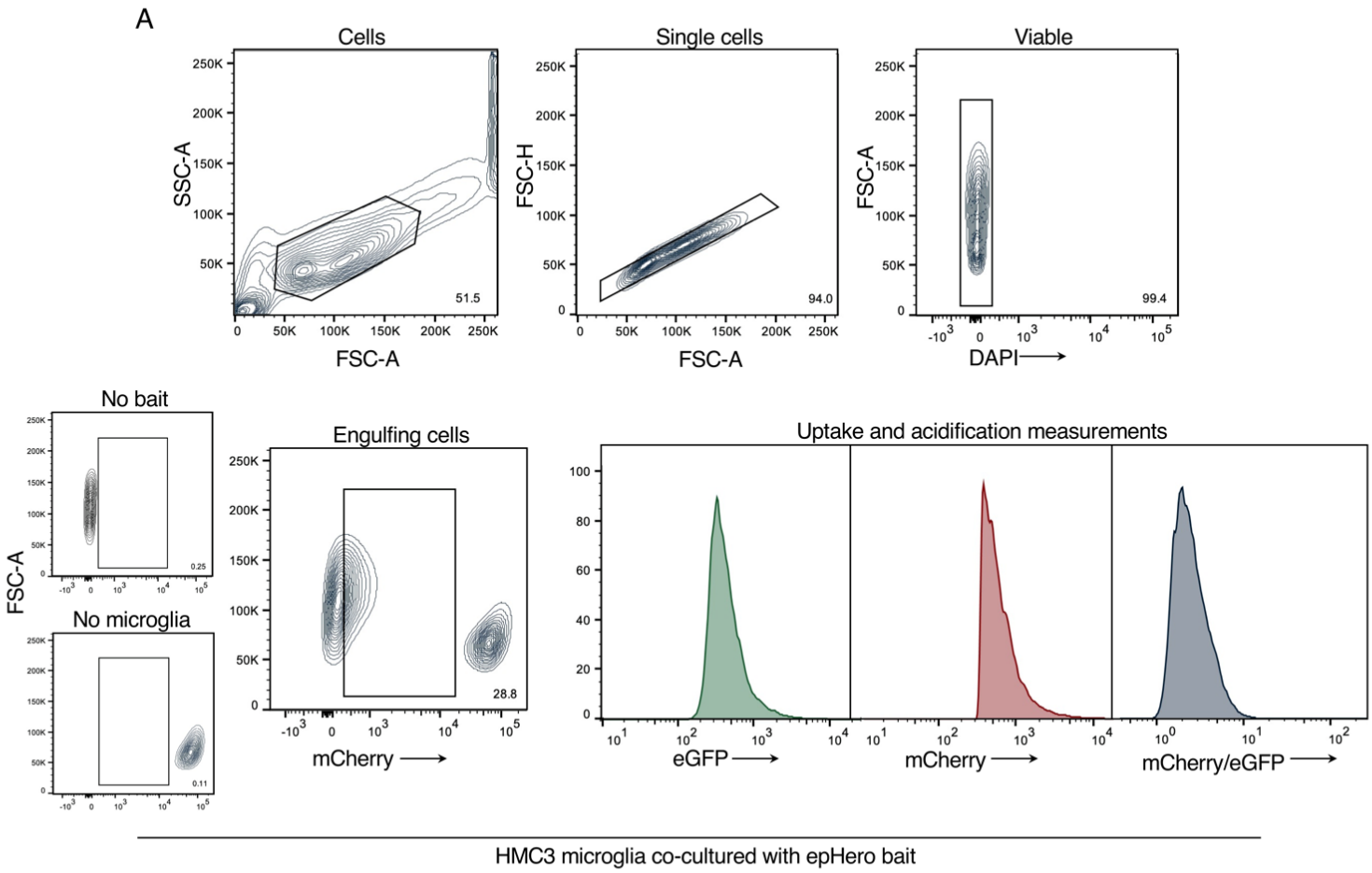

Supplementary Figure 4.1 Gating strategy for efferocytosis experiments.

(A) Schematic depicting the gating strategy used in efferocytosis assays. Viable cells were gated based on forward, side scatter, and DAPI staining. Leftover epHero bait cells were excluded, and microglia that had engulfed cargo were gated and analysed based on mCherry and eGFP fluorescence.

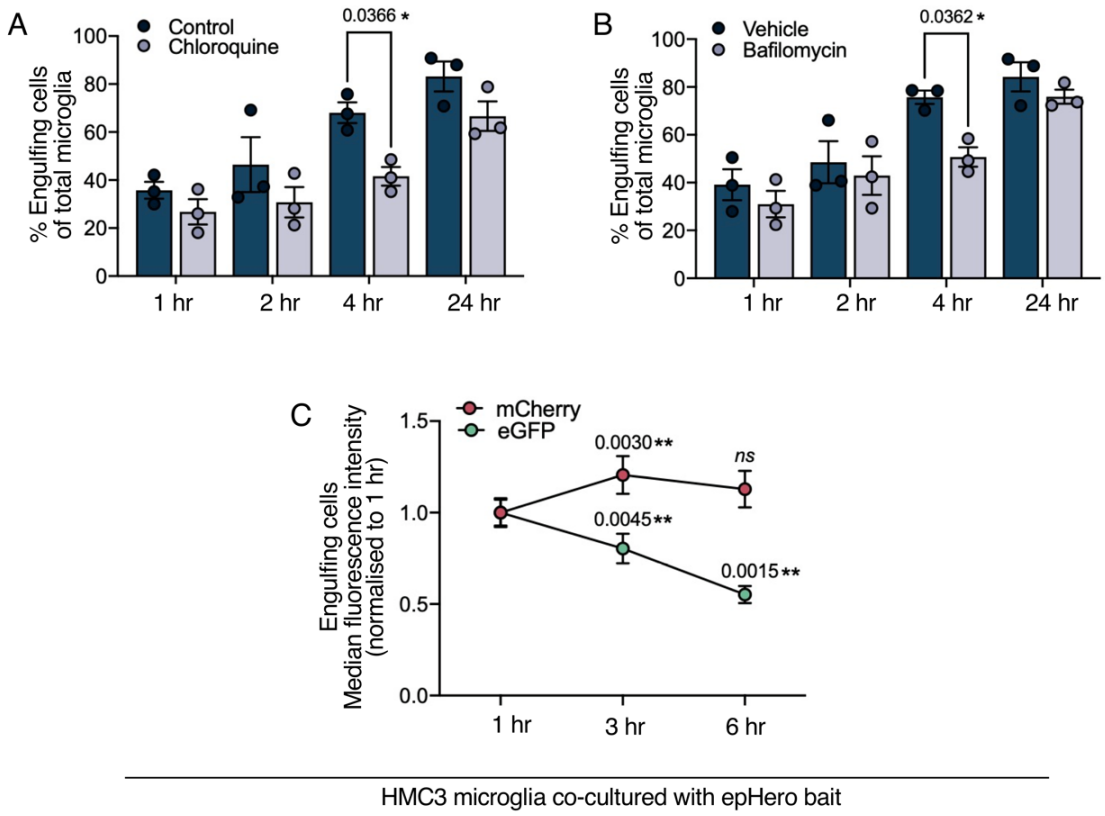

Supplementary Figure 4.2 Uptake and acidification of cargo during pH modulation of efferocytosis as measured via the epHero reporter. (A) Percentage of phagocytosing microglia when co-cultured with apoptotic epHero bait for 1-, 2-, 4- or 24-hr and pre-treated with 50 μM chloroquine. **(B)** Percentage of phagocytosing microglia when co-cultured with apoptotic epHero bait for 1-, 2-, 4- or 24-hr and pre-treated with 100 nM bafilomycin. (*A),(B)* Individual data points plotted from three independent experiments with error bars representing SEM (two-way ANOVA with Šídák's multiple comparisons test). **(C)** Relative mCherry and eGFP fluorescence from microglia phagocytosing apoptotic epHero bait for 1-, 3- and 6- hr. Data points represent mean ± SEM with n = 6-8 from three- to four independent experiments (two-way ANOVA with Šídák's multiple comparisons test; p values represent comparison between different time-points within the mCherry or eGFP groups). *Abbreviations:* ns - not significant.

4.6 REFERENCES

Alliot, F., Godin, I. and Pessac, B. (1999) 'Microglia derive from progenitors, originating from the yolk sac, and which proliferate in the brain', *Brain Res Dev Brain Res,* 117(2), pp. 145-152.

Aziz, M., Yang, W.L. and Wang, P. (2013) 'Measurement of phagocytic engulfment of apoptotic cells by macrophages using pHrodo succinimidyl ester', *Curr Protoc Immunol,* Chapter 14, p. Unit 14.31.

Cai, B., Thorp, E.B., Doran, A.C., Subramanian, M., Sansbury, B.E., Lin, C.S., Spite, M., Fredman, G. and Tabas, I. (2016) 'MerTK cleavage limits proresolving mediator biosynthesis and exacerbates tissue inflammation', *Proc Natl Acad Sci U S A,* 113(23), pp. 6526-6531.

Campbell, R.E., Tour, O., Palmer, A.E., Steinbach, P.A., Baird, G.S., Zacharias, D.A. and Tsien, R.Y. (2002) 'A monomeric red fluorescent protein', *Proc Natl Acad Sci U S A,* 99(12), pp. 7877-7882.

Casella, J.F., Flanagan, M.D. and Lin, S. (1981) 'Cytochalasin D inhibits actin polymerization and induces depolymerization of actin filaments formed during platelet shape change', *Nature,* 293(5830), pp. 302-305.

Doran, A.C., Yurdagul, A., Jr. and Tabas, I. (2020) 'Efferocytosis in health and disease', *Nat Rev Immunol,* 20(4), pp. 254-267.

Etchegaray, J.I., Elguero, E.J., Tran, J.A., Sinatra, V., Feany, M.B. and McCall, K. (2016) 'Defective Phagocytic Corpse Processing Results in Neurodegeneration and Can Be Rescued by TORC1 Activation', *J Neurosci,* 36(11), pp. 3170-3183.

Fadok, V.A., Bratton, D.L., Konowal, A., Freed, P.W., Westcott, J.Y. and Henson, P.M. (1998) 'Macrophages that have ingested apoptotic cells in vitro inhibit proinflammatory cytokine production through autocrine/paracrine mechanisms involving TGF-beta, PGE2, and PAF', *J Clin Invest,* 101(4), pp. 890-898.

Fedele, A.O. and Proud, C.G. (2020) 'Chloroquine and bafilomycin A mimic lysosomal storage disorders and impair mTORC1 signalling', *Biosci Rep,* 40(4).

Geng, L., Zhao, J., Deng, Y., Molano, I., Xu, X., Xu, L., Ruiz, P., Li, Q., Feng, X., Zhang, M., Tan, W., Kamen, D.L., Bae, S.C., Gilkeson, G.S., Sun, L. and Tsao, B.P. (2022) 'Human SLE variant NCF1-R90H promotes kidney damage and murine lupus through enhanced Tfh2 responses induced by defective efferocytosis of macrophages', *Ann Rheum Dis,* 81(2), pp. 255-267.

Haupts, U., Maiti, S., Schwille, P. and Webb, W.W. (1998) 'Dynamics of fluorescence fluctuations in green fluorescent protein observed by fluorescence correlation spectroscopy', *Proc Natl Acad Sci U S A,* 95(23), pp. 13573-13578.

Hein, L.K., Apaja, P.M., Hattersley, K., Grose, R.H., Xie, J., Proud, C.G. and Sargeant, T.J. (2017) 'A novel fluorescent probe reveals starvation controls the commitment of amyloid precursor protein to the lysosome', *Biochim Biophys Acta Mol Cell Res,* 1864(10), pp. 1554-1565.

Jorge, A.M., Lao, T., Kim, R., Licciardi, S., El Khoury, J., Luster, A.D., Means, T.K. and Ramirez-Ortiz, Z.G. (2022) 'SCARF1-Induced Efferocytosis Plays an Immunomodulatory Role in Humans, and Autoantibodies Targeting SCARF1 Are Produced in Patients with Systemic Lupus Erythematosus', *J Immunol,* 208(4), pp. 955-967.

Katayama, H., Yamamoto, A., Mizushima, N., Yoshimori, T. and Miyawaki, A. (2008) 'GFP-like proteins stably accumulate in lysosomes', *Cell Struct Funct,* 33(1), pp. 1-12.

Kimura, S., Noda, T. and Yoshimori, T. (2007) 'Dissection of the autophagosome maturation process by a novel reporter protein, tandem fluorescent-tagged LC3', *Autophagy,* 3(5), pp. 452-460.

Kneen, M., Farinas, J., Li, Y. and Verkman, A.S. (1998) 'Green fluorescent protein as a noninvasive intracellular pH indicator', *Biophys J,* 74(3), pp. 1591-1599.

Kumaran Satyanarayanan, S., El Kebir, D., Soboh, S., Butenko, S., Sekheri, M., Saadi, J., Peled, N., Assi, S., Othman, A., Schif-Zuck, S., Feuermann, Y., Barkan, D., Sher, N., Filep, J.G. and Ariel, A. (2019) 'IFN-β is a macrophage-derived effector cytokine facilitating the resolution of bacterial inflammation', *Nat Commun,* 10(1), p. 3471.

Lang, C., Roy, S., Wang, Y., Graves, D., Xu, Y., Serezani, C.H., Korrer, M. and Kim, Y.J. (2022) 'Efferocytosis drives myeloid NLRP3 dependent inflammasome signaling secretion of IL-1β to promote tumor growth', *Front Immunol,* 13, p. 993771.

Márquez-Ropero, M., Benito, E., Plaza-Zabala, A. and Sierra, A. (2020) 'Microglial Corpse Clearance: Lessons From Macrophages', *Front Immunol,* 11, p. 506.

Miksa, M., Komura, H., Wu, R., Shah, K.G. and Wang, P. (2009) 'A novel method to determine the engulfment of apoptotic cells by macrophages using pHrodo succinimidyl ester', *J Immunol Methods,* 342(1-2), pp. 71-77.

Overholtzer, M., Mailleux, A.A., Mouneimne, G., Normand, G., Schnitt, S.J., King, R.W., Cibas, E.S. and Brugge, J.S. (2007) 'A nonapoptotic cell death process, entosis, that occurs by cell-in-cell invasion', *Cell,* 131(5), pp. 966-979.

Raymond, M.H., Davidson, A.J., Shen, Y., Tudor, D.R., Lucas, C.D., Morioka, S., Perry, J.S.A., Krapivkina, J., Perrais, D., Schumacher, L.J., Campbell, R.E., Wood, W. and Ravichandran, K.S. (2022) 'Live cell tracking of macrophage efferocytosis during Drosophila embryo development in vivo', *Science,* 375(6585), pp. 1182-1187.

Rehemtulla, A., Hamilton, C.A., Chinnaiyan, A.M. and Dixit, V.M. (1997) 'Ultraviolet radiation-induced apoptosis is mediated by activation of CD-95 (Fas/APO-1)', *J Biol Chem,* 272(41), pp. 25783-25786.

Riazanski, V., Sui, Z. and Nelson, D.J. (2020) 'Kinetic Separation of Oxidative and Non-oxidative Metabolism in Single Phagosomes from Alveolar Macrophages: Impact on Bacterial Killing', *iScience,* 23(11), p. 101759.

Schappe, M.S., Stremska, M.E., Busey, G.W., Downs, T.K., Seegren, P.V., Mendu, S.K., Flegal, Z., Doyle, C.A., Stipes, E.J. and Desai, B.N. (2022) 'Efferocytosis requires periphagosomal Ca(2+)-signaling and TRPM7-mediated electrical activity', *Nat Commun,* 13(1), p. 3230.

Sender, R. and Milo, R. (2021) 'The distribution of cellular turnover in the human body', *Nat Med,* 27(1), pp. 45-48.

Shin, S., Choi, J.W., Moon, H., Lee, C.Y., Park, J.H., Lee, J., Seo, H.H., Han, G., Lim, S., Lee, S., Kim, S.W. and Hwang, K.C. (2019) 'Simultaneous Suppression of Multiple

Programmed Cell Death Pathways by miRNA-105 in Cardiac Ischemic Injury', *Mol Ther Nucleic Acids,* 14, pp. 438-449.

Stöhr, R., Deckers, N., Schurgers, L., Marx, N. and Reutelingsperger, C.P. (2018) 'AnnexinA5-pHrodo: a new molecular probe for measuring efferocytosis', *Sci Rep,* 8(1), p. 17731.

Turner, C., Devitt, A., Parker, K., MacFarlane, M., Giuliano, M., Cohen, G.M. and Gregory, C.D. (2003) 'Macrophage-mediated clearance of cells undergoing caspase-3-independent death', *Cell Death Differ,* 10(3), pp. 302-312.

van Delft, M.F., Smith, D.P., Lahoud, M.H., Huang, D.C. and Adams, J.M. (2010) 'Apoptosis and non-inflammatory phagocytosis can be induced by mitochondrial damage without caspases', *Cell Death Differ,* 17(5), pp. 821-832.

Wang, Y., Subramanian, M., Yurdagul, A., Jr., Barbosa-Lorenzi, V.C., Cai, B., de Juan-Sanz, J., Ryan, T.A., Nomura, M., Maxfield, F.R. and Tabas, I. (2017) 'Mitochondrial Fission Promotes the Continued Clearance of Apoptotic Cells by Macrophages', *Cell,* 171(2), pp. 331-345.e322.

Westman, J. and Grinstein, S. (2020) 'Determinants of Phagosomal pH During Host-Pathogen Interactions', *Front Cell Dev Biol,* 8, p. 624958.

Yoshimori, T., Yamamoto, A., Moriyama, Y., Futai, M. and Tashiro, Y. (1991) 'Bafilomycin A1, a specific inhibitor of vacuolar-type H(+)-ATPase, inhibits acidification and protein degradation in lysosomes of cultured cells', *J Biol Chem,* 266(26), pp. 17707-17712.

Yu, Y., Zhang, Z., Walpole, G.F.W. and Yu, Y. (2022) 'Kinetics of phagosome maturation is coupled to their intracellular motility', *Commun Biol,* 5(1), p. 1014.

Yurdagul, A., Jr., Doran, A.C., Cai, B., Fredman, G. and Tabas, I.A. (2017) 'Mechanisms and Consequences of Defective Efferocytosis in Atherosclerosis', *Front Cardiovasc Med,* 4, p. 86.

Yurdagul, A., Jr., Subramanian, M., Wang, X., Crown, S.B., Ilkayeva, O.R., Darville, L., Kolluru, G.K., Rymond, C.C., Gerlach, B.D., Zheng, Z., Kuriakose, G., Kevil, C.G., Koomen, J.M., Cleveland, J.L., Muoio, D.M. and Tabas, I. (2020) 'Macrophage Metabolism of Apoptotic Cell-Derived Arginine Promotes Continual Efferocytosis and Resolution of Injury', *Cell Metab,* 31(3), pp. 518-533.e510.

CHAPTER 5

Amino acid starvation promotes the acidification of phagosomes during apoptotic corpse clearance

Rationale: The work presented in this chapter addresses research objective 2, i.e. to determine whether microglial corpse clearance changes in response to nutrient deprivation. Here, I show that amino acid starvation increases acidification of efferocytic cargo, and perform proteomics to try and elucidate the pathways involved in this.

5.1 INTRODUCTION

The removal of dead cells via efferocytosis is critical for maintaining tissue homeostasis and the resolution of inflammation. This involves the mobilisation of phagocytes towards the site of injury, phagocytes binding to one or more apoptotic corpses via receptors and bridging molecules, and subsequent engulfment and digestion of apoptotic material in lysosomes (Doran, Yurdagul and Tabas, 2020). To date, there has been limited dissemination of the terminal stages of efferocytosis, likely driven by the lack of available techniques to adequately track the fate of apoptotic corpses following their engulfment.

There is an emerging body of evidence linking apoptotic corpse clearance to amino acid metabolism. Macrophages performing efferocytosis obtain arginine from the digestion of apoptotic cargo, which is subsequently converted to ornithine (Yurdagul *et al.*, 2020). This activates actin-mobilising pathways, facilitating the engulfment of

additional corpses. Moreover, efferocytosis triggers the endocytic import of arginine-derived polyamines spermine and spermidine, which helps dampen pro-inflammatory signalling (McCubbrey *et al.*, 2022). The essential amino acid methionine is also derived from engulfed apoptotic corpses and contributes to efferocytosis-mediated resolution via epigenetic regulation of a transforming growth factor β repair program (Ampomah *et al.*, 2022). Recent work has also implicated the hydrolysis of another amino acid, glutamine, into glutamate, in fuelling energy requirements during continual efferocytosis (Merlin *et al.*, 2021). Thus, several lines of evidence suggest that amino acids serve as immune signalling molecules responsible for mediating the engulfment of apoptotic material, cytokine production, and energy demands of efferocytosis. However, whether they play a role in the post-engulfment processing of apoptotic corpses remains unknown.

Autophagy is a catabolic process where cytosolic cargo is delivered to lysosomes for degradation and recycling. This process involves the formation of intermediary double-membraned structures called autophagosomes, which contain the protein LC3 on both inner and outer membranes (Kabeya *et al.*, 2000, Kirisako *et al.*, 1999). Autophagy is typically activated during periods of stress, such as during amino acid starvation (Onodera and Ohsumi, 2005). The autophagic protein LC3 can also be conjugated onto single membranes during endocytosis (Heckmann *et al.*, 2019) and phagocytosis (Martinez *et al.*, 2011, Martinez *et al.*, 2015), facilitating the lysosomal degradation of cargo via non-canonical autophagy pathways by promoting fusion of phagosomes with lysosomes.

During efferocytosis, apoptotic corpses not only serve as phagocytic targets for the ingesting cell but may also provide a source of nutrients, as macrophages that have engulfed cargo show elevated amino acid levels (McCubbrey *et al.*, 2022). Given the connections between amino acids, autophagy, and efferocytosis, we investigated the efferocytic degradation of apoptotic cargo during amino acid starvation, a condition known to stimulate autophagy. Previous research has focused on the engulfment of cargo and cytokine production by phagocytes during efferocytosis. Here, we employed our newly developed epHero probe – capable of simultaneously measuring apoptotic cell uptake and acidification – to track the fate of apoptotic corpses during prolonged amino acid starvation in microglia. We show that amino acid starvation increased the acidification of cargo during microglial efferocytosis. Proteomic analyses were also performed to identify novel proteins and pathways that may be involved in apoptotic corpse metabolism.

5.2 METHODS

Cell culture

HMC3 microglial cells were obtained from ATCC and cultured in EMEM containing 10% FCS. THP1 monocytes stably expressing epHero were prepared as described in Chapter 4 and maintained in RPMI 1640 medium supplemented with 10% FCS and 2 mM L-glutamine. All cell lines used in this study were maintained at 37°C with 5% CO_2 and routinely screened for mycoplasma infection.

In vitro efferocytosis assay

HMC3 microglia were seeded in a 12-well plate at 1 X 10^5 cells per well and maintained

overnight. The following day, THP1 bait cells stably expressing epHero were rendered apoptotic via UV irradiation at 316 nm for 3-4 min, followed by incubation for 3 hr at 37°C with 5% CO_2. Apoptotic bait cells were then added to the phagocytes at a 5:1 bait to phagocyte ratio for the indicated times. Phagocytes underwent three PBS washes to remove any unattached bait, were dissociated from the plate using trypsin to cleave un-internalised bait, and then analysed using flow cytometry. Flow cytometry measurements were performed on a BDFortessa with appropriate gating controls, with >10000 phagocyte events recorded per sample. All flow cytometry data were analysed on FlowJo™ version 10.8 (BD Life Sciences).

For amino acid starvation experiments, HMC3 microglia were treated for 12 hr in Earle's Balanced Salt Solution (EBSS) containing 10% dialysed FCS ± amino acids prior to performing the efferocytosis assay. For amino acid re-stimulation experiments, HMC3 microglia were starved for 12 hr as described above and re-stimulated with amino acids immediately prior to performing the efferocytosis assay.

For serum starvation experiments, HMC3 microglia were treated for 12 hr in EBSS containing amino acids ± 10% dialysed FCS prior to performing the efferocytosis assay. HMC3 microglia were either starved for the entire assay duration or re-stimulated with serum immediately prior to the addition of apoptotic bait.

Proteomics

Relative label-free quantitation proteomics was performed on cell lysates from amino acid-starved and -fed microglia (with or without apoptotic corpses). Samples were

prepared via universal solid phase protein preparation, and run on a timsTOF2 using a standard 48 min method with a 30 min gradient (Dagley *et al.*, 2019), with six biologically independent replicates run per group. Raw intensities were log2-transformed, and principal component and relative log expression analysis was performed to assess sample quality and exclude any potential outliers from subsequent analyses. Proteins were filtered based on identification of ≥ 2 unique peptides in > 50-60% of all samples per group. Log intensities were normalised using cyclicloess implemented in limma version 3.52.2 (Law *et al.*, 2014), and missing values imputed via the barycenter approach in msImpute version1.7.0 (Hediyeh-Zadeh, Webb and Davis, 2023). Proteins in amino acid-starved vs -fed microglia (with or without apoptotic corpses) were compared in limma, with a protein considered differentially expressed between two conditions if the adjusted p-value was ≤ 0.1. Pathway enrichment analysis was performed on differentially expressed proteins using ShinyGO version 0.77 (Ge, Jung and Yao, 2020) based on gene ontology, KEGG, Reactome and WikiPathways databases.

Western blotting

HMC3 microglia were amino acid-fed or -starved (with or without apoptotic corpses) as described above, in the presence of either vehicle or 100 nM of bafilomycin A1, a lysosomal inhibitor. Samples were pelleted and resuspended in cell lysis buffer containing protease and phosphatase inhibitors and sonicated on ice. Protein concentration was determined via a BCA assay, with 10 μg protein loaded per well and electrophoresed through 4-12% SDS-PAGE gels before being transferred to a PVDF membrane as previously described (Hein *et al.*, 2017). Membranes were

blocked in Tris-buffered saline containing 0.1% (v/v) Tween 20 and 5% (w/v) skim milk or 2% (w/v) BSA and incubated overnight at 4°C with anti-LC3, anti-p62, anti-ATG2B, anti-STAT3 or anti-SNX17 antibodies. All primary antibodies were used at a 1:1,000 dilution. Membranes were washed, and incubation with HRP-conjugated anti-mouse or anti-rabbit secondary antibodies (1:10,000) was performed at room temperature for 1 hr. To detect β-actin, membranes were incubated with an HRP-conjugated anti-β-actin antibody (1:10,000) for 1 hr at room temperature. Membranes were developed on the LAS4000 Luminescent Image Analyser (Fujifilm Life Science) using the West Pico or West Femto ECL systems.

Data analysis

Proteomics data were analysed as described above. All other statistical analyses were performed using GraphPad version 8. Data were analysed via two-way ANOVA; sample size for each experiment is detailed in the Figure legend. Gaussian distribution was verified using a Shapiro-Wilk test, and either parametric or non-parametric analyses were performed accordingly. Data are presented as individual data points with standard error bars, as indicated in the Figure legends. Given the exploratory nature of our proteomics analyses, we used an adjusted p-value cut-off of ≤ 0.1. For all other experiments $p \leq 0.05$ was considered statistically significant. All p-values are reported in the Figures.

5.3 RESULTS

5.3.1 Amino acid starvation increases acidification of the apoptotic corpse-containing phagosome during efferocytosis

Amino acid starvation is a potent inducer of autophagy (Onodera and Ohsumi, 2005). Recently, several groups have shown that amino acid metabolism also affects apoptotic corpse clearance by macrophages (Yurdagul *et al.*, 2020, Merlin *et al.*, 2021, Ampomah *et al.*, 2022). To determine whether this also held true in microglia, HMC3 microglia were pre-treated with either complete or amino acid-deficient medium containing dialysed serum for 12 hr, and then co-cultured with apoptotic epHero bait for varying lengths of time (Figure 5.1A). Apoptotic bait cells containing the epHero reporter exhibit dual mCherry and eGFP fluorescence, where mCherry remains stable and eGFP quenches in an acidic environment. When they are engulfed by microglia, the mCherry/eGFP ratio can be used as a measure of cargo acidification (and thereby phagosomal maturation) over time. Amino acid starvation did not affect the uptake of apoptotic cargo (Figure 5.2A). However, amino acid-starved microglia had markedly increased flux of efferocytic material with time, as evidenced by the increased mCherry/eGFP ratio (Figure 5.2B–C).

Next, we investigated whether this starvation-mediated increase in phagosomal acidification was transient or if it could be rescued upon the re-addition of amino acids. For this, HMC3 microglia were pre-treated in either complete or amino acid-deficient medium for 12 hr, as before. However, this time, microglia were re-stimulated with amino acids before being co-cultured with apoptotic epHero bait (Figure 5.1B).

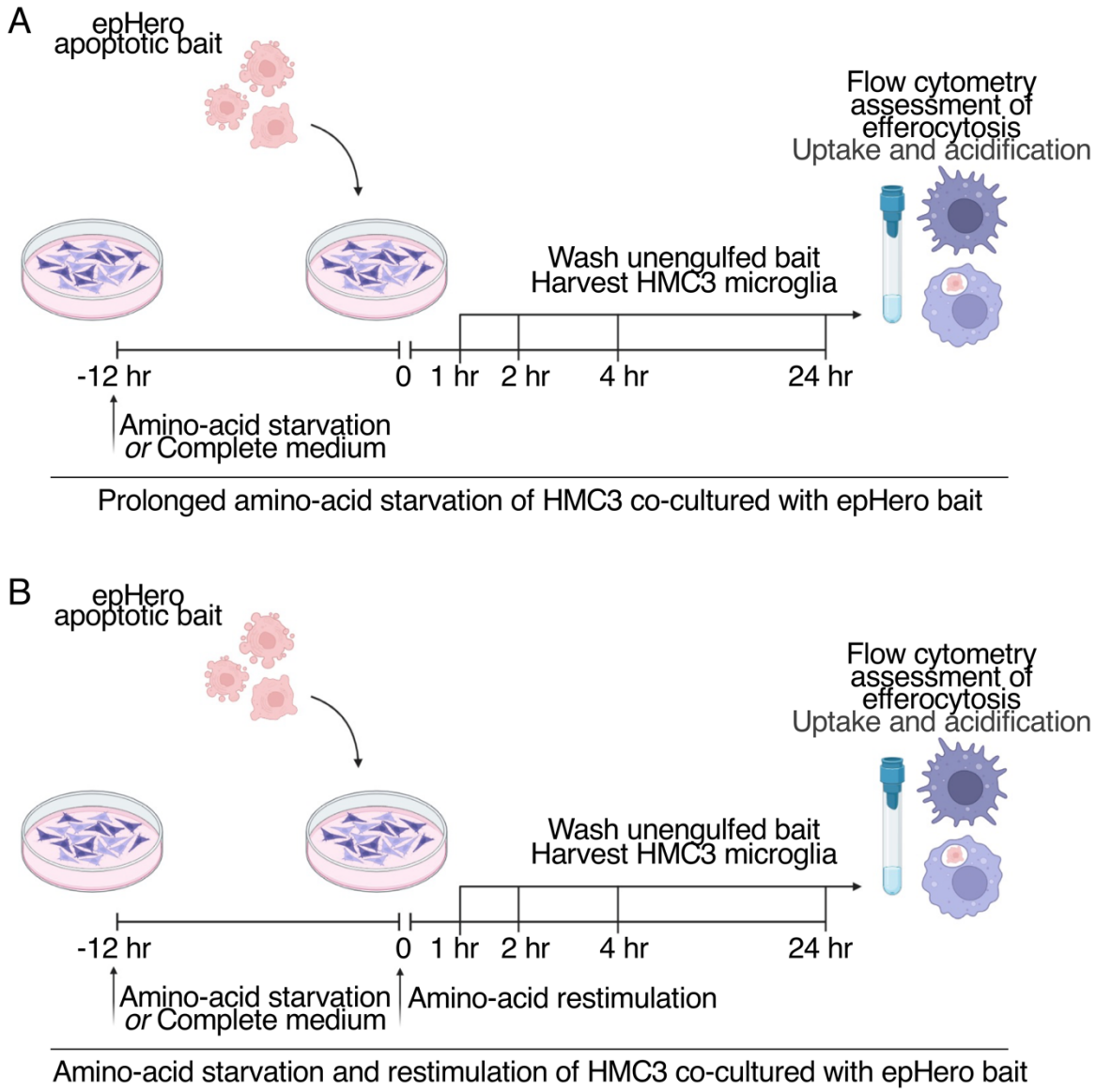

Figure 5.1 Schematic of amino acid starvation and efferocytosis experiments. **(A)** HMC3 microglia were amino acid-starved for 12 h before being co-cultured with epHero apoptotic bait. (B) Microglia were amino acid-starved for 12 h and re-stimulated with amino acids immediately before incubation with apoptotic cells.

Intriguingly, we observed increased uptake of corpses by amino acid-starved (and re-stimulated) microglia at all time-points (Figure 5.2D). Further, amino acid starvation

(and re-stimulation) also increased phagosomal acidification in these microglia (Figure 5.2E–F). This effect persisted even 24 hr after the re-addition of amino acids, indicating that prolonged starvation reprograms microglia to be more efficient at phagocytosing apoptotic cargo.

To validate our epHero-based method for measuring efferocytosis, we serum-starved microglia (in the presence of amino acids) for 12 hr before co-culturing them with epHero-expressing bait. Serum contains several pro-opsonisation molecules, including the complement component C1q, which facilitate the binding of apoptotic cells to phagocytes, an important first step in efferocytosis (Hulsebus *et al.*, 2016, Pulanco *et al.*, 2017, Liang *et al.*, 2014). Serum starvation should therefore reduce the engulfment of apoptotic cargo by microglia, with minimal impact on its subsequent processing. As expected, serum starvation reduced the uptake of apoptotic cells by microglia (Supplementary Figure 5.1A). In serum-starved microglia that had engulfed apoptotic bait, phagosomal acidification was unaltered compared to their serum-fed counterparts (Supplementary Figure 5.1B–C). Importantly, this engulfment defect could be restored upon the re-addition of serum (Supplementary Figure 5.1D–F).

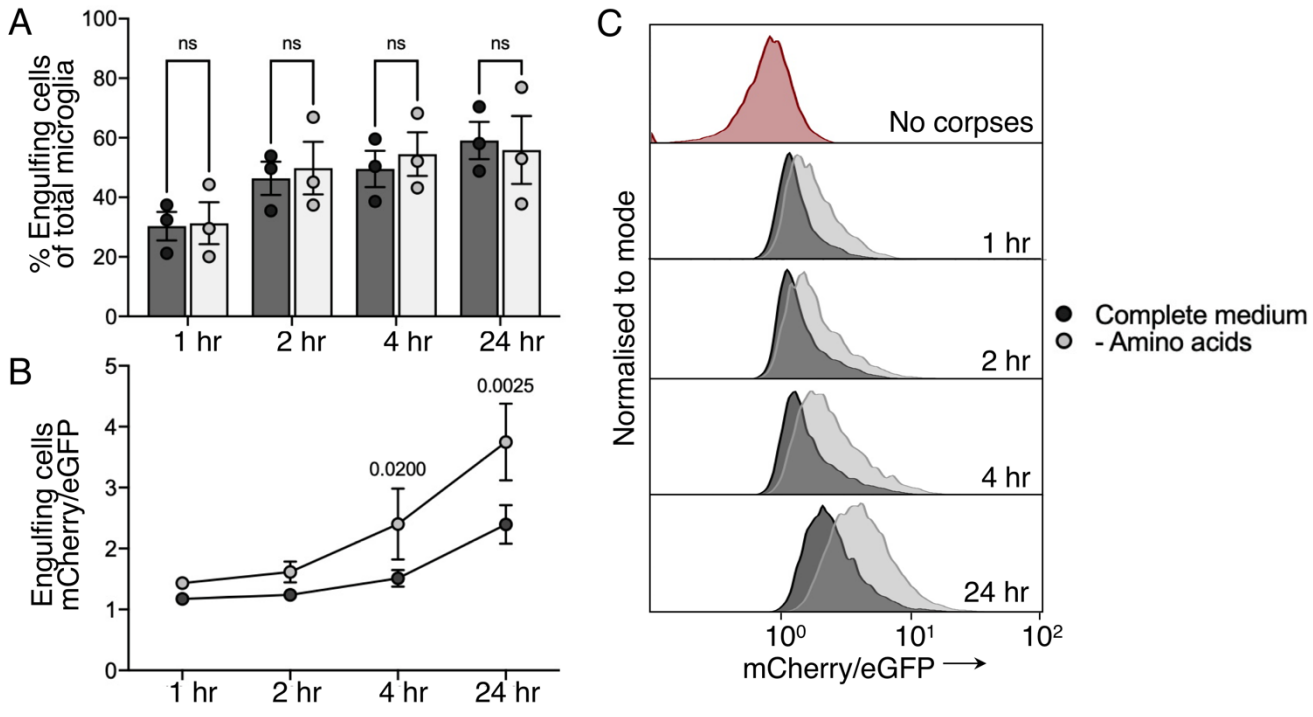

Prolonged amino-acid starvation of HMC3 co-cultured with epHero bait

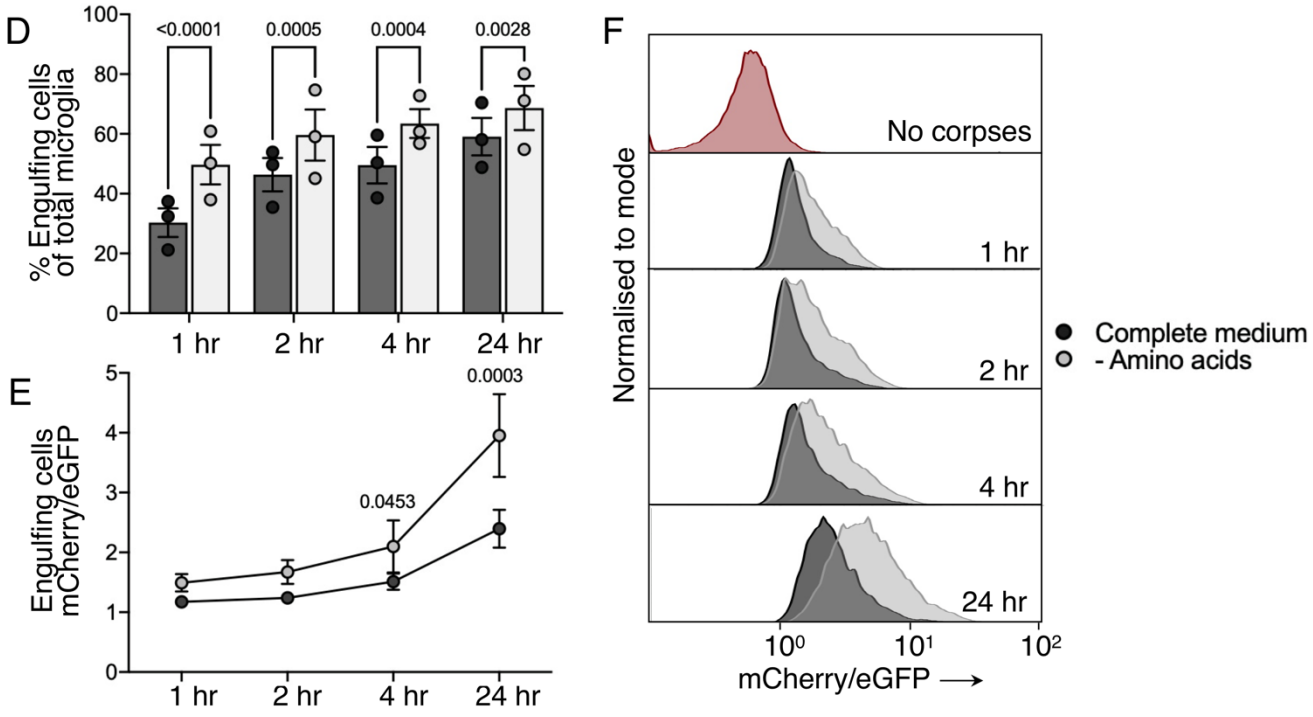

Amino-acid starvation and restimulation of HMC3 co-cultured with epHero bait

Figure 5.2 Amino acid starvation increases apoptotic corpse acidification during microglial efferocytosis. (A) Quantification of the percentage of phagocytosing cells from amino acid-fed or -starved microglia co-cultured with epHero bait for up to 24 hr.

(B) mCherry/eGFP ratio from microglia that have phagocytosed cargo after being co-cultured with apoptotic epHero bait for up to 24 hr, with or without amino acid starvation. **(C)** Representative histograms from *(B).* **(D)** Quantification of the percentage of phagocytosing cells from amino acid-fed or -starved (and re-stimulated) microglia incubated with epHero apoptotic cells for up to 24 hr. **(E)** mCherry/eGFP ratio from microglia that have phagocytosed cargo after being co-cultured with apoptotic epHero bait for up to 24 hr, with or without amino acid starvation (and re-stimulation). **(F)** Representative histograms from *(E). (A*),*(B),(D)* and *(E)*: all data points depict mean ± SEM from three independent experiments (two-way ANOVA with Šídák's multiple comparisons test).

5.3.2 Establishing a proteomics workflow to detect differences between amino acid-fed and -starved microglia during efferocytosis

Next, we devised a proteomics strategy to elucidate mechanisms driving the amino acid starvation-mediated increase in phagosomal cargo acidification during efferocytosis. Proteomics of phagocytosis can be challenging, as part of the protein signal could be derived from the apoptotic cells themselves and not the phagocyte. Although a SILAC-based approach – where apoptotic bait is labelled with heavy amino acids and peptides containing these heavy amino acids are excluded from analyses – can help counter this, we chose not to employ it as recent work has shown that material derived from apoptotic cargo itself can be used by phagocytes to fuel subsequent rounds of efferocytosis (Ampomah *et al.*, 2022, Yurdagul *et al.*, 2020). Therefore, excluding all SILAC-labelled peptides may not be ideal, as phagocytes could incorporate heavy amino acids recycled from the breakdown of apoptotic cargo into

their own proteome. We decided to compare microglia that had engulfed apoptotic bait and had either been amino acid-fed or -starved for the entire efferocytosis experiment (Figure 5.3A). Given that we observed no differences in cargo engulfment between these two conditions, we reasoned that the portion of apoptotic bait-derived signal would be comparable between amino acid-fed and -starved microglia. In addition, we also performed proteomic profiling of the apoptotic bait itself as a qualitative control to assist with the selection of proteins for further validation. Lastly, since we expected that prolonged amino acid starvation itself would drastically alter the microglial proteome, we sought to compare the protein signature of microglia that were either fed or starved of amino acids as a baseline. We did not perform a direct comparison between the 'no corpse' and 'corpse' conditions (*i.e.* amino acid-fed/-starved vs amino acid-fed/-starved + apoptotic corpses) because signal from the ingested apoptotic corpses would confound this analysis.

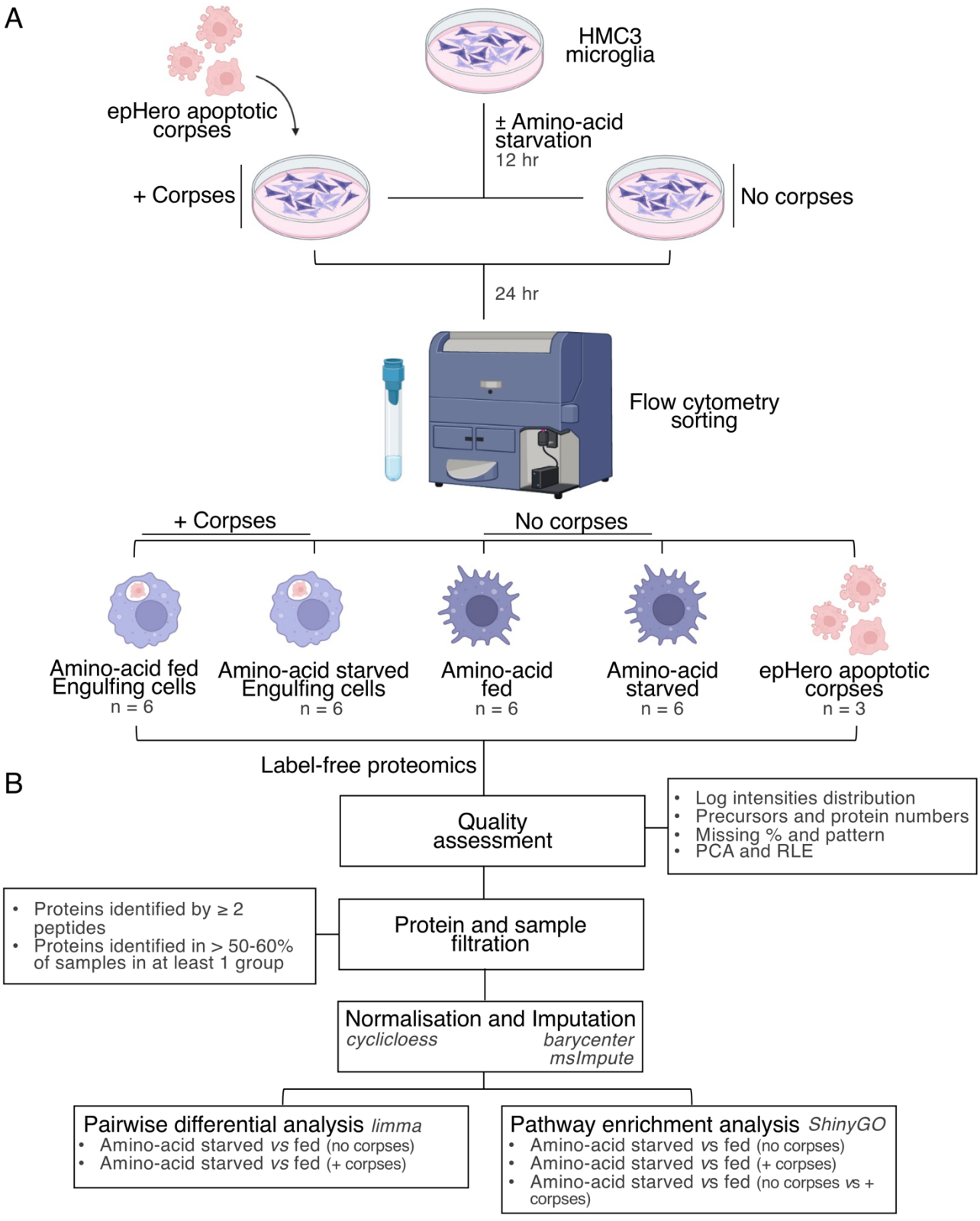

Figure 5.3 Schematic for proteomic analysis of amino acid-fed or -starved microglia during efferocytosis. (A) HMC3 microglia were amino acid-fed or -starved for 12 hr before being incubated for a further 24 hr either alone or in the presence of

apoptotic corpses, and then sorted via flow cytometry for proteomic analysis. **(B)** Label-free proteomics was performed on samples from *(A).* Data were filtered, normalised, and analysed for differentially expressed proteins and enriched pathways. *Abbreviations:* PCA - Principal Component Analysis; RLE - Relative Log Expression.

We performed label-free proteomics on six independent replicates per condition and three apoptotic bait-only samples (Figure 5.3B). Proteins were filtered based on identification of ≥ 2 unique peptides in > 50-60% of samples in at least one group. Raw intensities were log2-transformed, and missing values imputed using a barycentre approach. This method utilises a weighted average of data distributions under the missing-at-random and missing-not-at-random assumptions to estimate missing values (Hediyeh-Zadeh, Webb and Davis, 2023). This yielded a list of 3744 filtered proteins, which was used for all subsequent analyses.

5.3.3 Proteomic profiling of microglia during prolonged amino acid starvation

Since we anticipated that prolonged amino acid starvation would have a profound effect on the microglial proteome, we first sought to establish a proteomic signature for starved microglia. For our analysis, we only included high confidence proteins where ≥ 2 unique peptides had been identified in at least 50-60% of samples from one group. An ANOVA with empirical Bayesian variance estimation was used to determine whether proteins were differentially expressed (adjusted p value ≤ 0.1). Based on these parameters, we identified 3744 proteins; of these, 751 proteins were differentially expressed between the amino acid-starved and -fed conditions (Figure 5.4A–B, Appendix Table 8.1–8.2): 351 proteins were up-regulated in amino acid-

starved cells, with a significant subset of these proteins being involved in DNA replication (*n* = 12), binding (*n* = 6), and repair (*n* = 7) pathways as well as ribosomal (*n* = 7) and messenger RNA (*n* = 4) regulation (Figure 5.4C). Interestingly, we also observed enrichment of the pathway involved in salvage and *de novo* synthesis of the essential amino acid methionine – the precursor for S-adenosylmethionine (SAM) – a master regulator of DNA and RNA methylation (Chiang *et al.*, 1996)) in the proteome of starved microglia (*n* = 3).

The expression of 400 proteins was reduced during prolonged amino acid starvation in microglia. As expected, proteins involved in catabolic pathways such as the proteasome (*n* = 6), proteolysis (*n* = 10), and amino acid degradation (*n* = 11) were down-regulated during prolonged starvation (Figure 5.4D). Further, proteins participating in the synthesis of cholesterol and fatty acids (*n* = 12) were also reduced, likely to conserve nutrients during scarcity. Pathway analysis also revealed that several proteins involved in collagen processing (*n* = 31) and extracellular matrix (ECM) organisation (*n* = 7) decreased during prolonged starvation in microglia, which was somewhat surprising considering the bi-directional relationship between autophagy and several ECM components (Carmignac *et al.*, 2011, Nakamura *et al.*, 2021, Fung *et al.*, 2008).

Collectively, our findings suggest a proteomic signature for starved microglia characterised by heightened DNA and RNA metabolism, amino acid prioritisation via enhanced salvage and reduced degradation mechanisms, and decreased ECM, collagen, and lipid synthesis.

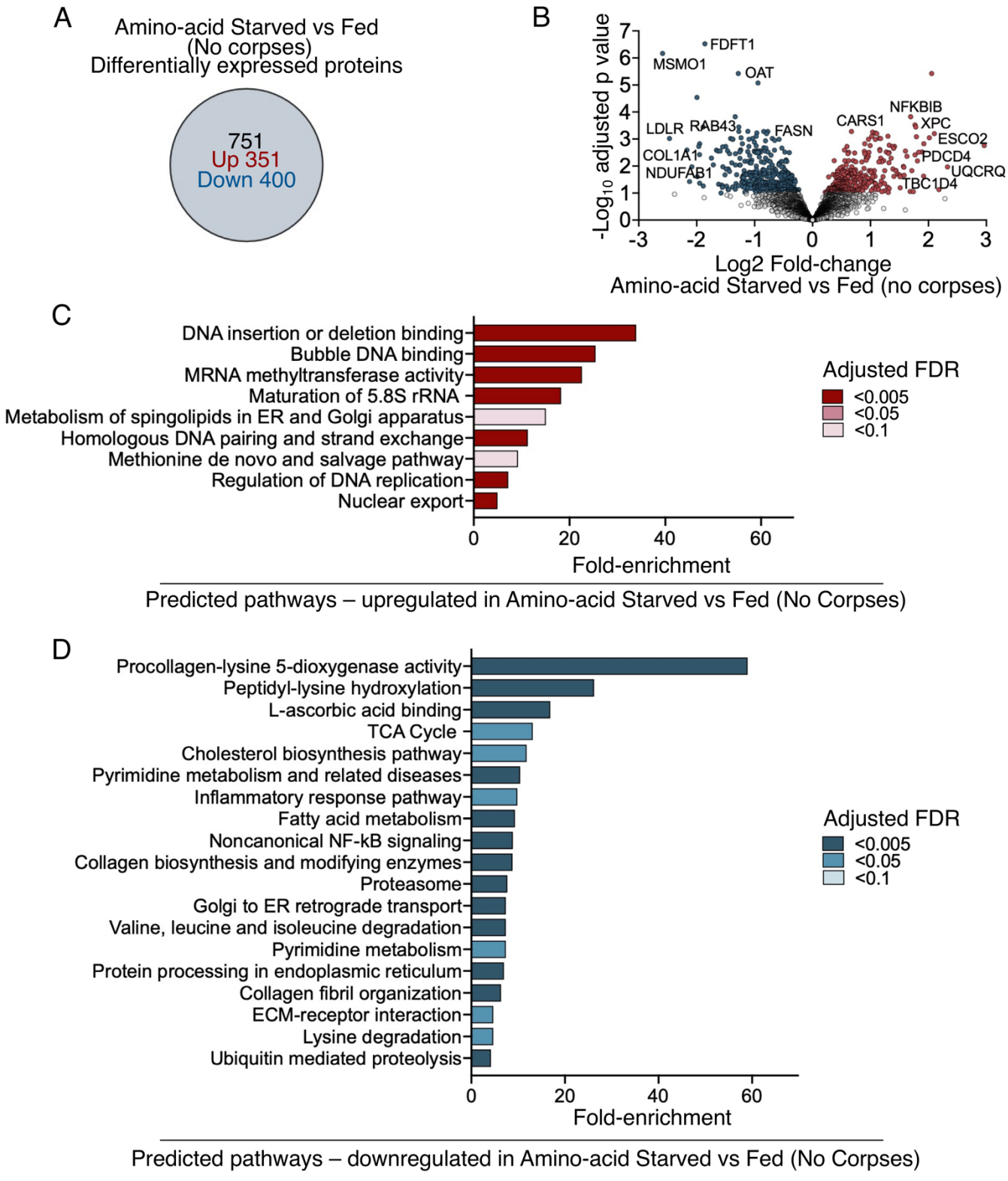

Figure 5.4 Proteomic signature of amino acid-starved microglia. (A) Number of differentially expressed proteins between HMC3 microglia cultured in either amino acid-deficient or complete medium. **(B)** Volcano plot showing differentially expressed

proteins from *(A).* Data derived from n = 6 independent experiments (limma-based one-way ANOVA, adjusted p-value ≤ 0.1). **(C)** Pathway enrichment analysis of proteins up-regulated between amino acid-starved and -fed cells (ShinyGO , adjusted FDR ≤ 0.1). **(D)** Pathway enrichment analysis of proteins down-regulated between amino acid-starved vs -fed cells (ShinyGO, adjusted FDR ≤ 0.1). *Abbreviations:* FDR - False Discovery Rate.

5.3.4 Proteomics of amino acid-starved microglia during efferocytosis

Next, we examined the proteomic profile of amino acid-starved and -fed microglia during efferocytosis. In the presence of apoptotic corpses, 279 proteins were differentially expressed between starved and fed microglia; of these, 125 were up-regulated and 154 were down-regulated (Figure 5.5A). Given that we observed increased acidification of the apoptotic corpse-containing phagosome in these cells, we questioned whether there was altered expression of any pH-modifying proteins. Of the 16 proteins involved in organelle acidification that were detected in our proteomics experiment, none were differentially expressed between amino acid-starved and -fed cells during efferocytosis (Figure 5.5B). Pathway analysis revealed an increase in proteins involved in the transport and metabolism of several amino acids, including glutamine (*n* = 7), cysteine and methionine (*n* = 7), and serine (*n* = 7) during efferocytosis in amino acid-starved microglia (Figure 5.5C). Similar to amino acid starvation alone, amino acid starvation during efferocytosis down-regulated ECM and collagen-related pathways (Figure 5.5D). Intriguingly, despite an overall spike in amino acid transport and salvage mechanisms, proteins involved in the metabolism of arginine – an amino acid capable of being derived from apoptotic cells themselves

during efferocytosis (Yurdagul *et al.*, 2020) – were reduced in amino acid-starved microglia that had ingested corpses.

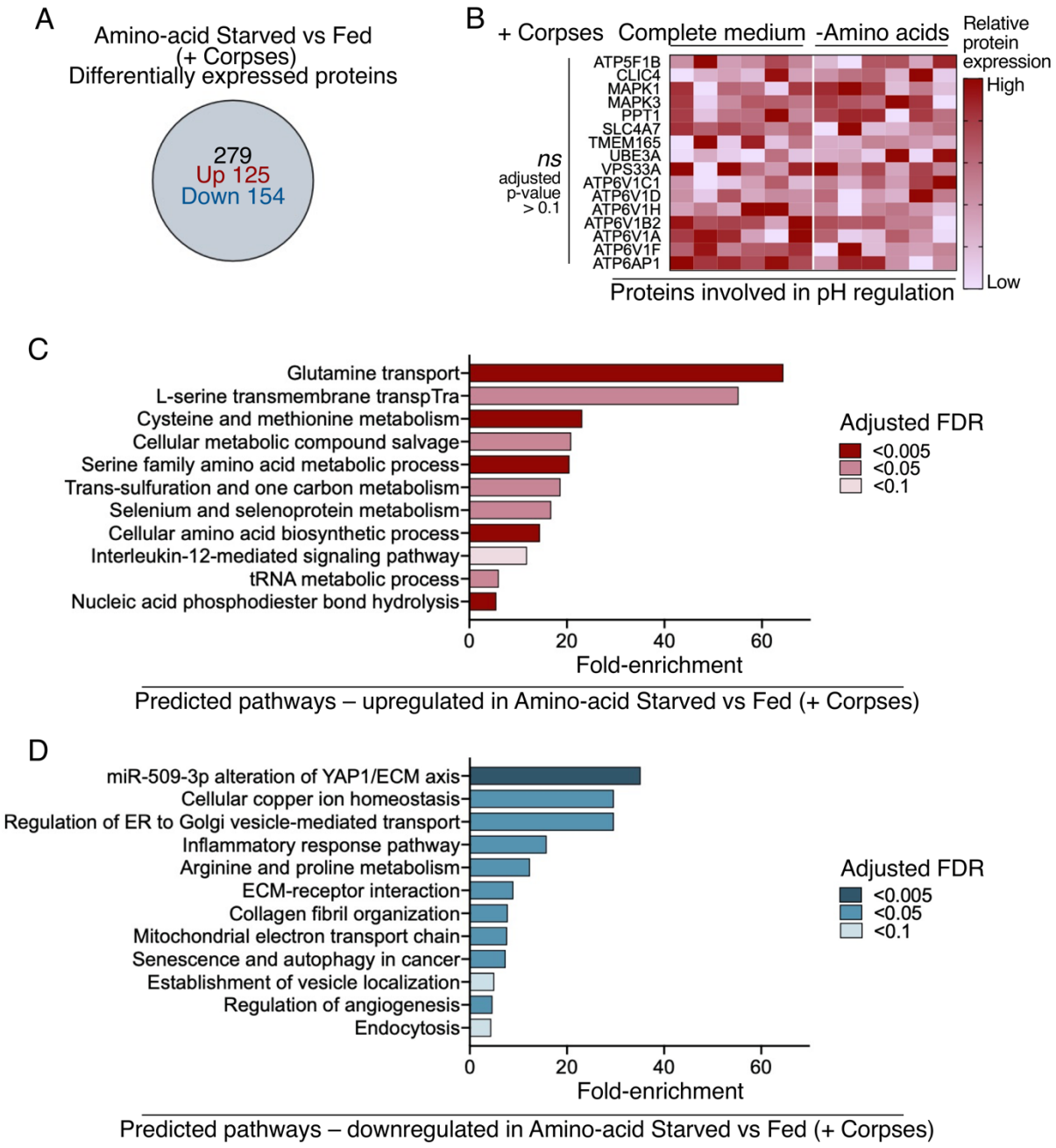

Figure 5.5 Proteomic signature of amino acid-starved microglia performing efferocytosis (A) Number of differentially expressed proteins between HMC3 microglia cultured in either amino acid-deficient or complete medium and co-cultured

with apoptotic bait for 24 hr. **(B)** Heatmap showing expression of proteins involved in intracellular pH regulation in amino acid-starved and -fed microglia that have ingested corpses. **(C)** Pathway enrichment analysis of proteins up-regulated between amino acid-starved and -fed cells during efferocytosis (ShinyGO, adjusted FDR ≤ 0.1). **(D)** Pathway enrichment analysis of proteins down-regulated between amino acid-starved vs -fed phagocytosing microglia (ShinyGO, adjusted FDR ≤ 0.1). *Abbreviations:* FDR - False Discovery Rate.

5.3.5 Comparison of starvation-induced changes to the proteomic profile of microglia in the presence or absence of efferocytosis

Based on our initial findings, we devised a follow-up strategy whereby we analysed differentially expressed proteins between amino acid-starved and -fed microglia, either in the presence or absence of apoptotic corpses to identify proteins that were shared or unique across the two comparisons. Of the 279 proteins differentially expressed between amino acid-starved and -fed cells during efferocytosis (Figure 5.6A), 147 were unique to efferocytosis, *i.e.* not differentially expressed in the absence of apoptotic corpses (Figure 5.6B). These unique proteins could therefore play a role in apoptotic corpse engulfment or processing. We expanded upon our previous pathway enrichment analysis by manually curating subcategories of interest based on a combination of database and literature mining, with differentially expressed proteins that were unique to efferocytosis highlighted in bold (Figure 5.6C). This revealed that during efferocytosis, amino acid-starved microglia had more autophagy-related proteins and fewer proteins involved in mTOR signalling and vesicle trafficking. Amino

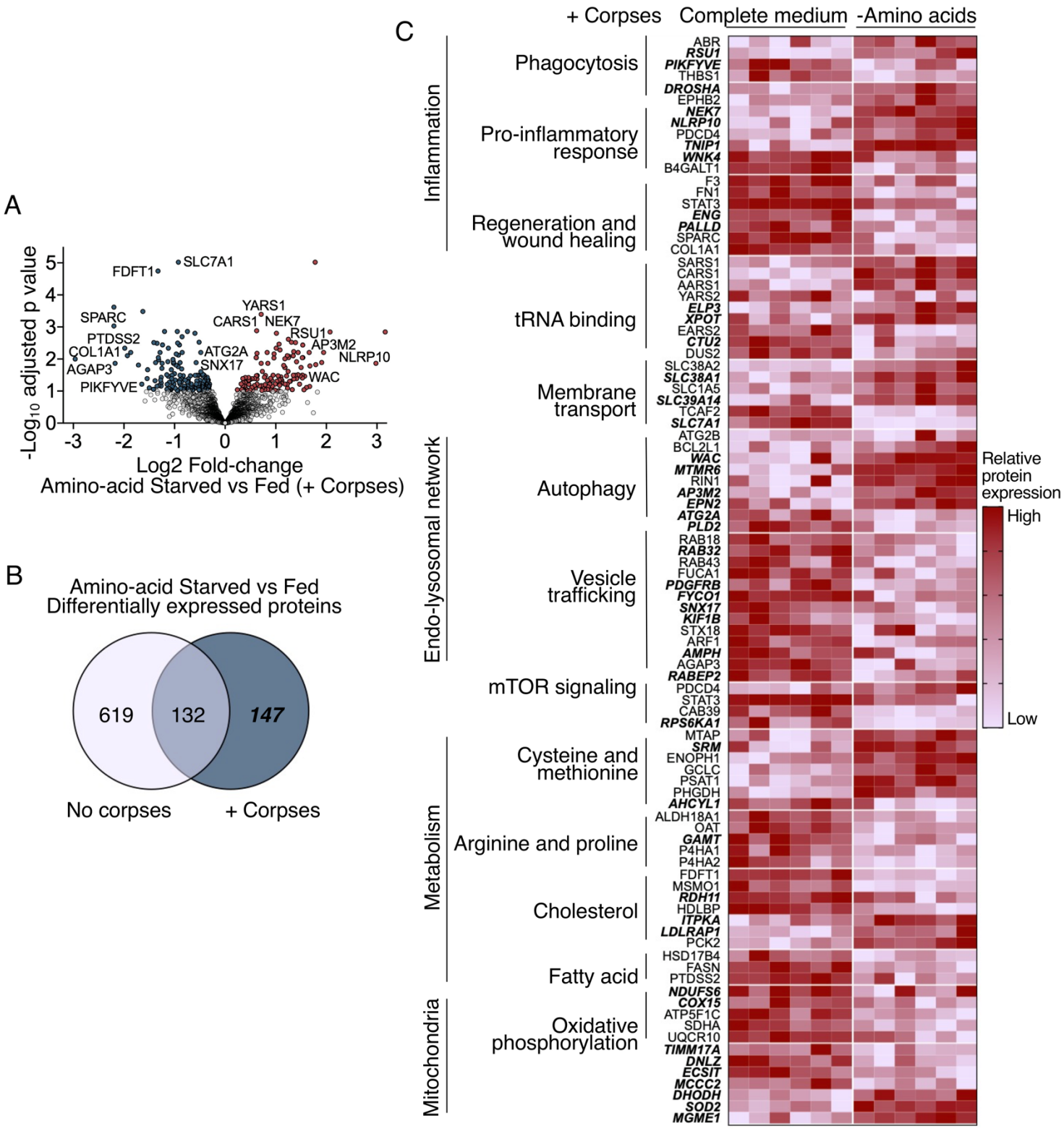

Figure 5.6 Proteins differentially expressed between amino acid-starved and -fed microglia during efferocytosis. (A) Volcano plot showing differentially expressed proteins between amino acid-starved and -fed microglia following 24 hr of

efferocytosis. Data derived from n = 6 independent experiments (limma-based one-way ANOVA, adjusted p-value ≤ 0.1). **(B)** Venn diagram depicting differentially expressed proteins that were shared or unique between amino acid-starved vs -fed microglia that were either cultured alone or in the presence of apoptotic corpses. **(C)** Heatmap depicting a subset of proteins from *(A)* that were categorised according to their primary function. Proteins in bold were unique to the amino acid-starved vs -fed (+ corpses) comparison.

acid-starved microglia performing efferocytosis had an up-regulation of inflammation and membrane transport pathway proteins and, with the exception of cysteine and methionine, proteins involved in the metabolism of most substrates were reduced. Of note, a large subset of differentially expressed proteins that were unique to efferocytosis were localised to the mitochondria.

Next, we examined unique proteins that were differentially expressed between amino acid-starved and -fed microglia but *not* differentially expressed in the presence of apoptotic corpses. We identified 304 proteins that were down-regulated during amino acid starvation but not when amino acid starvation was coupled with efferocytosis (Figure 5.7A). Consequently, this meant that expression of these proteins increased during efferocytosis in amino acid-starved microglia. We reasoned that these proteins may be involved in pathways that were essential for apoptotic corpse clearance. Pathway analysis on these proteins revealed an enrichment in proteins involved in mitochondrial fatty acid oxidation, degradation of branched chain amino acids (valine, leucine, and isoleucine), ornithine decarboxylase regulation, and proteasomal

degradation. Finally, we examined 331 proteins that were up-regulated in amino acid-starved microglia but not during amino acid starvation combined with efferocytosis (Figure 5.7B), indicating that expression of these proteins was reduced during efferocytosis. Pathway analysis highlighted that most of the up-regulated DNA and RNA metabolic pathways previously implicated during amino acid starvation reverted to normal upon the addition of apoptotic corpses.

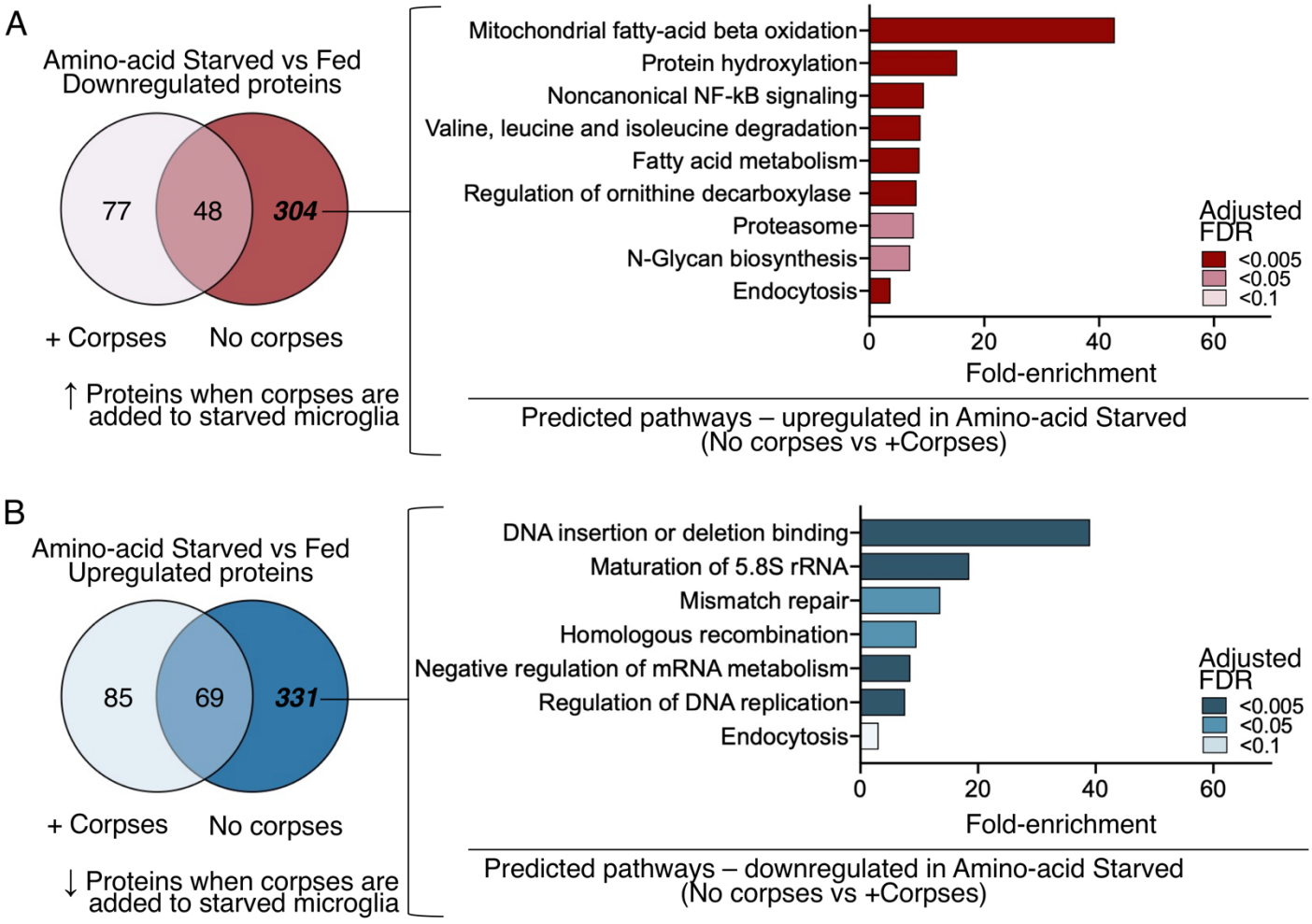

Figure 5.7 Pathway analysis of proteins differentially expressed following amino acid starvation, performed alone or during efferocytosis. (A) Pathway analysis of proteins down-regulated only in starved microglia that were not performing

efferocytosis (ShinyGO, adjusted FDR ≤ 0.1). **(B)** Pathway enrichment analysis of proteins upregulated in starved microglia only in the absence of apoptotic corpses (ShinyGO, adjusted FDR ≤ 0.1). *Abbreviations:* FDR - False Discovery Rate.

Finally, given that amino acid starvation induces autophagy and that the autophagic protein LC3 is also involved in the phagocytosis of dead cells, we sought to investigate whether any of the differentially expressed proteins from our analyses contained an LC3-interacting region (LIR), characterised by a [W/F/Y]-X-X-[L/I/V] motif, where X can be any amino acid (Pankiv *et al.*, 2007). We observed 59 differentially expressed proteins containing an LIR (Jacomin *et al.*, 2016): 35 were unique to the amino acid-starved vs -fed microglia (no corpses) comparison; 15 were unique to the amino acid-starved vs -fed (+ corpses) comparison; and 9 were shared across both (Figure 5.8A–B).

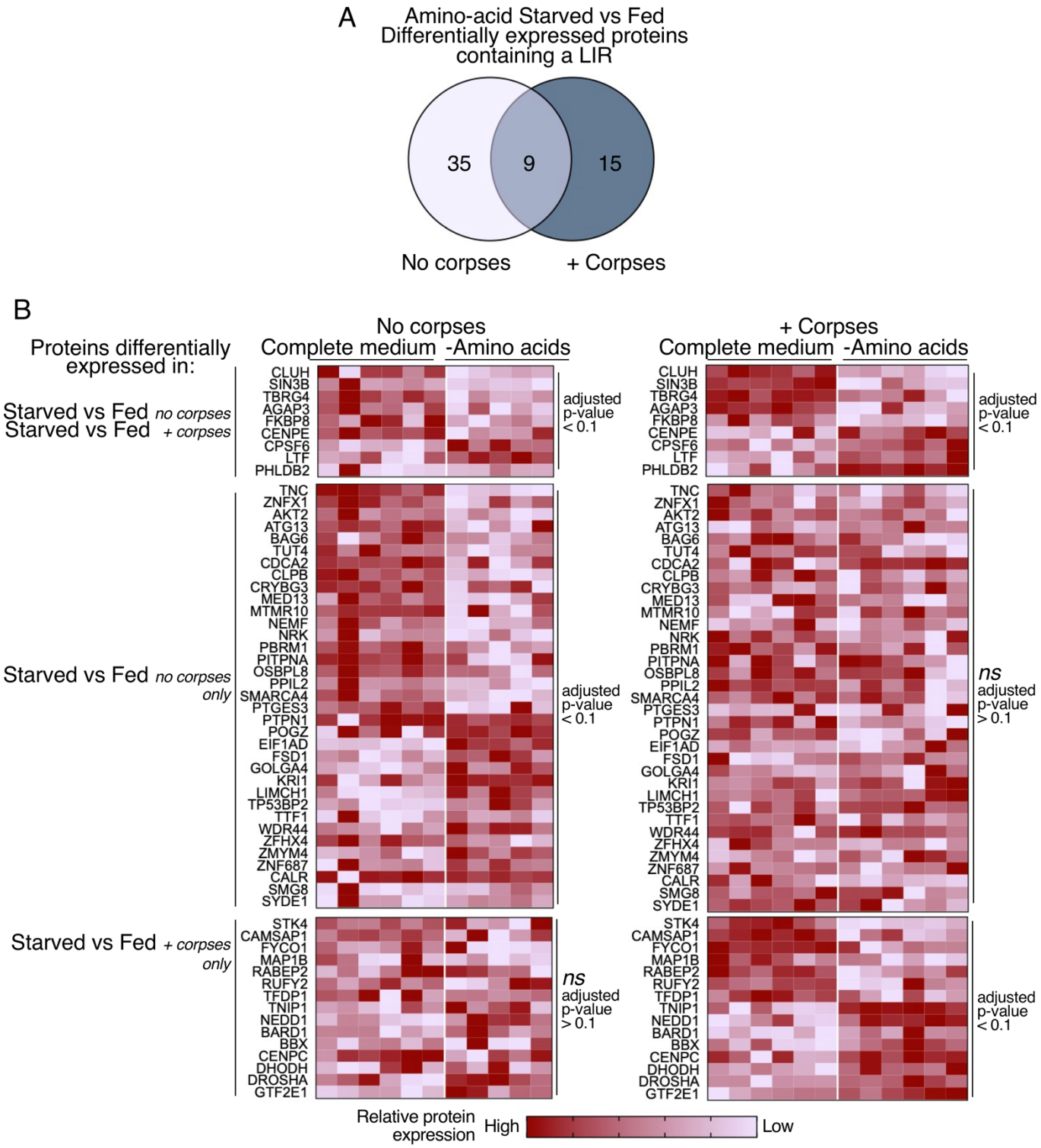

Figure 5.8 LC3-interacting region (LIR) containing differentially expressed proteins between amino acid-starved and -fed microglia. (A) Venn diagram showing overlapping and unique differentially expressed proteins containing an LIR.

(B) Heatmap depicting expression of LIR-containing proteins across the different comparisons.

5.3.6 Validating candidate regulators of phagosomal acidification from the proteome of amino acid-starved microglia

We studied the proteome of amino acid-starved microglia during efferocytosis for candidate regulators driving heightened phagosomal corpse acidification in these cells. The autophagy components ATG2A and ATG2B, which are involved in lipid transfer (Osawa *et al.*, 2019) and the growth and closure of the autophagosome membrane (Broadbent *et al.*, 2023, Velikkakath *et al.*, 2012), were differentially expressed in amino acid-starved and -fed microglia that had engulfed apoptotic cargo. Given that starvation is a known inducer of autophagy and autophagy components have previously been linked to phagocytosis, we shortlisted these as candidates for further validation. We also examined the sorting nexin SNX17, which plays a role in vesicle trafficking (Steinberg *et al.*, 2012, Zhou *et al.*, 2022), and the transcription factor STAT3, which is involved in both immune system (Campana *et al.*, 2018) and lysosomal protease regulation (Liu *et al.*, 2018, Lloyd-Lewis *et al.*, 2018). We performed western blotting to validate that these targets. However, we did not detect differences in protein levels of SNX17, ATG2B or phosphorylated STAT3 between amino acid- fed and -starved during efferocytosis (Figure 5.9).

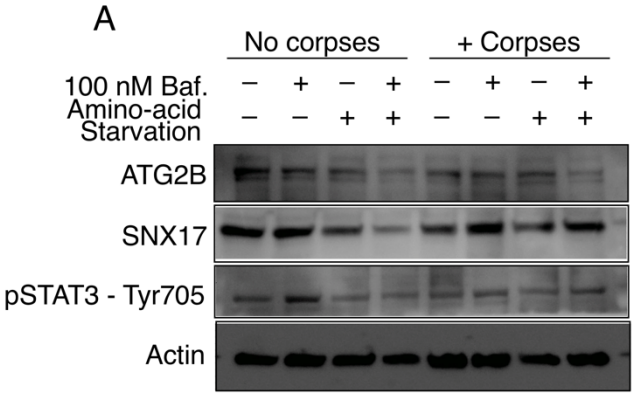

Figure 5.9 Validating candidate drivers of apoptotic cargo acidification in amino acid-starved microglia during efferocytosis. (A) Western blot of amino acid-fed or -starved HMC3 microglia co-cultured with or without epHero bait and 100 nM bafilomycin for 24 hr. Representative immunoblot of two independent experiments is shown.

5.4 DISCUSSION

Here, we employed our previously developed epHero probe to show that prolonged amino acid starvation increases the acidification of phagosomes containing apoptotic corpses in microglia and that, notably, this occurs without any discernible changes to the engulfment of apoptotic cargo. Surprisingly, even when microglia were re-stimulated with amino acids following a period of starvation, this heightened phagosomal acidification persisted, indicating that the impact of amino acid deprivation on efferocytosis extends beyond the period of starvation itself. Proteomic comparison between fed and starved microglia revealed that prolonged amino acid starvation caused an up-regulation in DNA and RNA binding and repair processes.

However, when amino acid starvation was combined with efferocytosis, proteins involved in these pathways reverted to normal levels.

Recently, several groups have reported links between amino acid metabolism and apoptotic corpse clearance. For instance, following an initial round of efferocytosis, apoptotic cell-derived arginine and ornithine are required to activate the actin regulator Rac1 and facilitate the engulfment of subsequent apoptotic corpses (Yurdagul *et al.*, 2020). Consistent with this, we observed that although amino acid metabolic pathways were generally up-regulated during efferocytosis in amino acid-starved microglia, arginine metabolism was depressed. This suggests that microglia prioritise obtaining arginine through efferocytosis mechanisms. Further, compared to microglia that have not engulfed apoptotic corpses, amino acid-starved microglia also up-regulated the pathway involved in the regulation of ornithine decarboxylase, the enzyme that facilitates ornithine-mediated Rac1 activation. The amino acids glutamine and methionine have also been implicated in efferocytosis. Apoptotic cell methionine and its derivative SAM are required for the epigenetic regulation of efferocytosis-mediated tissue resolution (Ampomah *et al.*, 2022), while glutamine metabolism is required to meet the high energy demands of cytoskeletal rearrangements during efferocytosis (Merlin *et al.*, 2021). Consistent with these findings, our proteomic analysis of amino acid-starved microglia during efferocytosis revealed an enrichment in pathways related to glutamine and methionine transport and metabolism. Moreover, we observed an increase in proteins involved in the synthesis of serine, an amino acid also involved in SAM generation (Maddocks *et al.*, 2016), and those involved in the degradation of branched chain amino acids (BCAA) leucine, valine and isoleucine.

Considering that neither serine nor BCAAs have been previously associated with efferocytosis, coupled with the recent paradigm shift implicating amino acids as immune system modulators rather than mere protein building blocks, future work to investigate the precise contribution of these amino acids during apoptotic corpse clearance is warranted.

Surprisingly, despite the amino acid starvation-mediated increase in cargo acidification during efferocytosis, no changes were observed to proteins involved in the regulation of intracellular pH, indicating that amino acid starvation may play a role in the trafficking of cargo to acidic compartments rather than directly modulating phagolysosomal pH itself. In line with this, several proteins involved in vesicle trafficking were down-regulated in amino acid-starved cells during efferocytosis. Of note, expression of SNX17 – a sorting nexin that mediates cargo recycling by directing it away from lysosomal degradation (Steinberg *et al.*, 2012, Zhou *et al.*, 2022) – was reduced in amino acid-starved microglia during efferocytosis. Given its role in recycling pathways, reduced SNX17 could, therefore, result in increased lysosomal delivery of phagosomal material. We also observed alterations in the levels of the autophagy-related proteins ATG2A and ATG2B in amino acid-starved microglia that had ingested apoptotic corpses. In addition to its role in autophagy (Broadbent *et al.*, 2023, Velikkakath *et al.*, 2012), ATG2B has recently been linked to a non-canonical form of autophagy involving the recruitment of LC3 machinery to single membranes during lysosome damage (Cross *et al.*, 2023), endocytosis (Heckmann *et al.*, 2019), and phagocytosis (Martinez *et al.*, 2011, Martinez *et al.*, 2015). ATG2B could therefore play a role in the phagosomal acidification of apoptotic cargo, either via canonical or

non-canonical autophagy-dependent mechanisms. However, we did not detect any changes to protein levels of ATG2B or SNX17 via western blot. One possible explanation for this discrepancy between our proteomics and western blot results could be that the proteomic analysis was performed on microglia that had engulfed apoptotic cargo, as determined via flow cytometry, whereas immunoblotting was done on a bulk microglial population. Microglia that had not engulfed cargo may have contributed to the protein signal detected in our western blots, confounding our analysis. In the future, immunoblotting for these targets on a sorted microglial population, coupled with functional screens may yield more conclusive information.

5.5 SUPPLEMENTARY INFORMATION

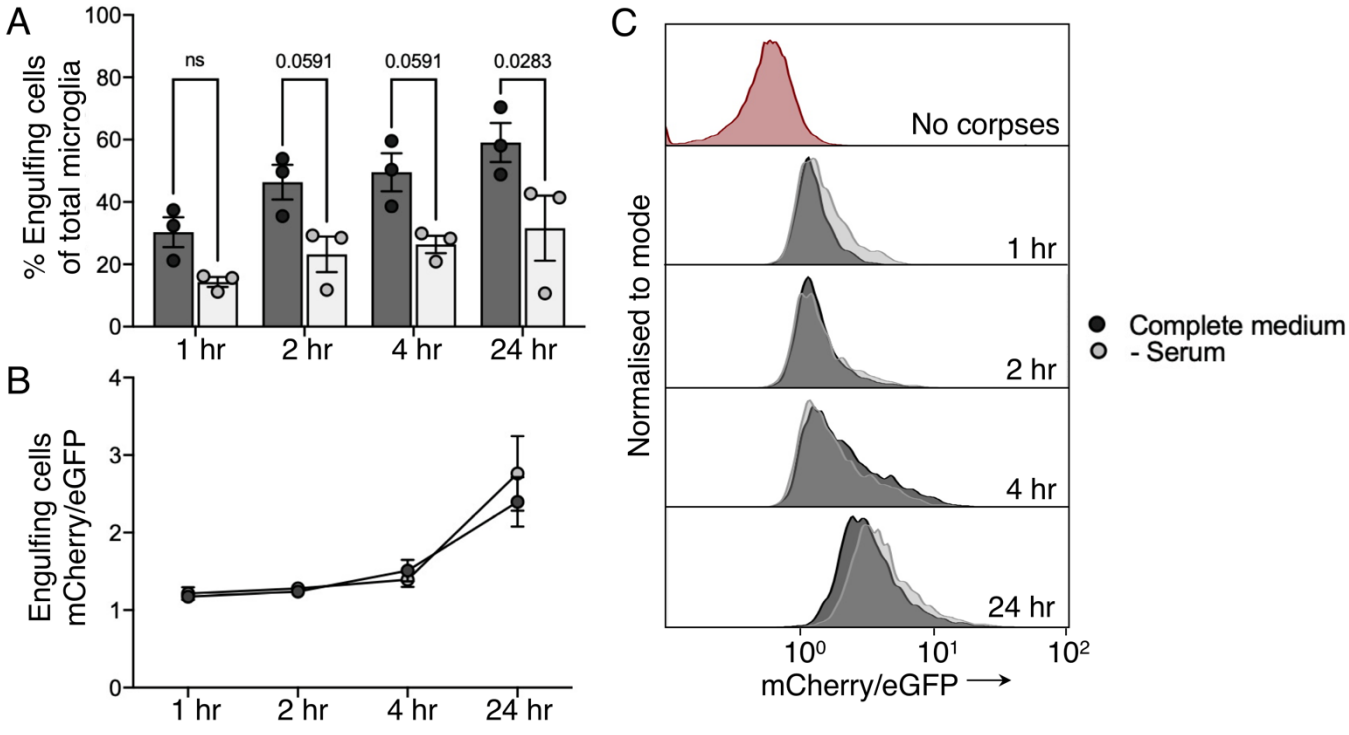

Prolonged serum starvation of HMC3 co-cultured with epHero bait

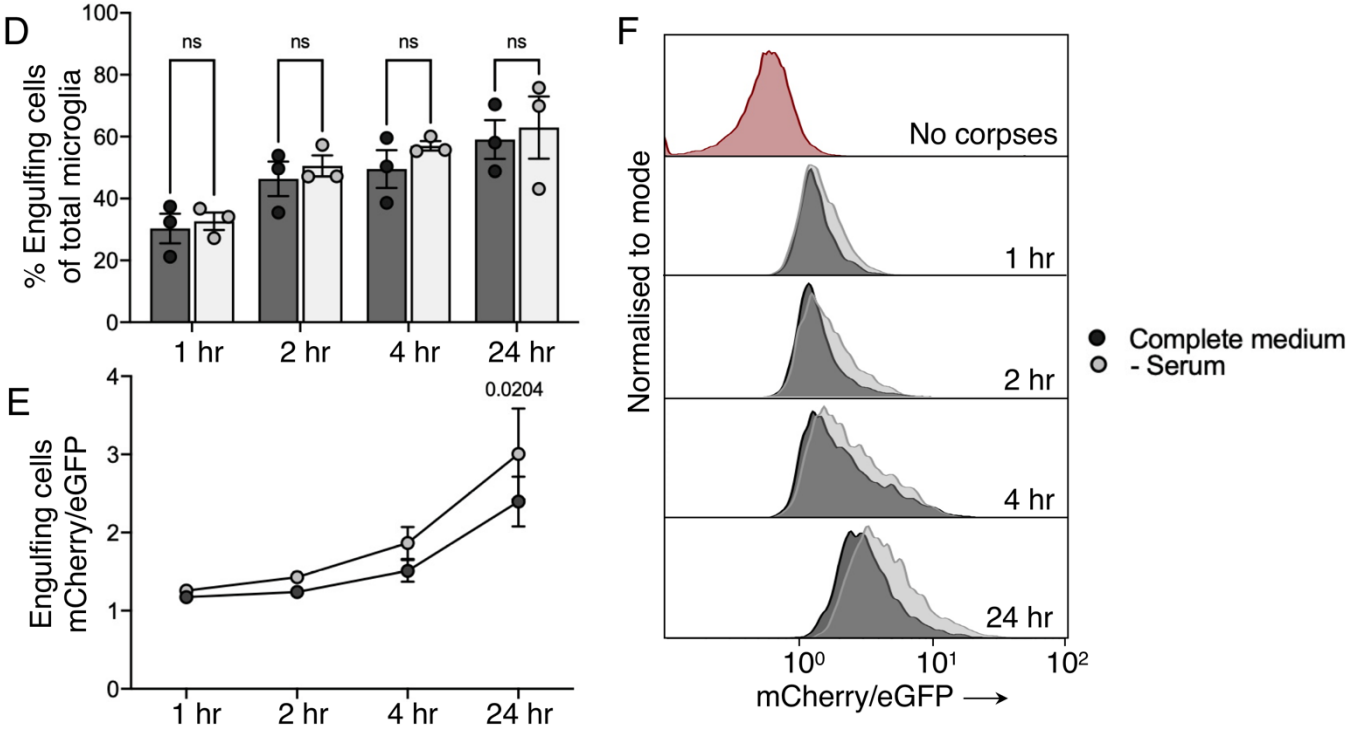

Serum starvation and restimulation of HMC3 co-cultured with epHero bait

Supplementary Figure 5.1 Serum starvation reduces apoptotic corpse uptake during microglial efferocytosis. (A) Quantification of the percentage of

phagocytosing cells from serum-fed or -starved microglia co-cultured with epHero bait for up to 24 hr. **(B)** mCherry/eGFP ratio from microglia that have phagocytosed cargo after being co-cultured with apoptotic epHero bait for up to 24 hr, with or without serum. **(C)** Representative histograms from *(B).* **(D)** Quantification of the percentage of phagocytosing cells from serum-fed or -starved (and re-stimulated) microglia incubated with epHero apoptotic cells for up to 24 hr. **(E)** mCherry/eGFP ratio from microglia that have phagocytosed cargo after being co-cultured with apoptotic epHero bait for up to 24r h, with or without serum starvation (and re-stimulation). **(F)** Representative histograms from *(E). (A*),*(B),(D)* and *(E).* All data points depict mean ± SEM from three independent experiments (two-way ANOVA with Šídák's multiple comparisons test).

5.6 REFERENCES

Ampomah, P.B., Cai, B., Sukka, S.R., Gerlach, B.D., Yurdagul, A., Jr., Wang, X., Kuriakose, G., Darville, L.N.F., Sun, Y., Sidoli, S., Koomen, J.M., Tall, A.R. and Tabas, I. (2022) 'Macrophages use apoptotic cell-derived methionine and DNMT3A during efferocytosis to promote tissue resolution', *Nat Metab,* 4(4), pp. 444-457.

Broadbent, D.G., Barnaba, C., Perez, G.I. and Schmidt, J.C. (2023) 'Quantitative analysis of autophagy reveals the role of ATG9 and ATG2 in autophagosome formation', *J Cell Biol,* 222(7).

Campana, L., Starkey Lewis, P.J., Pellicoro, A., Aucott, R.L., Man, J., O'Duibhir, E., Mok, S.E., Ferreira-Gonzalez, S., Livingstone, E., Greenhalgh, S.N., Hull, K.L., Kendall, T.J., Vernimmen, D., Henderson, N.C., Boulter, L., Gregory, C.D., Feng, Y., Anderton, S.M., Forbes, S.J. and Iredale, J.P. (2018) 'The STAT3-IL-10-IL-6 Pathway Is a Novel Regulator of Macrophage Efferocytosis and Phenotypic Conversion in Sterile Liver Injury', *J Immunol,* 200(3), pp. 1169-1187.

Carmignac, V., Svensson, M., Körner, Z., Elowsson, L., Matsumura, C., Gawlik, K.I., Allamand, V. and Durbeej, M. (2011) 'Autophagy is increased in laminin α2 chain-deficient muscle and its inhibition improves muscle morphology in a mouse model of MDC1A', *Hum Mol Genet,* 20(24), pp. 4891-4902.

Chiang, P.K., Gordon, R.K., Tal, J., Zeng, G.C., Doctor, B.P., Pardhasaradhi, K. and McCann, P.P. (1996) 'S-Adenosylmethionine and methylation', *Faseb j,* 10(4), pp. 471-480.

Cross, J., Durgan, J., McEwan, D.G. and Florey, O. (2023) 'Lysosome damage triggers direct ATG8 conjugation and ATG2 engagement via CASM', *bioRxiv*, p. 2023.2003.2022.533754.

Dagley, L.F., Infusini, G., Larsen, R.H., Sandow, J.J. and Webb, A.I. (2019) 'Universal Solid-Phase Protein Preparation (USP(3)) for Bottom-up and Top-down Proteomics', *J Proteome Res,* 18(7), pp. 2915-2924.

Doran, A.C., Yurdagul, A., Jr. and Tabas, I. (2020) 'Efferocytosis in health and disease', *Nat Rev Immunol,* 20(4), pp. 254-267.

Fung, C., Lock, R., Gao, S., Salas, E. and Debnath, J. (2008) 'Induction of autophagy during extracellular matrix detachment promotes cell survival', *Mol Biol Cell,* 19(3), pp. 797-806.

Ge, S.X., Jung, D. and Yao, R. (2020) 'ShinyGO: a graphical gene-set enrichment tool for animals and plants', *Bioinformatics,* 36(8), pp. 2628-2629.

Heckmann, B.L., Teubner, B.J.W., Tummers, B., Boada-Romero, E., Harris, L., Yang, M., Guy, C.S., Zakharenko, S.S. and Green, D.R. (2019) 'LC3-Associated Endocytosis Facilitates beta-Amyloid Clearance and Mitigates Neurodegeneration in Murine Alzheimer's Disease', *Cell,* 178(3), pp. 536-551.e514.

Hediyeh-Zadeh, S., Webb, A.I. and Davis, M.J. (2023) 'MsImpute: Estimation of missing peptide intensity data in label-free quantitative mass spectrometry', *Mol Cell Proteomics*, p. 100558.

Hein, L.K., Apaja, P.M., Hattersley, K., Grose, R.H., Xie, J., Proud, C.G. and Sargeant, T.J. (2017) 'A novel fluorescent probe reveals starvation controls the commitment of amyloid precursor protein to the lysosome', *Biochim Biophys Acta Mol Cell Res,* 1864(10), pp. 1554-1565.

Hulsebus, H.J., O'Conner, S.D., Smith, E.M., Jie, C. and Bohlson, S.S. (2016) 'Complement Component C1q Programs a Pro-Efferocytic Phenotype while Limiting TNFα Production in Primary Mouse and Human Macrophages', *Front Immunol,* 7, p. 230.

Jacomin, A.C., Samavedam, S., Promponas, V. and Nezis, I.P. (2016) 'iLIR database: A web resource for LIR motif-containing proteins in eukaryotes', *Autophagy,* 12(10), pp. 1945-1953.

Kabeya, Y., Mizushima, N., Ueno, T., Yamamoto, A., Kirisako, T., Noda, T., Kominami, E., Ohsumi, Y. and Yoshimori, T. (2000) 'LC3, a mammalian homologue of yeast Apg8p, is localized in autophagosome membranes after processing', *Embo j,* 19(21), pp. 5720-5728.

Kirisako, T., Baba, M., Ishihara, N., Miyazawa, K., Ohsumi, M., Yoshimori, T., Noda, T. and Ohsumi, Y. (1999) 'Formation process of autophagosome is traced with Apg8/Aut7p in yeast', *J Cell Biol,* 147(2), pp. 435-446.

Law, C.W., Chen, Y., Shi, W. and Smyth, G.K. (2014) 'voom: Precision weights unlock linear model analysis tools for RNA-seq read counts', *Genome Biol,* 15(2), p. R29.

Liang, Y.Y., Arnold, T., Michlmayr, A., Rainprecht, D., Perticevic, B., Spittler, A. and Oehler, R. (2014) 'Serum-dependent processing of late apoptotic cells for enhanced efferocytosis', *Cell Death Dis,* 5(5), p. e1264.

Liu, B., Palmfeldt, J., Lin, L., Colaço, A., Clemmensen, K.K.B., Huang, J., Xu, F., Liu, X., Maeda, K., Luo, Y. and Jäättelä, M. (2018) 'STAT3 associates with vacuolar H(+)-ATPase and regulates cytosolic and lysosomal pH', *Cell Res,* 28(10), pp. 996-1012.

Lloyd-Lewis, B., Krueger, C.C., Sargeant, T.J., D'Angelo, M.E., Deery, M.J., Feret, R., Howard, J.A., Lilley, K.S. and Watson, C.J. (2018) 'Stat3-mediated alterations in lysosomal membrane protein composition', *J Biol Chem,* 293(12), pp. 4244-4261.

Maddocks, O.D., Labuschagne, C.F., Adams, P.D. and Vousden, K.H. (2016) 'Serine Metabolism Supports the Methionine Cycle and DNA/RNA Methylation through De Novo ATP Synthesis in Cancer Cells', *Mol Cell,* 61(2), pp. 210-221.

Martinez, J., Almendinger, J., Oberst, A., Ness, R., Dillon, C.P., Fitzgerald, P., Hengartner, M.O. and Green, D.R. (2011) 'Microtubule-associated protein 1 light chain 3 alpha (LC3)-associated phagocytosis is required for the efficient clearance of dead cells', *Proc Natl Acad Sci U S A,* 108(42), pp. 17396-17401.

Martinez, J., Malireddi, R.K., Lu, Q., Cunha, L.D., Pelletier, S., Gingras, S., Orchard, R., Guan, J.L., Tan, H., Peng, J., Kanneganti, T.D., Virgin, H.W. and Green, D.R. (2015) 'Molecular characterization of LC3-associated phagocytosis reveals distinct roles for Rubicon, NOX2 and autophagy proteins', *Nat Cell Biol,* 17(7), pp. 893-906.

McCubbrey, A.L., McManus, S.A., McClendon, J.D., Thomas, S.M., Chatwin, H.B., Reisz, J.A., D'Alessandro, A., Mould, K.J., Bratton, D.L., Henson, P.M. and Janssen, W.J. (2022) 'Polyamine import and accumulation causes immunomodulation in macrophages engulfing apoptotic cells', *Cell Rep,* 38(2), p. 110222.

Merlin, J., Ivanov, S., Dumont, A., Sergushichev, A., Gall, J., Stunault, M., Ayrault, M., Vaillant, N., Castiglione, A., Swain, A., Orange, F., Gallerand, A., Berton, T., Martin, J.C., Carobbio, S., Masson, J., Gaisler-Salomon, I., Maechler, P., Rayport, S., Sluimer, J.C., Biessen, E.A.L., Guinamard, R.R., Gautier, E.L., Thorp, E.B., Artyomov, M.N. and Yvan-Charvet, L. (2021) 'Non-canonical glutamine transamination sustains efferocytosis by coupling redox buffering to oxidative phosphorylation', *Nat Metab,* 3(10), pp. 1313-1326.

Nakamura, T., Yamashita, M., Ikegami, K., Suzuki, M., Yanagita, M., Kitagaki, J., Kitamura, M. and Murakami, S. (2021) 'Autophagy facilitates type I collagen synthesis in periodontal ligament cells', *Sci Rep,* 11(1), p. 1291.

Onodera, J. and Ohsumi, Y. (2005) 'Autophagy is required for maintenance of amino acid levels and protein synthesis under nitrogen starvation', *J Biol Chem,* 280(36), pp. 31582-31586.

Osawa, T., Kotani, T., Kawaoka, T., Hirata, E., Suzuki, K., Nakatogawa, H., Ohsumi, Y. and Noda, N.N. (2019) 'Atg2 mediates direct lipid transfer between membranes for autophagosome formation', *Nat Struct Mol Biol,* 26(4), pp. 281-288.

Pankiv, S., Clausen, T.H., Lamark, T., Brech, A., Bruun, J.A., Outzen, H., Øvervatn, A., Bjørkøy, G. and Johansen, T. (2007) 'p62/SQSTM1 binds directly to Atg8/LC3 to facilitate degradation of ubiquitinated protein aggregates by autophagy', *J Biol Chem,* 282(33), pp. 24131-24145.

Pulanco, M.C., Cosman, J., Ho, M.M., Huynh, J., Fing, K., Turcu, J. and Fraser, D.A. (2017) 'Complement Protein C1q Enhances Macrophage Foam Cell Survival and Efferocytosis', *J Immunol,* 198(1), pp. 472-480.

Steinberg, F., Heesom, K.J., Bass, M.D. and Cullen, P.J. (2012) 'SNX17 protects integrins from degradation by sorting between lysosomal and recycling pathways', *J Cell Biol,* 197(2), pp. 219-230.

Velikkakath, A.K., Nishimura, T., Oita, E., Ishihara, N. and Mizushima, N. (2012) 'Mammalian Atg2 proteins are essential for autophagosome formation and important for regulation of size and distribution of lipid droplets', *Mol Biol Cell,* 23(5), pp. 896-909.

Yurdagul, A., Jr., Subramanian, M., Wang, X., Crown, S.B., Ilkayeva, O.R., Darville, L., Kolluru, G.K., Rymond, C.C., Gerlach, B.D., Zheng, Z., Kuriakose, G., Kevil, C.G., Koomen, J.M., Cleveland, J.L., Muoio, D.M. and Tabas, I. (2020) 'Macrophage Metabolism of Apoptotic Cell-Derived Arginine Promotes Continual Efferocytosis and Resolution of Injury', *Cell Metab,* 31(3), pp. 518-533.e510.

Zhou, C., Wu, Z., Du, W., Que, H., Wang, Y., Ouyang, Q., Jian, F., Yuan, W., Zhao, Y., Tian, R., Li, Y., Chen, Y., Gao, S., Wong, C.C.L. and Rong, Y. (2022) 'Recycling

of autophagosomal components from autolysosomes by the recycler complex', *Nat Cell Biol,* 24(4), pp. 497-512.

CHAPTER 6

mTORC1 mediates cross-talk between corpse clearance and autophagic pathways in microglia

Rationale: The work presented in this chapter relates to research objectives 3 and 4, i.e. to determine how modulating efferocytosis impacts canonical autophagy and vice-versa, and to investigate potential mechanism/s driving this interaction. The results herein indicate that mTORC1 is involved in communication between these two synergistic pathways in microglia.

6.1 INTRODUCTION

The phagocytic removal of dead cells via efferocytosis is indispensable for maintaining tissue homeostasis. It involves the binding of phagocytes to apoptotic cells via an assortment of receptors and bridging molecules, triggering downstream pathways that lead to cytoskeletal rearrangements, actin mobilisation, and the formation of a phagocytic cup (Doran, Yurdagul and Tabas, 2020). Material is then engulfed by phagocytes and trafficked towards lysosomes for degradation, activating either antigen presentation (Salina *et al.*, 2022, Campisi *et al.*, 2016) or inflammation resolution pathways (Meriwether *et al.*, 2022, Ampomah *et al.*, 2022, Bhattacharya *et al.*, 2023) in a context-specific manner. Perturbations to efferocytosis have been implicated in several pathologies, including cardiovascular disease (Yurdagul *et al.*, 2017), autoimmune conditions (Geng *et al.*, 2022, Jorge *et al.*, 2022), and neurodegeneration (Etchegaray *et al.*, 2016).

Autophagy is the catabolic process by which intracellular material is sequestered within a double-membraned structure termed an autophagosome, and subsequently delivered to the lysosome for destruction. Under the influence of the master nutritional sensor mTORC1, this process is strongly stimulated by starvation (Onodera and Ohsumi, 2005, Deleyto-Seldas and Efeyan, 2021) which facilitates the breakdown and recycling of non-essential cargo to enable cells to maintain homeostasis during periods of scarcity. A key step in autophagy is the tethering and lipidation of LC3-I to generate LC3-II on the membrane of the nascent double-membraned autophagosome, mediated by two ubiquitin-like conjugation cascades. Cargo can also enter the autophagic pathway via endocytic trafficking, where material is either directed towards the autophagy-lysosome axis for degradation (Coelho *et al.*, 2022, Tian *et al.*, 2013) or packaged into recycling endosomes for delivery to other cellular structures (Fraser *et al.*, 2019).

In addition to its role in autophagy, LC3 can be lipidated onto single membranes during efferocytosis and bacterial phagocytosis, in a process termed CASM, to facilitate lysosomal fusion (Martinez *et al.*, 2011, Martinez *et al.*, 2015, Sanjuan *et al.*, 2007), although the mechanisms underpinning this are unclear. For the most part, this is distinct from autophagy, although the ubiquitin-like conjugation systems are required for both canonical autophagy and CASM (Martinez *et al.*, 2015, Martinez *et al.*, 2011, Fletcher *et al.*, 2018). Beyond this shared lipidation machinery, the CASM and autophagy pathways are considered largely independent of each other. However, seminal works comparing efferocytosis-induced CASM to canonical autophagy solely utilised apoptotic cargo engulfment as a readout for efferocytosis. Key autophagy

proteins that do not affect apoptotic cell uptake may play a role in their post-engulfment trafficking and degradation. Further, recent work in *Caenorhabditis elegans* has demonstrated that canonical double-membraned autophagosomes fuse to phagosomes, and that blocking autophagosome biogenesis results in delayed acidification and degradation of phagosomal contents (Peña-Ramos *et al.*, 2022). Thus, canonical autophagy and CASM are two cellular catabolic pathways whose final destination is the lysosome; they diverge predominantly on the basis of the origin of their cargo: autophagy degrades intracellular material whereas CASM involves the uptake and destruction of extracellular cargo. However, beyond the characterisation of key components involved in CASM, very little is known about other potential interactions between efferocytosis and autophagy.

To date, research into CASM and efferocytosis has predominantly been performed in macrophage-like cells, with results extrapolated for other cell types. Microglia are the resident phagocytes in the brain, and defects in microglial phagocytosis and autophagy have been associated with poorer outcomes in a range of pathological settings, including stroke (Beccari *et al.*, 2023, Buckley *et al.*, 2014, Cai *et al.*, 2019) and neurodegeneration (Cheng *et al.*, 2020, Heckmann *et al.*, 2019, Cho *et al.*, 2014). Here, we investigated autophagy during apoptotic corpse clearance and showed that there is cross-talk between autophagy and efferocytosis in microglia. Autophagic flux is reduced during corpse clearance, and stimulating autophagy with amino acid starvation improves acidification of apoptotic cargo in microglia performing efferocytosis via an mTOR- and protein synthesis-dependent mechanism.

6.2 METHODS

Cell Culture

HMC3 microglial cells were obtained from ATCC and cultured in EMEM containing 10% FCS. Wild-type or epHero-expressing THP1 monocytes were maintained in RPMI 1640 medium supplemented with 10% FCS and 2 mM L-glutamine. All cell lines were maintained at 37°C with 5% CO_2 and were routinely screened for mycoplasma infection.

In vitro efferocytosis assay

For flow cytometry experiments, HMC3 microglia were seeded in 12-well plates at 1 X 10^5 cells per well and maintained overnight. For experiments involving western blots, HMC3 microglia were seeded in six-well plates at 2.5 X 10^5 cells per well and incubated overnight. The following day, wild-type or epHero THP1 bait cells were rendered apoptotic via UV irradiation at 316 nm for 3-4 min and incubated for 3 hr at 37°C with 5% CO_2. Apoptotic bait cells were overlaid onto HMC3 microglia at a 5:1 bait to phagocyte ratio for 4 hr. For flow cytometry measurements, microglia underwent three PBS washes to remove any unattached bait, were dissociated from the plate using trypsin to cleave un-internalised bait, and then analysed on a BDFortessa with appropriate gating controls, with >10000 phagocyte events recorded per sample. All flow cytometry data were analysed on FlowJo™ version 10.8 (BD Life Sciences). For western blots, microglia were washed 4-5 times with PBS to remove un-internalised bait and harvested via scraping into lysis buffer as described below.

For amino acid starvation experiments, HMC3 microglia were treated in EBSS containing 10% dialysed FCS ± amino acids. Where indicated, HMC3 cells were also treated with 100 nM bafilomycin, 1 μM AZD8055, 50 μM chloroquine or 355 μM cycloheximide. All treatments were performed for 4 hr and added to the phagocyte at the same time as the corpses.

Western blotting

HMC3 microglia were treated as described above, harvested via scraping into cell lysis buffer containing protease and phosphatase inhibitors, sonicated on ice, and protein concentration determined via a BCA assay; 10-15 μg protein was loaded per well and electrophoresed through 4-12% SDS-PAGE gels before being transferred to a PVDF membrane as previously described (Hein *et al.*, 2017). For some experiments, a total protein stain was performed with the No-Stain Labelling Reagent as per manufacturer's instructions. Membranes were blocked in tris-buffered saline containing 0.1% (v/v) Tween 20 and 5% (w/v) skim milk or 2% (w/v) BSA, and incubated overnight at 4°C with anti-LC3, anti-SQSTM1, anti-COL1A1, anti-cathepsin D, anti-phospho-STAT3, anti-phospho-4E-BP1, anti-phospho-S6K, anti-S6K or anti-STAT3 antibodies. Membranes were washed and incubated with HRP-conjugated anti-mouse, -goat or -rabbit secondary antibodies (1:10,000) at room temperature for 1 hr. To detect β-actin, membranes were incubated with an HRP-conjugated anti-β-actin antibody (1:10,000) for 1 hr at room temperature. Membranes were developed on the LAS4000 Luminescent Image Analyser (Fujifilm Life Science) using the West Pico or West Femto ECL systems.

Confocal Imaging

HMC3 cells were seeded into 12-well plates containing poly-L-lysine-coated coverslips at 1.5 x 10^5 cells per well and grown overnight. HMC3 cells were treated as described above, either alone or in the presence of THP1 apoptotic corpses at a 5:1 bait: phagocyte ratio. Phagocytes were washed three times with PBS to remove unengulfed bait, and coverslips were fixed with ice-cold 100% methanol for 10 min at -20°C. Coverslips were blocked in PBS containing 5% (w/v) BSA and 0.01% (w/v) saponin for 30 min, and incubated for 1 hr in blocking solution containing anti-LC3 (1:100), anti-SQSTM1 (1:200) and anti-LAMP1 (1:200) primary antibodies. Cells were washed and incubated with secondary antibodies at a 1:500 dilution for 40 min. Coverslips were washed a further three times with PBS, mounted onto slides using Vectashield HardSet with DAPI, and sealed with nail polish.

For live imaging, HMC3 cells were seeded into two-well chambered coverslips at 1.25 x 10^5 cells per well. Cells were treated as described above, and live imaging was performed in a humidified chamber at 37°C and 5% CO_2, with z-stacks (4-6 optical sections, z range ~ 3 μm) taken for each field of view.

All images were acquired using a TCS SP8X confocal microscope with LASX (Leica, Germany) and imported into ImageJ for analysis. For LC3 fluorescence measurements, images from the LC3 channel were manually thresholded and the fluorescence intensity of each cell was analysed via the 'measure' function. For colocalisation analyses, Mander's correlation coefficients were derived using the JACoP plugin (Bolte and Cordelières, 2006).

Lysosome activity measurements

HMC3 microglia underwent phagocytosis-, autophagy- or mTOR-modulating interventions for 4 hr as described above and were stained with Lysotracker Green in accordance with manufacturer's instructions. In brief, 50 nM Lysotracker Green was added to microglia during the final 30 min of treatment. Microglia were then washed three times with PBS, harvested using trypsin, and analysed via flow cytometry. For cathepsin proteolytic activity measurements, HMC3 microglia were seeded into two-well chambered coverslips and treated for 4 hr as detailed above. Cells were incubated with cathepsin L Magic Red during final 30 min of treatment, at the manufacturer-recommended working concentration (1:260). Microglia then underwent three PBS washes, were incubated with fresh cell culture medium with or without amino acids and inhibitors, with live confocal imaging performed immediately after.

Data analysis

All statistical analyses were performed using GraphPad Prism version 8. Sample size and statistical tests for each experiment are detailed in the Figure legend. In general, data were analysed via either one-way or two-way ANOVA. Gaussian distribution was determined via a Shapiro-Wilk test, after which either parametric or non-parametric analyses were performed. For all imaging experiments, *n* denotes a cell or field of view (taken from two to three independent experiments) – statistical analyses and SEM for imaging experiments were based on *n*. All data are presented with individual data points or mean ± SEM, as indicated in the Figure legends. $p \leq 0.05$ was set as the threshold for statistical significance.

6.3 RESULTS

6.3.1 Flux of autophagic cargo is reduced during microglial efferocytosis

We examined flux of key autophagy proteins SQSTM1 and LC3 during microglial efferocytosis (Figure 6.1A). We treated microglia with bafilomycin, a compound that blocks autophagy by inhibiting lysosomal acidification and vesicle fusion (Mauvezin and Neufeld, 2015), and measured the build-up of LC3 and SQSTM1 within lysosomes. Although bafilomycin robustly blocked autophagic flux, causing the accumulation of LC3, this was diminished when microglia were co-cultured with apoptotic corpses (Figure 6.1B). Further, lysosomal delivery of LC3 and SQSTM1 was also curtailed, as evidenced by reduced colocalisation of these proteins with the lysosome marker LAMP1 (Figure 6.1C–D).

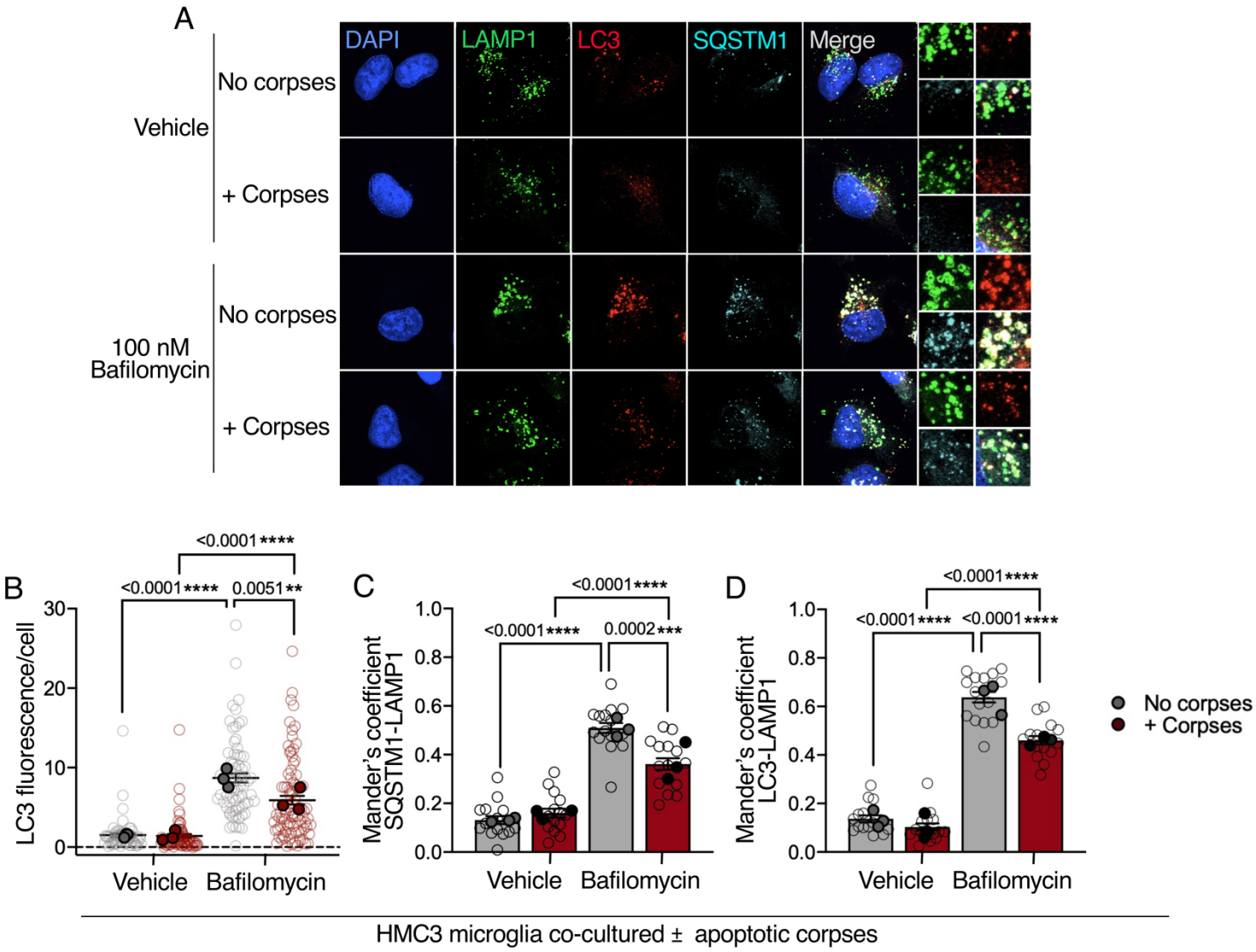

Figure 6.1 Lysosomal delivery of autophagic cargo is compromised during microglial efferocytosis. (A) Confocal images of HMC3 microglia co-cultured with or without apoptotic corpses for 4 hr, in the presence or absence of 100 nM bafilomycin. **(B)** LC3 signal quantification from *(A).* Data points centered on mean ± SEM from n = 60-85 individual cells in three independent experiments (Kruskal-Wallis test with Dunn's multiple comparison correction). **(C)** Colocalisation between SQSTM1 and LAMP1 measured using Mander's overlap coefficient. Error bars denote mean ± SEM from n = 14-15 equal fields of view across three independent experiments (two-way

ANOVA with Turkey's multiple comparisons test). **(D)** Colocalisation between LC3 and LAMP1 as measured using Mander's overlap coefficient. Error bars denote mean ± SEM with n = 14-15 equal fields of view from three independent experiments (two-way ANOVA with Turkey's multiple comparisons test). *(B–D)* Open circles denote measurements taken from each cell or field of view. Closed circles represent the mean from each biologically independent replicate.

6.3.2 Amino acid starvation restores autophagic flux during microglial efferocytosis

Amino acid starvation is a potent inducer of autophagy (Onodera and Ohsumi, 2005) and acts, in part, by repressing mTORC1 activity (Zhou *et al.*, 2013). We treated microglia with bafilomycin for 4 hr and examined starvation-induced autophagic flux during apoptotic corpse clearance. In line with our imaging data, we observed that lipidated LC3 flux was reduced in microglia co-cultured with corpses. Strikingly, this defect was restored upon amino acid starvation (Figure 6.2A–B). Although lipidated LC3-II is commonly used as a marker for autophagy, LC3 is also known to be lipidated onto single membranes during CASM, in response to several stimuli including efferocytosis (Durgan and Florey, 2022). We treated microglia with chloroquine, a lysosomotropic agent known to stimulate both autophagy and non-canonical LC3 lipidation onto single membranes (Jacquin *et al.*, 2017), and showed that, consistent with previous reports (Florey *et al.*, 2015), bafilomycin ablated chloroquine-induced LC3 flux, likely by inhibiting CASM (Supplementary Figure 6.1A). Thus, we reasoned that any LC3-II signal during bafilomycin treatment represented true autophagic flux, with very little contribution from other LC3 lipidation pathways. Nonetheless, we

decided to assess flux of two additional endolysosomal cargoes during efferocytosis. SQSTM1 is a ubiquitin binding selective autophagy receptor that accumulates in lysosomes upon autophagy inhibition (Bjørkøy *et al.*, 2009). Similar to our LC3 results, bafilomycin-generated SQSTM1 flux decreased during efferocytosis and reverted to normal when corpse clearance was coupled with amino acid starvation (Figure 6.2C). We also examined flux of COL1A1, a substrate that is trafficked to lysosomes via endoplasmic reticulum (ER)-phagy (Forrester *et al.*, 2019), a selective autophagy pathway whereby ER components are delivered for lysosomal degradation. In amino acid-fed microglia, bafilomycin increased COL1A1 levels but not during efferocytosis (Figure 6.2D). During amino acid starvation, there was no difference in COL1A1 flux between microglia incubated with and without apoptotic corpses, although starvation itself dramatically reduced COL1A1 levels.

Amino acid starvation represses mTORC1 activity and this induces autophagy (Zhou *et al.*, 2013). In line with this, we observed reduced phosphorylation of the mTORC1 targets ULK1 and ribosomal protein S6 kinase (S6K) during amino acid starvation in microglia. Phosphorylation of these mTORC1 substrates was partially restored during apoptotic corpse clearance, likely because efferocytosis increases amino acid levels in engulfing microglia (McCubbrey *et al.*, 2022).

Taken together, these data indicate that flux of autophagic cargo is compromised during microglial efferocytosis, and this defect can be restored by coupling corpse clearance with amino acid starvation.

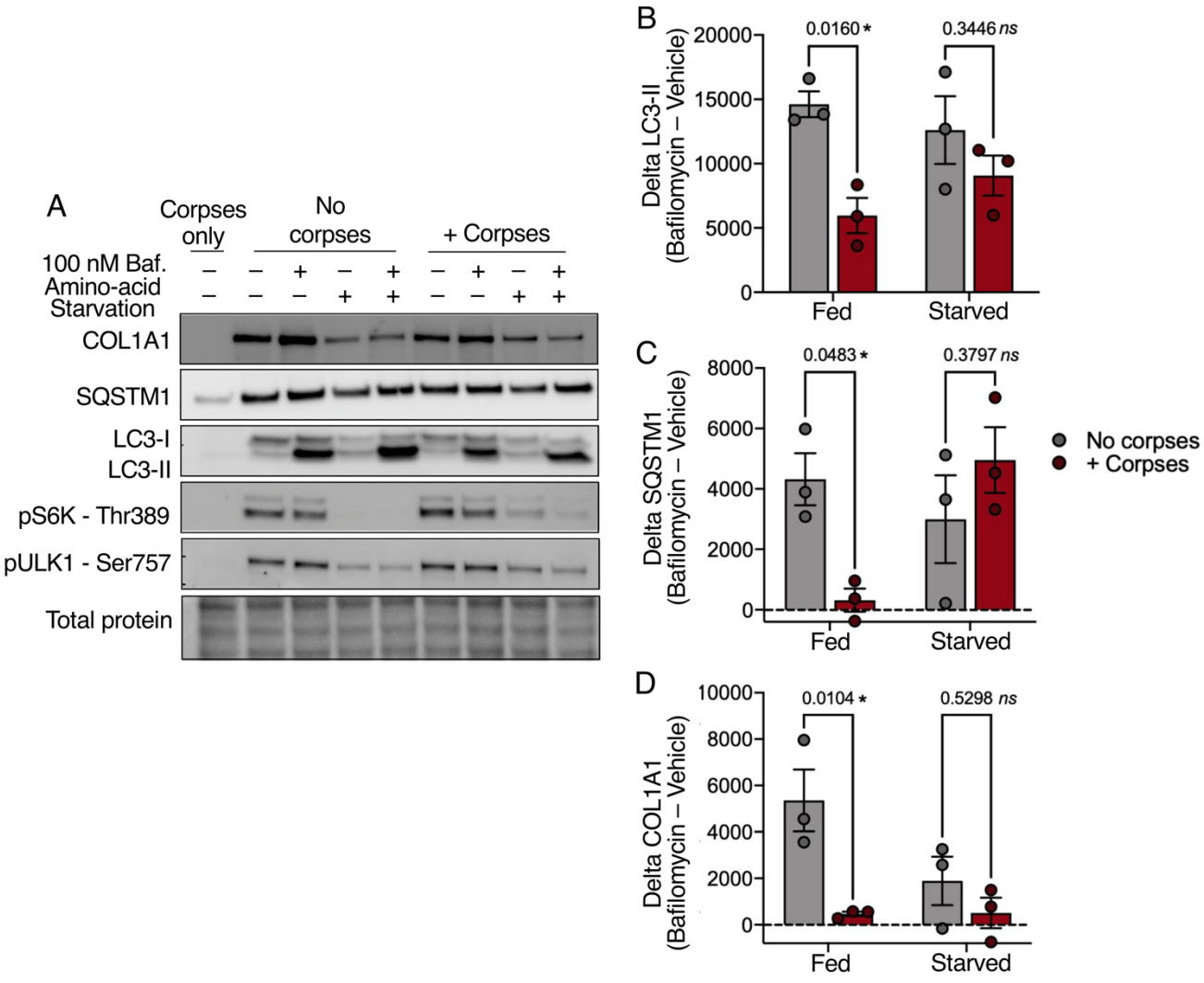

Figure 6.2 Autophagic flux is reduced during apoptotic corpse clearance in microglia (A) Western blot of HMC3 microglia during autophagy induction via 4 hr amino-acid starvation, 100 nM bafilomycin treatment, or both, co-cultured in the presence or absence of apoptotic corpses. **(B)** Densitometric quantification LC3-II flux from *(A).* Flux is defined as the difference in LC3-II signal (normalised to total protein) between bafilomycin and vehicle-treated cells for each condition. Error bars depict

mean ± SEM from three independent experiments (Two-way ANOVA with Šídák's multiple comparisons test). **(C)** Quantification of bafilomycin-induced SQSTM1 flux, measured as described for *(B).* Data centred on mean ± SEM from three biologically independent experiments (two-way ANOVA with Šídák's multiple comparisons test). **(D)** COL1A1 flux during microglial efferocytosis, quantified as described for *(B).* Error bars denote mean ± SEM from three independent experiments (two-way ANOVA with Šídák's multiple comparisons test). *Abbreviations:* ns - not significant.

6.3.3 Amino acid starvation and mTOR inhibition partially restore lysosomal delivery of autophagy proteins during apoptotic corpse clearance

Next, we examined bafilomycin-generated flux of autophagic cargo in microglia that were treated with both apoptotic corpses and pro-autophagy stimuli. Consistent with our previous observations, we noted less LC3 accumulation in microglia when corpses were present (Figure 6.3A–B). Stimulating autophagy via amino acid starvation and the mTOR inhibitor AZD8055 (Chresta *et al.*, 2010) ameliorated this defect, with amino acid starvation exerting a stronger effect compared to mTOR inhibition. Despite this, neither amino acid starvation nor AZD8055 treatment restored lysosomal delivery of LC3, as evidenced by its reduced colocalisation with the LAMP1 marker (Figure 6.3D). Similarly, lysosomal targeting of the selective autophagy receptor SQSTM1 was also compromised during microglial efferocytosis. Interestingly, we observed that this efferocytosis-induced SQSTM1 trafficking defect disappeared in amino acid-starved microglia, although we cannot rule out the possibility that this was driven by the fact that amino acid starvation appeared to reduce total SQSTM1 levels in these cells (Figure 6.3C).

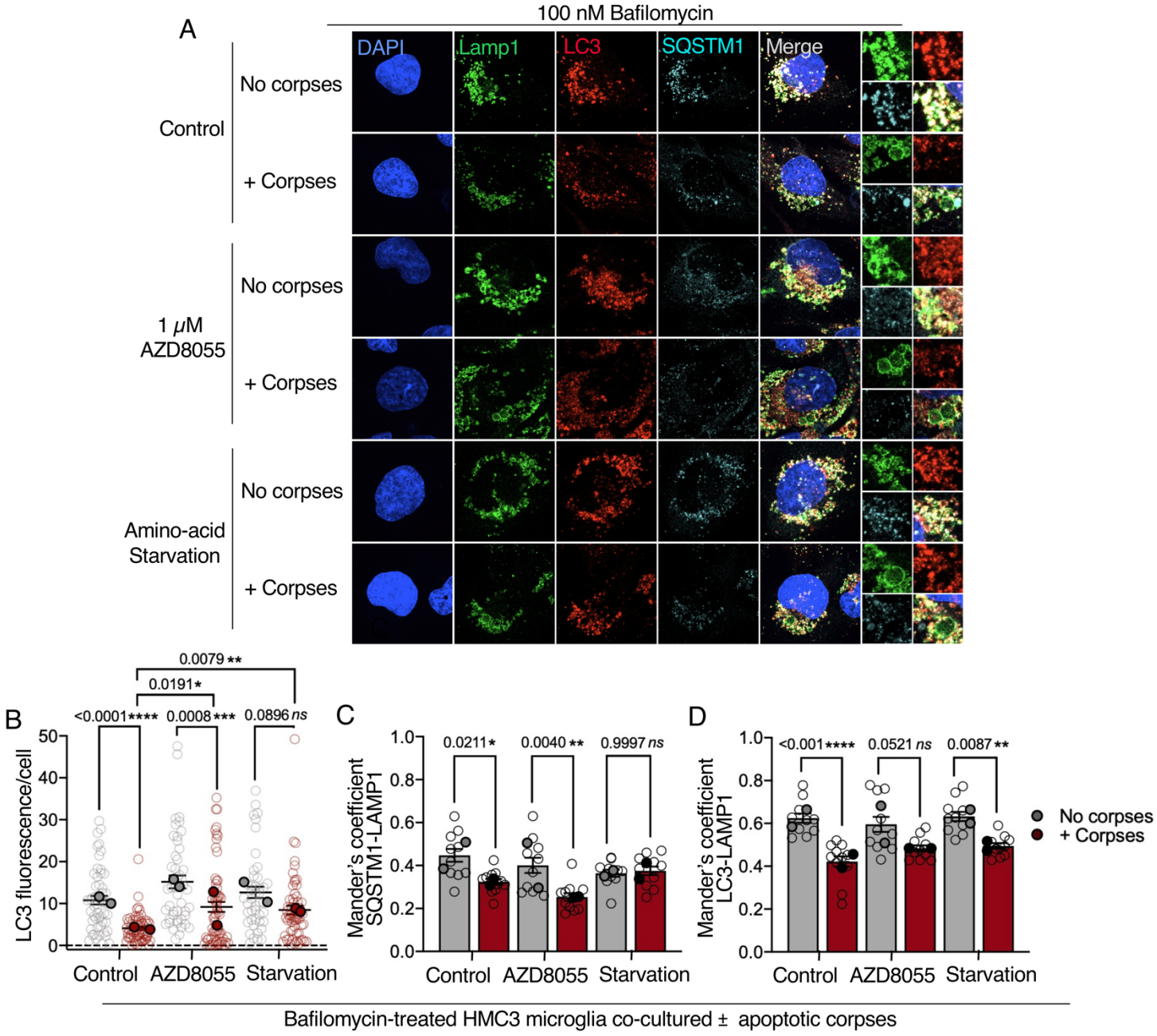

Figure 6.3 Autophagy stimulation partly restores lysosomal flux of autophagic cargo during microglial efferocytosis. (A) Confocal images of 100 nM bafilomycin-treated HMC3 microglia co-cultured with or without apoptotic corpses, during autophagy stimulation via either amino-acid starvation or 1 μM AZD8055-mediated mTOR inhibition. All treatments were performed for 4 hr. **(B)** LC3 fluorescence signal quantification from *(A).* Data points centred on mean ± SEM with n = 44-62 individual

cells from two independent experiments (Kruskal-Wallis test with Dunn's multiple comparison correction). **(C)** Colocalisation between SQSTM1 and LAMP1 measured using Mander's overlap coefficient. Error bars denote mean ± SEM from n = 10-11 equal fields of view across two independent experiments (two-way ANOVA with Turkey's multiple comparisons test). **(D)** Colocalisation between LC3 and LAMP1 as measured using Mander's overlap coefficient. Error bars denote mean ± SEM from n = 10-11 equal fields of view in two independent experiments (two-way ANOVA with Turkey's multiple comparisons test). *(B–D)* Open circles denote measurements taken from each cell or field of view. Closed circles represent the mean for each biologically independent replicate. *Abbreviations:* ns - not significant.

6.3.4 Amino acid starvation during efferocytosis increases corpse acidification in an mTOR- and protein synthesis-dependent manner

Previously, we reported that amino acid starvation – a stimulus which strongly induces autophagy (Onodera and Ohsumi, 2005) – increased acidification of apoptotic cargo during efferocytosis. Starvation-induced autophagy is partially mediated by a repression in mTORC1 activity (Zhou *et al.*, 2013). In line with this, we observed reduction in phosphorylation of the mTORC1 targets S6K and ULK1 during amino acid starvation. We therefore sought to determine whether suppressing mTORC1 activity could recapitulate the starvation-induced increase in phagosomal efferocytosis. We employed the epHero reporter – which provides information on both the uptake and acidification of apoptotic material – to examine efferocytosis in HMC3 microglia that were undergoing either amino acid starvation, treatment with the mTOR inhibitor AZD8055 or a combination of the two interventions. Given that mTORC1 activity

modulates protein synthesis (Holz *et al.*, 2005), we also treated cells with cycloheximide, a protein synthesis inhibitor (Baliga, Pronczuk and Munro, 1969, Schneider-Poetsch *et al.*, 2010) to determine whether the starvation-mediated increase in apoptotic cargo acidification involved the synthesis of new proteins. We verified the efficacy of our cycloheximide treatment in blocking protein translation (Supplementary Figure 6.1B) by measuring the incorporation of puromycin to newly synthesised proteins (Schmidt *et al.*, 2009).

Consistent with our previous results, amino acid starvation increased the acidification of apoptotic corpses during microglial efferocytosis (Figure 6.4A–B). Surprisingly, mTOR inhibition with AZD8055 reduced efferocytic flux, as indicated by a decrease in the mCherry/eGFP ratio. Further, combining amino acid starvation with AZD8055 treatment abolished the previously observed increase in cargo acidification caused by starvation alone. Although cycloheximide by itself did not affect corpse acidification, cycloheximide coupled with starvation eliminated the heightened corpse acidification induced by amino acid starvation. Additionally, amino acid starvation, cycloheximide and AZD8055 treatment all slightly reduced the engulfment of apoptotic material (Figure 6.4C). As expected, blocking lysosomal acidification with bafilomycin completely abolished efferocytic flux in microglia, and there were no differences in cargo acidification between any of the tested conditions when bafilomycin was present (Figure 6.4D–E). However, similar to our previous findings, both amino acid starvation and AZD8055 resulted in a small reduction to corpse uptake in bafilomycin-treated microglia (Figure 6.4F).

Together, these data indicate a role for mTOR in phagosomal cargo acidification and, counter-intuitively, suggest that both mTOR activity and protein synthesis are required for the amino acid restriction-mediated increase in corpse acidification during efferocytosis.

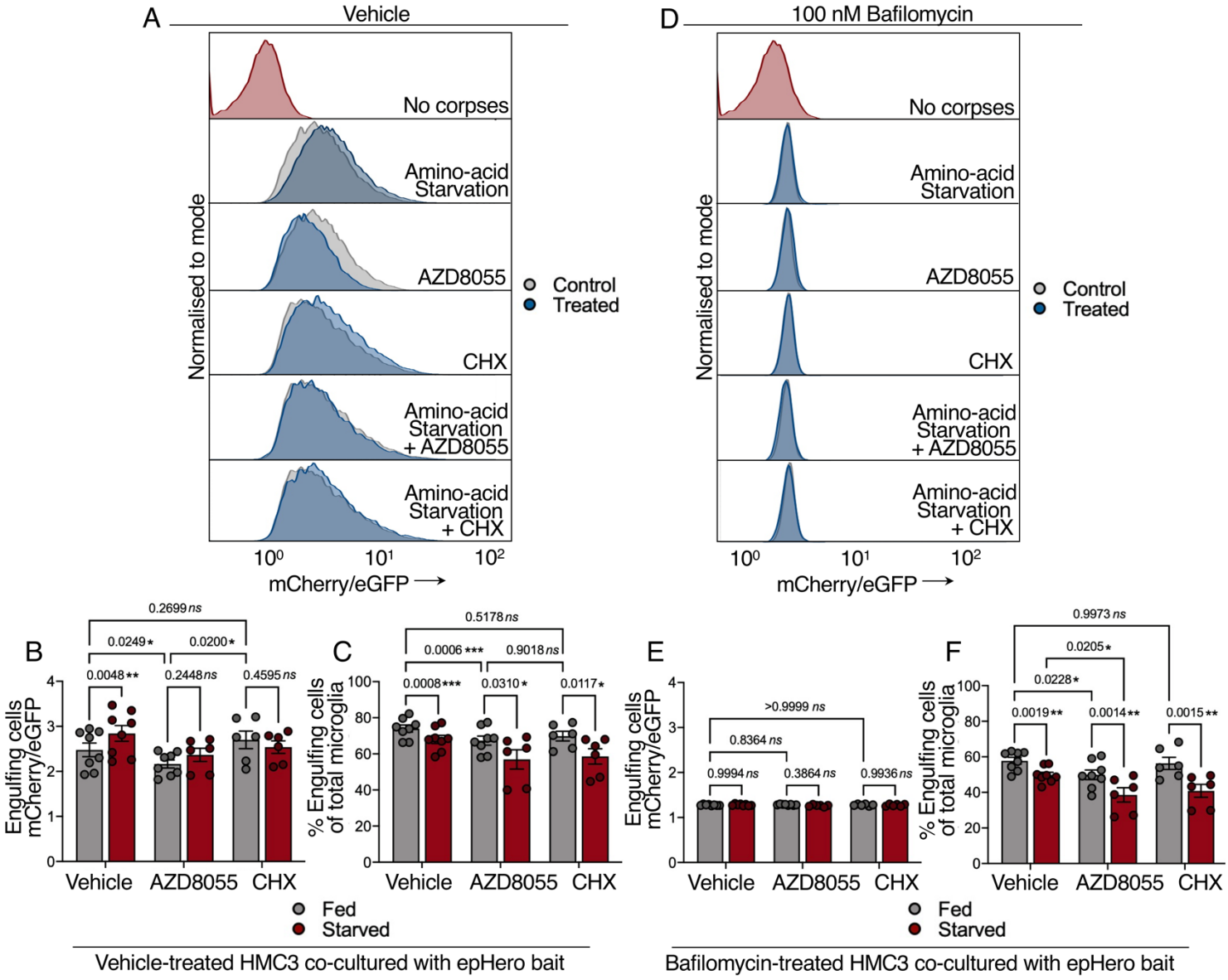

Figure 6.4 Amino acid starvation increases phagolysosomal acidification during microglial corpse clearance via an mTOR-dependent mechanism. (A) Histograms of the mCherry/eGFP signal from HMC3 microglia containing phagocytosed cargo 4 hr after being co-cultured with apoptotic epHero bait and treated with the following:

amino acid starvation, 1 μM AZD8055 or 355 μM cycloheximide (CHX). **(B)** mCherry/eGFP ratio from microglia containing engulfed cargo after being treated as described in *(A).* Error bars represent mean ± SEM; n = 6-8 measurements from three- to four biologically independent experiments (two-way ANOVA followed by Turkey's multiple comparisons test). **(C)** Percentage of phagocytosing cells from microglia co-cultured with epHero apoptotic bait for 4 hr. Data centred on mean ± SEM; n = 6-8 from three- to four independent experiments (two-way ANOVA with Turkey's multiple comparisons test). **(D)** Representative histograms depicting mCherry/eGFP signal in 100 nM bafilomycin-treated HMC3 microglia containing engulfed cargo after being co-cultured with apoptotic epHero bait, with the following interventions: amino acid starvation, 1 μM AZD8055 or 355 μM CHX, for 4 hr. **(E)** mCherry/eGFP ratio in microglia engulfing cargo after being treated as described in *(E).* Data centred on mean ± SEM, with n = 6-8 measurements from three- to four biologically independent experiments (two-way ANOVA followed by Turkey's multiple comparisons test). **(F)** Percentage of phagocytosing cells from bafilomycin-treated microglia incubated with epHero apoptotic bait for 4 hr. Error bars denote mean ± SEM; n = 6-8 from three to four independent experiments (two-way ANOVA with Turkey's multiple comparisons test). *Abbreviations:* ns - not significant.

6.3.5 Amino acid starvation and mTOR inhibition increase lysosomal biogenesis and activity

We surveyed the lysosomal landscape of microglia during amino acid starvation and AZD8055 treatment. Since we observed that amino acid starvation and mTOR inhibition had opposite effects on phagosomal cargo acidification during microglial

efferocytosis, we posited that our interventions may directly modulate lysosomal function. We stained microglia with the acidotrophic compound Lysotracker Green, which diffuses into cells and sequesters in acidic compartments, predominantly lysosomes (Chazotte, 2011). Both amino acid starvation and mTOR inhibition increased Lysotracker staining in microglia (Figure 6.5A–B). Further, AZD8055 stimulated Lysotracker staining to a greater degree than amino acid starvation alone. Blocking protein synthesis with cycloheximide abolished the starvation-mediated increase in Lysotracker intensity. We also measured lysosome proteolytic capacity using Cathepsin L Magic Red, which contains a substrate linked to a quenched cresyl violet fluorophore via a cathepsin-cleavable site. Upon substrate cleavage, cresyl violet is released and able to fluoresce: an increase in cresyl violet signal therefore indicates better Cathepsin L proteolysis (Creasy *et al.*, 2007). In line with our Lysotracker results, both amino acid starvation and mTOR inhibition increased Cathepsin L Magic Red signal in microglia (Figure 6.5C–D). Treatment with cycloheximide blocked the amino acid starvation-mediated increase in lysosomal proteolysis, indicating that protein synthesis may be required to boost lysosomal capacity in starved cells. Notably, mTOR inhibition via AZD8055 treatment resulted in a larger increase in Cathepsin L protease activity compared to starvation alone. These findings show that both amino acid starvation and mTOR inhibition enhance lysosome biogenesis and proteolysis, with mTOR inhibition being the stronger stimulus of the two.

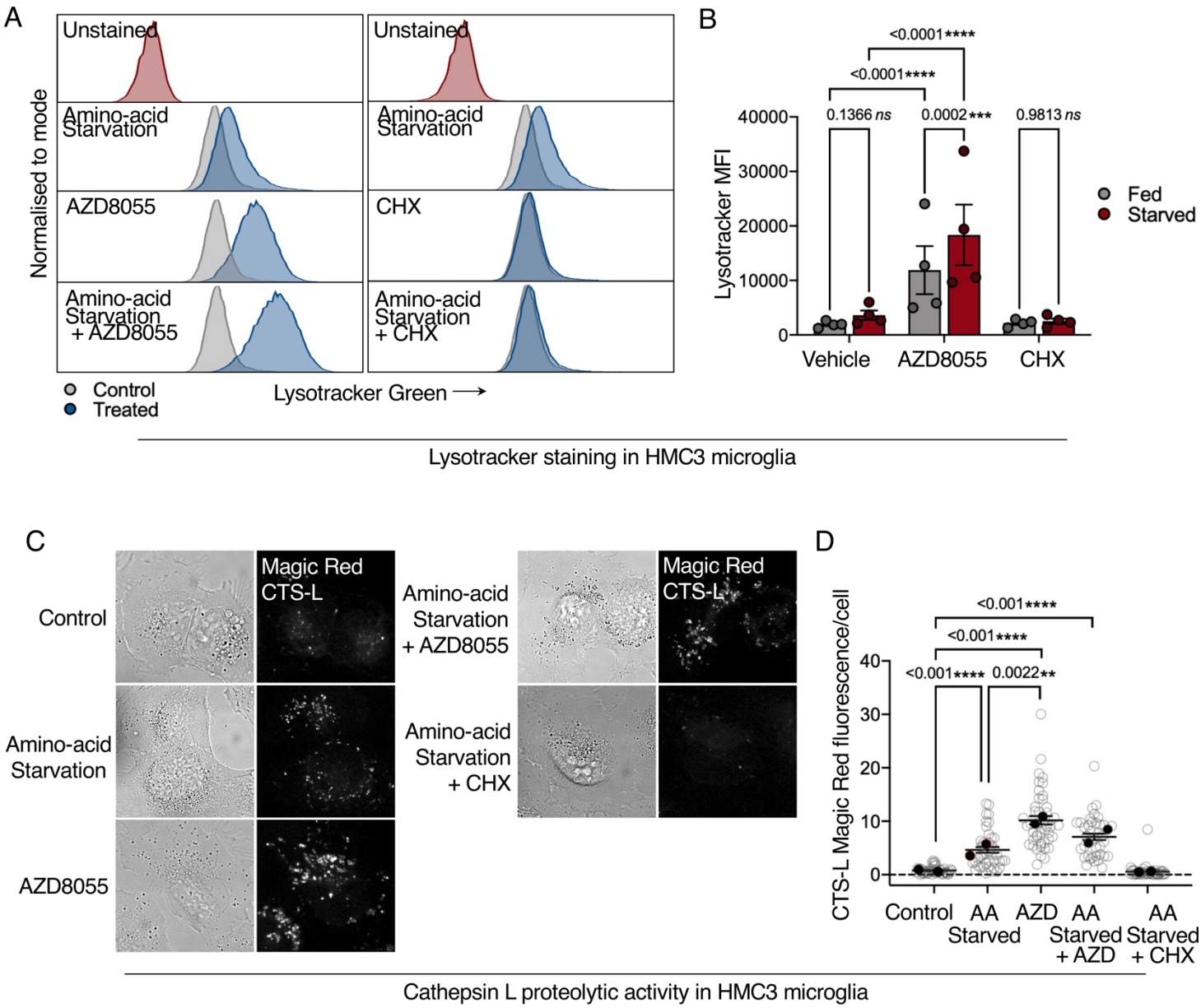

Figure 6.5 Stimulating autophagy via amino acid starvation and mTOR inhibition increases lysosome biogenesis and proteolytic capacity. (A) Representative histograms of Lysotracker staining in amino acid (AA)-fed or -starved HMC3 microglia treated with 1 μM AZD8055 or 355 μM cycloheximide (CHX) for 4 hr. **(B)** Comparison of Lysotracker fluorescence intensity between the treatments described in *(A).* Data centred on mean ± SEM from four independent experiments (two-way ANOVA

followed by Turkey's multiple comparisons test). **(C)** Confocal live-imaging stills depicting degradation of Cathepsin L (CTS-L) magic red substrates in microglia stimulated with 4 hr of amino acid starvation, 1 μM AZD8055 or 355 μM CHX. **(D)** CTS-L Magic Red signal quantification from *(C).* Error bars represent SEM; n = 38-44 individual cells from two independent experiments (Kruskal-Wallis test with Dunn's correction). *Abbreviations:* ns - not significant; MFI - Median fluorescence intensity.

6.3.6 mTORC1 is reactivated during corpse clearance in amino acid-starved microglia

Since we observed that amino acid starvation and mTORC1 inhibition had opposite effects on cargo acidification during microglial efferocytosis, we assessed mTORC1 function in these cells. We noted that blocking protein synthesis with cycloheximide robustly activated mTORC1 in amino acid-starved microglia, as evidenced by phosphorylation of two mTORC1 targets: S6K and eukaryotic translation initiation factor 4E-binding protein 1 (4E-BP1). Surprisingly, we were able to detect low levels of phosphorylated S6K (p70 and p85) and 4E-BP1 during amino acid starvation in microglia, indicating residual mTORC1 activity under these conditions (Figure 6.7A–C). In addition, when apoptotic corpses were co-cultured with starved microglia, we observed a trend where phosphorylation of both 4E-BP1 and S6K increased further. In contrast, AZD8055 treatment completely blocked phosphorylation of mTORC1 downstream substrates, even in the presence of corpses. Thus, mTORC1 can be activated in amino acid-starved microglia performing efferocytosis, likely through the recycling of nutrients derived from the apoptotic cargo itself, and this re-activation cannot occur during pharmacological mTORC1 inhibition.

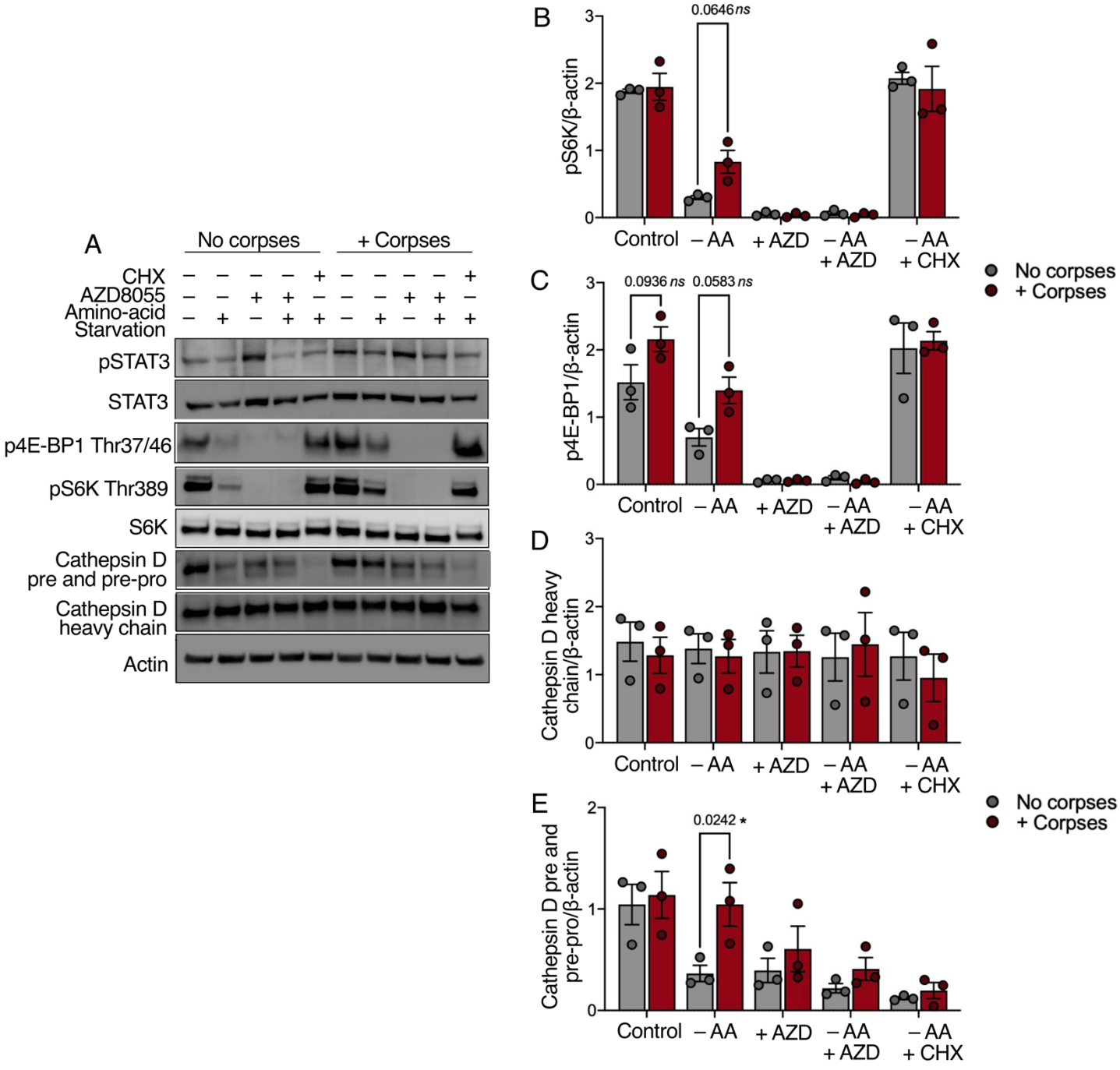

Figure 6.6 mTORC1 is reactivated in amino acid-starved microglia during efferocytosis. (A) Western blot of amino acid (AA)-fed or -starved HMC3 microglia treated with 1 μM AZD8055 or 355 μM cycloheximide (CHX) for 4 hr and co-cultured in the presence or absence of apoptotic corpses. **(B)** Densitometric quantification of pS6K; **(C)** p4E-BP1; **(D)** mature Cathepsin D; and **(E)** pre- and pre-pro Cathepsin D

from *(A).* All densitometric quantifications are presented relative to β-actin. Error bars denote mean ± SEM from three independent experiments (two-way ANOVA with Šídák's multiple comparisons test). *Abbreviations:* ns - not significant.

Given the regulatory role that mTORC1 plays in lysosome biogenesis and activity, we also assessed protein levels of the lysosomal protease Cathepsin D. The glycosylated pre- and pre-pro forms of Cathepsin D undergo a series of processing steps, culminating in the formation of a mature, functional protease localised to the lysosome. We observed no differences in mature Cathepsin D levels across any of the tested conditions (Figure 6.7D). However, efferocytosis increased levels of pre- and pre-pro Cathepsin D in amino acid-starved, but not mTOR-inhibited, microglia (Figure 6.7E). These high molecular weight Cathepsin D precursors disappeared in cycloheximide-treated cells, indicating that protein levels of immature Cathepsin D may represent synthesis of this protease. Thus, even though we previously observed that AZD8055-mediated mTOR inhibition was more potent at inducing lysosome activity compared to amino acid starvation, starvation may selectively modulate specific lysosome proteases.

6.4 DISCUSSION

Efferocytosis and autophagy are two major quality control mechanisms which involve the degradation and recycling of surrounding dead cells and intracellular cargo, respectively, and are crucial for maintaining homeostasis. This is particularly important in the brain, which requires a tightly regulated microenvironment for optimal function. In the present study, we showed that autophagic flux was reduced during microglial

efferocytosis and that stimulating autophagy via either amino acid starvation or mTOR inhibition could partially restore this defect. Further, although both amino acid starvation and mTOR inhibition increased lysosomal biogenesis and proteolytic capacity, only amino acid starvation increased acidification of apoptotic material during efferocytosis. To date, canonical autophagy and efferocytosis have been considered parallel yet independent processes, sharing only the LC3 conjugation machinery during CASM (Martinez *et al.*, 2011, Martinez *et al.*, 2015, Fletcher *et al.*, 2018). Here, we employed a model where CASM is pharmacologically inhibited, and demonstrated that autophagic flux is reduced during corpse clearance in microglia. Thus, we show a relationship between autophagy and efferocytosis beyond CASM.

Amino acid starvation is a potent suppressor of mTORC1 activity (Zhou *et al.*, 2013). In line with previous reports (Ratto *et al.*, 2022, Zhou *et al.*, 2013), we observed that both amino acid starvation and mTOR inhibition increased lysosomal biogenesis and activity. However, when we stimulated autophagy via these two seemingly related mechanisms in microglia, they had opposite effects on efferocytosis efficiency. In contrast to amino acid starvation which improves efferocytosis, why does AZD8055-mediated mTOR inhibition reduce, rather than drive, corpse acidification? In a *Drosophila melanogaster* model of neurodegeneration, stimulating glial mTORC1 activity via over-expression of its upstream promoter Rheb resulted in improved corpse processing (Etchegaray *et al.*, 2016). Further, recent work has shown that once cargo is delivered to the lysosome, a series of phagolysosomal tubulation and fission events facilitate its degradation (Lancaster *et al.*, 2021) in an mTORC1-dependent manner, whereby depletion of mTORC1 results in reduced phagosomal vesiculation,

delaying the clearance of cargo (Fazeli *et al.*, 2018, Fazeli *et al.*, 2023, Krajcovic *et al.*, 2013). Together, these results suggest that although conventionally considered an inhibitor of lysosomal function, mTORC1 can, counter-intuitively, promote lysosomal catabolism of material under certain conditions.

We found key differences in mTORC1 activity levels between amino acid starvation and pharmacological mTOR inhibition in microglia. mTORC1 function was only partially suppressed in amino acid-starved microglia – as evidenced by phosphorylation of its targets S6K and 4E-BP – and increased further when corpses were added to microglia. In contrast, AZD8055 treatment completely abolished mTORC1 substrate phosphorylation. Thus, amino acid starvation enables some residual mTORC1 activity to occur, which may be required for the efficient acidification and clearance of apoptotic material by microglia. Previous reports connecting mTORC1 to the fission and subsequent clearance of phagosomal cargo support this theory (Fazeli *et al.*, 2023, Krajcovic *et al.*, 2013). At present, there is no evidence that directly links phagosomal fission to acidification, however, our data suggest that mTORC1 promotes the acidification of corpse-containing phagosomes during microglial efferocytosis. Whether this occurs as part of its role in phagosomal fission or via an additional unrelated mechanism is yet to be determined.

We observed that inhibiting protein synthesis with cycloheximide did not impact cargo acidification under nutrient-replete conditions. However, in amino acid-starved microglia, cycloheximide reduced apoptotic corpse acidification, lysosomal biogenesis, and proteolytic capacity. While we initially posited that these effects were

driven by its blockage of protein synthesis, subsequent experiments showed that mTORC1 activity was high in amino acid-starved cells that had also been treated with cycloheximide. This likely occurred due to a cycloheximide-mediated increase in intracellular amino acid levels and consequent inhibition of autophagy, as has been documented previously (Watanabe-Asano, Kuma and Mizushima, 2014). Thus, it is difficult to determine whether cycloheximide's ability to block cargo acidification in starved microglia was driven by a reduction in protein synthesis, the stimulation of mTORC1 or both; this will need to be investigated further.

We noted that amino acid starvation increased lysosome biogenesis and degradative capacity but not to the same extent as AZD8055 treatment. This was likely due to the residual mTORC1 activity in starved cells, as mTORC1 inhibition directly modulates lysosomal pH and proteolysis (Ratto *et al.*, 2022, Zhou *et al.*, 2013). Based on this, we hypothesise that amino acid starvation balances increased lysosomal capacity with mTORC1-dependent phagosomal fission: it suppresses mTORC1 sufficiently to activate catabolic pathways whilst allowing low levels of mTORC1 to facilitate efficient phagosome maturation, thus providing a 'happy medium' which promotes cargo acidification during microglial corpse clearance (Figure 6.7). This theory is bolstered by our observation that amino acid-starved microglia, where mTORC1 was partially on, had increased efferocytosis cargo acidification compared to fed or cycloheximide-treated microglia, in which mTORC1 activity was high. We present this model with two important caveats: (i) while we showed a role for mTORC1 activity in driving efferocytic cargo acidification, we did not directly test whether this occurred via phagolysosomal fission or a different mechanism. Recently, the machinery operating

downstream of mTORC1 in phagolysosomal vesiculation has been characterised in nematodes (Fazeli *et al.*, 2023). Future experiments targeting these components in our efferocytosis model may yield additional insights; and (ii) like most mTOR inhibitors, AZD8055 acts on both mTORC1 and mTORC2 (Chresta *et al.*, 2010). Consequently, we cannot exclude the possibility that some of our observations were driven by mTORC2 inhibition. Specifically targeting mTORC1 activity via genetic ablation or newer, small molecular inhibitors would help untangle the contribution of each mTOR complex towards microglial corpse clearance.

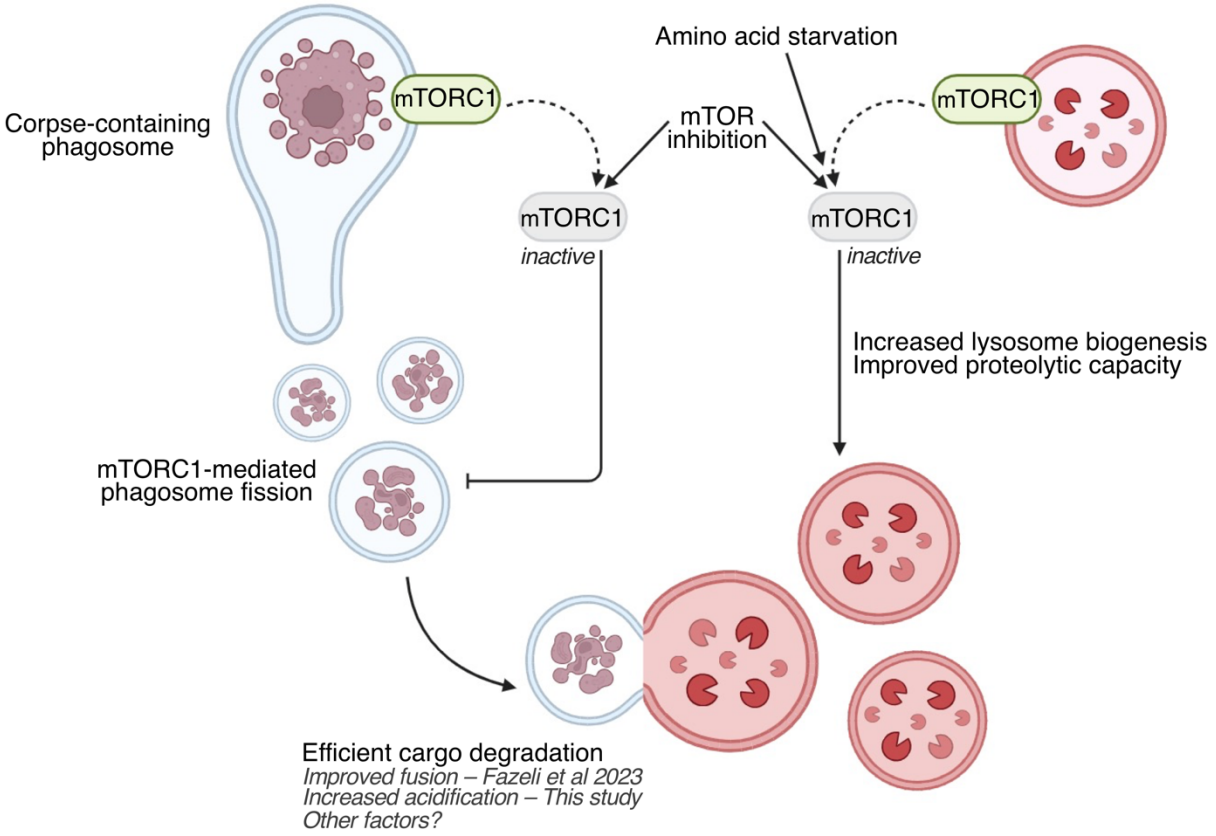

Figure 6.7 A proposed model for the dual role of mTORC1 in both blocking and facilitating catabolism of efferocytic cargo. Pharmacological mTORC1 inhibition which completely suppresses mTORC1. In contrast, amino acid starvation only partly blocks mTORC1 activity, increasing lysosomal activity yet allowing mTORC1-mediated efficient clearance of cargo to occur.

6.5 SUPPLEMENTARY INFORMATION

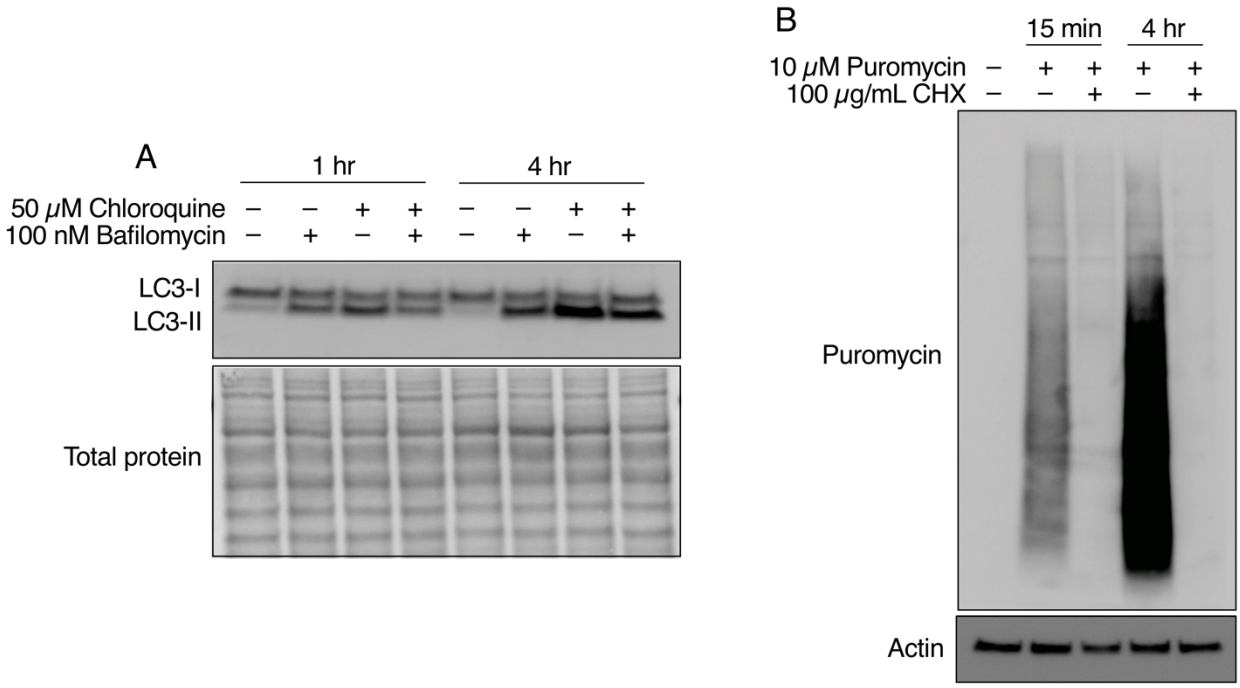

Supplementary Figure 6.1 Verification of efficacy for pharmacological reagents. **(A)** LC3-II lipidation in HMC3 microglia incubated with 50 μM chloroquine or 100 nM bafilomycin for 1 or 4 hr to block flux. When cells were treated with both chloroquine and bafilomycin, bafilomycin was added 15 min prior to chloroquine. **(B)** Protein synthesis in microglia treated with 100 μg/mL cycloheximide (CHX) for 15 min or 4 hr, measured via puromycin incorporation into nascent proteins.

6.6 REFERENCES

Ampomah, P.B., Cai, B., Sukka, S.R., Gerlach, B.D., Yurdagul, A., Jr., Wang, X., Kuriakose, G., Darville, L.N.F., Sun, Y., Sidoli, S., Koomen, J.M., Tall, A.R. and Tabas, I. (2022) 'Macrophages use apoptotic cell-derived methionine and DNMT3A during efferocytosis to promote tissue resolution', *Nat Metab,* 4(4), pp. 444-457.

Baliga, B.S., Pronczuk, A.W. and Munro, H.N. (1969) 'Mechanism of cycloheximide inhibition of protein synthesis in a cell-free system prepared from rat liver', *J Biol Chem,* 244(16), pp. 4480-4489.

Beccari, S., Sierra-Torre, V., Valero, J., Pereira-Iglesias, M., García-Zaballa, M., Soria, F.N., De Las Heras-Garcia, L., Carretero-Guillen, A., Capetillo-Zarate, E., Domercq, M., Huguet, P.R., Ramonet, D., Osman, A., Han, W., Dominguez, C., Faust, T.E., Touzani, O., Pampliega, O., Boya, P., Schafer, D., Mariño, G., Canet-Soulas, E., Blomgren, K., Plaza-Zabala, A. and Sierra, A. (2023) 'Microglial phagocytosis dysfunction in stroke is driven by energy depletion and induction of autophagy', *Autophagy,* 19(7), pp. 1952-1981.

Bhattacharya, P., Dhawan, U.K., Hussain, M.T., Singh, P., Bhagat, K.K., Singhal, A., Austin-Williams, S., Sengupta, S. and Subramanian, M. (2023) 'Efferocytes release extracellular vesicles to resolve inflammation and tissue injury via prosaposin-GPR37 signaling', *Cell Rep,* 42(7), p. 112808.

Bjørkøy, G., Lamark, T., Pankiv, S., Øvervatn, A., Brech, A. and Johansen, T. (2009) 'Monitoring autophagic degradation of p62/SQSTM1', *Methods Enzymol,* 452, pp. 181-197.

Bolte, S. and Cordelières, F.P. (2006) 'A guided tour into subcellular colocalization analysis in light microscopy', *J Microsc,* 224(Pt 3), pp. 213-232.

Buckley, K.M., Hess, D.L., Sazonova, I.Y., Periyasamy-Thandavan, S., Barrett, J.R., Kirks, R., Grace, H., Kondrikova, G., Johnson, M.H., Hess, D.C., Schoenlein, P.V., Hoda, M.N. and Hill, W.D. (2014) 'Rapamycin up-regulation of autophagy reduces infarct size and improves outcomes in both permanent MCAL, and embolic MCAO, murine models of stroke', *Exp Transl Stroke Med,* 6, p. 8.

Cai, W., Dai, X., Chen, J., Zhao, J., Xu, M., Zhang, L., Yang, B., Zhang, W., Rocha, M., Nakao, T., Kofler, J., Shi, Y., Stetler, R.A., Hu, X. and Chen, J. (2019) 'STAT6/Arg1 promotes microglia/macrophage efferocytosis and inflammation resolution in stroke mice', *JCI Insight,* 4(20).

Campisi, L., Barbet, G., Ding, Y., Esplugues, E., Flavell, R.A. and Blander, J.M. (2016) 'Apoptosis in response to microbial infection induces autoreactive TH17 cells', *Nat Immunol,* 17(9), pp. 1084-1092.

Chazotte, B. (2011) 'Labeling lysosomes in live cells with LysoTracker', *Cold Spring Harb Protoc,* 2011(2), p. pdb.prot5571.

Cheng, J., Liao, Y., Dong, Y., Hu, H., Yang, N., Kong, X., Li, S., Li, X., Guo, J., Qin, L., Yu, J., Ma, C., Li, J., Li, M., Tang, B. and Yuan, Z. (2020) 'Microglial autophagy defect causes parkinson disease-like symptoms by accelerating inflammasome activation in mice', *Autophagy,* 16(12), pp. 2193-2205.

Cho, M.H., Cho, K., Kang, H.J., Jeon, E.Y., Kim, H.S., Kwon, H.J., Kim, H.M., Kim, D.H. and Yoon, S.Y. (2014) 'Autophagy in microglia degrades extracellular β-amyloid fibrils and regulates the NLRP3 inflammasome', *Autophagy,* 10(10), pp. 1761-1775.

Chresta, C.M., Davies, B.R., Hickson, I., Harding, T., Cosulich, S., Critchlow, S.E., Vincent, J.P., Ellston, R., Jones, D., Sini, P., James, D., Howard, Z., Dudley, P., Hughes, G., Smith, L., Maguire, S., Hummersone, M., Malagu, K., Menear, K., Jenkins, R., Jacobsen, M., Smith, G.C., Guichard, S. and Pass, M. (2010) 'AZD8055 is a potent, selective, and orally bioavailable ATP-competitive mammalian target of rapamycin kinase inhibitor with in vitro and in vivo antitumor activity', *Cancer Res,* 70(1), pp. 288-298.

Coelho, P.P., Hesketh, G.G., Pedersen, A., Kuzmin, E., Fortier, A.N., Bell, E.S., Ratcliffe, C.D.H., Gingras, A.C. and Park, M. (2022) 'Endosomal LC3C-pathway selectively targets plasma membrane cargo for autophagic degradation', *Nat Commun,* 13(1), p. 3812.

Creasy, B.M., Hartmann, C.B., White, F.K. and McCoy, K.L. (2007) 'New assay using fluorogenic substrates and immunofluorescence staining to measure cysteine cathepsin activity in live cell subpopulations', *Cytometry A,* 71(2), pp. 114-123.

Deleyto-Seldas, N. and Efeyan, A. (2021) 'The mTOR-Autophagy Axis and the Control of Metabolism', *Front Cell Dev Biol,* 9, p. 655731.

Doran, A.C., Yurdagul, A., Jr. and Tabas, I. (2020) 'Efferocytosis in health and disease', *Nat Rev Immunol,* 20(4), pp. 254-267.

Durgan, J. and Florey, O. (2022) 'Many roads lead to CASM: Diverse stimuli of noncanonical autophagy share a unifying molecular mechanism', *Sci Adv,* 8(43), p. eabo1274.

Etchegaray, J.I., Elguero, E.J., Tran, J.A., Sinatra, V., Feany, M.B. and McCall, K. (2016) 'Defective Phagocytic Corpse Processing Results in Neurodegeneration and Can Be Rescued by TORC1 Activation', *J Neurosci,* 36(11), pp. 3170-3183.

Fazeli, G., Levin-Konigsberg, R., Bassik, M.C., Stigloher, C. and Wehman, A.M. (2023) 'A BORC-dependent molecular pathway for vesiculation of cell corpse phagolysosomes', *Curr Biol,* 33(4), pp. 607-621.e607.

Fazeli, G., Stetter, M., Lisack, J.N. and Wehman, A.M. (2018) 'C. elegans Blastomeres Clear the Corpse of the Second Polar Body by LC3-Associated Phagocytosis', *Cell Rep,* 23(7), pp. 2070-2082.

Fletcher, K., Ulferts, R., Jacquin, E., Veith, T., Gammoh, N., Arasteh, J.M., Mayer, U., Carding, S.R., Wileman, T., Beale, R. and Florey, O. (2018) 'The WD40 domain of ATG16L1 is required for its non-canonical role in lipidation of LC3 at single membranes', *Embo j,* 37(4).

Florey, O., Gammoh, N., Kim, S.E., Jiang, X. and Overholtzer, M. (2015) 'V-ATPase and osmotic imbalances activate endolysosomal LC3 lipidation', *Autophagy,* 11(1), pp. 88-99.

Forrester, A., De Leonibus, C., Grumati, P., Fasana, E., Piemontese, M., Staiano, L., Fregno, I., Raimondi, A., Marazza, A., Bruno, G., Iavazzo, M., Intartaglia, D., Seczynska, M., van Anken, E., Conte, I., De Matteis, M.A., Dikic, I., Molinari, M. and

Settembre, C. (2019) 'A selective ER-phagy exerts procollagen quality control via a Calnexin-FAM134B complex', *Embo j,* 38(2).

Fraser, J., Simpson, J., Fontana, R., Kishi-Itakura, C., Ktistakis, N.T. and Gammoh, N. (2019) 'Targeting of early endosomes by autophagy facilitates EGFR recycling and signalling', *EMBO Rep,* 20(10), p. e47734.

Geng, L., Zhao, J., Deng, Y., Molano, I., Xu, X., Xu, L., Ruiz, P., Li, Q., Feng, X., Zhang, M., Tan, W., Kamen, D.L., Bae, S.C., Gilkeson, G.S., Sun, L. and Tsao, B.P. (2022) 'Human SLE variant NCF1-R90H promotes kidney damage and murine lupus through enhanced Tfh2 responses induced by defective efferocytosis of macrophages', *Ann Rheum Dis,* 81(2), pp. 255-267.

Heckmann, B.L., Teubner, B.J.W., Tummers, B., Boada-Romero, E., Harris, L., Yang, M., Guy, C.S., Zakharenko, S.S. and Green, D.R. (2019) 'LC3-Associated Endocytosis Facilitates β-Amyloid Clearance and Mitigates Neurodegeneration in Murine Alzheimer's Disease', *Cell,* 178(3), pp. 536-551.e514.

Hein, L.K., Apaja, P.M., Hattersley, K., Grose, R.H., Xie, J., Proud, C.G. and Sargeant, T.J. (2017) 'A novel fluorescent probe reveals starvation controls the commitment of amyloid precursor protein to the lysosome', *Biochim Biophys Acta Mol Cell Res,* 1864(10), pp. 1554-1565.

Holz, M.K., Ballif, B.A., Gygi, S.P. and Blenis, J. (2005) 'mTOR and S6K1 mediate assembly of the translation preinitiation complex through dynamic protein interchange and ordered phosphorylation events', *Cell,* 123(4), pp. 569-580.

Jacquin, E., Leclerc-Mercier, S., Judon, C., Blanchard, E., Fraitag, S. and Florey, O. (2017) 'Pharmacological modulators of autophagy activate a parallel noncanonical pathway driving unconventional LC3 lipidation', *Autophagy,* 13(5), pp. 854-867.

Jorge, A.M., Lao, T., Kim, R., Licciardi, S., El Khoury, J., Luster, A.D., Means, T.K. and Ramirez-Ortiz, Z.G. (2022) 'SCARF1-Induced Efferocytosis Plays an Immunomodulatory Role in Humans, and Autoantibodies Targeting SCARF1 Are Produced in Patients with Systemic Lupus Erythematosus', *J Immunol,* 208(4), pp. 955-967.

Krajcovic, M., Krishna, S., Akkari, L., Joyce, J.A. and Overholtzer, M. (2013) 'mTOR regulates phagosome and entotic vacuole fission', *Mol Biol Cell,* 24(23), pp. 3736-3745.

Lancaster, C.E., Fountain, A., Dayam, R.M., Somerville, E., Sheth, J., Jacobelli, V., Somerville, A., Terebiznik, M.R. and Botelho, R.J. (2021) 'Phagosome resolution regenerates lysosomes and maintains the degradative capacity in phagocytes', *J Cell Biol,* 220(9).

Martinez, J., Almendinger, J., Oberst, A., Ness, R., Dillon, C.P., Fitzgerald, P., Hengartner, M.O. and Green, D.R. (2011) 'Microtubule-associated protein 1 light chain 3 alpha (LC3)-associated phagocytosis is required for the efficient clearance of dead cells', *Proc Natl Acad Sci U S A,* 108(42), pp. 17396-17401.

Martinez, J., Malireddi, R.K., Lu, Q., Cunha, L.D., Pelletier, S., Gingras, S., Orchard, R., Guan, J.L., Tan, H., Peng, J., Kanneganti, T.D., Virgin, H.W. and Green, D.R.

(2015) 'Molecular characterization of LC3-associated phagocytosis reveals distinct roles for Rubicon, NOX2 and autophagy proteins', *Nat Cell Biol,* 17(7), pp. 893-906.

Mauvezin, C. and Neufeld, T.P. (2015) 'Bafilomycin A1 disrupts autophagic flux by inhibiting both V-ATPase-dependent acidification and Ca-P60A/SERCA-dependent autophagosome-lysosome fusion', *Autophagy,* 11(8), pp. 1437-1438.

McCubbrey, A.L., McManus, S.A., McClendon, J.D., Thomas, S.M., Chatwin, H.B., Reisz, J.A., D'Alessandro, A., Mould, K.J., Bratton, D.L., Henson, P.M. and Janssen, W.J. (2022) 'Polyamine import and accumulation causes immunomodulation in macrophages engulfing apoptotic cells', *Cell Rep,* 38(2), p. 110222.

Meriwether, D., Jones, A.E., Ashby, J.W., Solorzano-Vargas, R.S., Dorreh, N., Noori, S., Grijalva, V., Ball, A.B., Semis, M., Divakaruni, A.S., Mack, J.J., Herschman, H.R., Martin, M.G., Fogelman, A.M. and Reddy, S.T. (2022) 'Macrophage COX2 Mediates Efferocytosis, Resolution Reprogramming, and Intestinal Epithelial Repair', *Cell Mol Gastroenterol Hepatol,* 13(4), pp. 1095-1120.

Onodera, J. and Ohsumi, Y. (2005) 'Autophagy is required for maintenance of amino acid levels and protein synthesis under nitrogen starvation', *J Biol Chem,* 280(36), pp. 31582-31586.

Peña-Ramos, O., Chiao, L., Liu, X., Yu, X., Yao, T., He, H. and Zhou, Z. (2022) 'Autophagosomes fuse to phagosomes and facilitate the degradation of apoptotic cells in Caenorhabditis elegans', *Elife,* 11.

Ratto, E., Chowdhury, S.R., Siefert, N.S., Schneider, M., Wittmann, M., Helm, D. and Palm, W. (2022) 'Direct control of lysosomal catabolic activity by mTORC1 through regulation of V-ATPase assembly', *Nat Commun,* 13(1), p. 4848.

Salina, A.C.G., Dos-Santos, D., Rodrigues, T.S., Fortes-Rocha, M., Freitas-Filho, E.G., Alzamora-Terrel, D.L., Castro, I.M.S., Fraga da Silva, T.F.C., de Lima, M.H.F., Nascimento, D.C., Silva, C.M., Toller-Kawahisa, J.E., Becerra, A., Oliveira, S., Caetité, D.B., Almeida, L., Ishimoto, A.Y., Lima, T.M., Martins, R.B., Veras, F., do Amaral, N.B., Giannini, M.C., Bonjorno, L.P., Lopes, M.I.F., Benatti, M.N., Batah, S.S., Santana, R.C., Vilar, F.C., Martins, M.A., Assad, R.L., de Almeida, S.C.L., de Oliveira, F.R., Arruda Neto, E., Cunha, T.M., Alves-Filho, J.C., Bonato, V.L.D., Cunha, F.Q., Fabro, A.T., Nakaya, H.I., Zamboni, D.S., Louzada-Junior, P., Oliveira, R.D.R. and Cunha, L.D. (2022) 'Efferocytosis of SARS-CoV-2-infected dying cells impairs macrophage anti-inflammatory functions and clearance of apoptotic cells', *Elife,* 11.

Sanjuan, M.A., Dillon, C.P., Tait, S.W., Moshiach, S., Dorsey, F., Connell, S., Komatsu, M., Tanaka, K., Cleveland, J.L., Withoff, S. and Green, D.R. (2007) 'Toll-like receptor signalling in macrophages links the autophagy pathway to phagocytosis', *Nature,* 450(7173), pp. 1253-1257.

Schmidt, E.K., Clavarino, G., Ceppi, M. and Pierre, P. (2009) 'SUnSET, a nonradioactive method to monitor protein synthesis', *Nat Methods,* 6(4), pp. 275-277.

Schneider-Poetsch, T., Ju, J., Eyler, D.E., Dang, Y., Bhat, S., Merrick, W.C., Green, R., Shen, B. and Liu, J.O. (2010) 'Inhibition of eukaryotic translation elongation by cycloheximide and lactimidomycin', *Nat Chem Biol,* 6(3), pp. 209-217.

Tian, Y., Chang, J.C., Fan, E.Y., Flajolet, M. and Greengard, P. (2013) 'Adaptor complex AP2/PICALM, through interaction with LC3, targets Alzheimer's APP-CTF for terminal degradation via autophagy', *Proc Natl Acad Sci U S A,* 110(42), pp. 17071-17076.

Watanabe-Asano, T., Kuma, A. and Mizushima, N. (2014) 'Cycloheximide inhibits starvation-induced autophagy through mTORC1 activation', *Biochem Biophys Res Commun,* 445(2), pp. 334-339.

Yurdagul, A., Jr., Doran, A.C., Cai, B., Fredman, G. and Tabas, I.A. (2017) 'Mechanisms and Consequences of Defective Efferocytosis in Atherosclerosis', *Front Cardiovasc Med,* 4, p. 86.

Zhou, J., Tan, S.H., Nicolas, V., Bauvy, C., Yang, N.D., Zhang, J., Xue, Y., Codogno, P. and Shen, H.M. (2013) 'Activation of lysosomal function in the course of autophagy via mTORC1 suppression and autophagosome-lysosome fusion', *Cell Res,* 23(4), pp. 508-523.

CHAPTER 7

General Discussion

7.1 KEY FINDINGS

I hypothesised that microglial efferocytosis interacts with autophagy to co-ordinate cargo clearance in a nutrient-sensitive manner. The primary objectives of this project were to –

7.1.1 Develop a probe capable of tracking both early and late stages of efferocytosis simultaneously

In Chapter 4, I generated epHero, a novel tandem fluorescent reporter for the measurement of efferocytosis. Other tools commonly used to track efferocytosis are either unable to discriminate between changes to uptake and acidification of apoptotic material by phagocytes (Miksa *et al.*, 2009, Aziz, Yang and Wang, 2013, Stöhr *et al.*, 2018), are costly and require specialised equipment (Hill *et al.*, 2017), or have not been validated in mammals (Raymond *et al.*, 2022). In contrast, epHero is a pH-sensitive probe that can be used to measure both the engulfment and acidification of cargo during corpse clearance, and has been tested in two different phagocyte cell lines, as well as a mouse model of efferocytosis. Further, it can be used for live imaging and flow cytometry, two of the most common techniques used to assay efferocytosis. In the future, epHero could developed further to assay *in vivo* efferocytosis in the brain – for instance, via stereotaxic injection of apoptotic cells, or by generating a transgenic mouse with neuronal-specific expression of the epHero reporter.

7.1.2 Determine if microglial corpse clearance changes in response to nutrient deprivation

Previous reports have shown phagocytes obtain 'food' from the breakdown of apoptotic cells during efferocytosis, which can be used to fuel additional cargo engulfment (Yurdagul *et al.*, 2020) or tissue repair programs (Ampomah *et al.*, 2022). However, it is not known whether extracellular nutrient availability can modulate efferocytosis. In Chapter 5, I employed the epHero reporter to show that amino acid starvation increases the acidification, but not uptake, of apoptotic cargo during microglial efferocytosis. Further, this increase in corpse acidification persists even after restimulation with amino acids. In contrast, serum starvation reduces the uptake, but not acidification, of apoptotic corpses by microglia, and this engulfment defect can be rescued via the re-addition of serum.

7.1.3 Investigate if modulating efferocytosis alters canonical autophagy, and vice-versa

Although interplay between efferocytosis and canonical autophagy has been documented during CASM (Martinez *et al.*, 2011, Martinez *et al.*, 2015), it is not known whether these two pathways interact with each other beyond CASM. In Chapter 6, I showed that when CASM is pharmacologically inhibited, efferocytosis reduces autophagy – as evidenced by impaired lysosomal flux of key autophagy proteins LC3 and SQSTM1 – and this defect can be partially restored via amino acid starvation. Conversely, stimulating autophagy modifies efferocytosis, but with mixed results. Amino acid starvation improves microglial efferocytosis, increasing the acidification of apoptotic cargo. However, stimulating autophagy through a different mechanism,

mTORC1 inhibition, decreases apoptotic corpse acidification by microglia. Amino acid starvation inhibits mTORC1 to promote autophagy (Zhou *et al.*, 2013); so why does stimulating autophagy via these two related pathways have opposite effects on corpse clearance?

7.1.4 Elucidate the mechanisms driving the potential interaction between efferocytosis and autophagy in microglia

In Chapter 5, I showed that inducing autophagy through amino acid starvation increases the acidification of apoptotic material by microglia without affecting its uptake. Proteomic profiling revealed that when apoptotic corpses were added to starved microglia, proteins involved in pathways known to impact efferocytosis – such as fatty acid (Zhang *et al.*, 2019) and ornithine decarboxylase metabolism (Yurdagul *et al.*, 2020) – were upregulated. In addition, I observed changes to novel pathways such as such as BCAA metabolism, which have not previously been linked to efferocytosis, providing an exciting new avenue to explore in future work.

Amino acid starvation induces autophagy by suppressing mTORC1, its negative regulator. In Chapter 6, I used the epHero reporter to demonstrate that, unlike amino acid starvation which increases cargo acidification, stimulating autophagy via mTORC1 inhibition decreases corpse acidification during microglial efferocytosis. This occurs despite both amino acid starvation and mTORC1 inhibition increasing lysosomal biogenesis and proteolysis. Thus, even though overall lysosomal capacity is augmented under both conditions, apoptotic cargo is trafficked and processed differently. I observed that mTORC1 is re-activated in amino acid starved microglia during efferocytosis, and this does not occur when mTORC1 is pharmacologically

inhibited. My results indicate that low levels of mTORC1 activity are required to drive corpse acidification during microglial efferocytosis. In line with this, mTORC1 has been implicated in phagosome resolution (Krajcovic *et al.*, 2013, Fazeli *et al.*, 2023), and more recently, in lysosomal pH regulation (Ratto *et al.*, 2022, Zi *et al.*, 2022). Future work exploring the dynamics between mTORC1, phagosome acidification and autophagy may yield additional insights into how these processes interact to co-ordinate cargo clearance in microglia.

7.2 LIMITATIONS AND FUTURE DIRECTIONS

There are some caveats to the work presented in this thesis. While the epHero reporter developed in Chapter 4 was validated in two different cell types and a mouse model of efferocytosis, subsequent work in Chapters 5 and 6 was only performed using the human microglial HMC3 cell line. It was necessary to conduct these initial studies *in vitro*, to determine whether there was a relationship between autophagy and efferocytosis beyond CASM. However, in the future, this work will need to be validated in a more physiological setting – using primary microglia, or in the mouse brain. In addition, recent work indicates that metabolites obtained from the breakdown of apoptotic cargo play a role in corpse clearance by macrophages (Yurdagul *et al.*, 2020, Ampomah *et al.*, 2022, Zhang *et al.*, 2019); it will be interesting to test whether my findings related to the impact of extracellular nutrient availability on microglial efferocytosis also hold true in other types of phagocytes. In Chapter 5, proteomics of amino acid starved microglia that had engulfed and acidified apoptotic cargo surprisingly revealed no changes to proteins known to acidify the lysosomal lumen, such as v-ATPase components. Instead, altered expression of proteins involved in

trafficking and BCAA metabolic pathways was observed in these cells. I was unable to verify changes in protein levels of SNX17 and ATG2B, shortlisted from our proteomics dataset based on their role in lysosomal trafficking (Steinberg *et al.*, 2012, Zhou *et al.*, 2022) and CASM (Cross *et al.*, 2023) respectively, via western blot. Other potential candidates mediating the increased acidification of apoptotic cargo in starved microglia will need to be selected for further testing, via both immunoblotting and functional screens. Further, changes to cargo acidification may be mediated by differences in protein localisation or phosphorylation rather than total expression, something that would not have been detectable with the approach used in this thesis. In Chapter 6, I observed that stimulating autophagy via mTORC1 inhibition and amino acid starvation had opposite results on corpse acidification during microglial efferocytosis. Some of these effects may be mediated by CASM, future experiments performed in CASM-deficient and autophagy-deficient cells may yield additional insights into this phenomenon. Lastly, the findings from this thesis are well suited for testing in a mouse model of neuronal efferocytosis. For instance, recent work has shown that feeding mice a low protein diet – which mimics some aspects of amino acid starvation in cells – improves neurological outcomes after stroke (Silva de Carvalho *et al.*, 2022). Are any of these effects mediated by an improvement of corpse clearance in mice on a low protein diet? These questions should be addressed in future work.

7.3 PROJECT SIGNIFICANCE AND FINAL PERSPECTIVES

Microglia play a vital role in maintaining brain homeostasis; consequently, a compromised brain is associated with unique microglial signatures. A disease-

associated microglia transcriptional profile is linked to Alzheimer's disease pathology (Deczkowska *et al.*, 2018). Similarly, microglia situated around white matter debris in the ageing brain adopt their own transcriptional phenotype (Safaiyan *et al.*, 2021). While the specifics of each microglial signature are different, they all contain phagocytosis, lysosome and autophagy-related genes. Further, genetic variants associated with Alzheimer's (Romero-Molina *et al.*, 2022) and Parkinson's disease (Gan-Or, Dion and Rouleau, 2015) also implicate these pathways. Loss of lysosomal, autophagic or phagocytic function has been linked to neurodegeneration (Heckmann *et al.*, 2020, Xu *et al.*, 2021, Qin *et al.*, 2021, Heckmann *et al.*, 2019, Kollmann *et al.*, 2012, Song *et al.*, 2018). Taken together, this evidence underscores the importance of waste catabolism in the brain, particularly by microglia. Given that autophagy and phagocytosis are two mechanisms for delivering cargo to the lysosome, it is important to study how these processes interact with each other in microglia. Although the phagocytosis of toxic protein aggregates during neurodegeneration is a popular area of research, the removal of neuronal debris is relatively under-studied. This is surprising, as several lines of evidence implicate microglial corpse clearance in Alzheimer's disease, which is the most common cause of dementia: (i) many Alzheimer's risk factor genes such as TREM2, PLCG2 and APOE are involved in the recognition and clearance of apoptotic material (Huang *et al.*, 2017, Romero-Molina *et al.*, 2022); (ii) neurons containing toxic tau protein aggregates (Brelstaff *et al.*, 2018), and those exposed to oligomers of the amyloid-beta protein (Rueda-Carrasco *et al.*, 2023), express the efferocytosis 'eat-me' signal phosphatidylserine on their plasma and synaptic membranes respectively, triggering their removal by microglia; and (iii)

disruption of the CASM machinery leads to neurodegeneration in both wild-type aged (Heckmann *et al.*, 2020), and transgenic Alzheimer's mice (Heckmann *et al.*, 2019).

The work presented in this thesis shows that microglial autophagy and corpse clearance pathways interact with each other beyond CASM. Efferocytosis reduces the lysosomal delivery of autophagic material, but this defect can be partly rescued by stimulating autophagy via amino acid starvation. Further, amino acid starvation also promotes the acidification of apoptotic cargo by microglia, thus providing a shared mechanism by which both autophagic and efferocytic degradation can be stimulated. Dietary interventions can modify the levels of at least *some* amino acids, such as BCAAs, in both the plasma and cerebrospinal fluid surrounding the brain (Russin *et al.*, 2021, Grimes, Cameron and Fernstrom, 2009). This presents an exciting possibility that modifying nutrition may improve disease outcomes in conditions where there is both autophagic and corpse burden in microglia. In line with this, a recent study showed that a low protein diet in mice boosted their recovery after stroke (Silva de Carvalho *et al.*, 2022), where there is both a large amount of cell death and increased autophagy in the brain. Similarly, reducing dietary protein in multiple sclerosis mice lowered disease severity (Choi *et al.*, 2016). While the reports on dietary protein restriction in neurodegeneration are mixed, there is some evidence to suggest that this may be beneficial during Alzheimer's and Parkinson's disease (Bensalem *et al.*, 2023, Wang *et al.*, 2017). Findings from this thesis should be expanded upon by testing the effect of nutritional interventions in mouse models of stroke or neurodegeneration, and specifically assaying for flux of autophagic and efferocytic cargo by microglia.

Importantly, this thesis presented data showing that not all autophagy interventions are created equal: while both amino acid starvation and mTORC1 inhibition induced autophagy and lysosomal catabolism, only amino acid starvation was able to improve efferocytosis. In fact, mTORC1 inhibition counter-intuitively reduced microglia's ability to acidify apoptotic corpses. Immunoblotting revealed that microglia digesting corpses start to re-activate mTORC1, even under conditions of amino acid starvation, which normally blocks mTORC1 activity. In this scenario, mTORC1 may be suppressed enough to stimulate lysosomal function, but still sufficiently active for its recently reported role in efficient phagosomal trafficking and cargo clearance. This may also explain why inhibiting mTORC1 to stimulate autophagy has mixed results in the brain. Inhibiting mTORC1 with rapamycin improves pathological and neurological deficits in transgenic Alzheimer's mice when administered during early stages, but appears to have limited therapeutic effect on late stage disease (Carosi and Sargeant, 2019). On the other hand, activating microglial mTORC1 in Alzheimer's disease mice improves microglial phagocytosis and reduces the build-up of toxic protein aggregates (Shi *et al.*, 2022). In a different report examining the impact of autophagy in stroke, rapamycin-mediated mTORC1 inhibition improved microglial corpse clearance after stroke in mice, but conversely worsened it *ex vivo* (Beccari et al., 2023). These conflicting results may have been driven by the fact that mTORC1-rapaymycin binding was completely saturated *ex vivo*, but not *in vivo*, enabling residual mTORC1 activity to occur in the mice and having an overall beneficial effect. Thus, modulating mTORC1 can have vastly different outcomes even in the same study. Given the opposing roles of mTORC1 in autophagy and phagocytic clearance, it may be difficult to strike a

balance between beneficial and detrimental levels of mTORC1 activity. In recent years, there has been burgeoning interest in utilising rapamycin to promote longevity and brain health in humans. However, several lines of evidence, including the work presented in this thesis, show that modifying cellular catabolism is complex, and selectively targeting one pathway may come at a cost to others. These nuances should be carefully explored before any therapeutic recommendations can be made.

7.4 REFERENCES

Ampomah, P.B., Cai, B., Sukka, S.R., Gerlach, B.D., Yurdagul, A., Jr., Wang, X., Kuriakose, G., Darville, L.N.F., Sun, Y., Sidoli, S., Koomen, J.M., Tall, A.R. and Tabas, I. (2022) 'Macrophages use apoptotic cell-derived methionine and DNMT3A during efferocytosis to promote tissue resolution', *Nat Metab,* 4(4), pp. 444-457.

Aziz, M., Yang, W.L. and Wang, P. (2013) 'Measurement of phagocytic engulfment of apoptotic cells by macrophages using pHrodo succinimidyl ester', *Curr Protoc Immunol,* Chapter 14, p. Unit 14.31.

Beccari, S., Sierra-Torre, V., Valero, J., Pereira-Iglesias, M., García-Zaballa, M., Soria, F.N., De Las Heras-Garcia, L., Carretero-Guillen, A., Capetillo-Zarate, E., Domercq, M., Huguet, P.R., Ramonet, D., Osman, A., Han, W., Dominguez, C., Faust, T.E., Touzani, O., Pampliega, O., Boya, P., Schafer, D., Mariño, G., Canet-Soulas, E., Blomgren, K., Plaza-Zabala, A. and Sierra, A. (2023) 'Microglial phagocytosis dysfunction in stroke is driven by energy depletion and induction of autophagy', *Autophagy,* 19(7), pp. 1952-1981.

Bensalem, J., Hein, L.K., Hassiotis, S., Trim, P.J., Proud, C.G., Heilbronn, L.K. and Sargeant, T.J. (2023) 'Modifying Dietary Protein Impacts mTOR Signaling and Brain Deposition of Amyloid β in a Knock-In Mouse Model of Alzheimer Disease', *J Nutr,* 153(5), pp. 1407-1419.

Brelstaff, J., Tolkovsky, A.M., Ghetti, B., Goedert, M. and Spillantini, M.G. (2018) 'Living Neurons with Tau Filaments Aberrantly Expose Phosphatidylserine and Are Phagocytosed by Microglia', *Cell Rep,* 24(8), pp. 1939-1948.e1934.

Carosi, J.M. and Sargeant, T.J. (2019) 'Rapamycin and Alzheimer disease: a double-edged sword?', *Autophagy,* 15(8), pp. 1460-1462.

Choi, I.Y., Piccio, L., Childress, P., Bollman, B., Ghosh, A., Brandhorst, S., Suarez, J., Michalsen, A., Cross, A.H., Morgan, T.E., Wei, M., Paul, F., Bock, M. and Longo, V.D. (2016) 'A Diet Mimicking Fasting Promotes Regeneration and Reduces Autoimmunity and Multiple Sclerosis Symptoms', *Cell Rep,* 15(10), pp. 2136-2146.

Cross, J., Durgan, J., McEwan, D.G. and Florey, O. (2023) 'Lysosome damage triggers direct ATG8 conjugation and ATG2 engagement via CASM', *bioRxiv*, p. 2023.2003.2022.533754.

Deczkowska, A., Keren-Shaul, H., Weiner, A., Colonna, M., Schwartz, M. and Amit, I. (2018) 'Disease-Associated Microglia: A Universal Immune Sensor of Neurodegeneration', *Cell,* 173(5), pp. 1073-1081.

Fazeli, G., Levin-Konigsberg, R., Bassik, M.C., Stigloher, C. and Wehman, A.M. (2023) 'A BORC-dependent molecular pathway for vesiculation of cell corpse phagolysosomes', *Curr Biol,* 33(4), pp. 607-621.e607.

Gan-Or, Z., Dion, P.A. and Rouleau, G.A. (2015) 'Genetic perspective on the role of the autophagy-lysosome pathway in Parkinson disease', *Autophagy,* 11(9), pp. 1443-1457.

Grimes, M.A., Cameron, J.L. and Fernstrom, J.D. (2009) 'Cerebrospinal fluid concentrations of large neutral and basic amino acids in Macaca mulatta: diurnal variations and responses to chronic changes in dietary protein intake', *Metabolism,* 58(1), pp. 129-140.

Heckmann, B.L., Teubner, B.J.W., Boada-Romero, E., Tummers, B., Guy, C., Fitzgerald, P., Mayer, U., Carding, S., Zakharenko, S.S., Wileman, T. and Green, D.R. (2020) 'Noncanonical function of an autophagy protein prevents spontaneous Alzheimer's disease', *Sci Adv,* 6(33), p. eabb9036.

Heckmann, B.L., Teubner, B.J.W., Tummers, B., Boada-Romero, E., Harris, L., Yang, M., Guy, C.S., Zakharenko, S.S. and Green, D.R. (2019) 'LC3-Associated Endocytosis Facilitates beta-Amyloid Clearance and Mitigates Neurodegeneration in Murine Alzheimer's Disease', *Cell,* 178(3), pp. 536-551.e514.

Hill, R.A., Damisah, E.C., Chen, F., Kwan, A.C. and Grutzendler, J. (2017) 'Targeted two-photon chemical apoptotic ablation of defined cell types in vivo', *Nat Commun,* 8, p. 15837.

Huang, K.L., Marcora, E., Pimenova, A.A., Di Narzo, A.F., Kapoor, M., Jin, S.C., Harari, O., Bertelsen, S., Fairfax, B.P., Czajkowski, J., Chouraki, V., Grenier-Boley, B., Bellenguez, C., Deming, Y., McKenzie, A., Raj, T., Renton, A.E., Budde, J., Smith, A., Fitzpatrick, A., Bis, J.C., DeStefano, A., Adams, H.H.H., Ikram, M.A., van der Lee,

S., Del-Aguila, J.L., Fernandez, M.V., Ibanez, L., Sims, R., Escott-Price, V., Mayeux, R., Haines, J.L., Farrer, L.A., Pericak-Vance, M.A., Lambert, J.C., van Duijn, C., Launer, L., Seshadri, S., Williams, J., Amouyel, P., Schellenberg, G.D., Zhang, B., Borecki, I., Kauwe, J.S.K., Cruchaga, C., Hao, K. and Goate, A.M. (2017) 'A common haplotype lowers PU.1 expression in myeloid cells and delays onset of Alzheimer's disease', *Nat Neurosci,* 20(8), pp. 1052-1061.

Kollmann, K., Damme, M., Markmann, S., Morelle, W., Schweizer, M., Hermans-Borgmeyer, I., Röchert, A.K., Pohl, S., Lübke, T., Michalski, J.C., Käkelä, R., Walkley, S.U. and Braulke, T. (2012) 'Lysosomal dysfunction causes neurodegeneration in mucolipidosis II 'knock-in' mice', *Brain,* 135(Pt 9), pp. 2661-2675.

Krajcovic, M., Krishna, S., Akkari, L., Joyce, J.A. and Overholtzer, M. (2013) 'mTOR regulates phagosome and entotic vacuole fission', *Mol Biol Cell,* 24(23), pp. 3736-3745.

Martinez, J., Almendinger, J., Oberst, A., Ness, R., Dillon, C.P., Fitzgerald, P., Hengartner, M.O. and Green, D.R. (2011) 'Microtubule-associated protein 1 light chain 3 alpha (LC3)-associated phagocytosis is required for the efficient clearance of dead cells', *Proc Natl Acad Sci U S A,* 108(42), pp. 17396-17401.

Martinez, J., Malireddi, R.K., Lu, Q., Cunha, L.D., Pelletier, S., Gingras, S., Orchard, R., Guan, J.L., Tan, H., Peng, J., Kanneganti, T.D., Virgin, H.W. and Green, D.R. (2015) 'Molecular characterization of LC3-associated phagocytosis reveals distinct roles for Rubicon, NOX2 and autophagy proteins', *Nat Cell Biol,* 17(7), pp. 893-906.

Miksa, M., Komura, H., Wu, R., Shah, K.G. and Wang, P. (2009) 'A novel method to determine the engulfment of apoptotic cells by macrophages using pHrodo succinimidyl ester', *J Immunol Methods,* 342(1-2), pp. 71-77.

Qin, Y., Qiu, J., Wang, P., Liu, J., Zhao, Y., Jiang, F. and Lou, H. (2021) 'Impaired autophagy in microglia aggravates dopaminergic neurodegeneration by regulating NLRP3 inflammasome activation in experimental models of Parkinson's disease', *Brain Behav Immun,* 91, pp. 324-338.

Ratto, E., Chowdhury, S.R., Siefert, N.S., Schneider, M., Wittmann, M., Helm, D. and Palm, W. (2022) 'Direct control of lysosomal catabolic activity by mTORC1 through regulation of V-ATPase assembly', *Nat Commun,* 13(1), p. 4848.

Raymond, M.H., Davidson, A.J., Shen, Y., Tudor, D.R., Lucas, C.D., Morioka, S., Perry, J.S.A., Krapivkina, J., Perrais, D., Schumacher, L.J., Campbell, R.E., Wood, W. and Ravichandran, K.S. (2022) 'Live cell tracking of macrophage efferocytosis during Drosophila embryo development in vivo', *Science,* 375(6585), pp. 1182-1187.

Romero-Molina, C., Garretti, F., Andrews, S.J., Marcora, E. and Goate, A.M. (2022) 'Microglial efferocytosis: Diving into the Alzheimer's disease gene pool', *Neuron,* 110(21), pp. 3513-3533.

Rueda-Carrasco, J., Sokolova, D., Lee, S.E., Childs, T., Jurčáková, N., Crowley, G., De Schepper, S., Ge, J.Z., Lachica, J.I., Toomey, C.E., Freeman, O.J., Hardy, J., Barnes, S.J., Lashley, T., Stevens, B., Chang, S. and Hong, S. (2023) 'Microglia-synapse engulfment via PtdSer-TREM2 ameliorates neuronal hyperactivity in Alzheimer's disease models', *Embo j*, p. e113246.

Russin, K.J., Nair, K.S., Montine, T.J., Baker, L.D. and Craft, S. (2021) 'Diet Effects on Cerebrospinal Fluid Amino Acids Levels in Adults with Normal Cognition and Mild Cognitive Impairment', *J Alzheimers Dis,* 84(2), pp. 843-853.

Safaiyan, S., Besson-Girard, S., Kaya, T., Cantuti-Castelvetri, L., Liu, L., Ji, H., Schifferer, M., Gouna, G., Usifo, F., Kannaiyan, N., Fitzner, D., Xiang, X., Rossner, M.J., Brendel, M., Gokce, O. and Simons, M. (2021) 'White matter aging drives microglial diversity', *Neuron,* 109(7), pp. 1100-1117.e1110.

Shi, Q., Chang, C., Saliba, A. and Bhat, M.A. (2022) 'Microglial mTOR Activation Upregulates Trem2 and Enhances β-Amyloid Plaque Clearance in the 5XFAD Alzheimer's Disease Model', *J Neurosci,* 42(27), pp. 5294-5313.

Silva de Carvalho, T., Singh, V., Mohamud Yusuf, A., Wang, J., Schultz Moreira, A.R., Sanchez-Mendoza, E.H., Sardari, M., Nascentes Melo, L.M., Doeppner, T.R., Kehrmann, J., Scholtysik, R., Hitpass, L., Gunzer, M. and Hermann, D.M. (2022) 'Post-ischemic protein restriction induces sustained neuroprotection, neurological recovery, brain remodeling, and gut microbiota rebalancing', *Brain Behav Immun,* 100, pp. 134-144.

Song, W.M., Joshita, S., Zhou, Y., Ulland, T.K., Gilfillan, S. and Colonna, M. (2018) 'Humanized TREM2 mice reveal microglia-intrinsic and -extrinsic effects of R47H polymorphism', *J Exp Med,* 215(3), pp. 745-760.

Steinberg, F., Heesom, K.J., Bass, M.D. and Cullen, P.J. (2012) 'SNX17 protects integrins from degradation by sorting between lysosomal and recycling pathways', *J Cell Biol,* 197(2), pp. 219-230.

Stöhr, R., Deckers, N., Schurgers, L., Marx, N. and Reutelingsperger, C.P. (2018) 'AnnexinA5-pHrodo: a new molecular probe for measuring efferocytosis', *Sci Rep,* 8(1), p. 17731.

Wang, L., Xiong, N., Huang, J., Guo, S., Liu, L., Han, C., Zhang, G., Jiang, H., Ma, K., Xia, Y., Xu, X., Li, J., Liu, J.Y. and Wang, T. (2017) 'Protein-Restricted Diets for Ameliorating Motor Fluctuations in Parkinson's Disease', *Front Aging Neurosci,* 9, p. 206.

Xu, Y., Propson, N.E., Du, S., Xiong, W. and Zheng, H. (2021) 'Autophagy deficiency modulates microglial lipid homeostasis and aggravates tau pathology and spreading', *Proc Natl Acad Sci U S A,* 118(27).

Yurdagul, A., Jr., Subramanian, M., Wang, X., Crown, S.B., Ilkayeva, O.R., Darville, L., Kolluru, G.K., Rymond, C.C., Gerlach, B.D., Zheng, Z., Kuriakose, G., Kevil, C.G., Koomen, J.M., Cleveland, J.L., Muoio, D.M. and Tabas, I. (2020) 'Macrophage Metabolism of Apoptotic Cell-Derived Arginine Promotes Continual Efferocytosis and Resolution of Injury', *Cell Metab,* 31(3), pp. 518-533.e510.

Zhang, S., Weinberg, S., DeBerge, M., Gainullina, A., Schipma, M., Kinchen, J.M., Ben-Sahra, I., Gius, D.R., Yvan-Charvet, L., Chandel, N.S., Schumacker, P.T. and Thorp, E.B. (2019) 'Efferocytosis Fuels Requirements of Fatty Acid Oxidation and the Electron Transport Chain to Polarize Macrophages for Tissue Repair', *Cell Metab,* 29(2), pp. 443-456.e445.

Zhou, C., Wu, Z., Du, W., Que, H., Wang, Y., Ouyang, Q., Jian, F., Yuan, W., Zhao, Y., Tian, R., Li, Y., Chen, Y., Gao, S., Wong, C.C.L. and Rong, Y. (2022) 'Recycling

of autophagosomal components from autolysosomes by the recycler complex', *Nat Cell Biol,* 24(4), pp. 497-512.

Zhou, J., Tan, S.H., Nicolas, V., Bauvy, C., Yang, N.D., Zhang, J., Xue, Y., Codogno, P. and Shen, H.M. (2013) 'Activation of lysosomal function in the course of autophagy via mTORC1 suppression and autophagosome-lysosome fusion', *Cell Res,* 23(4), pp. 508-523.

Zi, Z., Zhang, Z., Feng, Q., Kim, C., Wang, X.D., Scherer, P.E., Gao, J., Levine, B. and Yu, Y. (2022) 'Quantitative phosphoproteomic analyses identify STK11IP as a lysosome-specific substrate of mTORC1 that regulates lysosomal acidification', *Nat Commun,* 13(1), p. 1760.

CHAPTER 8

Appendix figures

FIGURE 8.1 Original western blots for Figure 4.1D

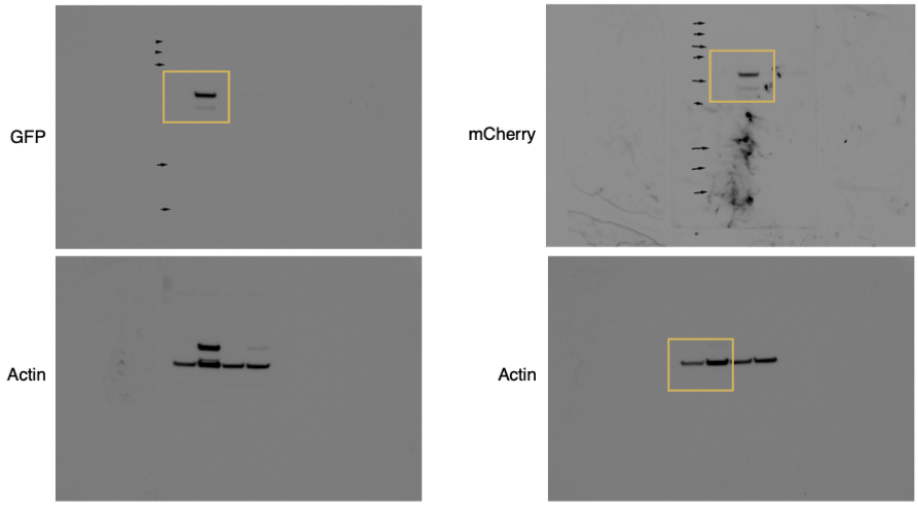

FIGURE 8.2 Plasmid map for epHero construct.

Image provided using Benchling software.

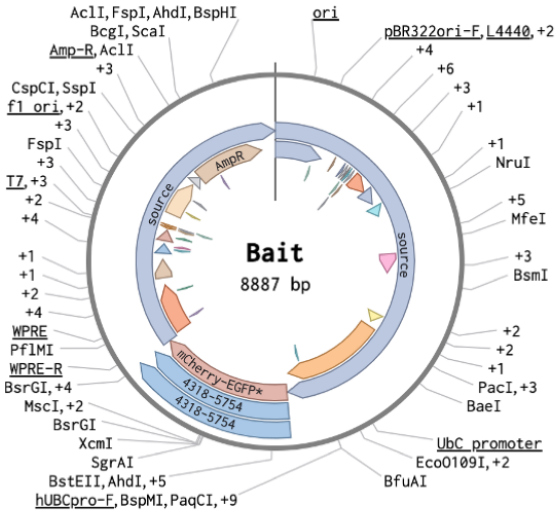

FIGURE 8.3 Original western blots for Figure 5.9A

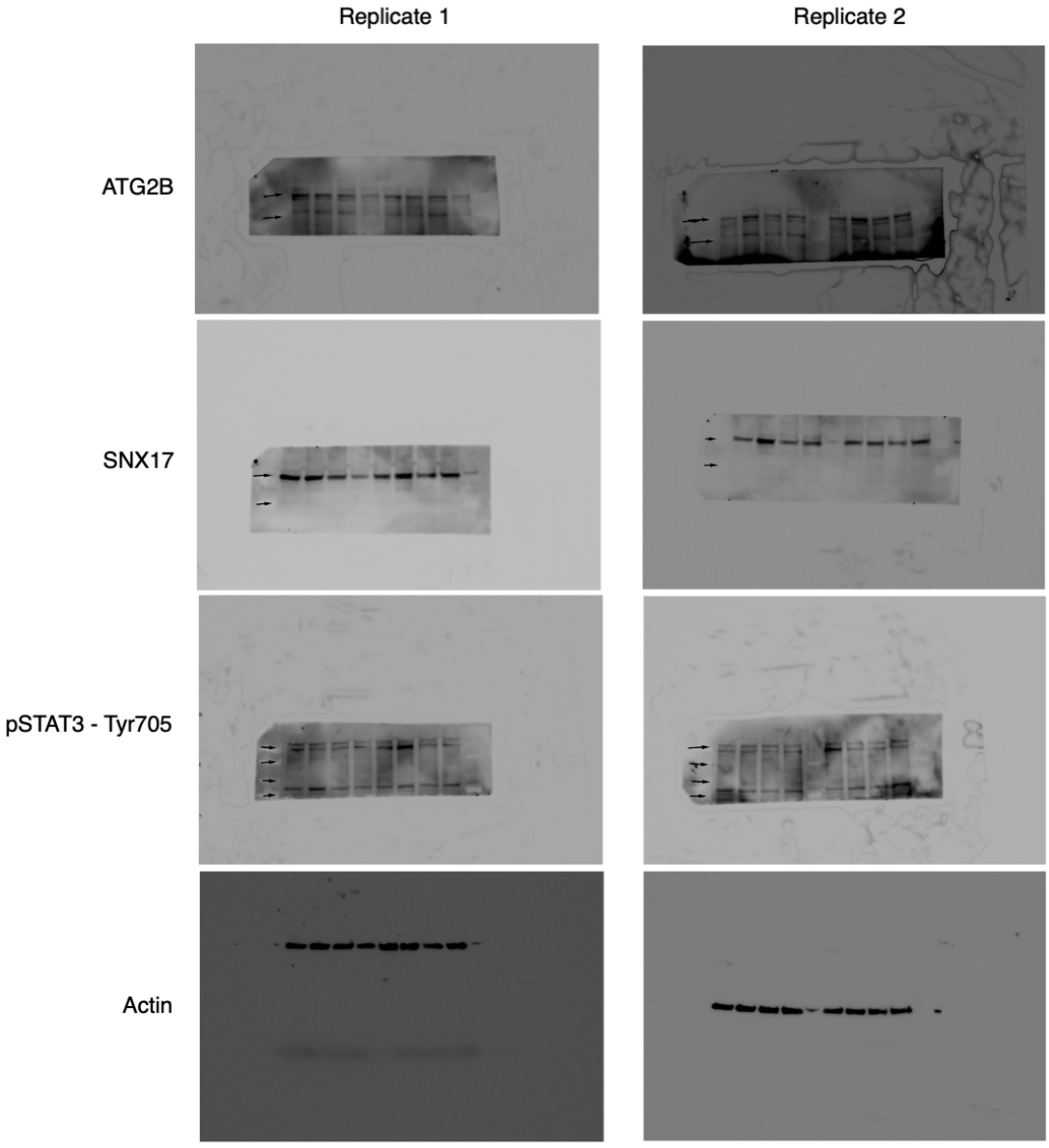

FIGURE 8.4 Original western blots for Figure 6.2A

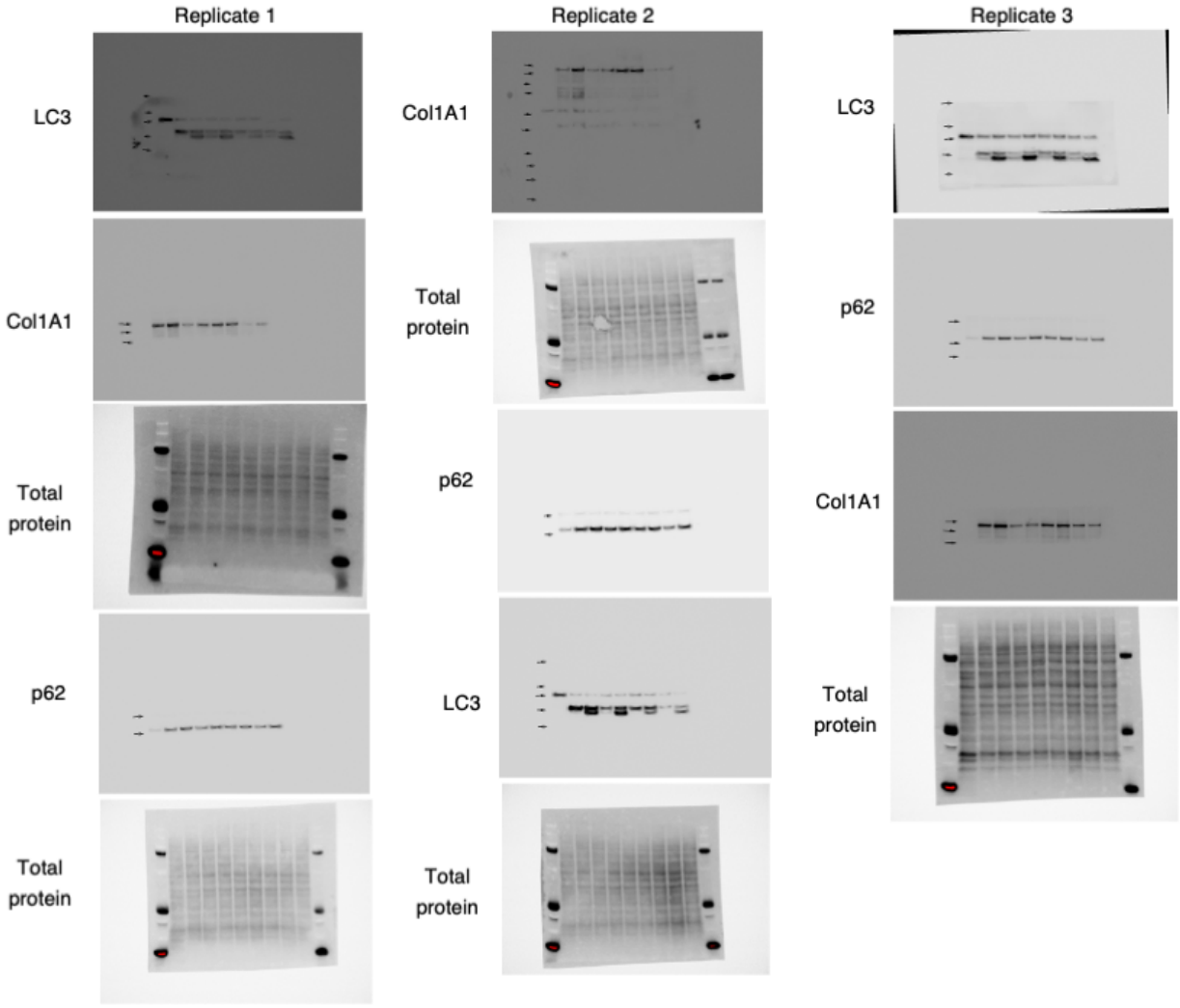

FIGURE 8.5 Original western blots for Figure 6.6A

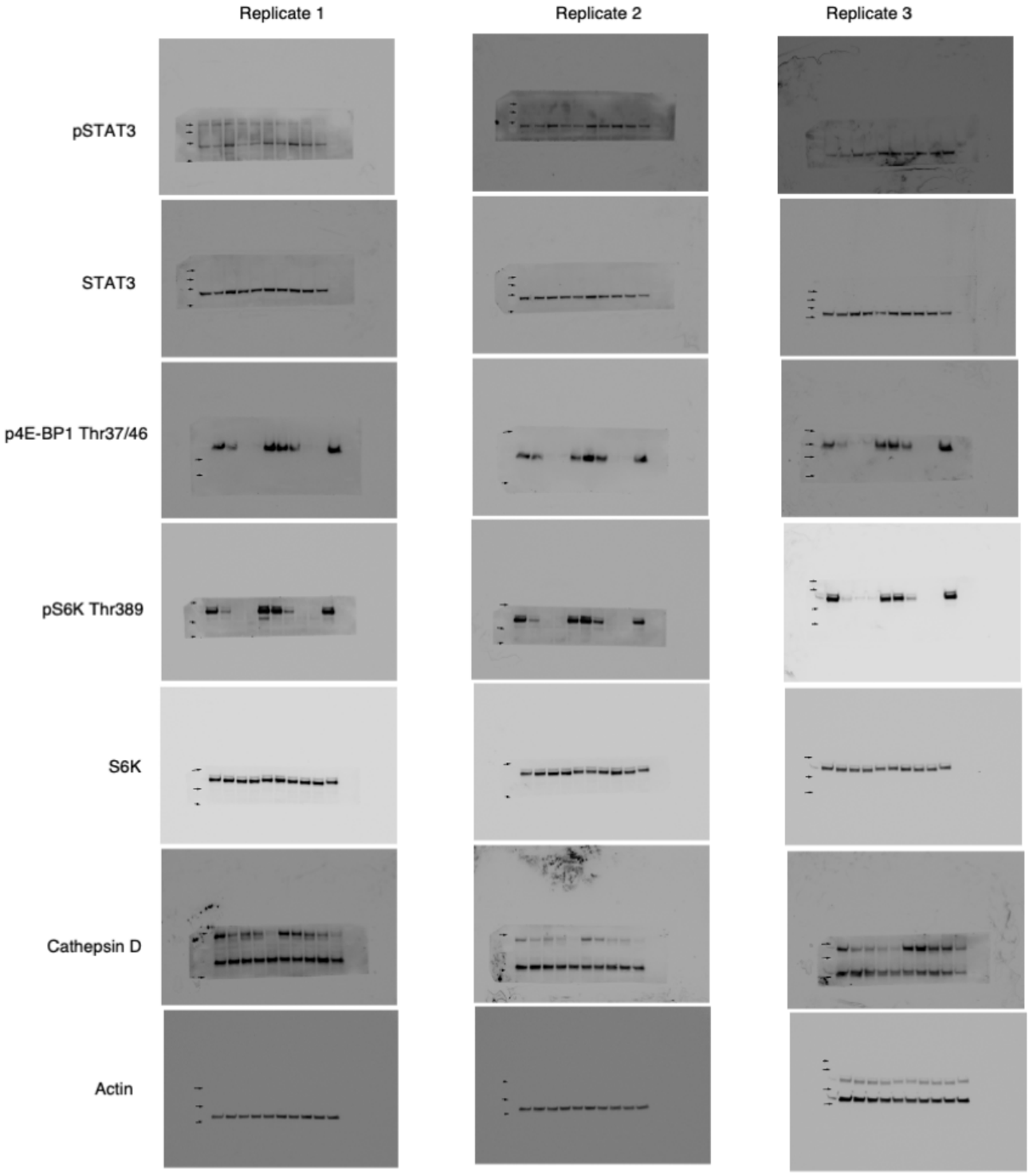

Appendix tables

TABLE 8.1 Proteins upregulated in amino acid starved- vs fed-microglia (no corpses)

Gene symbol	Log FC	Adj. p value	Gene symbol	Log FC	Adj. p value
C1orf52	2.96	1.7E-03	MED25	0.97	3.8E-02
UQCRQ	2.33	1.1E-02	FGF2	0.97	1.0E-03
PXMP2	2.18	7.4E-02	POLR2D	0.96	4.3E-03
XPC	2.10	6.3E-04	LSM7	0.96	4.0E-02
ZNF830	2.06	3.7E-06	LUC7L2	0.96	2.8E-02
ESCO2	2.02	9.0E-04	HIP1R	0.94	5.1E-03
CCNT1	1.92	1.5E-03	LTF	0.94	5.4E-02
NOL8	1.92	2.4E-02	TRIM58	0.93	2.7E-02
TES	1.89	3.0E-03	AGO2	0.93	5.1E-03
SCAMP1	1.83	3.1E-03	TGM2	0.93	6.1E-03
PDCD4	1.81	6.4E-03	ERCC6	0.92	2.2E-02
SHFL	1.79	8.2E-04	ADH5	0.92	6.3E-02
CEP152	1.78	3.6E-04	KRR1	0.90	5.8E-02
TIMM8A	1.77	3.9E-03	ABL1	0.90	3.5E-03
YTHDC1	1.77	3.0E-04	DLC1	0.90	1.5E-03
GNB1	1.74	8.8E-02	BRAP	0.90	4.0E-02
ZFAND1	1.71	1.5E-02	HS1BP3	0.90	2.8E-03
NFKBIB	1.69	1.5E-04	NCAPH2	0.89	3.9E-02
MFSD10	1.68	8.7E-02	EPHB2	0.89	1.2E-02
DIS3L2	1.63	4.4E-03	ETS1	0.89	4.6E-02
LRRC1	1.60	2.8E-03	XYLT2	0.88	5.4E-02
BROX	1.58	2.2E-02	SNIP1	0.87	2.4E-02
EIF1AD	1.58	1.1E-02	RPP38	0.87	6.6E-02
MSI1	1.57	1.0E-02	NT5E	0.86	8.5E-02
CYBC1	1.51	6.3E-02	ANXA5	0.85	7.1E-03

TBC1D4	1.51	2.5E-02	CNRIP1	0.85	7.9E-02
CNPY2	1.51	2.2E-02	BICC1	0.85	3.2E-02
SYDE1	1.47	2.0E-02	CDC45	0.84	3.9E-02
FAS	1.44	1.5E-02	BTN2A1	0.84	2.3E-02
SLC35E1	1.44	1.5E-02	PCIF1	0.83	2.8E-02
SEPTIN8	1.42	1.9E-03	RIOK1	0.83	1.8E-02
GPATCH4	1.41	2.4E-02	RRP8	0.83	7.4E-02
UPF2	1.40	2.2E-03	SEPTIN10	0.83	6.6E-02
KRI1	1.39	1.3E-02	CUTA	0.82	5.4E-02
KIF18A	1.38	1.9E-03	CDC40	0.82	3.3E-02
CHEK1	1.36	5.1E-03	WDR76	0.81	5.4E-02
NOCT	1.32	1.7E-03	FAM111B	0.80	7.1E-02
MAP3K2	1.32	6.8E-02	BAG4	0.80	2.1E-02
SH3PXD2B	1.32	3.2E-03	VTI1B	0.79	2.7E-02
ACYP2	1.32	7.5E-03	SMG6	0.78	8.0E-02
RBP7	1.31	3.4E-03	AAGAB	0.76	8.0E-02
MED13L	1.31	9.4E-02	SUB1	0.75	8.9E-02
RHPN2	1.30	7.8E-04	RTF1	0.75	1.0E-01
TTF1	1.30	6.0E-02	RNMT	0.75	6.9E-03
INPP4B	1.27	3.0E-03	ITPR3	0.75	5.0E-02
NDRG1	1.25	1.5E-02	SLC35F2	0.74	1.4E-02
SCRN3	1.24	4.4E-02	FHL3	0.74	5.8E-02
PTPN9	1.24	8.3E-02	LENG8	0.74	1.5E-02
ERI3	1.23	6.3E-03	RECQL5	0.74	3.4E-02
ACTR5	1.22	2.5E-02	ABR	0.74	7.9E-02
NUDCD3	1.20	8.9E-02	MYL6B	0.73	9.5E-02
BCL2L1	1.20	6.9E-03	HAGH	0.73	3.6E-02
DENR	1.19	3.6E-02	PHF8	0.73	4.2E-02
URI1	1.18	5.1E-03	RAD51C	0.73	8.8E-02
RAD23A	1.17	9.6E-04	PPIL4	0.73	3.3E-03
STXBP6	1.17	4.9E-02	ARMT1	0.72	1.9E-02
TBC1D7	1.16	2.7E-03	GABPA	0.72	4.4E-02

TAF6L	1.16	2.4E-03	NUTF2	0.72	8.0E-02
LIMCH1	1.15	9.3E-04	SRSF1	0.72	2.6E-02
DUS2	1.14	7.0E-03	N4BP1	0.72	9.3E-02
RNF113A	1.14	7.4E-02	DNM1	0.72	2.5E-02
NEDD4L	1.11	6.3E-04	EPN1	0.71	8.1E-02
EBNA1BP2	1.11	6.4E-02	SETD7	0.71	1.6E-02
SLC12A2	1.09	7.4E-02	MPP2	0.71	2.7E-02
UGCG	1.09	6.1E-02	FARP2	0.71	3.2E-02
PSAT1	1.09	6.0E-04	KATNB1	0.70	6.3E-03
BLM	1.09	4.6E-02	SDR39U1	0.70	9.6E-02
SLC38A2	1.08	1.0E-03	RHOT2	0.69	3.8E-02
RIC1	1.08	4.3E-02	TRMT6	0.68	1.1E-02
APTX	1.08	2.4E-02	MED23	0.68	7.1E-02
STK38	1.07	1.5E-02	SELENOM	0.67	7.6E-02
CSTF2T	1.06	2.1E-02	BRD2	0.67	9.8E-02
POGZ	1.05	6.8E-02	CARS1	0.67	5.2E-04
CKAP2	1.04	5.6E-04	ECT2	0.67	2.0E-02
OTUD4	1.04	2.5E-02	SSB	0.67	3.8E-02
EPB41	1.03	3.6E-02	WBP11	0.67	2.1E-02
PCK2	1.02	8.0E-04	MOB2	0.67	6.4E-02
GPATCH1	1.02	3.6E-02	TLN2	0.66	1.5E-02
HMGB2	1.01	8.1E-02	ARHGAP10	0.66	1.8E-02
PHLDB2	1.01	1.5E-02	REXO4	0.66	1.5E-02
RNPS1	1.01	1.7E-02	RRM2B	0.66	2.0E-02
VPS51	1.00	3.8E-02	MVK	0.65	3.8E-02
MAT2B	0.99	1.7E-03	SACS	0.64	7.5E-02
PPCDC	0.98	1.5E-02	INTS10	0.64	1.0E-01
TBCEL	0.97	3.1E-03	ATP1B1	0.64	5.4E-02
MTMR12	0.97	4.2E-02	FHL1	0.63	3.1E-03
CSRP2	0.62	1.8E-02	LEMD3	0.63	2.2E-02
GNPDA1	0.62	6.8E-02	RAB22A	0.63	7.9E-02
NBN	0.62	2.2E-02	NARS1	0.62	6.3E-03

STAG1	0.62	3.8E-02	SSRP1	0.47	8.8E-02
ARF6	0.62	8.8E-02	GIT2	0.47	9.6E-02
CERT1	0.62	9.4E-02	NIBAN1	0.46	8.2E-02
COBLL1	0.62	2.5E-02	ZMYM4	0.46	7.5E-02
FMR1	0.61	1.4E-02	MRTO4	0.46	4.8E-02
SPHK1	0.61	2.4E-02	AP1S2	0.46	8.3E-02
SLC1A5	0.61	3.6E-02	TBC1D9B	0.45	7.8E-02
ACTR6	0.61	3.5E-03	NEPRO	0.45	6.0E-02
NPM1	0.61	2.6E-02	ZNF143	0.45	9.2E-02
ELL	0.60	3.6E-02	LNPEP	0.45	3.1E-02
CRK	0.60	1.8E-02	BCAT1	0.45	6.8E-02
PHF5A	0.60	3.6E-02	VCPIP1	0.45	3.2E-02
VPS18	0.60	5.5E-02	THRAP3	0.45	3.6E-02
ZNF687	0.60	4.0E-02	L2HGDH	0.45	3.8E-02
RBM12	0.60	1.9E-03	UTP20	0.44	9.9E-02
ENOPH1	0.59	4.6E-02	IFI16	0.44	2.2E-02
DCAF13	0.59	7.3E-02	CHD2	0.44	9.2E-02
VRK1	0.59	5.9E-02	KIF22	0.44	8.7E-02
SARS1	0.58	9.1E-03	EXOC6B	0.44	3.7E-02
B4GALT1	0.58	9.8E-02	DPYSL4	0.44	9.0E-02
KDSR	0.57	4.1E-02	TP53	0.44	2.7E-02
FRMD6	0.57	7.9E-02	ADPRS	0.44	2.2E-02
SH3BP1	0.57	9.3E-02	EXOSC7	0.43	1.5E-02
PITHD1	0.57	5.1E-02	EIF2S2	0.43	1.7E-02
SMG8	0.56	5.9E-02	TMPO	0.43	7.8E-02
MAK16	0.56	3.0E-02	ARMC6	0.43	9.3E-02
MAP4K5	0.56	6.2E-02	SMC5	0.43	6.2E-02
GLOD4	0.56	6.3E-03	RRP1B	0.43	8.8E-02
ARAP1	0.56	3.2E-02	TXNRD2	0.42	9.2E-02
C11orf68	0.55	4.6E-02	PDXK	0.42	2.1E-02
TRIM3	0.55	1.7E-02	MSH3	0.42	5.8E-02
YARS1	0.55	2.6E-03	DCTD	0.42	6.7E-02

NAE1	0.55	7.8E-02	KPNA4	0.42	9.3E-02
HNRNPUL2	0.55	4.3E-02	BNIP2	0.42	7.3E-02
MMTAG2	0.55	5.8E-02	ETFA	0.42	7.6E-02
HMG20A	0.54	7.5E-02	HMBS	0.42	3.8E-02
FSD1	0.54	3.0E-02	DEK	0.42	4.7E-02
RASA1	0.54	1.0E-01	PSMD5	0.41	2.7E-02
TP53BP2	0.54	2.1E-02	MCAM	0.41	7.0E-02
PHGDH	0.54	1.4E-02	PFN1	0.40	9.7E-02
DNAJC9	0.54	1.4E-02	SUPT5H	0.40	5.4E-02
GOLGA4	0.53	4.3E-02	WDR75	0.40	8.3E-02
ADAM17	0.53	3.9E-02	IGF2R	0.40	6.6E-02
MYLK	0.53	3.6E-02	PELP1	0.40	2.1E-02
MYO6	0.53	3.9E-02	PI4K2A	0.39	9.8E-02
DUS3L	0.53	3.9E-02	GNL1	0.39	3.9E-02
HNRNPA2B1	0.53	8.8E-02	U2AF2	0.39	7.4E-02
TACC3	0.53	7.4E-02	BOP1	0.39	5.9E-02
KMT2A	0.53	8.8E-02	ESD	0.39	8.9E-02
LIMS1	0.53	5.4E-02	GCLC	0.39	5.8E-02
NCL	0.53	9.2E-02	SERPINB8	0.38	9.0E-02
PPIF	0.52	5.9E-02	IGF2BP1	0.38	6.3E-02
PCNA	0.52	9.8E-02	EEA1	0.38	6.2E-02
POLR3E	0.52	4.5E-02	GTF3C1	0.38	7.4E-02
POLD1	0.52	1.8E-02	ALDH4A1	0.38	8.9E-02
NOP56	0.52	1.5E-02	RPA1	0.37	6.3E-03
SUPT16H	0.52	6.0E-02	MTAP	0.37	7.2E-02
WDR18	0.52	9.2E-02	ARIH1	0.37	8.9E-02
TPX2	0.52	2.7E-02	GTF3C4	0.37	9.5E-02
CPSF6	0.52	1.1E-02	GOPC	0.36	5.0E-02
RFC4	0.52	3.6E-02	GSTZ1	0.36	6.3E-02
DIAPH3	0.51	1.6E-02	HNRNPH3	0.36	6.7E-02
EIF6	0.51	4.7E-02	H4-16	0.36	6.5E-02
ANAPC7	0.51	3.7E-02	LANCL1	0.36	6.5E-02

DKC1	0.51	3.3E-02	EXOSC9	0.36	6.5E-02
NPM3	0.51	3.8E-02	API5	0.36	2.1E-02
ERCC3	0.51	8.8E-02	TRMT10C	0.35	8.9E-02
IFIT5	0.51	6.6E-02	CWF19L1	0.35	5.0E-02
KIF14	0.51	5.4E-02	PPFIA1	0.35	6.6E-02
WDR44	0.50	5.4E-02	SMC3	0.35	9.2E-02
UTP6	0.50	4.5E-02	METTL3	0.34	7.1E-02
ZC3H7A	0.50	8.0E-02	RBM14	0.33	9.2E-02
LGALSL	0.50	8.9E-02	LMO7	0.33	8.2E-02
ENO2	0.50	9.1E-02	TPI1	0.33	7.1E-02
TPD52L2	0.50	4.3E-02	EIF3J	0.32	9.2E-02
UBE3A	0.48	8.3E-02	WDR12	0.32	8.2E-02
MRE11	0.48	6.0E-02	NIFK	0.31	6.6E-02
THUMPD3	0.48	7.0E-02	PDS5A	0.30	6.6E-02
PSMD8	0.48	9.4E-02	RCL1	0.29	6.4E-02
PGM2	0.48	5.5E-02	TPR	0.28	8.9E-02
ARHGAP35	0.48	5.5E-02	FLNB	0.28	2.5E-02
GRWD1	0.47	1.2E-02	AARS1	0.27	7.8E-02
TSG101	0.47	8.8E-02	TXNRD1	0.27	8.8E-02
DHX33	0.47	8.8E-02	SART3	0.25	9.2E-02
ANXA3	0.47	2.4E-02	RANBP2	0.25	1.0E-01
LEMD2	0.47	9.8E-02	SEPTIN9	0.24	9.6E-02
KANK2	0.47	3.6E-02	HNRNPM	0.22	9.4E-02

TABLE 8.2 Proteins downregulated in amino acid-starved vs fed microglia (no corpses)

Gene symbol	Log FC	Adj. p value	Gene symbol	Log FC	Adj. p value
MSMO1	-2.59	6.8E-07	TOMM40	-1.07	2.4E-02
LDLR	-2.47	9.6E-04	TMED9	-1.06	6.8E-02
COL1A1	-2.17	2.6E-03	NT5DC2	-1.06	7.7E-03
POP7	-2.12	3.8E-02	MED13	-1.06	4.7E-02
NDUFAB1	-2.08	1.1E-02	PPIL2	-1.05	1.8E-02
MT-CO1	-2.00	2.9E-05	SDHAF2	-1.05	6.0E-03
CD63	-1.99	2.5E-02	VPS13A	-1.04	2.7E-02
ARPC4	-1.96	1.9E-03	HACL1	-1.04	1.9E-02
MT-CO2	-1.95	3.8E-03	IFIH1	-1.04	2.2E-02
SPARC	-1.95	1.5E-03	FN1	-1.04	9.6E-04
COTL1	-1.95	4.3E-02	P3H4	-1.03	2.2E-02
RAB43	-1.89	3.6E-04	PTRH2	-1.02	3.2E-02
ZFYVE26	-1.89	5.4E-02	WDR5	-1.01	3.0E-02
FDFT1	-1.86	3.0E-07	LAMP1	-1.01	2.4E-02
SETX	-1.74	5.1E-03	STRIP1	-1.01	1.7E-02
PTDSS2	-1.71	9.1E-03	GSPT2	-1.01	6.6E-02
GALNT14	-1.66	2.6E-03	KCTD9	-1.00	2.8E-03
MRPS34	-1.63	2.8E-03	LOXL2	-1.00	2.9E-03
TUT4	-1.62	4.7E-02	THBS1	-1.00	1.3E-03
CYP51A1	-1.59	2.8E-03	MTMR1	-1.00	5.8E-02
GSTM3	-1.58	1.0E-01	DKK3	-1.00	4.4E-02
PHPT1	-1.57	5.1E-02	PSAP	-1.00	6.3E-02
HSD17B11	-1.55	6.2E-02	PI4KB	-1.00	5.4E-02
FBXW11	-1.55	1.9E-03	RPSA	-1.00	7.7E-02
NME1	-1.55	5.4E-02	USP13	-0.99	5.4E-02
GIT1	-1.55	1.1E-02	FPGS	-0.99	1.8E-02
SERPINE1	-1.51	2.1E-02	RBM3	-0.98	9.6E-02

ADAMTS1	-1.50	1.9E-03	RPLP0	-0.98	3.1E-03
MRPL23	-1.49	1.3E-02	EARS2	-0.98	2.4E-02
HLA-C	-1.48	5.7E-02	P3H1	-0.97	8.0E-04
SIL1	-1.47	2.7E-03	SLC7A6	-0.97	8.0E-02
TRMT112	-1.46	7.4E-02	DPM1	-0.97	1.8E-03
RCOR1	-1.45	1.3E-02	IDH3G	-0.97	3.2E-03
AGAP3	-1.45	7.4E-02	ARHGEF28	-0.97	1.0E-02
FADS2	-1.43	1.6E-02	SENP2	-0.97	6.0E-02
MGAT4B	-1.43	3.5E-03	PDF	-0.97	4.5E-02
FKBP9	-1.41	9.6E-04	MICU2	-0.97	1.4E-02
UBE2M	-1.40	7.6E-03	RAB2A	-0.96	5.9E-04
HACD2	-1.38	5.9E-02	SMARCD2	-0.96	6.5E-02
TPM2	-1.38	1.0E-03	COG4	-0.96	3.6E-02
GLT8D1	-1.38	1.0E-03	HEXA	-0.95	8.3E-02
LSS	-1.33	1.5E-04	CEP250	-0.95	2.7E-03
RBM7	-1.33	7.2E-02	FKBP14	-0.95	3.8E-02
TCAF2	-1.33	9.1E-03	NCKIPSD	-0.94	3.2E-03
PAIP2	-1.33	3.5E-03	PLOD1	-0.94	8.4E-06
GOLGA5	-1.32	4.4E-02	CRYBG3	-0.94	8.6E-02
CPA4	-1.31	2.1E-02	AASDHPPT	-0.94	2.4E-02
OAT	-1.28	3.7E-06	STX18	-0.93	6.8E-02
SPC25	-1.28	5.4E-02	RPS10	-0.93	4.0E-02
DHCR24	-1.27	5.2E-04	RAB35	-0.93	3.1E-03
TYMS	-1.27	3.6E-04	TBCC	-0.93	2.7E-02
TMEM14C	-1.26	9.1E-03	DENND3	-0.93	4.9E-02
TXNDC5	-1.26	3.0E-03	LOX	-0.92	7.9E-02
GGA2	-1.25	5.2E-03	FLAD1	-0.92	5.9E-02
QSOX1	-1.25	9.1E-03	TJAP1	-0.92	3.4E-02
TAOK2	-1.25	2.7E-03	ATG2B	-0.92	4.7E-03
ABCD3	-1.24	2.5E-03	MAP3K6	-0.92	2.2E-02
TBRG4	-1.23	9.0E-04	YIF1A	-0.92	3.2E-02
SYPL1	-1.22	3.9E-02	PARP2	-0.91	5.0E-02

MB21D2	-1.21	2.6E-02	POLE2	-0.91	1.8E-02
GGCX	-1.21	1.5E-03	ATAD5	-0.91	5.4E-02
FAR1	-1.21	3.9E-02	HADH	-0.91	2.4E-02
NFU1	-1.20	5.8E-02	LMAN1	-0.91	2.7E-03
AGPAT2	-1.20	2.4E-02	ACTG1	-0.90	1.8E-02
UBE2Z	-1.20	4.0E-02	IFIT1	-0.90	6.8E-02
HYPK	-1.19	2.8E-02	KANSL1	-0.90	3.1E-03
SNTA1	-1.19	3.9E-02	VPS36	-0.90	9.3E-02
MTX2	-1.19	2.4E-02	RRAGB	-0.90	8.0E-02
BCAT2	-1.19	2.1E-02	PTGES3	-0.89	9.4E-02
IGBP1	-1.18	1.5E-02	NUDT2	-0.89	2.2E-02
RAVER1	-1.17	4.5E-02	POGLUT3	-0.88	6.9E-03
RPS15A	-1.17	6.1E-02	ANXA7	-0.88	2.8E-02
TMPO	-1.17	9.2E-02	SEC22B	-0.86	4.2E-02
VPS4A	-1.17	6.6E-03	LZTFL1	-0.86	7.0E-02
SLC25A6	-1.16	5.8E-02	LSM8	-0.86	9.7E-02
GOLIM4	-1.16	2.0E-02	UCK2	-0.86	1.5E-02
CYB5A	-1.15	3.6E-02	LRRC41	-0.86	6.0E-02
CAT	-1.15	2.1E-02	ZNRD2	-0.85	1.3E-02
ABCB7	-1.14	8.9E-02	SNX8	-0.84	4.2E-02
SMARCC1	-1.13	2.0E-02	POLR3C	-0.84	5.9E-02
RIN1	-1.13	5.9E-02	NELFA	-0.84	5.2E-04
PITPNA	-1.13	5.9E-02	SIN3B	-0.84	2.1E-03
PCMT1	-1.13	5.0E-02	OBSL1	-0.84	5.4E-02
CCN1	-1.12	2.9E-03	DDX60	-0.84	7.5E-03
TNC	-1.12	5.2E-04	RAB11FIP5	-0.84	4.1E-02
PAFAH1B2	-1.11	6.6E-02	MAPKAPK2	-0.83	1.5E-02
POLG	-1.11	6.6E-03	BABAM2	-0.83	6.5E-02
ZNFX1	-1.10	4.9E-02	EIF2B1	-0.83	2.0E-02
TXN	-1.10	5.0E-02	PFDN5	-0.83	6.8E-02
ERGIC1	-1.10	1.9E-03	MYDGF	-0.82	4.1E-02
POLR3B	-1.10	3.6E-02	BUB1	-0.82	1.8E-02

AKT2	-1.10	1.0E-03	CDCA2	-0.82	3.8E-02
MED4	-1.09	1.7E-02	NOSIP	-0.82	2.8E-03
FUCA1	-1.08	4.1E-03	FSTL1	-0.81	5.1E-03
KDELR1	-1.08	1.8E-02	RRBP1	-0.81	1.2E-03
ECD	-1.08	7.6E-03	HMGCS1	-0.81	4.3E-02
NEMF	-1.08	6.6E-03	MRPS9	-0.81	5.0E-02
STRN4	-1.08	5.1E-02	CAB39	-0.80	2.2E-03
ATG13	-0.80	5.4E-02	UBAP1	-0.80	5.8E-02
CHID1	-0.79	1.5E-02	CASP2	-0.80	5.8E-02
FASN	-0.79	6.3E-04	GALNT2	-0.51	1.0E-01
FANCD2	-0.79	2.4E-02	YEATS2	-0.51	5.8E-02
TEX2	-0.78	5.8E-02	POFUT2	-0.80	6.6E-02
DOHH	-0.78	8.9E-02	SPTLC2	-0.50	1.8E-02
SPART	-0.77	6.4E-02	GBA	-0.50	1.1E-02
ACOX3	-0.77	5.2E-02	LAMB1	-0.49	4.6E-02
CLPB	-0.77	5.2E-04	ACTR10	-0.49	7.5E-02
OAS1	-0.77	2.5E-02	TCF25	-0.49	3.6E-02
TECR	-0.77	3.0E-03	GPRASP2	-0.48	4.2E-02
UFSP2	-0.77	3.9E-02	USP22	-0.48	7.4E-02
P4HB	-0.76	6.3E-03	VDAC1	-0.48	9.2E-02
GRAMD2B	-0.76	4.3E-02	DNAJC10	-0.48	2.4E-02
TMEM245	-0.76	7.1E-02	SAR1A	-0.48	3.1E-02
TIMMDC1	-0.76	8.8E-02	CLUH	-0.48	3.0E-03
NT5C2	-0.75	2.0E-02	BIRC2	-0.48	5.9E-02
CPPED1	-0.75	9.5E-02	ACACA	-0.48	1.4E-02
SMARCA4	-0.75	1.1E-02	DHX30	-0.48	6.8E-03
HECTD3	-0.74	2.5E-02	OSBPL8	-0.48	6.8E-02
TRIM21	-0.74	5.8E-02	MTDH	-0.47	1.4E-02
TCP11L1	-0.73	4.9E-02	LAMC1	-0.47	4.4E-02
TOR1B	-0.73	6.8E-03	DBN1	-0.47	2.1E-02
L1CAM	-0.73	3.8E-02	MTMR10	-0.46	9.7E-02
ATAD3B	-0.73	9.2E-02	PSMD2	-0.46	6.4E-03

COA3	-0.73	7.2E-02	UBXN4	-0.46	5.0E-02
SCFD2	-0.72	7.2E-02	NDUFAF7	-0.46	5.9E-02
RER1	-0.72	8.9E-02	TRIP12	-0.46	5.9E-03
TNS1	-0.72	8.3E-02	SSR4	-0.46	1.7E-02
NAA30	-0.72	9.6E-02	TAP1	-0.45	3.7E-02
RBM19	-0.72	4.0E-03	PLOD2	-0.45	3.8E-02
COL8A1	-0.70	3.2E-02	USP48	-0.44	5.5E-02
CLPX	-0.70	1.6E-02	PDIA4	-0.44	3.2E-02
BRD9	-0.69	9.1E-03	EHD2	-0.44	2.0E-02
RRM1	-0.69	9.6E-04	CHMP7	-0.44	6.7E-03
ZFHX4	-0.69	1.5E-02	OGDH	-0.43	8.9E-02
ARF1	-0.69	3.8E-02	RNF40	-0.43	9.4E-02
CLPTM1	-0.69	2.4E-02	BAIAP2L1	-0.43	8.4E-02
UBE2C	-0.68	6.0E-02	IPO7	-0.43	3.9E-02
MVP	-0.68	1.8E-02	MCCC1	-0.43	2.1E-02
LDHB	-0.67	5.4E-02	QTRT2	-0.43	9.3E-02
PITPNB	-0.67	3.8E-02	DDX5	-0.43	1.8E-02
COL6A2	-0.67	9.2E-02	BAG6	-0.42	9.4E-02
GNA13	-0.67	7.1E-02	PARP14	-0.42	3.8E-02
R3HCC1	-0.67	5.9E-02	GTPBP10	-0.42	9.4E-02
PUM2	-0.66	2.1E-02	ATP5PB	-0.42	3.6E-02
RGP1	-0.66	3.8E-02	GALNT7	-0.42	2.1E-02
NFS1	-0.66	2.6E-03	PDCL3	-0.42	8.3E-02
ATL3	-0.65	1.1E-03	UHRF1	-0.42	2.4E-02
F3	-0.65	1.3E-02	CALR	-0.42	7.5E-02
USP34	-0.65	5.6E-02	CAPRIN1	-0.41	6.2E-02
PTCD1	-0.65	8.3E-02	ERP44	-0.41	5.4E-02
TIMM50	-0.65	5.9E-02	ABCF2	-0.41	1.8E-02
UQCR10	-0.65	6.6E-02	SEC63	-0.41	2.8E-02
P4HA2	-0.64	1.8E-02	GANAB	-0.41	7.2E-02
GRSF1	-0.63	1.4E-02	SLC25A13	-0.40	3.2E-03
MARCHF5	-0.63	6.6E-02	DAP3	-0.40	7.4E-02

BSDC1	-0.63	5.5E-02	EMC3	-0.40	4.2E-02
MRPS23	-0.62	4.5E-02	SEC61A1	-0.39	5.3E-02
CMTM6	-0.62	7.5E-02	HSD17B4	-0.39	2.5E-02
MESD	-0.61	7.6E-02	DDOST	-0.39	3.6E-02
IGHMBP2	-0.61	6.8E-02	DHX29	-0.38	5.9E-02
RBBP4	-0.61	9.8E-02	HECTD1	-0.38	9.3E-02
PSMG2	-0.61	8.0E-02	HELLS	-0.38	4.6E-02
AHSA1	-0.61	5.4E-02	SDHA	-0.38	4.0E-02
PSMD7	-0.61	3.9E-02	EEF2	-0.38	2.6E-02
EIF4ENIF1	-0.61	9.6E-02	IMPDH2	-0.37	4.5E-02
CDC25C	-0.60	4.9E-02	CORO1B	-0.36	7.4E-02
MRPS5	-0.60	1.9E-02	ATP2A2	-0.36	6.3E-02
ITM2C	-0.59	8.2E-02	NR2F2	-0.36	7.4E-02
UBE4B	-0.59	4.9E-02	ATP5F1C	-0.36	6.3E-02
WASL	-0.59	6.8E-02	LRPPRC	-0.36	2.2E-02
PSMA5	-0.59	5.9E-02	PSMD6	-0.36	3.2E-02
DGKA	-0.58	7.5E-02	SLC25A3	-0.35	2.3E-02
ACSL4	-0.58	8.8E-03	EEF1G	-0.35	8.9E-02
BICD2	-0.58	4.6E-02	TRIM25	-0.34	6.7E-02
LGALS3BP	-0.58	4.2E-02	ALDH18A1	-0.33	7.4E-02
PLOD3	-0.58	9.1E-03	STAT3	-0.33	8.7E-02
PSMB4	-0.58	2.2E-02	RPS24	-0.33	9.2E-02
HDLBP	-0.58	1.0E-03	KPNA2	-0.33	7.7E-02
MAPK3	-0.57	8.9E-02	HLTF	-0.32	6.5E-02
PRDX4	-0.57	9.9E-02	RPN2	-0.32	5.0E-02
TFCP2	-0.57	9.8E-02	MTA1	-0.32	8.1E-02
RMND5A	-0.57	9.2E-02	BIRC6	-0.32	3.8E-02
BTF3	-0.57	7.7E-02	NACC1	-0.31	7.4E-02
EMC1	-0.57	7.7E-03	ITCH	-0.31	3.8E-02
NRK	-0.56	6.3E-02	SCYL1	-0.31	3.2E-02
PBRM1	-0.56	4.0E-02	RANBP9	-0.30	9.3E-02
RAB18	-0.55	2.5E-02	HADHA	-0.30	3.8E-02

CENPE	-0.54	5.0E-02	PTK7	-0.30	9.2E-02
INF2	-0.54	6.8E-03	OGT	-0.29	9.8E-02
CCDC25	-0.53	4.6E-02	HSDL2	-0.29	8.2E-02
ZKSCAN8	-0.53	7.4E-02	MOGS	-0.29	9.3E-02
FKBP8	-0.53	2.2E-02	PSMD12	-0.29	9.2E-02
HSPH1	-0.53	1.1E-02	CAD	-0.28	8.9E-02
ESYT1	-0.53	2.2E-03	MSN	-0.28	7.4E-02
SRPK1	-0.53	1.8E-02	PRKCI	-0.28	9.2E-02
PALM	-0.53	7.8E-02	ZW10	-0.27	7.8E-02
ANXA6	-0.52	3.1E-02	HADHB	-0.26	9.8E-02
TRIP6	-0.52	9.4E-02	PTPN1	-0.25	9.6E-02
P4HA1	-0.52	1.8E-02	MDH2	-0.25	9.9E-02
DNAJA1	-0.52	2.1E-02	PSMD11	-0.24	7.4E-02

TABLE 8.3 Proteins upregulated in amino acid-starved vs fed microglia during efferocytosis

Gene symbol	Log FC	Adj. p value	Gene symbol	Log FC	Adj. p value
C1orf52	3.16	1.4E-03	AP3M2	1.35	7.9E-03
NLRP10	2.98	1.4E-02	CPSF4	1.33	9.1E-02
NEDD1	2.07	1.4E-03	PPCDC	1.31	3.0E-03
SLC39A14	1.95	6.2E-03	CLGN	1.29	4.9E-02
SLC38A1	1.91	1.3E-02	SEPHS2	1.27	5.0E-02
ZFAND1	1.79	1.5E-02	CCNY	1.26	8.3E-03
TBCEL	1.78	9.5E-06	MGME1	1.25	9.0E-03
RNF113A	1.67	1.6E-02	MOB2	1.25	2.4E-03
SOD2	1.67	7.2E-02	BARD1	1.24	2.4E-02
GLTP	1.66	6.2E-03	CENPC	1.23	8.1E-02
PAIP1	1.61	7.8E-02	SRM	1.23	6.1E-02
WAC	1.57	3.4E-02	SKA3	1.23	7.9E-03
FAM50A	1.56	9.1E-02	SMARCD2	1.21	3.4E-02
ZNF318	1.54	9.0E-03	PRTFDC1	1.18	1.8E-02
RPP38	1.53	3.7E-03	UCKL1	1.18	6.0E-02
PARG	1.53	3.2E-02	CCNA2	1.18	9.8E-03
BROX	1.53	3.9E-02	WDR5	1.18	1.8E-02
GEMIN6	1.52	9.1E-03	MTMR6	1.16	1.6E-02
MSI1	1.50	1.8E-02	ZHX3	1.12	4.7E-02
PDCD4	1.48	3.3E-02	ACTR5	1.11	5.7E-02
PTPN9	1.47	6.1E-02	EPN2	1.10	3.6E-02
RSU1	1.44	6.2E-03	PDE4DIP	1.10	4.3E-02
RIN1	1.44	3.1E-02	TTL	1.09	5.2E-03
ELP3	1.41	4.1E-02	ITPKA	1.08	6.1E-02
MED21	1.41	1.2E-02	CD2BP2	1.08	6.6E-02
NUDT16L1	1.39	3.1E-03	LTF	1.07	4.5E-02
UBE2Z	1.38	3.2E-02	WASL	1.07	3.4E-03

FBXO38	1.36	4.2E-02	SCAMP1	1.06	9.7E-02
TNIP1	1.36	5.9E-03	EPC2	1.05	3.3E-02
USP19	1.35	3.2E-02	BCL9L	1.02	4.9E-02
NSRP1	0.99	9.4E-02	NEK7	1.01	1.6E-03
WDR89	0.97	6.9E-03	IFT81	1.01	4.6E-03
ZNF830	0.96	9.3E-03	IGF2BP3	0.99	6.1E-02
PHLDB2	0.95	3.2E-02	GLE1	0.63	3.3E-02
EPM2AIP1	0.93	7.0E-02	CARS1	0.62	1.3E-03
ABR	0.92	4.6E-02	REXO4	0.62	3.3E-02
NDRG1	0.90	9.4E-02	DROSHA	0.58	4.1E-02
INTS10	0.89	4.0E-02	SLC1A5	0.58	6.8E-02
BCL2L1	0.88	5.8E-02	CBFB	0.55	9.5E-02
UHRF2	0.88	6.1E-02	ENOPH1	0.55	9.4E-02
CYHR1	0.85	7.5E-02	RRP1	0.53	4.1E-02
GTF2E1	0.84	1.4E-02	CENPE	0.53	7.8E-02
SREK1	0.84	9.0E-02	RNMT	0.49	9.3E-02
SELENOM	0.83	4.6E-02	DHODH	0.49	4.4E-02
PSAT1	0.83	6.2E-03	PHF2	0.47	6.1E-02
NSL1	0.80	3.3E-02	SARS1	0.47	4.7E-02
STK17B	0.79	6.4E-02	WDR74	0.46	4.5E-02
CEP152	0.78	8.9E-02	GCLC	0.46	3.8E-02
IRGQ	0.78	3.7E-02	TPX2	0.43	9.1E-02
SKA1	0.74	8.1E-02	GNL1	0.40	5.1E-02
SLC38A2	0.74	2.4E-02	RBM12	0.40	3.8E-02
BBX	0.73	9.6E-02	MTAP	0.40	8.1E-02
LDLRAP1	0.72	6.8E-02	CASP3	0.39	5.4E-02
PCK2	0.71	1.4E-02	CPSF6	0.38	7.0E-02
YARS1	0.71	4.0E-04	UBA2	0.37	9.1E-02
EPHB2	0.68	6.8E-02	GLOD4	0.36	9.5E-02
YEATS2	0.63	3.3E-02	PELP1	0.35	5.5E-02
PHGDH	0.63	6.6E-03	TXNRD1	0.35	4.1E-02
HMG20A	0.63	6.1E-02	RPP30	0.35	6.7E-02

PHF5A	0.63	4.2E-02	XPOT	0.33	9.0E-02
ASNS	0.62	9.1E-03	AARS1	0.32	6.0E-02
ZNF185	0.61	9.0E-03	RPA1	0.24	9.1E-02
AGO2	0.60	8.3E-02			

TABLE 8.4 Proteins upregulated in amino acid-starved vs fed microglia during efferocytosis

Gene symbol	Log FC	Adj. p value	Gene symbol	Log FC	Adj. p value
PRNP	-2.96	9.98E-03	CAMSAP1	-1.12	3.43E-02
SPARC	-2.20	9.32E-04	GAMT	-1.12	9.85E-02
TCAF2	-2.20	2.40E-04	B4GALT1	-1.12	4.60E-03
AGAP3	-2.17	1.36E-02	AHCYL1	-1.12	8.20E-02
PTDSS2	-1.98	4.60E-03	DLGAP4	-1.11	9.08E-02
COL1A1	-1.93	7.86E-03	TIMM17A	-1.10	5.37E-02
MAP7D3	-1.87	6.24E-03	FAR1	-1.09	8.98E-02
ATOX1	-1.71	1.55E-02	TAB1	-1.07	9.10E-02
PIKFYVE	-1.65	6.11E-02	EARS2	-1.06	2.16E-02
TPM2	-1.63	3.28E-04	SMYD5	-1.06	4.07E-02
RBPMS	-1.54	4.07E-02	BTBD2	-1.05	5.14E-02
PROCR	-1.53	2.16E-02	RAB43	-1.05	3.20E-02
WNK4	-1.50	7.93E-02	AUP1	-1.05	7.39E-02
NDUFS6	-1.42	8.84E-02	PLD2	-1.03	1.03E-02
WDR76	-1.41	3.07E-03	STK4	-1.02	1.23E-02
CNPY2	-1.39	4.76E-02	EDIL3	-1.02	1.36E-02
GALNT14	-1.37	1.30E-02	EXOSC2	-1.01	6.11E-02
FPGS	-1.35	3.21E-03	AGRN	-1.00	2.86E-02
HSBP1	-1.35	7.05E-02	CTU2	-0.99	8.10E-02
FDFT1	-1.33	1.79E-05	TRAPPC10	-0.99	4.50E-02
THOC6	-1.32	9.02E-03	GNA13	-0.97	1.55E-02
CRIM1	-1.31	1.06E-02	PDGFRB	-0.97	6.96E-03
DMAP1	-1.31	6.77E-02	CLMN	-0.95	9.36E-02
RER1	-1.29	6.24E-03	SIN3B	-0.95	1.38E-03
UGCG	-1.28	4.57E-02	THBS1	-0.94	3.18E-03
TANGO6	-1.27	7.02E-02	STX18	-0.93	9.94E-02
CPA4	-1.26	3.72E-02	FUCA1	-0.93	1.72E-02

TYW3	-1.26	5.58E-02	SLC7A1	-0.92	9.52E-06
ZYG11B	-1.25	1.95E-02	LOXL2	-0.92	7.63E-03
IGBP1	-1.24	1.36E-02	ATG2A	-0.91	5.25E-02
JUP	-1.24	3.64E-03	FN1	-0.90	3.64E-03
COL8A1	-1.20	1.38E-03	WRN	-0.90	5.92E-02
GOLIM4	-1.15	3.10E-02	MRPS9	-0.89	4.57E-02
SPAG1	-1.15	8.82E-02	MSMO1	-0.89	3.20E-02
FYCO1	-1.15	6.18E-02	ARF1	-0.89	1.29E-02
AMPH	-1.13	1.21E-02	TMEM14C	-0.88	8.20E-02
BICC1	-0.87	4.12E-02	COX15	-0.52	9.10E-02
VARS2	-0.86	5.14E-02	LMAN1	-0.52	9.37E-02
DNLZ	-0.86	2.03E-02	CLUH	-0.51	2.98E-03
CAB39	-0.85	2.02E-03	RAB18	-0.51	5.71E-02
IVNS1ABP	-0.85	6.24E-03	SAR1B	-0.50	7.09E-02
UQCR10	-0.83	3.31E-02	ACTR2	-0.50	9.31E-02
SRSF11	-0.83	9.08E-02	FKBP8	-0.50	4.59E-02
ADAMTS1	-0.82	9.10E-02	HDLBP	-0.48	6.22E-03
TFDP1	-0.81	9.81E-02	STAT3	-0.48	2.48E-02
EXOSC3	-0.81	8.38E-02	RAB32	-0.46	7.23E-02
DUS2	-0.81	7.02E-02	MAP1B	-0.45	6.11E-02
KEAP1	-0.80	7.23E-02	PDCL3	-0.44	9.56E-02
TRIM58	-0.80	8.10E-02	SDHA	-0.44	2.98E-02
THBS2	-0.79	4.56E-02	FBXO22	-0.44	7.16E-02
RABEP2	-0.76	8.10E-02	RRM1	-0.44	3.34E-02
FASN	-0.75	1.38E-03	RDH11	-0.44	6.77E-02
C17orf80	-0.75	5.20E-02	HSPH1	-0.43	4.99E-02
POLE2	-0.74	7.02E-02	P4HA1	-0.43	6.68E-02
TMEM263	-0.73	5.68E-02	TAP1	-0.41	7.61E-02
CD59	-0.73	4.99E-02	ARPC1B	-0.41	8.70E-02
TBRG4	-0.73	4.18E-02	PON2	-0.41	3.22E-02
HPF1	-0.72	9.15E-02	ALDH18A1	-0.41	4.76E-02
MICU2	-0.69	9.31E-02	RPS6KA1	-0.40	6.86E-02

TYMS	-0.69	3.34E-02	GBP1	-0.40	3.69E-02
RUFY2	-0.68	8.06E-02	HLA-B	-0.40	4.90E-02
RGL2	-0.67	5.97E-02	SSR4	-0.38	5.79E-02
RHPN2	-0.67	7.02E-02	ATP5F1C	-0.38	7.08E-02
KIF1B	-0.65	7.39E-02	PALLD	-0.36	3.72E-02
L1CAM	-0.64	9.31E-02	PSMD2	-0.35	4.59E-02
UCK2	-0.63	9.01E-02	ECSIT	-0.35	9.49E-02
GALNT2	-0.60	8.20E-02	RANBP9	-0.34	9.08E-02
PLOD1	-0.60	1.57E-03	TRIP12	-0.34	4.90E-02
F3	-0.59	3.25E-02	SNX17	-0.34	4.90E-02
OAT	-0.57	1.29E-02	HSD17B4	-0.34	7.23E-02
FSTL1	-0.57	6.02E-02	BIRC6	-0.33	4.46E-02
P4HA2	-0.56	4.80E-02	SLC25A3	-0.33	4.57E-02
ENG	-0.56	3.20E-02	NACA	-0.33	9.08E-02
RRBP1	-0.53	3.22E-02	RPS2	-0.33	9.45E-02
QTRT2	-0.53	5.97E-02	ABCF2	-0.32	8.70E-02
RPL18	-0.53	6.68E-02	ESYT1	-0.31	7.02E-02
TPT1	-0.52	6.86E-02	MCCC2	-0.31	6.11E-02